

QUANTITATIVE STUDIES OF THE EFFECTS  
OF INTERFACIAL BONDING STRENGTH ON THE  
MECHANICAL AND RHEOLOGICAL PROPERTIES OF POLYMER COMPOSITES

BY

SHAYE-WEN SHANG

A DISSERTATION PRESENTED TO THE GRADUATE SCHOOL  
OF THE UNIVERSITY OF FLORIDA IN PARTIAL  
FULFILLMENT OF THE REQUIREMENTS  
FOR THE DEGREE OF DOCTOR OF PHILOSOPHY

UNIVERSITY OF FLORIDA

1989

UNIVERSITY OF FLORIDA



3 1262 08552 3180

TO MY FAMILY

## ACKNOWLEDGEMENTS

I would like to express my sincerest gratitude and appreciation to my advisors professor Christopher D. Batich and Dr. Jerry J. Williams in 3M for their invaluable guidance and understanding during the course of this work.

I am also grateful to professor Robert T. DeHoff for the discussion of the model proposed in this study, and to professor Eugene P. Goldberg and professor Denish O. Shah for their helpful comments and kind assistance, and to professor Kevis S. Jones for the help with the TEM micrograph, and to professor Michael D. Sacks for his kind assistance with the Rheometrics Dynamic Spectrometer.

Special thanks are given to professor Karl-Johan M. Söderholm of the Department of Dental Biomaterials for his introducing me to the art of thorough scientific investigation and for his unforgettable assistance as well as encouragement during the time of my research as a graduate student.

Meanwhile, I would like to express my gratitude to my parents and sister for their constant support, without their backup, this work cannot be done.

## TABLE OF CONTENTS

	<u>Page</u>
ACKNOWLEDGEMENTS.....	iii
LIST OF TABLES.....	ix
LISTS OF FIGURES.....	x
ABSTRACT.....	xix
 CHAPTERS	
1. INTRODUCTION.....	1
1.1 General.....	1
1.2 Outline of This Study.....	2
2. BACKGROUND.....	7
2.1 Effect of Filler Particles in Polymer Matrix.....	7
2.2 Interfacial Bonding.....	7
2.2.1 Bonding and Force across an Interface.....	8
2.2.1.1 Aided Bonding by Coupling Agents....	8
2.2.1.2 Direct Intermolecular Interactions..	9
2.2.2 Ways to Characterize Forces at the	
Interface.....	15
2.2.2.1 Work of Adhesion and Wetting.....	15
2.2.2.2 Relationship between Work of	
Adhesion and Force Attraction	
Constant.....	18
2.2.2.3 Work of Adhesion and Surface	
Energy.....	19
2.2.2.3.1 Harmonic-Mean Approach...20	
2.2.2.3.2 Geometric-Mean Approach..20	
2.2.2.4 Surface Energy.....	21
2.2.2.4.1 Surface Energy and	
Contact Angle.....	21
2.2.2.4.2 Surface Energy and	
Cohesive Energy Density..23	
2.2.2.4.3 Hamilton Methods.....	24
2.2.2.4.4 Captive Air Bubble	
Technique.....	26
2.2.2.5 Work of Adhesion and Acid-Base	
Interaction.....	27

2.3	Quantitative Evaluation of Interfacial Bonding Strength of Polymer Composites.....	29
2.4	Mechanical Properties of Particulate Filled Polymer Composite.....	32
2.4.1	Effect of Properties of Interface/ Interphase on a Polymer Composite.....	34
2.4.2	Effect of Volume Fraction and Particle Size on the Modulus of a Composite.....	36
2.4.3	Effect of Volume Fraction and Particle Size on the Tensile Strength of a composite.....	42
2.4.4	Effect of Temperature and Testing Rate on the Mechanical Properties of a composite...	46
2.5	Rheological Properties of Particulate Filled Polymer Melts.....	48
2.5.1	Effect of Volume Fraction, Particle Size and Size Distribution of Filler on Polymer Melts.....	49
2.5.2	Effect of Testing Rate and Temperature.....	52
2.6	Dispersion of Filler Particles in the Polymer Matrices.....	54
2.7	Friction in a Filled Polymer System.....	56
2.7.1	Coefficient of Friction.....	56
2.7.1.1	Effect of Polar Functional Groups on the Coefficient of Friction.....	58
2.7.1.2	Effect of Temperature on the Coefficient of Friction.....	58
2.7.2	Friction Factor.....	59
2.7.2.1	Types of Friction Factor in a Polymer System.....	61
2.7.2.2	Segmental Friction of an Unfilled Polymer Matrix.....	61
2.7.2.3	Surface Skin and Form Friction on Particulate Filled Polymer Melts...	62
3.	MATERIALS AND METHODS.....	64
3.1	Materials.....	64
3.1.1	Filler.....	64
3.1.1.1	Stöber Silica.....	64
3.1.1.2	Cab-O-Sil Silica.....	64
3.1.1.3	Quartz Plates.....	65
3.1.2	Polymer.....	65
3.1.3	Chemical for Surface Modification.....	66
3.2	Techniques.....	67
3.2.1	Preparation of Stöber Silica.....	67
3.2.2	Surface Modification on Silica Particle...	68
3.2.2.1	Heat Treatment.....	68
3.2.2.2	Chemical Treatment by Trimethylchlorosilane (TMCS).....	69
3.2.3	Contact Angle Measurement.....	69
3.2.4	Titration by Indicator Dye.....	71
3.2.5	Diffuse Reflectance Infrared Fourier Transform (DRIFT) Spectrometry.....	72

3.2.6	Thermogravimetric Analysis (TGA).....	74
3.2.7	Polymer Adsorption on the Silica Surface.....	75
3.2.8	Preparation of Polymer Composites.....	76
3.2.9	Mechanical and Rheological Measurements....	77
3.2.10	Scanning Electron Microscopy (SEM) and Scanning Transmission Electron Microscopy (STEM) Studies.....	79
4.	CHARACTERIZATION AND MODIFICATION OF SURFACE OF SILICA PARTICLES.....	81
4.1	Characterization of Silica Particles.....	81
4.1.1	Stöber Silica.....	81
4.1.2	Cab-O-Sil Silica.....	84
4.2	Modification of the Silica Surface.....	88
4.2.1	Contact Angles on Amorphous Fused Quartz Plates.....	88
4.2.2	Fourier Transform Infrared (FTIR) and Thermogravity Analysis (TGA) Studies of Silica Particles.....	89
4.2.2.1	Heat Treatment.....	89
4.2.2.2	Chemical Treatment.....	96
4.2.2.2.1	Cab-O-Sil Silica.....	97
4.2.2.2.2	Stöber Silica.....	99
4.3	Concentration of Hydroxyl Groups on the Silica Surface.....	102
4.4	Polymer Adsorption on Silica Surface.....	104
4.4.1	Evidence of Hydrogen Bonding Studied by FTIR.....	105
4.4.2	Effect of Hydrogen Bonding on the Polymer Adsorption.....	107
4.4.3	Ratio of Hydrogen-Bonded to Non- Hydrogen-Bonded Carbonyl Group.....	115
4.5	Temperature Dependence of the Interfacial Bonding.....	122
4.5.1	Heating Effect on the Silica-Surface- Adsorbed Polymer.....	122
4.5.2	Cooling Effect on the Silica-Surface- Adsorbed Polymer.....	128
4.5.3	Quasi-Equilibrium Constant of Hydrogen Bonding.....	131
4.5.3.1	Thermodynamic Approach.....	131
4.5.3.2	Temperature Dependence of Quasi- Equilibrium Constant of Hydrogen Bonding at the Interface.....	132
5.	RESULTS.....	137
5.1	Work of Adhesion between Silica Particles and E-Va Copolymer.....	137
5.1.1	Work of Adhesion of Weak Interfacial Bonding.....	137

5.1.2	Work of Adhesion of Strong Interfacial Bonding.....	139
5.1.3	Work of Adhesion and Surface Energy of Silica Particles.....	142
5.1.4	The Hydrogen Bonding Component of Work of Adhesion.....	144
5.2	The Mechanical Properties of Silica Filled Filled Composites.....	145
5.2.1	Effects of Particle Size and Volume Fraction of Silica Filler.....	145
5.2.2	Effect of Work of Adhesion.....	149
5.2.2.1	Young's Modulus.....	149
5.2.2.2	Extension of Guth-Smallwood Equation.....	154
5.2.2.3	Tensile Strength.....	156
5.3	The Rheological Properties of Silica Filled Composites.....	160
5.3.1	Shear Storage Modulus of Polymer Composites.....	160
5.3.1.1	Dependence of Frequency and Solid Loading on the Shear Modulus.....	160
5.3.1.1.1	Cab-O-Sil Silica Filled Composites.....	160
5.3.1.1.2	Stöber Silica Filled Composites.....	163
5.3.1.2	Dependence of Work of Adhesion on the Shear Modulus.....	163
5.3.1.2.1	Cab-O-Sil Silica Filled Composites.....	163
5.3.1.2.2	Stöber Silica Filled Composites.....	172
5.3.2	Melt Viscosity of Silica Filled Polymer Melt.....	186
5.3.2.1	Dependence of Frequency and Solid Loading on the Melt Viscosity.....	186
5.3.2.1.1	Cab-O-Sil Silica Filled Composites.....	186
5.3.2.1.2	Stöber Silica Filled Composites.....	187
5.3.2.2	Dependence of Work of Adhesion on the Melt Viscosity.....	199
5.3.2.2.1	Cab-O-Sil Silica Filled Composites.....	199
5.3.2.2.2	Stöber Silica Filled Composites.....	199
5.4	Effect of Temperature on the Viscosity of Silica Filled Polymer Composites.....	213
5.5.1	Dependence of Volume Fraction of Silica.....	215
5.5.2	Dependence of Silica Surface Properties.....	221
5.6	Dispersion of Silica Filler Particles in the Polymer Matrix.....	232

6.	DISCUSSION.....	256
6.1	Effective Silica Particle Size.....	256
6.2	Interphase Dependence of Mechanical Properties of Polymer Composites.....	260
6.2.1	Interphase Dependence of Young's Modulus.....	260
6.2.2	Interphase Dependence of Tensile Strength.....	262
6.3	Effect of Temperature on Work of Adhesion.....	268
6.3.1	Temperature Dependence of Weak Interfacial Bonding.....	268
6.3.2	Temperature Dependence of Strong Interfacial Bonding.....	269
6.3.3	Discussion of Temperature Dependence of Work of Adhesion.....	270
6.4	Effect of Interphase on the Rheological Properties of Silica Filled Polymer melt.....	272
6.4.1	Frequency Dependence of the Effective Particle Size.....	272
6.4.2	Interphase Dependence of Shear Modulus.....	274
6.4.3	Interphase Dependence of Melt Viscosity.....	275
6.4.3.1	Flow Process of a Filled Polymer Melt.....	275
6.4.3.2	Effect of Friction Factor on Melt Viscosity.....	276
6.4.3.3	Low Frequency Dependence of Surface Friction Factor.....	277
6.4.3.4	High Frequency Dependence of Surface Friction Factor.....	280
6.5	Mathematical Model.....	281
6.6	Effect of Frequency on the Activation Energy of Polymer Melt.....	290
6.7	The Extended Arrhenius Equation on the Melt Viscosity of Silica Filled Polymer Melts.....	292
7.	CONCLUSIONS.....	299
8.	FUTURE RESEARCH.....	303
	REFERENCES.....	312
	BIOGRAPHICAL SKETCH.....	337

## LIST OF TABLES

<u>Tables</u>	<u>Pages</u>
2.1 Bond Types and Typical Bond Energy.....	14
4.1 Contact Angles Versus Surface Modification on Amorphous Fused Quartz Plates.....	91
4.2 Surface Hydroxyl Groups Per Unit Area.....	103
4.3 Amount of Polymer Adsorbed on Unit Area of Silica Surface.....	110
4.4 Ratio of Hydrogen-Bonded to Non-Hydrogen-Bonded Carbonyl Groups.....	120
5.1 Surface Energy of Silica and E-Va Copolymer Evaluated by Contact Angles.....	140
5.2 Calculated Work of Adhesion Between Silica Surface and E-Va Copolymer.....	141
5.3 Slopes of the Young's Modulus of Silica Filled E-Va Copolymers.....	155
5.4 Slopes of the Tensile Strength of Silica Filled E-Va Copolymers.....	159
5.5 Activation Energy of Viscosity of Stöber Silica Filled Ethylene-Vinyl Acetate Copolymer.....	224

## LIST OF FIGURES

<u>Figures</u>	<u>Pages</u>
2.1 Relationship between Contact Angle and Young's Equation.....	17
2.2 Components of Surface Free Energy for the Hamilton Technique.....	25
2.3 Components of Surface Free Energy for Air Bubble Technique.....	25
4.1 Shape and Size of Stöber Silica by SEM.....	82
4.2 The Three Dimensional Random Branching of the Aggregates of Cab-O-Sil Silica.....	85
4.3 The Isolated Individual Aggregates of Cab-O-Sil Silica.....	86
4.4 The Individual Particles in the Aggregates of Cab-O-Sil Silica.....	87
4.5 Contact Angles of Water on the Surface of the Fused Quartz Plates Treated by Heat and/or TMCS....	90
4.6 FTIR Spectrum of Stöber Silica Heat Treated at Different Temperatures.....	92
4.7 FTIR Spectrum of Cab-O-Sil Silica Heat Treated at Different Temperatures.....	93
4.8 TGA Spectrum of the Weight Loss of Cab-O-Sil and Stöber Silica by the Heating Process.....	95
4.9 FTIR Spectrum of Cab-O-Sil Silica at Different Heat/TMCS Treatments.....	98
4.10 FTIR Spectrum of Stöber Silica at Different Heat/TMCS Treatments.....	100
4.11 The Wavenumber Shift of the Carbonyl Groups of E-Va Copolymer after Hydrogen Bonding with the Hydroxyl Groups on the Silica Surface.....	106

4.12	Effects of Volume Concentrations of Polymer Solution on the Extent of Polymer Adsorbed on 110°C and 750°C/TMCS Cab-O-Sil Silica Surfaces'....	108
4.13	Effect of Silica Surface Properties on Polymer Bonded and/or Adsorbed on the Cab-O-Sil Silica Surface from 6% Volume of Polymer Solution.....	112
4.14	Effect of Silica Surface Properties on Polymer Bonded and/or Adsorbed on the Cab-O-Sil Silica Surface from 2% Volume of Polymer Solution.....	113
4.15	Effect of Silica Surface Properties and Volume Concentration of Polymer Solution on the Extent of Adsorbed Polymer per Unit Silica Surface.....	114
4.16	The Extent of Polymer Bonded and/or Adsorbed on the Silica Surface versus Work of Adhesion from Different Solution Concentrations.....	116
4.17	Effect of Concentrations of Polymer Solution on the Ratio of Hydrogen-Bonded to Non-Hydrogen-Bonded Carbonyl Groups of 110°C Treated Silica....	118
4.18	Effect of Concentrations of Polymer Solution on the Ratio of Hydrogen-Bonded to Non-Hydrogen-Bonded Carbonyl Groups of 750°C/TMCS Silica.....	119
4.19	Effect of Environmental Temperature on the Carbonyl Groups Bonded/Adsorbed on the Cab-O-Sil Silica Treated at 110°C.....	123
4.20	Effect of Environmental Temperature on the Intensity of Hydroxyl Groups of the Cab-O-Sil Silica Treated at 110°C.....	125
4.21	Effect of Environmental Temperature on the Carbonyl Groups Bonded/Adsorbed on the Cab-O-Sil Silica Treated by 750°C/TMCS.....	126
4.22	Effect of Environmental Temperature on the Intensity of Hydroxyl Groups of the Cab-O-Sil Silica Treated by 750°C/TMCS.....	127
4.23	FTIR Spectrum of Temperature Cooling Process on the Hydrogen-Bonded Carbonyl Groups Adsorbed on the Cab-O-Sil Silica Treated at 110°C.....	129
4.24	FTIR Spectrum of Temperature Cooling Process on the Hydrogen-Bonded Carbonyl Groups Adsorbed on the Cab-O-Sil Silica Treated by 750°C/TMCS.....	130

4.25	Quasi-Equilibrium Constant between Hydrogen-Bonded and Non-Hydrogen-Bonded Carbonyl Groups at the Interface.....	134
4.26	Effect of Temperature on the Quasi-Equilibrium Constant between Hydrogen-Bonded and Non-Hydrogen-Bonded Carbonyl Groups at the Interface..	136
5.1	Work of Adhesion versus Surface Energy of Silica..	143
5.2	Hydrogen Component of Work of Adhesion versus Hydrogen Component of Surface Energy of Silica....	146
5.3	Effect of Volume Fraction and Surface Properties of Stöber Silica Filler Particles on the Modulus of Polymer Composites.....	147
5.4	Effect of Volume Fraction and Surface Properties of Cab-O-Sil Silica Filler Particles on the Modulus of Polymer Composites.....	148
5.5	Effect of Volume Fraction and Surface Properties of Stöber Silica Filler on the Tensile Strength of Polymer Composites.....	150
5.6	Effect of Volume Fraction and Surface Properties of Cab-O-Sil Silica Filler on the Tensile Strength of Polymer Composites.....	151
5.7	Effect of Work of Adhesion, Volume Fraction and Particle Size of Silica Filler on the Modulus of Polymer Composites.....	153
5.8	Effect of Work of Adhesion, Volume Fraction and Particle Size of Silica Filler on the Tensile Strength of Polymer Composites.....	157
5.9	Effect of Frequency and Surface Properties of Silica on the Shear Modulus of 5% Volume Cab-O-Sil Filled E-Va Copolymer.....	161
5.10	Relative Shear Storage Modulus versus Frequency of Various Surface Properties of 5% Volume Cab-O-Sil Filled Copolymer.....	162
5.11	Effect of Frequency and Surface Properties of Silica on the Shear Modulus of 20% Volume Stöber Silica Filled Copolymer.....	164
5.12	Effect of Frequency and Surface Properties of Silica on the Shear Modulus of 15% Volume Stöber Silica Filled Copolymer.....	165

5.13	Effect of Frequency and Surface Properties of Silica on the Shear Modulus of 10% Volume Stöber Silica Filled Copolymer.....	166
5.14	Effect of Frequency and Surface Properties of Silica on the Shear Modulus of 5% Volume Stöber Silica Filled Copolymer.....	167
5.15	Relative Shear Modulus versus Frequency of Various Surface Properties of 20% Volume Stöber Silica Filled Copolymer.....	168
5.16	Relative Shear Modulus versus Frequency of Various Surface Properties of 15% Volume Stöber Silica Filled Copolymer.....	169
5.17	Relative Shear Modulus versus Frequency of Various Surface Properties of 10% Volume Stöber Silica Filled Copolymer.....	170
5.18	Relative Storage Modulus versus Frequency of Various Surface Properties of 5% Volume Stöber Silica Filled Copolymer.....	171
5.19	Effect of Work of Adhesion and Frequency on the Relative Shear Modulus of 5% Volume Cab-O-Sil Silica Filled E-Va Copolymer.....	173
5.20	Effect of Work of Adhesion and Frequency on the Relative Shear Modulus of 20% Volume Stöber Silica Filled E-Va Copolymer.....	174
5.21	Effect of Work of Adhesion and Frequency on the Relative Shear Modulus of 15% Volume Stöber Silica Filled E-Va Copolymer.....	176
5.22	Effect of Work of Adhesion and Frequency on the Relative Shear Modulus of 10% Volume Stöber Silica Filled E-Va Copolymer.....	177
5.23	Effect of Work of Adhesion and Frequency on the Relative Shear Modulus of 5% Volume Stöber Silica Filled E-Va Copolymer.....	178
5.24	Effect of Work of Adhesion and Volume Fraction on the Relative Shear Modulus of Stöber Silica Filled E-Va Copolymer Measured at 0.1 rad/sec.....	179
5.25	Effect of Work of Adhesion and Volume Fraction on the Relative Shear Modulus of Stöber Silica Filled E-Va Copolymer Measured at 1.0 rad/sec.....	180

5.26	Effect of Work of Adhesion and Volume Fraction on the Relative Shear Modulus of Stöber Silica Filled E-Va Copolymer Measured at 10 rad/sec.....	181
5.27	Effect of Volume Fraction of Stöber Silica and Frequency on the Apparent Surface Energy Barrier of Shear Modulus.....	183
5.28	Effect of Frequency on the Intercept Values in Figure 5.27.....	184
5.29	Effect of Frequency and Surface Properties of Silica on the Melt Viscosity of 5% Volume Cab-O-Sil Filled Copolymer.....	188
5.30	Relative Melt Viscosity versus Frequency of Various Surface Properties of 5% Volume Cab-O-Sil Filled Copolymer.....	189
5.31	Effect of Frequency and Surface Properties of Silica on the Melt Viscosity of 20% Volume Stöber Filled Copolymer.....	191
5.32	Effect of Frequency and Surface Properties of Silica on the Melt Viscosity of 15% Volume Stöber Filled Copolymer.....	192
5.33	Effect of Frequency and Surface Properties of Silica on the Melt Viscosity of 10% Volume Stöber Filled Copolymer.....	193
5.34	Effect of Frequency and Surface Properties of Silica on the Melt Viscosity of 5% Volume Stöber Filled Copolymer.....	194
5.35	Relative Melt Viscosity versus Frequency of Various Surface Properties of 20% Volume Stöber Filled Copolymer.....	195
5.36	Relative Melt Viscosity versus Frequency of Various Surface Properties of 15% Volume Stöber Filled Copolymer.....	196
5.37	Relative Melt Viscosity versus Frequency of Various Surface Properties of 10% Volume Stöber Filled Copolymer.....	197
5.38	Relative Melt Viscosity versus Frequency of Various Surface Properties of 5% Volume Stöber Filled Copolymer.....	198

5.39	Effect of Work of Adhesion and Frequency on the Relative Viscosity of 5% Volume Cab-O-Sil Silica Filled E-Va Copolymer.....	200
5.40	Effect of Work of Adhesion and Frequency on the Relative Viscosity of 20% Volume Stöber Silica Filled E-Va Copolymer.....	201
5.41	Effect of Work of Adhesion and Frequency on the Relative Viscosity of 15% Volume Stöber Silica Filled E-Va Copolymer.....	203
5.42	Effect of Work of Adhesion and Frequency on the Relative Viscosity of 10% Volume Stöber Silica Filled E-Va Copolymer.....	204
5.43	Effect of Work of Adhesion and Frequency on the Relative Viscosity of 5% Volume Stöber Silica Filled E-Va Copolymer.....	205
5.44	Effect of Work of Adhesion and Volume Fraction on the Relative Viscosity of Stöber Silica Filled E-Va Copolymer Measured at 0.1 rad/sec.....	206
5.45	Effect of Work of Adhesion and Volume Fraction on the Relative Viscosity of Stöber Silica Filled E-Va Copolymer Measured at 1.0 rad/sec.....	207
5.46	Effect of Work of Adhesion and Volume Fraction on the Relative Viscosity of Stöber Silica Filled E-Va Copolymer Measured at 10 rad/sec.....	208
5.47	Effect of Volume Fraction of Stöber Silica and Frequency on the Apparent Surface Energy Barrier of Melt Viscosity.....	210
5.48	Effect of Frequency on the Slope Values in Figure 5.47.....	211
5.49	Effect of Frequency and Temperature on the Melt Viscosity of Polymer Filled by 20% Stöber Silica with 110°C Treatment.....	214
5.50	Effect of Frequency and Temperature on the Melt Viscosity of Polymer Filled by 15% Stöber Silica with 500°C Treatment.....	216
5.51	Effect of Frequency and Temperature on the Melt Viscosity of Polymer Filled by 10% Stöber Silica with 500°C/TMCS Treatment.....	217

5.52	Effect of Frequency and Temperature on the Melt Viscosity of Polymer Filled by 5% Stöber Silica with 110°C Treatment.....	218
5.53	Effect of Frequency and Temperature on the Melt Viscosity of E-Va Copolymer.....	219
5.54	Effect of Environmental Testing Temperature and Solid Loading on the Melt Viscosity of Stöber Silica Filled Polymer Measured at 0.1 rad/sec.....	220
5.55	Effect of Environmental Testing Temperature and Solid Loading on the Melt Viscosity of Stöber Silica Filled Polymer Measured at 1.0 rad/sec.....	222
5.56	Effect of Environmental Testing Temperature and Solid Loading on the Melt Viscosity of Stöber Silica Filled Polymer Measured at 10 rad/sec.....	223
5.57	Effect of Frequency and Solid Loading on the Change of Melt Viscosity with Temperature.....	225
5.58	Effect of Frequency and Temperature on the Melt Viscosity of Polymer Filled by 20% Stöber Silica with 110°C Treatment.....	226
5.59	Effect of Frequency and Temperature on the Melt Viscosity of Polymer Filled by 20% Stöber Silica with 500°C Treatment.....	227
5.60	Effect of Frequency and Temperature on the Melt Viscosity of Polymer Filled by 20% Stöber Silica with 750°C Treatment.....	228
5.61	Effect of Frequency and Temperature on the Melt Viscosity of Polymer Filled by 20% Stöber Silica with 750°C/TMCS Treatment.....	229
5.62	Effect of Frequency and Temperature on the Melt Viscosity of Polymer Filled by 20% Stöber Silica with 500°C/TMCS Treatment.....	230
5.63	Effect of Frequency and Temperature on the Melt Viscosity of Polymer Filled by 20% Stöber Silica with 110°C/TMCS Treatment.....	231
5.64	Effect of Temperature and Work of Adhesion on the Melt Viscosity of 20% Volume Stöber Filled Polymer at 0.1 rad/sec.....	233

5.65	Effect of Temperature and Work of Adhesion on the Melt Viscosity of 20% Volume Stöber Filled Polymer at 1.0 rad/sec.....	234
5.66	Effect of Temperature and Work of Adhesion on the Melt Viscosity of 20% Volume Stöber Filled Polymer at 10 rad/sec.....	235
5.67	Effect of Testing Temperature on the Change of Melt Viscosity with Work of Adhesion for 20% Stöber Silica Filled Polymer at 0.1 rad/sec.....	236
5.68	Effect of Testing Temperature on the Change of Melt Viscosity with Work of Adhesion for 20% Stöber Silica Filled Polymer at 1.0 rad/sec.....	237
5.69	Effect of Testing Temperature on the Change of Melt Viscosity with Work of Adhesion for 20% Stöber Silica Filled Polymer at 10 rad/sec.....	238
5.70	SEM Micrograph of the Brittle Fracture Surface of 15% Volume Stöber Silica Particles in E-Va Copolymer Matrix. Silica Treated at 110°C.....	239
5.71	SEM Micrograph of the Brittle Fracture Surface of 15% Volume Stöber Silica Particles in E-Va Copolymer Matrix. Silica Treated by 110°C/TMCS....	241
5.72	SEM Micrograph of the Brittle Fracture Surface of 15% Volume Stöber Particles in E-Va Matrix. Silica Treated at (a) 750°C (b) 750°C/TMCS.....	244
5.73	SEM Micrograph of the Tensile Fracture Surface of 5% Volume Stöber Particles in E-Va Matrix. Silica Treated at (a) 110°C (b) 110°C/TMCS.....	246
5.74	SEM Micrograph of the Tensile Fracture Surface of 15% Volume Stöber Particles in E-Va Matrix. Silica Treated at (a) 750°C (b) 750°C/TMCS.....	247
5.75	SEM Micrograph of the Brittle Fracture Surface of 5% Volume Cab-O-Sil Silica in E-Va Matrix. Silica Treated at 110°C.....	248
5.76	SEM Micrograph of the Brittle Fracture Surface of 5% Volume Cab-O-Sil Silica in E-Va Matrix. Silica Treated by 110°C/TMCS.....	249
5.77	TEM Micrographs of 5% Volume Cab-O-Sil Silica in E-Va Matrix. Silica with Various Surface Modification. (a) 110°C (b) 500°C (c) 750°C (d) 750°C/TMCS (e) 500°C/TMCS (f) 110°C/TMCS.....	252

5.78	TEM Micrographs of 5% Volume Cab-O-Sil Silica in E-Va Matrix. Silica with Various Surface Modification at High Magnification.....	255
6.1	Schematic Representation of the Interface Model .....	257
6.2	Effect of Work of Adhesion on the Gradient of Properties of Polymer within the Interphase Layer.	259
6.3	The Change of Effective Particle Size of Silica with Frequency at Different Levels of Work of Adhesion.....	273
6.4	The Apparent Surface Energy Barrier of Polymer Flowing Through Different Surface Properties of Silica Filler Particles.....	283
8.1	DSC Spectrum of 20% Volume Stöber Silica and 5% Volume Cab-O-Sil Silica filled E-Va Copolymer.....	308
8.2	DSC Spectrum of Unfilled and 20% Volume Stöber Silica Filled E-Va Copolymer.....	309
8.3	DSC Spectrum of Unfilled and 5% Volume Cab-O-Sil Silica Filled E-Va Copolymer.....	310

Abstract of Dissertation Presented to the Graduate School  
of the University of Florida in Partial Fulfillment of the  
Requirement for the Degree of Doctor of Philosophy

QUANTITATIVE STUDIES OF THE EFFECTS  
OF INTERFACIAL BONDING STRENGTH ON THE  
MECHANICAL AND RHEOLOGICAL PROPERTIES OF POLYMER COMPOSITES

BY

SHAYE-WEN SHANG

August 1989

Chairman: Dr. Christopher D. Batich  
Major Department: Materials Science and Engineering

The aims of this study are to develop a model polymer composite system which will allow one to (1) quantify interfacial bonding, (2) relate the interfacial bonding strength quantitatively to the mechanical and rheological properties of polymer composites, and (3) interpret the interfacial bonding at a molecular level.

The interfacial bonding strength is characterized in terms of work of adhesion ( $W_a$ ). Models used to evaluate work of adhesion for strong and weak interfacial bonding are proposed. The magnitude of the work of adhesion can be controlled by modifying the surface properties of silica filler particles.

The value of  $W_a$  is increased with increasing interfacial bonding strength. The calculated  $W_a$  ranges from 63 to 301 erg  $\text{cm}^{-2}$ . The Young's modulus, tensile strength, shear modulus and melt viscosity of composites are directly proportional to the work of adhesion. The relationship is exponential. Since hydrogen and/or polar component of work of adhesion ( $W_a^h$ ) varies significantly when silica surface is modified,  $W_a^h$  is the main component in determining the performance of polymer composites.

The effects of interfacial bonding on the mechanical and rheological properties of composites are studied at different testing rates, temperatures, volume fractions of filler, and particle sizes. At a constant temperature,  $W_a$  has a greater effect on the melt viscosity of a filled polymer measured at a low frequency.  $W_a$  has little effect, however, on the change of melt viscosity with temperature at a low volume fraction of silica filled polymers.

The effective particle size of filler is increased with increasing work of adhesion. The thickness of the interphase layer around filler surface has a great effect on the performance of polymer composites. The idea of friction factors is proposed, from a molecular level, to interpret the importance of this interphase layer to control the properties of composites. The skin friction plays an important role from the flow process viewpoint.

## CHAPTER 1 INTRODUCTION

### 1.1. General

Most studies dealing with the effect of the interfacial bonding on the mechanical and rheological properties of polymer composites have been qualitative rather than quantitative (1-31). The effects of the interfacial bonding are described as leading to either good adhesion or poor adhesion. From the qualitative studies, it has been concluded that the mechanical and physical properties of particulate filled polymer composites can be improved by optimizing the interfacial bonding between the filler particles and polymer matrix (1-10). However, very few quantitative studies relate the mechanical and rheological properties of polymer composites to the interfacial bonding (15,16,30,31).

One of the reasons for this is that there is no generally accepted method to evaluate the strength of interfacial bonding. Therefore, it is important to develop a quantitative and measurable technique to evaluate the quality of the interface and relate this interface to the composite properties. The effect of interfacial bonding on the composite properties can then be systematically studied.

In general, the interactions at the filler-matrix interface can be classified into three types: (a) interactions due to intermolecular forces between the two phases, (b) chemical bonding, and (c) physical bonding or mechanical interlocking (17).

The interaction due to intermolecular forces between the filler surface and polymer matrix is a simple case of intermolecular interaction. These forces include dispersion forces (Van der Waals), hydrogen bonding, dipole-dipole, and dipole-induced dipole forces. Hydrogen bonding and/or polar forces can be evaluated by using an acid-base concept (18,19,20). A useful approach has been developed by Fowkes et al. (18,21-25), based on acid-base concepts proposed by Drago et al. (26,27).

The degree of intermolecular interaction can be determined by controlling the surface properties of filler particles through either heat or chemical treatment. The polymer composites are prepared from these well-designed filler surfaces. The mechanical and rheological properties of these polymer composites are then examined and correlated with the strength of the interfacial interaction.

### 1.2. Outline of This Study

The specific objectives of this study are to develop a model system which will allow one to (a) quantify interfacial bonding, (b) relate interfacial bonding to the

mechanical and rheological properties of filled polymers, and (c) interpret interfacial bonding at a molecular level.

The materials used in the model study are silica filler particles and ethylene-vinyl acetate (E-Va) copolymer.

This study focuses on the intermolecular interaction between two phases in which a thermodynamic approach is used to characterize the interfacial bonding. The strength of the interfacial bonding is expressed in terms of the work of adhesion ( $W_a$ ).

Work of adhesion is defined as the change in free energy when two surfaces are brought into contact. It has the same numerical value but opposite sign as the amount of work reversibly expended under equilibrium conditions to disrupt the interface. In this study, the work of adhesion is partitioned into two contributors (28,29). One contributor comes from hydrogen bonding and/or polar forces. The other comes from dispersion forces. The magnitude of work of adhesion can be varied by modifying the surface properties of the silica filler particles.

The surface silanol concentrations on the spherical silica particles can be changed by heat and/or chemical treatments. These silanol groups can form hydrogen bonds with the carbonyl groups in the polymer molecular chain. The hydrogen and/or polar contribution of work of adhesion varies significantly with the concentration of surface

silanol groups. However, the dispersion component of work of adhesion shows little change with these treatments.

The work of adhesion between the silica filler surface and the E-Va copolymer matrix is examined by combinations of measurement techniques: Fourier Transform Infrared Spectroscopy (FTIR), contact angle measurements and titration with indicator dyes.

The mechanical properties of silica filled composites are examined by an Instron tensile tester at room temperature. The rheological properties of silica filled polymer melts are measured by a Rheometrics Dynamic Spectrometer.

When the values of the work of adhesion, and the mechanical and rheological properties of silica filled polymer composites are available, the quantitative studies of the relationship between the mechanical and rheological properties of polymer composites and the strength of the interfacial bonding is then possible.

Since the hydrogen and/or polar contribution of the work of adhesion is the dominant variation in this study, it mainly determines the mechanical and physical properties of the investigated polymer composites.

The study shows that an exponential relationship exists between the work of adhesion and the mechanical and rheological properties of the composites (30,31). A mathematical model is proposed to account for the effects of

interfacial interactions on the observed properties of composites.

The effects of the interfacial bonding on the mechanical and rheological properties of composites are dependent on the materials characteristics and environmental test conditions (16,31). For example, the work of adhesion has a greater effect on rheological properties at lower testing rates (31). Volume fraction of filler and filler surface area ( $\text{m}^2/\text{g}$ ) are examples of materials characteristics of the polymer composites. Temperature and testing rate such as strain rate or frequency used to test the mechanical and rheological properties of materials are examples of environmental test conditions.

The molecular model of the microstructure around the filler particle gives insight into the nature of the interfacial bonding, and explains the effect of the bonding on the mechanical and rheological properties. The polymer around a particle is hydrogen bonds or physical entanglement by other polymers. These polymer molecules establish an interphase layer. The extent of polymer interaction with the silica surface is evaluated by FTIR spectroscopy. The thickness of the interphase layer is dependent on the work of adhesion. The effective particle size is thus increased with an increase in work of adhesion. The friction factor (32,33) in the flow process is higher when the interphase layer is thicker.

In summary, a model is proposed to evaluate the interfacial bonding strength between filler particles and the polymer matrix in terms of the work of adhesion. Quantitative studies of the effect of interfacial bonding strength on the mechanical and rheological properties of polymer composites are obtained. The observed mechanical and rheological phenomena are interpreted from the molecular level in terms of the effective particle size.

## CHAPTER 2 BACKGROUND

### 2.1 Effect of Filler Particles in a Polymer Matrix

The incorporation of filler particles in a polymer matrix can be used to improve the properties of the matrix (34). These improvements include (a) increased modulus of elasticity, (b) reduced coefficient of thermal expansion, (c) improved heat resistance, (d) higher creep resistance, (e) lower permeability behavior of gases and liquids, (f) increased mechanical strength, (g) improved rheological properties, (h) improved electrical properties, (i) increased flame retardancy, (j) improved wear resistance, (k) modified damping properties, (l) lower curing shrinkage, and (m) lower material cost.

Most of the properties discussed above are strongly dependent upon the interfacial bonding strength. It is therefore important to study the interface of the filler-matrix system (35-49) and its effect on the properties of filled polymer materials.

### 2.2 Interfacial Bonding

The interaction between a filler and polymer matrix can be basically classified into three types: (a) chemical bonding, (b) intermolecular forces, and (c) mechanical interlocking on the filler surface (17).

The Interfacial interactions may be primary or secondary forces (17,42). These interactions can be optimized by the application of a silane coupling agent to the reinforcing or filler surface. The silane improves these interactions by forming chemical bonds to both the filler surface and the matrix, or by forming interpenetrating network bonded to the filler surface (11-13,17,35-41). The primary forces, such as chemical bonds, are usually stronger. The secondary forces, such as dispersion, polar and hydrogen bonds, are generally weaker and are often due to interaction between hydroxyl groups on the filler surface and polar groups of the matrix. For mechanical interlocking, polymer wets a rough surface and flows into the interstices of the substrate, solidifies and forms a mechanical interlock (17,42-44).

### 2.2.1 Bonding and Force across an Interface

#### 2.2.1.1 Aided bonding by coupling agents

A coupling agent is defined as a chemical compound which has two differently reactive functional groups and can be used to form a link between filler surface and polymer matrix (11). One end of the coupling agent may react with the filler surface and the other end with the matrix material. Silane coupling agents are the most important coupling agents currently used in the composite industry.

The structure and utility of the silane coupling agent strongly depend upon the application method, solvent, pH, organofunctionality, concentration, drying process and temperature as well as other variables (13,35-41,45-49).

Besides the chemical bonding at the interface, silane coupling agents can also polymerize and form a polymer network on a filler surface (11). This modifies the interphase region by forming an interpenetrating network, which strengthens the organic and inorganic boundary layers. In addition to improving the mechanical and physical properties of polymer composites, silane coupling agents can also improve wetting, dispersion, rheology, and other properties (11).

These coupling agent layers are not just homogeneous thin films, but may consist of chemisorbed and physisorbed layers with a structural and compositional gradient (13). Therefore, characterization of these molecular structures and their corresponding interactions will help explain the performance of silane treated particulate filler or glass fiber filled polymer composites (35-41).

#### 2.2.1.2 Direct intermolecular interactions

The characteristics of interfacial interactions can be simplified when there are no coupling agent layers at the interface.

Various intermolecular interactions between simple molecules have been compared with the average kinetic

energy of a vibrating pair of molecules (i.e.,  $kT$  at  $25^\circ\text{C}$ ) by Hirschfelder et al. (50), where  $k$  is the Boltzmann constant, and  $T$  is the absolute temperature ( $^\circ\text{K}$ ). The value for  $kT$  at room temperature is equal to  $4.1 * 10^{-14}$  ergs (or  $0.6$  kcal/mole).

The electronic charge is shown as  $q$ , dipole moment as  $\mu$ , and polarizability as  $\alpha$ . The attraction energies can be compared based on the molecular pairs at  $r_{12} = 4 \text{ \AA}$  separation and expressed in terms of  $kT$  at  $25^\circ\text{C}$ , where 1 and 2 represent molecule 1 (or phase 1) and molecule 2 (or phase 2).

(A) Charged force in ionic molecules

(a) Point charges,  $U^{qq}$  (e.g.,  $\text{Na}^+ \text{Cl}^-$ )

$$U^{qq} = \frac{q_1 q_2}{r_{12}} \quad ( 2.1 )$$

$$= -139 \text{ kT}$$

where

$$q = 4.8 * 10^{-10} \text{ esu}$$

$$= 1.6 * 10^{-19} \text{ coulomb}$$

and 1 and 2 represent different ionic molecules in this case.

(b) Charge-Dipole,  $U^{q\mu}$  (e.g.,  $\text{Na}^+ \text{H}_2\text{O}$ )

$$U^{q\mu} = \frac{-q_1\mu_2}{r_{12}^2} \quad ( 2.2 )$$

$$= -13.2 \text{ kT}$$

where

$$\begin{aligned} \mu_2 &= 1.84 * 10^{-18} \text{ esu-cm} \\ &= 6.1 * 10^{-30} \text{ coulomb-m} \end{aligned}$$

(c) Charge-Induced dipole,  $U^{q\alpha}$  (e.g.,  $\text{Na}^+ - \text{H}_2\text{O}$ )

$$U^{q\alpha} = \frac{-q_1^2\alpha_2}{r_{12}^4} \quad ( 2.3 )$$

$$= - 3.2 \text{ kT}$$

where

$$\alpha_2 = 1.48 * 10^{-24} \text{ cm}^3$$

(B) Polar force in neutral molecules

(d) Dipole-Dipole,  $U^{\mu\mu}$  (e.g., phenol-phenol)

$$U^{\mu\mu} = \frac{-2}{3kT} \cdot \frac{\mu_1^2\mu_2^2}{r_{12}^6} \quad ( 2.4 )$$

$$= -0.42 \text{ kT}$$

(e) Dipole-Induced dipole,  $U^{\mu\alpha}$  (e.g., phenol-benzene)

$$U^{\mu\alpha} = \frac{\mu_1^2 \alpha_2}{r_{12}^6} \quad ( 2.5 )$$

$$= -0.13 \text{ kT}$$

(f) Acid-Base interactions (26,51),  $U^{AB}$  (including Hydrogen bonds) (e.g., phenol-benzene)

$$U^{AB} = - ( C_A C_B + E_A E_B ) \quad ( 2.6 )$$

$$= -4.04 \text{ kT [ includes } U^{\mu\alpha} \text{ and } U^{\mu\mu} \text{ ]}$$

(C) Non-polar force in neutral molecules

(g) Dispersion forces,  $U^d$  (e.g., benzene-benzene)

$$U^d = \frac{-3}{4} \cdot \frac{\alpha^2 h \nu^\circ}{r_{12}^6} \quad ( 2.7 )$$

$$= -7.8 \text{ kT}$$

where

$$\nu^\circ = 2.54 * 10^{15} \text{ sec}^{-1}$$

$$h = 6.62 * 10^{-27} \text{ erg-sec}$$

The interactions between molecules usually include several of these interactions at once. The hydrogen and/or polar interactions in a neutral system which are due to intermolecular forces between a filler surface and a polymer matrix can be calculated using an acid-base concept (18,19,20) or adsorption theory (52,53). The extent of intermolecular interactions can be determined by the surface properties of each phase.

Polymer molecules may be bonded and/or adsorbed to the filler surface after the polymer wets its surface. In the neutral system, primary forces usually do not occur if there is no chemical bonding at the interface. Thus, secondary forces, such as the dispersion force, the dipole-dipole force, the dipole-induced dipole force, and hydrogen bonding, may be the main components in the neutral system which contribute to the intermolecular forces at the interface (41,54,55).

Hydrogen bonds are formed between proton acceptors and hydrogen atoms where the latter are attached to highly electronegative atoms or groups. The energy of hydrogen bonding depends upon the strength of the hydrogen bonds (56). In the case of shorter bond length (2.5 Å or less), the covalent character may be as much as 25%. However, for longer bond length (2.8 Å or greater), the covalent character may be negligible.

It is reported that the bond energy of the primary forces is more than 25 kcal/mole, while the bond energy of the secondary force is below 12 kcal/mole (42,57), as shown in Table 2.1.

TABLE 2.1

BOND TYPES AND TYPICAL BOND ENERGY (Kcal/Mole)<sup>41</sup>

<u>TYPE</u>	<u>BOND ENERGY</u>
Chemical bonds	(kcal/mole)
ionic	140-250
covalent	15-170
metallic	27-83
Intermolecular force	
hydrogen bonds	≤ 12
dipole-dipole	≤ 5.0
dispersion	≤ 10
dipole-induced dipole	≤ 0.5

---

The range of magnitude of the dispersion force, in Table 2.1, is for the interaction of small molecules, or in the case of extended molecular polymers, the interaction of segments, e.g., of a —CH<sub>2</sub>— group in one molecule with a —CH<sub>2</sub>— group in a neighboring molecule (41).

It has been reported that the attraction force between two planar bulk phases due solely to dispersion forces at a separation of 1 Å is approximately 100 MPa (58-60).

Although there is evidence (61-63) that adhesion arising from the secondary forces alone may provide adequate interfacial interaction for bond strength in composite systems, many investigators believe that the primary bonding will increase the bond strength and is a requirement for obtaining an interface which is environmentally stable.

### 2.2.2 Ways to Characterize Forces at the Interface

#### 2.2.2.1 Work of adhesion and wetting

The process of interfacial interaction involves (a) wetting and (b) adsorption of polymer on the surface of filler particles.

Wetting is necessary before a direct intermolecular interaction between any two phases can occur. A polymer able to wet the filler surface can increase the intermolecular contact and therefore improve the polymer adsorption and bonding. Incomplete wetting will produce interfacial defects and thereby lower the adhesive bond strength. The work of adhesion ( $W_a$ ) was stated by Dupré (64) as

$$W_a = \tau_l + \tau_s - \tau_{ls} \quad ( 2.8 )$$

where  $W_a$  is the thermodynamic work of adhesion of a liquid to a solid, and is expressed as the sum of the surface free energies of the liquid ( $\tau_l$ ) and solid ( $\tau_s$ ) minus that of the interface ( $\tau_{ls}$ ).

Equation ( 2.8 ) has been applied to the spreading of a liquid on a solid surface. When a drop of liquid is placed on the surface of a solid, the liquid may spread. If it does, the surface of the solid disappears, and is replaced by an equal area of interface and the liquid, provided that liquid spreads to a film. The change of surface free energy is defined as the spreading coefficient (65-67), which is expressed by S,

$$S = \tau_s - ( \tau_l + \tau_{sl} ) \quad ( 2.9 )$$

Since a liquid will not spread on a solid surface unless  $\tau_s$  is greater than  $\tau_l + \tau_{sl}$ , a positive spreading coefficient is required for spreading to occur.

As shown in Figure 2.1, when a drop does not spread on a solid surface, the contact angle of a liquid drop on a solid surface follows Young's equation, expressed as follows

$$\tau_{sv} = \tau_{sl} + \tau_{lv} \cos \theta \quad ( 2.10 )$$

$$\tau_{sv} = \tau_s - \pi_e \quad ( 2.11 )$$

where  $\pi_e$  in equation ( 2.11 ) is the equilibrium film pressure and reflects the reduction in surface energy of the solid due to adsorbed vapor. Note that  $\pi_e$  is very small on polymer surfaces and can be normally neglected.

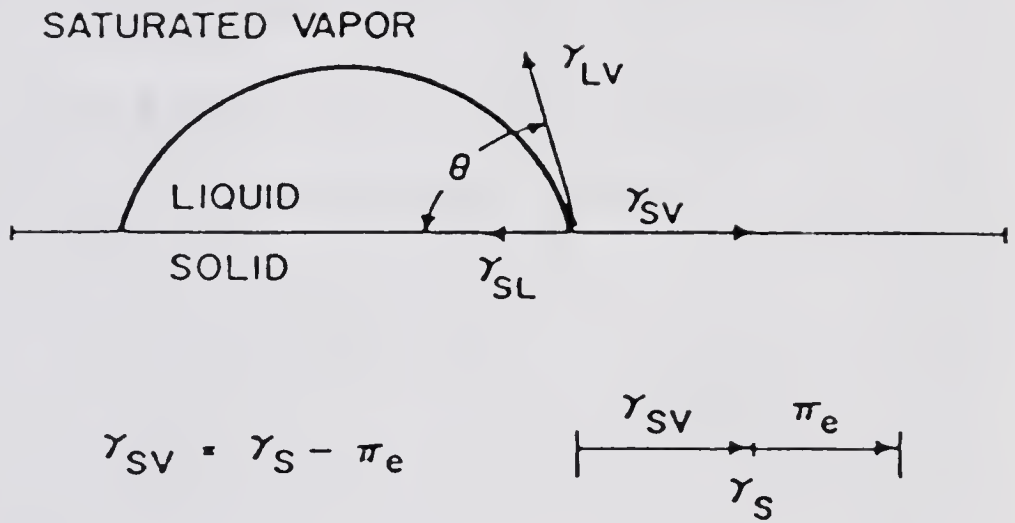


Figure 2.1 Relationship between Contact Angle and Silica Surface

Combining equations ( 2.8 ), ( 2.10 ) and ( 2.11 ) gives the well-known Young-Dupre' equation

$$\begin{aligned} W_a &= \tau_l + \tau_s - \tau_{ls} \\ &= \tau_{lv} (1 + \cos \theta) + \pi_e \end{aligned} \quad ( 2.12 )$$

This is the equation to express the work of adhesion for a liquid on a solid surface.

#### 2.2.2.2 Relationship between work of adhesion and force attraction constant

Summation of various energies across an interface in a neutral force system gives the total attraction energy, ( $U_{12}$ ), expressed as

$$U_{12} = U_{12}^d + U_{12}^{p^*} + U_{12}^i + U_{12}^h = \frac{-A_{12}}{r^6} \quad ( 2.13 )$$

where 1 and 2 represent phase 1 and phase 2. The  $A_{12}$  is the total attraction constant, and relates to the summation of forces across an interface discussed in section 2.2.1.2, and given by

$$A_{12} = A_{12}^d + A_{12}^{p^*} + A_{12}^i + A_{12}^h \quad ( 2.14 )$$

In equation ( 2.14 ),  $A_{12}^d$  is the attraction constant for dispersion interaction (68-70),  $A_{12}^{p^*}$  the attraction

constant for dipole interaction (71,72),  $A_{12}^i$  the attraction constant for induction (also called dipole-induced dipole) interaction (73,74), and  $A_{12}^h$  the attraction constant for hydrogen bonding (75).

The polar component (p) consists of dipole(p\*), induction (i), and hydrogen bonding (h) interaction.

Since

$$A_{12}^p = A_{12}^{p*} + A_{12}^i + A_{12}^h \quad ( 2.15 )$$

equation ( 2.14 ) can be simplified to

$$A_{12} = A_{12}^d + A_{12}^p \quad ( 2.16 )$$

Analogously, the surface free energy and work of adhesion can be separated into two components, a dispersion component and a polar component (28,29), where

$$\tau = \tau^d + \tau^p \quad ( 2.17 )$$

$$W_a = W_a^d + W_a^p \quad ( 2.18 )$$

### 2.2.2.3 Work of adhesion and surface energy

Several means of relating the work of adhesion and surface energy are discussed below.

### 2.2.2.3.1 Harmonic-mean approach

The  $Wa^d$  can be related to surface energy by

$$Wa^d = \frac{4\tau_1^d \tau_2^d}{\tau_1^d + \tau_2^d} \quad ( 2.19 )$$

which is called the harmonic-mean approximation, and is preferred between low-energy materials (76,77).

Similarly, the  $Wa^p$  can also be approached by the following harmonic-mean approximation (76,77).

$$Wa^p = \frac{4\tau_1^p \tau_2^p}{\tau_1^p + \tau_2^p} \quad ( 2.20 )$$

which adequately represents the combined polar interactions (p\*, i and h) in most cases and is valid for low-energy materials.

### 2.2.2.3.2 Geometric-mean approach

On the other hand, the geometric-mean relation, valid when the interaction is between a low-energy and a high-energy material, may be used as follows (76-78),

$$Wa^d = 2 ( \tau_1^d \tau_2^d )^{1/2} \quad ( 2.21 )$$

Using the appropriate approximations for the various polar attraction constants between a low-energy and a high-energy material gives

$$\begin{aligned}
 Wa^P &= Wa^{P^*} + Wa^i + Wa^h \\
 &= 2 ( \tau_1^{P^*} \tau_2^{P^*} )^{1/2} + ( \tau_1^i + \tau_2^i ) + \\
 &\quad ( \tau_1^{ha} \tau_2^{hd} + \tau_1^{hd} \tau_2^{ha} ) \quad ( 2.22 )
 \end{aligned}$$

which is the complete polar component of work of adhesion. The  $\tau^{ha}$  is the hydrogen-bond acceptor component, and  $\tau^{hd}$  is the hydrogen-bond donor component.

Several special cases deserve attention here (79):

(a) If the dipole-dipole interaction is predominant, then

$$Wa^P = 2 ( \tau_1^{P^*} \tau_2^{P^*} )^{1/2} \quad ( 2.23 )$$

(b) If the dipole-induced dipole interaction is predominant, then

$$Wa^P = \tau_1^i + \tau_2^i \quad ( 2.24 )$$

(c) If the hydrogen-bond interaction is predominant, then

$$Wa^P = \tau_1^{ha} \tau_2^{hd} + \tau_1^{hd} \tau_2^{ha} \quad ( 2.25 )$$

#### 2.2.2.4 Surface energy

##### 2.2.2.4.1 Surface energy and contact angle

A contact angle can be obtained when a drop of liquid is on a solid surface. The  $\tau^d$  and  $\tau^P$  could be calculated

from contact angles according to Owens and Wendt (80). They proposed a set of simultaneous equations to calculate  $\tau^d$  and  $\tau^p$  by measuring the contact angles of two various liquids against a solid as follows

$$1 + \cos \theta = 2\sqrt{\tau_s^d} \left( \frac{\sqrt{\tau_l^d}}{\tau_l} \right) + 2\sqrt{\tau_s^p} \left( \frac{\sqrt{\tau_l^p}}{\tau_l} \right) \quad ( 2.26 )$$

where  $\theta$  is the contact angle,  $l$  refers to the liquid and  $s$  refers to the solid. The  $\tau_s^d$  is the dispersion component of the surface energy of the solid, and  $\tau_s^p$  is the polar component of the surface energy of the solid. The surface energy of a solid is given by the summation of each component:  $\tau_s = \tau_s^d + \tau_s^p$ . The  $\tau_l$  and its components refer to the surface energy of the liquid used to measure the contact angle on the surface of a solid plate. The surface free energy of the polymer is dependent on the surface properties of the polymer. Using X-ray photoelectron spectroscopy (ESCA), Batich and Wendt (81) studied chemical labels to distinguish surface functional groups. The surface chemistry is usually dominated by the number and types of functional groups present on the surface. When the surface properties of a polymer are determined, the surface energy can then be evaluated.

#### 2.2.2.4.2 Surface energy and cohesive energy density

The cohesive energy density ( $\delta^2$ ) has been defined (82) as

$$\delta^2 = - ( \Delta U^{\text{vap}} / V^{\text{l}} ) \quad ( 2.27 )$$

where  $\Delta U^{\text{vap}}$  is the molar internal energy of vaporization, which means the energy change upon isothermal vaporization of the saturated liquid to the ideal gas state, and  $V^{\text{l}}$  is the molar volume of liquid.

A more useful definition is

$$\delta^2 = ( \Delta H^{\text{vap}} - RT ) / V^{\text{l}} \quad ( 2.28 )$$

where  $\Delta H^{\text{vap}}$  is the heat of vaporization,  $R$  is the gas constant and  $T$  is the absolute temperature.

An equation connecting surface free energy with molar volume and cohesive energy density was proposed by Hildebrand and Scott (82,83) as

$$\delta^2 = \Gamma^2 ( \tau / V^{0.33} )^{0.86} \quad ( 2.29 )$$

where  $\Gamma$  is a temperature dependent constant. This constant is fairly accurate for non-polar liquids, but when applied to polar liquids and polymers the limitations of equation ( 2.29 ) are revealed. An extended equation can be used for polymers, as demonstrated by Wu (84). However, it is

only applied to non-polar polymers since Wu's equation considers only the dispersion contribution of surface energy. Wu's equation is stated as

$$\tau = 0.327 [ (\Sigma F)_s / n_s ]^{1.85} [ n_s / V_s ]^{1.52} \quad ( 2.30 )$$

where  $(\Sigma F)_s$  is the summation of the Small force constants (85) for the segments,  $n_s$  is the number of atoms and  $V_s$  is the molar volume of the repeat unit.

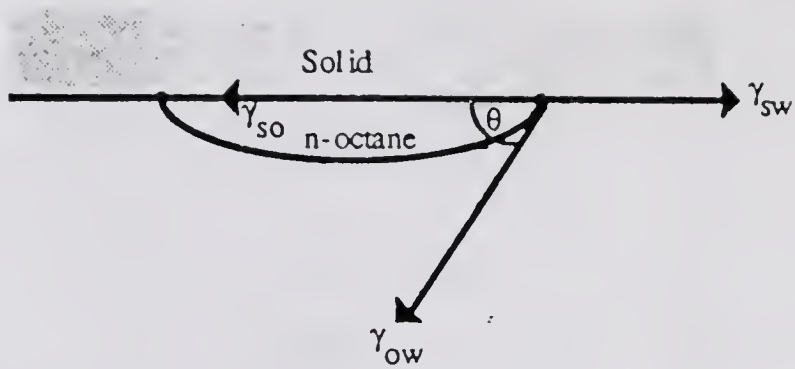
#### 2.2.2.4.3 Hamilton methods

Hamilton has developed a technique to characterize a hydrated solid surface (86,87). By measuring the contact angle of a small n-octane droplet on a solid surface under water, as shown in Figure 2.2, and assuming that the effect of gravity is negligible for such a small droplet, the polar component of the surface free energy can be determined.

An equation for the work of adhesion at a solid liquid interface has been developed by Fowkes (88) which assumes that there is no polar interaction across the interface. This equation is expressed as

$$\tau_{sl} = \tau_s + \tau_{lv} - 2( \tau_{lv}^d \tau_s^d )^{0.5} \quad ( 2.31 )$$

Although this equation contains a term  $[ 2( \tau_{lv}^d \tau_s^d )^{0.5} ]$ , which accounts for the dispersion forces, there is no term

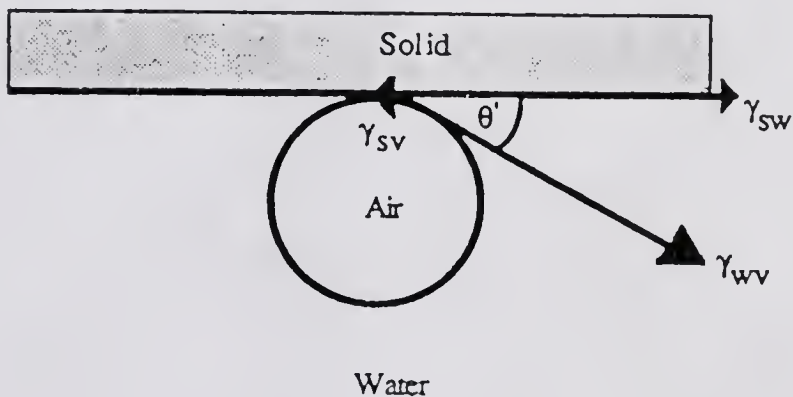


$\gamma_{sw}$  = solid - water interfacial free energy

$\gamma_{so}$  = solid - octane interfacial free energy

$\gamma_{ow}$  = octane - water interfacial free energy

Figure 2.2 Components of Surface Free Energy for the Hamilton Technique



$\gamma_{sw}$  = solid - water interfacial free energy

$\gamma_{wv}$  = water - vapour interfacial free energy (ie surface tension of water)

$\gamma_{sv}$  = solid - vapour interfacial free energy  $\approx \gamma_s$  = solid surface free energy

Figure 2.3 Components of Surface Free Energy for the Air Bubble Technique

to account for the dipole interaction and hydrogen bonding. A modified form of this expression was developed by Tamai et al. (89) which accounted for polar forces. This equation is written as

$$\tau_{sl} = \tau_s + \tau_{lv} - 2( \tau_{lv}^d \tau_s^d )^{0.5} - I_{sl} \quad ( 2.32 )$$

where

$$I_{sl} = 2( \tau_{lv}^p \tau_s^p )^{0.5} \quad ( 2.33 )$$

As n-octane has no polar components, and the dispersion components of n-octane and water ( $\tau_{lv}^d = 21.8$  dyne/cm) are identical, the combination of Young's equation (Eq. 2.10) and Tamai's equations (Eq. 2.32 and 2.33) leads to the determination of the polar component of the surface free energy of a solid surface.

The relationship between Hamilton's contact angle and the polar component of surface free energy has been shown (90-92); it is known that as the contact angle becomes larger,  $\tau_s^p$  also increases.

#### 2.2.2.4.4. Captive air bubble technique

The captive air bubble technique (93,94) uses air bubbles resting on a plane solid surface, as shown in Figure 2.3. This is similar to the Hamilton technique where liquid drops are used. Combining both the Hamilton and the captive air bubble technique, it is possible to

obtain values for  $\tau_s$ ,  $\tau_s^d$ ,  $\tau_s^p$  and  $r_{sl}$  for the solid-liquid interface.

#### 2.2.2.5 Work of adhesion and acid-base interaction

Drago and co-workers (26,27) have related enthalpy changes of acid-base interactions ( $\Delta H^{ab}$ ) in neutral solvents to the acidity and basicity of organic molecules. Drago (26,27,51) expressed the acid-base interaction  $\Delta H^{ab}$  with two constants for each base and acid ( $E_B$  and  $C_B$ , and  $E_A$  and  $C_A$ , respectively) as

$$-\Delta H^{ab} = C_A C_B + E_A E_B \quad ( 2.34 )$$

The two constants, C and E, for both the acid and the base reflect the idea that the strength of interaction of a pair of groups depends not only on the donor/acceptor characteristics, but also on the polarizability, where E is used to refer to the donor/acceptor characteristics, and C to the polarizability.

The ratio C/E is a measure of the relative ease of deforming outer electron orbitals by an electric field. The greater C/E, the "softer" the acid or base (25). Thus, the iodine and Bronsted acids behave as soft and hard acids, respectively, while sulfur and oxygen behave as soft and hard bases, respectively.

It is believed that maximum interaction occurs between soft acids and soft bases, or hard acids and hard bases

(25). Drago et al. were able to accurately predict values of  $\Delta H^{ab}$  for many systems involving hydrogen bonds and Bronsted and Lewis acids and bases (25). In addition, Drago et al. found a most interesting result: good correlations could be made by assuming the existence of only dispersion and acid-base interactions (the contribution of dipole-dipole interactions is usually very small or negligible).

Fowkes (21,22) has suggested that acid-base interaction across an interface may contribute to intrinsic adhesion forces. Fowkes (23) further postulated that hydrogen bonds across an interface can be considered as a subset of acid-base interactions and that the other polar (dipole-dipole or dipole-induced dipole) interactions are negligibly small in liquids and solids and can be ignored.

The dipole-dipole interaction, as measured by dipole moments, is not a significant factor in intermolecular interactions in solids and liquids (23). This is due to the fact that in condensed media, where equal sized molecules have ten or more nearest neighbors, conflicting local dipole fields are present which minimize dipole interactions. Due to the existence of conflicting local dipole fields, the dipole-induced dipole interaction is even smaller than dipole-dipole interaction.

Drago has developed a correlation of  $\Delta H^{ab}$ , the acid-base interaction energy, with the FTIR spectroscopic shifts

of the OH stretching frequency of dilute solution of phenol when interacting with a variety of bases in carbon tetrachloride (24,28). This is written as

$$\Delta H^{ab} = [ 3.08 + 0.0103 \Delta \nu_{OH} ( \text{cm}^{-1} ) ] \text{ kcal/mole} \quad ( 2.35 )$$

Fowkes studied the carbonyl polar group and found that the shift in the carbonyl stretching frequency,  $\Delta \nu_{C=O}$ , of esters correlates very well with the calorimetric acid-base interaction energy,  $\Delta H^{ab}$ , of these esters with acids such as chloroform and iodine (28,95).

$$\begin{aligned} \Delta H^{ab} &= 1.0 \Delta \nu_{C=O} ( \text{cm}^{-1} ) \text{ kJ/mole} \\ &= 0.236 \Delta \nu_{C=O} ( \text{cm}^{-1} ) \text{ kcal/mole} \quad ( 2.36 ) \end{aligned}$$

In general, without the involvement of the primary forces at an interface, the interactions of two phases involve some combinations of dispersion forces (or London forces), dipole-dipole forces, and specific interactions such as proton transfer in acid-base reactions (or hydrogen bonding). However, hydrogen bonding is the dominant factor controlling the interfacial adhesion in a condensed system.

### 2.3 Quantitative Evaluation of Interfacial Bonding Strength of Polymer Composites

There is no generally accepted method to quantitatively evaluate each individual type of interfacial bonding strength.

Chahal and St. Pierre (15,16) have proposed a technique to evaluate the interfacial bonding strength by an indirect approach. They described methods of changing the interfacial interaction energy of silica filler. The modification of the silica filler surface was accomplished by treating it with normal alcohols in the vapor phase (15). They also correlated changes in the interfacial interaction energy with the extent and nature of the alcohol coverage. The energy of interfacial interaction was expressed in terms of heat of adsorption of a model compound, octamethylcyclotetrasiloxane, on silica surface (15). The modified silica was then incorporated with polydimethylsiloxane polymer to study the effect of interfacial bonding strength on the mechanical properties of these polymer composites. When studied at a constant filler concentration, the relaxation modulus of uncrosslinked composites is an exponential function of the net heat of adsorption of octamethylcyclotetrasiloxane on the filler surface.

Schreiber et al. (96,97) first used inverse gas chromatography (IGC) as a technique for acid-base analysis. The interactions of a series of acidic, neutral and basic solvents with polyethylene (PE), polyvinylchloride (PVC) and plasma treated and untreated calcium carbonate ( $\text{CaCO}_3$ ) were measured.

By measuring the retention volume ( $V_g$ ) between a particular solvent and polymer or filler, the acid or base strength of the polymer or the filler can be determined (96). In order to compare acid and base strengths directly, Schreiber et al. (96,97) suggested an empirical comparison of these retention volumes using

$$\Omega = (V_g^\circ)_{\text{acid}} / (V_g^\circ)_{\text{base}} \quad (2.37)$$

where  $\Omega$  is a normalized acid/base interaction parameter.  $(V_g^\circ)_{\text{acid}}$  and  $(V_g^\circ)_{\text{base}}$  are the retention volumes for the acidic and basic probes respectively. Higher interaction gives a higher value of retention volume. The definition of this dimensionless parameter  $\Omega$  is arbitrary and based solely on experimental convenience. Values of  $\Omega < 1$  would be acidic and  $\Omega > 1$  would be basic.

Schreiber (96,97) suggested that the difference of  $\Omega_p - \Omega_f$  (the subscripts refer to polymer and filler, respectively) can be used as an index of the interaction strength between polymer and filler.

Using a thermodynamic approach, Williams and Shang (30,31) have proposed a set of techniques, based on surface energy and Fowkes's equation (24,28), to evaluate the interfacial bonding strength between filler surface and polymer matrix. The interfacial bonding strength is characterized in terms of work of adhesion ( $W_a$ ), which

mainly comes from two components, a dispersion component ( $W_a^d$ ) and a hydrogen bonding and/or polar component ( $W_a^p$ ). The value of work of adhesion can be evaluated by  $W_a = W_a^d + W_a^p$ , as shown in equation ( 2.18 ).

Williams and Shang modified the silica surface by heat and/or chemical treatments. The surface modified silica fillers were mixed with a polymer. Two different models were used to evaluate the work of adhesion for good and poor interfacial interaction, respectively.

When the quantitative value of interfacial bonding strength is available, it provide a quantitative tool to study the effect of adhesion on the mechanical and rheological properties of a filled polymer composite (15,16,30,31).

#### 2.4 Mechanical Properties of a Particulate Filled Polymer Composite

The mechanical properties of particulate filled polymers are dependent on many factors (34,98-102). Some of the materials characteristics influencing the mechanical properties are listed as follows: (a) particle size, (b) particle size distribution, (c) particle shape and its length-width aspect ratio, (d) volume fraction of filler particle, (e) elastic moduli of filler particles and polymer matrix, (f) adhesion bond between the two phases, (g) dispersion of filler particles in the polymer matrix, and (h) degree of particle agglomeration.

Unfortunately, these factors make the composite system very complex, and it is difficult to separate and evaluate individual variables.

However, when uniform spherical silica particles of narrow size distribution are used as filler particles in the polymer matrix, the effects of particle shape, size and size distribution can be excluded in determining the behavior of particulate filled polymers.

In many practical applications, the individual filler particles are not separated from one another and wetted individually by the matrix phase, especially the very fine filler particles. Instead, the filler particles are often agglomerates made up of many small particles. Thus, the individual effect of either interfacial adhesion, dispersion or particle agglomeration on the performance of the composite is not clearly known. This is due to the fact that there is no technology or instrument available currently which allows proper separation and evaluation of the individual variables in most experimental works (102-104). Nevertheless, the dispersion and particle agglomeration are more or less dependent on the interfacial bonding (102-104).

For a given polymer matrix, the surface properties of filler particles are the most important variables to affect the interfacial bonding, dispersion and particle agglomeration. Thus, surface modification of filler

particles by either heat or chemical treatment becomes very important in the field of polymer composites.

#### 2.4.1 Effect of Properties of Interface/Interphase on a Polymer Composite

Coupling agents such as silanes or titanates have long been used to modify the interfacial bonding and improve the mechanical properties of composites (11,36). Attention has also been given to the use of a polymeric interlayer between a reinforcing fiber or a filler particle and matrix to improve these properties (105-110).

For example, it has been claimed that a relatively soft interlayer provides a useful balance between stiffness and toughness in composite systems (105-108). A controlled crystalline morphology at the interface may also improve composite properties (109,110). The degree of dispersion of filler particles in the polymer matrix can be related to the acid-base interaction of the polymer-filler pair. This dispersion may vary widely with the surface treatments given to the filler (96). The mechanical properties at large deformations of the filled polymers, and their durability under different conditions, may also depend on the acid-base interaction (14,96).

With well bonded high modulus inclusions in the polymer matrix, the modulus, and sometimes the tensile strength and fracture energy, are increased (102,111). To obtain a combination of some specific properties, a proper balance

of the modulus of the interphase can be achieved by a deliberately developed interphase (105-110). When a composite with this well-controlled interphase is under large scale deformation, the interfacial bonding strength and interphase layer can change the balance between shearing and crazing (102,112).

It is often implied that "good" adhesion is generally to be desired. This is usually true for tensile strength and modulus in the filled polymer systems (1,16,30,31). However, the role of the adhesion on other properties and systems is more complex. For example, in many composites, maximum fracture energy, impact strength and fatigue resistance may actually require poor or moderate adhesion (1,113-115).

Thermodynamic and kinetic aspects must be considered for the interfacial bonding. Even though thermodynamics may favor a particular equilibrium state, and hence a particular set of properties, the nature of the interphase will depend on the history of the system, that is, on the conditions of film formation or solidification from melt (25,36,116-119). For example, the  $T_g$  of silica filled polystyrene composites was lower than the matrix when first formed, but became higher on annealing (118). Presumably the original interphase was not at equilibrium, and was relatively mobile, while subsequent annealing resulted in equilibrium with a less mobile conformation.

In another example, the blending of a matrix with a densely grafted filler which was compatible with the matrix led to poor strength (120). This was evidently because crowding at the filler surface inhibited interdiffusion with the matrix by creating an unfavorable entropy of mixing.

In general, the required strength of interfacial bonding in a composite system for a particular application is dependent the mode of applied stress and the failure mechanism.

#### 2.4.2 Effect of Volume Fraction and Particle Size on the Modulus of a Composite

Many models and equations have been derived to describe the Young's modulus of a filled glassy polymer (100-102, 121-130). In the simplest possible case, two bounds have been predicted for a composite elastic modulus  $E_c$  (102).

These are:

(a) Case of equal strains

$$\text{Upper bound: } E_c = V_p E_p + V_f E_f \quad ( 2.38 )$$

(b) Case of equal stresses

$$\text{Lower bound: } E_c = \frac{E_p E_f}{E_p V_f + E_f V_p} \quad ( 2.39 )$$

where  $E_c$ ,  $E_p$  and  $E_f$  are moduli of composite, polymer and filler, respectively.  $V_p$  and  $V_f$  are the volume fraction of polymer and filler, respectively.

On the other hand, the Kerner equation (131) is especially useful in predicting the modulus of the composite of spherical fillers being randomly dispersed in a glassy (not elastomeric) matrix. This equation assumes good adhesion between the phases and is expressed as

$$\frac{E_c}{E_p} = \frac{G_c}{G_p}$$

$$= \frac{\{G_f V_f / [(7-5\epsilon)G_p + (8-10\epsilon)G_f]\} + \{V_p / [15(1-\epsilon)]\}}{\{G_p V_f / [(7-5\epsilon)G_p + (8-10\epsilon)G_f]\} + \{V_p / [15(1-\epsilon)]\}}$$

( 2.40 )

where  $E_c$  and  $E_p$  are the Young's moduli of the composite and polymeric matrix, respectively;  $G_p$  and  $G_f$  are the shear moduli of the polymer and filler;  $\epsilon$  is Poisson's ratio of the polymer; and  $V_f$  and  $V_p$  are the volume fraction of filler and polymer, respectively.

Halpin and Tsai (132-134) have shown that the Kerner equation and many other equations for moduli can be put in a more general form. Lewis and Nielsen (98,99) showed that the equation can be generalized to

$$\frac{M_c}{M_p} = \frac{1 + ABV_f}{1 - B\phi V_f}$$

( 2.41 )

where  $M_c$  is any modulus — shear, Young's, or bulk. The constant A takes into account such factors as geometry of the filler phase and Poisson's ratio of the matrix. The constant B takes into account the relative moduli of filler and matrix phases; its value is 1.0 for very large  $M_f/M_p$  ratios. The quantity B is defined as

$$B = \frac{M_f/M_p - 1}{M_f/M_p + A} \quad ( 2.42 )$$

The factor  $\phi$  depends upon the maximum packing fraction  $\Phi_m$  of the filler. Two empirical functions which fulfill the necessary boundary conditions are

$$\phi = 1 + [ ( 1 - \Phi_m ) / \Phi_m^2 ] V_f \quad ( 2.43 )$$

$$\phi V_f = 1 - \exp \frac{1 - V_f}{1 - ( V_f / \Phi_m )} \quad ( 2.44 )$$

The quantity  $\phi V_f$  can be visualized as a reduced volume fraction. For  $\Phi_m = 1$ ,  $\phi = 1$ . The reduced concentration  $\phi V_f$  is a function of the concentration  $v_f$ .

The constant A is related to the generalized Einstein coefficient  $K_E$  by

$$A = K_E - 1 \quad ( 2.45 )$$

Einstein (125,126) pointed out that  $K_E = 2.5$  for a suspension of rigid spheres in a liquid with a Poisson's ratio of 0.5 when the type of deformation is shear. In general, for the case of the shear modulus with spherical fillers, the value of A for any Poisson's ratio of the matrix is

$$A = \frac{7 - 5 \epsilon}{8 - 10 \epsilon} \quad ( 2.46 )$$

For composites filled with particles of nearly spherical shape, the shear modulus, according to the modified Kerner's equation is given by

$$\frac{G_c}{G_p} = \frac{1 + ABV_f}{1 - B\phi V_f} \quad ( 2.47 )$$

where A can be evaluated by equation ( 2.46 ), and B by the modification of equation ( 2.42 ). Thus, B becomes

$$B = \frac{G_f/G_p - 1}{G_f/G_p + A} \quad ( 2.48 )$$

Most of these models or equations consider glassy continuous thermoplastic materials, and that Young's

modulus of filled polymers should not depend on the particle size, but only on the volume fraction of filler. However, as appears from experiments, the Young's modulus of a filled polymer is dependent on both volume fraction and filler particle size (121). Vollenberg et al. showed that the Young's modulus of bead filled polymer composites tended to be higher when particle size, in the same micro order, of the filler was increased (121).

Sumita et al. (122) studied spherical fine silica particles of various diameters (70, 160 and 400 Å and 35  $\mu\text{m}$ ) mixed with low density polyethylene (LDPE). The oriented silica filled composites were made by neck drawing. The Young's moduli of these oriented composites, filled with relatively small particles (70, 160 and 400 Å), increased when the filler content was increased or when the particle size was decreased; whereas the modulus of composites with the 35  $\mu\text{m}$  silica particle decreased with an increase in filler content. These results showed that extremely small particles comparable to the spherulite size of the LDPE in the crystalline region exerted considerable reinforcing effect on the oriented polymer matrix (122).

However, Kerner's and related equations are not suitable for quantitative predictions of moduli of particulate filled rubbery composites. Eiler's equation has frequently been used to describe the behavior of filled elastomeric systems (135). This equation is stated as

$$G_c/G_p = [ 1 + 1.25V_f / ( 1 - V_f/\Phi_m ) ]^2 \quad ( 2.49 )$$

where  $G_c/G_p$  is the relative modulus of the composite to polymer, and  $V_f$  and  $\Phi_m$  are the volume fraction of filler and maximum packing fraction, respectively (136).

The increase in modulus of a filled rubbery polymer may also be expressed in terms of the Mooney (137) or Guth-Smallwood (123,124) equations. For example, with glass bead filled epoxy resins, Lewis and Nielsen (99) found agreement between predicted and observed values of modulus in the rubbery region by using the Mooney (137) equation,

$$\ln ( G_c/G_p ) = K_E V_f / [ 1 - ( V_f/\Phi_m ) ] \quad ( 2.50 )$$

where  $K_E$  is the Einstein coefficient, which is equal to 2.5 for dispersed spheres. Guth (123) and Smallwood (124) developed a widely employed modulus equation expressing the shear modulus of the filled rubber directly in terms of filler concentration. The equation is based on the famous viscosity equation of Einstein (125,126). The Guth-Smallwood equation is given as

$$G_c = G_p ( 1 + 2.5V_f + 14.1 V_f^2 ) \quad ( 2.51 )$$

Generally speaking, the Guth-Smallwood equation correctly predicts the relatively modest increase in modulus developed by the addition of inactive or non-reinforcement fillers whose size is in micro or submicro order, but this equation has been found relatively unsatisfactory for highly reinforced systems where large positive deviations occur (102).

#### 2.4.3 Effect of Volume Fraction and Particle Size on the Tensile Strength of a Composite

Rigid particulate fillers always increase the modulus of a polymer matrix, but these fillers generally cause a dramatic decrease in elongation to break. Fillers also often decrease the tensile strength of a material; however, there are numerous exceptions to this tendency, especially with respect to fine filler particles such as carbon black in rubber (127).

The decrease in elongation to break in a rigid particulate filled composites comes from the fact that the actual elongation experienced by the polymer matrix is much greater than the measured elongation of the composite specimen. Since the specimen consists partly of filler and partly of matrix, most of the elongation comes from the polymer if the filler is much more rigid than the matrix.

When the adhesion at the interface is perfect, and the fracture path tends to go from particle to particle rather

than giving a perfectly smooth fracture surface, this can be expressed by Nielsen's equation (99) as follows

$$\epsilon_c \approx \epsilon_p ( 1 - V_f^{1/3} ) \quad ( 2.52 )$$

where  $\epsilon_c$  and  $\epsilon_p$  are the elongations to break of the composite and unfilled polymer, respectively.

When the interfacial bonding is poor, the filler does not adhere to the matrix, and the filler particles cannot carry any of load. In addition to the effective porosity thus introduced by poor adhesion under tensile strength, stress concentrations around the particles will also reduce the strength. Nielsen (99) proposed that the tensile strength ( $\sigma$ ) should be given approximately by an equation of the following general form

$$\sigma_c/\sigma_p \approx ( 1 - K'V_f^{2/3} ) \cdot S' \quad ( 2.53 )$$

In Nielsen's treatment, the constant  $K'$  is equal to unity, and the value of  $S'$ , which symbolizes the stress concentration factor, is assumed to be about 0.5 for typical cases.

When the primary filler particle sizes are small enough, in the range of several hundred angstroms, it is well known that these small filler particles have more pronounced reinforcing properties (127). A filled polymer

has higher tensile strength than an unfilled polymer if the size of filler is small enough to reinforce the composite system, while the opposite is true if the filler particle size is large. The reason for this is not completely clear. The increase in interfacial area per unit volume of filler as particle size decreases is an important factor. A second factor which may also be important is the stress field near a particle, which by itself is independent of the size of filler particle (101). However, the volume of polymer around a filler which is involved in the dewetting processes increases with increasing particle size, and therefore, the probability of finding a large flaw within this volume also increases. The tensile strength will be reduced if a large flaw exists within an area of stress concentration (101).

Landon et al. (128) proposed a linear relationship between the mean particle diameter and the tensile strength of a composite with a negative slope at a given volume fraction. The strength of a particulate filled polymeric composite can be expressed by

$$\sigma_c = \sigma_p \cdot (1 - V_f) - k(V_f) \cdot d \quad ( 2.54 )$$

where  $d$  is the average particle diameter and  $k(V_f)$  is the slope of the plot of tensile strength against mean particle diameter at the particular volume fraction in question.

Alter (129) showed a linear relationship between modulus as well as tensile strength and the reciprocal of particle diameter. This linear function expressed a dependence of modulus as well as tensile strength on the surface-to-volume ratio of the filler.

Leidner et al. (130) proposed a relationship from a mechanics viewpoint which related the ultimate strength of a composite to the filler size, volume fraction, and surface adhesion of a dispersed phase, respectively. With this relationship, it was shown that the ultimate strength of a composite, filled with spherical particles, was a linear function of volume fraction of filler. That is,

$$\sigma_c/\sigma_p = k_1V_f + c_1 \quad ( 2.55 )$$

where  $k_1$  and  $c_1$  are constants.

In the case of a fixed volume fraction of filler, the ultimate strength is inversely proportional to the square root of the sphere diameter, so that

$$\sigma_c/\sigma_p = k_2d^{-1/2} + c_2 \quad ( 2.56 )$$

where  $k_2$  and  $c_2$  are constants.

In general, the tensile strength of polymer composites filled with large filler particles usually decreases with an increase in volume fraction of filler (130,138-142).

#### 2.4.4 Effect of Temperature and Testing Rate on the Mechanical Properties of a composite

Nicolais and Narkis (143,144) studied the stress-strain curves of different concentrations of glass bead filled polymers measured at a constant strain rate above and below the glass transition temperature.

The influence of the filler concentrations on the yield stress is different in the brittle and rubbery states (143,144). When the polymer is in the rubbery state, the yield stress increases with an increase in filler concentration (144). On the other hand, Nicolais and Narkis have determined that the yield stress is the first point at which the tangent of the force-deformation curve becomes zero when the polymer is in the glassy state. Thus, the yield stress of a composite decreases with an increase in glass bead concentrations when the filled polymer is in the glassy state (143). Meanwhile, from the stress-strain curves of the glassy state, one can expect that the stresses at the break point of the polymers are not far from the corresponding yield stress.

When the polymer was in the glassy state, the yield stress was linearly increased with the logarithm value of the strain rate at a given temperature and filler concentration (143). The same linear dependence held even when studied at a wide range of different temperatures. A double shifting procedure to account for the temperature

and the filler effect on the yield stress ( $\sigma_{yc}$ ) as a function of strain rate was obtained (143). A single master curve that can be represented by the equation

$$\frac{\sigma_{yc}}{1 - 1.21 V_f^{2/3}} = A + B \ln(\dot{\epsilon} a_T) \quad ( 2.57 )$$

relates composite yield stress to strain rate ( $\dot{\epsilon}$ ), filler volume fraction ( $V_f$ ), and temperature (T). Nicolais and Narkis (143) found that the shifting factor,  $a_T$ , is practically independent of the filler concentration.

Moehlenpah et al. (145) pointed out that polymer changed from a brittle-to-ductile-to-rubbery failure mode with the transition temperature. The glass transition temperature is a function of strain rate, filler content, filler type, and filler surface properties.

Their results show that initial tangent moduli and stress relaxation of epoxy composites can be correlated by a time-temperature superposition principle. The time-temperature shift factors for initial tangent moduli and for stress relaxation are identical and are independent of mode of loading and type of filler. Thus, for their system the shift factors are properties of the matrix (145).

The yield stress of their epoxy composites can also be correlated by the time-temperature superposition principle to obtain master plots of yield stress versus logarithm of

shifted strain rate. The time-temperature shift factors are not affected by the mode of loading, the filler content, or the type of orientation, even though the actual values of yield stress, yield strain and transition temperatures for failure modes are affected by these variables. Thus the composite shift factors are a property of the matrix and not dependent on the state of stress (145).

Furthermore, the Young's modulus of a composite increases with a decrease in temperature and with an increase in strain rate (144). The tensile strength of an amorphous rubber was found to increase with both increasing strain rate and decreasing temperature (146,147).

### 2.5 Rheological Properties of Particulate Filled Polymer Melts

The rheological properties of a composite can be studied with the polymer in the melt phase by subjecting the samples primarily to shear deformation. The mechanical properties are usually evaluated at room temperature, with the polymer in the solid phase undergoing extensional deformations.

The loss modulus describes the viscous component of viscoelasticity; i.e., how easily the polymeric molecules can move over each other. The storage modulus shows the elastic or network entanglement structure of a polymer, and it is sensitive to the extent of physical and chemical

crosslinking. The dynamic viscosity includes the combined effect of both moduli, which are related to the overall dynamic response of a polymer.

The rheological behaviors of a filled polymer are very sensitive to environmental conditions. These conditions include the testing temperature and testing rate such as shear rate in the steady mode or frequency in the dynamic mode, and materials characteristics such as solid loading and particle size of filler as well as adhesion at the interface (148-150).

#### 2.5.1 Effect of Volume Fraction, Particle Size and Size Distribution of Filler on Polymer Melts

Generally speaking, the melt viscosity of a filled polymer is increased with the increasing volume fraction of filler (148-153). Einstein showed the viscosity of a suspension of rigid spherical particles as (126)

$$\eta = \eta_l ( 1 + k_E V_f ) \quad ( 2.58 )$$

The viscosity of a suspension ( $\eta$ ) is related to the viscosity of the suspending liquid ( $\eta_l$ ), the Einstein coefficient ( $k_E$ ), and the volume fraction of the filler ( $V_f$ ). The  $k_E$  is 2.5 for rigid spheres if there is no slippage of the liquid at the surface of the sphere. In composite materials, the subscripts l and f refer to the matrix or continuous phase and filler or dispersed phase,

respectively. Einstein's equation only holds for rigid particles in very dilute concentrations.

An equation that describes the viscosity of many kinds of suspensions over the entire concentration range is the Mooney equation (137)

$$\ln ( \eta/\eta_l ) = \frac{k_E V_f}{1 - V_f/\Phi_m} \quad ( 2.59 )$$

where  $\Phi_m$  is the maximum volume fraction that the filler can have because of packing difficulties from the particle-particle contacts.  $\Phi_m$  is the actual volume of the sphere divided by the volume that the sphere appears to occupy. It is the same form as equation ( 2.50 ), which is related to the modulus of a filled polymer in the rubbery state.

A second equation which fits many experimental data on viscosity of all kinds of suspensions is (154)

$$\eta/\eta_l = ( 1 - V_f/\Phi_m )^{-2.5} \quad ( 2.60 )$$

Chong et al. (155) showed that if the relative viscosity ( $\eta/\eta_l$ ) of a monodispersed as well as a bidispersed system is plotted as a function of the reduced solid volume (defined as  $V_f/\Phi_m$ ), all the data obtained fall on a single curve. This curve can be represented as

$$\frac{\eta}{\eta_1} = \frac{E}{E_1} = \left[ 1 + 0.75 \left( \frac{V_f/\Phi_m}{1 - V_f/\Phi_m} \right) \right]^2 \quad ( 2.61 )$$

Furthermore, the effect of particle size on the melt viscosity is studied over a wide range of particle diameters (153,155). As the particle size is decreased, both the magnitude of the melt viscosity and the degree of shear thinning increase. Shear thinning is exhibited by those materials whose structure breaks down with increasing shear rate. The shear thinning of particle filled polymer is due to breaking agglomerates of filler particles, since these small particles easily agglomerate. The melt viscosity is then decreased by breaking the agglomeration with an increase in shear rate.

The rheology of vinyl plastisol is known to be affected significantly by the particle size and size distribution of polyvinyl chloride (PVC) resin particles (156). A broad size distribution leads to elimination of the shear instability and a decrease in the shear thickening (dilatant) observed at high shear rates. The shear thickening in a polymer system is due to the fact that the melt viscosity increases with increasing shear rate. Addition of coarse particles to a suspension is also shown to result in a reduction in the viscosity at low shear rate. It has been suggested that this is achieved mainly by the alternation of voids between the particles (156).

### 2.5.2 Effect of Testing Rate and Temperature

The effect of filler on the resin viscosity has been studied at different shear rates or frequencies, and has shown that a decrease in relative viscosity occurs with increasing testing rate (148,149,157-159).

The Cross equation often holds for a non-Newtonian suspension if the apparent viscosity,  $\eta_a$ , decreases as the rate of shear,  $(\dot{\tau})$ , increases (160). This equation is

$$\eta_a = \eta_\infty + (\eta_0 - \eta_\infty) / (1 + \beta \cdot \dot{\tau}^m) \quad (2.62)$$

The constant  $\beta$  and  $m$  depend upon the system, where  $\beta$  is related to the rate constant for the formation and rupture of linkages between primary particles. The exponent  $m$  shows dependence on polydispersity and has an upper limit of unity for a monodisperse system. The value of  $m$  is usually located between 1/2 and 2/3. The viscosity at zero shear rate is  $\eta_0$ , while  $\eta_\infty$  is the viscosity at very high shear rate. For non-Newtonian behavior, the viscosity decreases with shear rate until some lower limit is reached. It is generally assumed that the shear rate dependency is due to some structural change in the suspension, such as the breaking up of agglomerates by the shear forces.

Fine filler particles usually form a weak structure in the polymer matrix, and therefore this structure remains

intact at very low frequencies or shear rates (157). However, at higher shear rates or frequencies, shearing causes segregation of the fillers and sometimes also degrades the polymer, which results in a decrease in the viscosity of the filled melt (159).

The effect of temperature on the melt viscosity has been studied (148,150,152,161-164). Melt viscosity decreases with increasing temperature. Generally speaking, polymer melts at temperatures within 100°C of the glass transition temperature follow the WLF equation (162). However, for polymers at temperatures far above the glass transition temperature or melting temperature, an Arrhenius type equation, proposed by Eyring (163), is the most commonly used equation to predict the temperature dependence of melt viscosity. This equation is written as (150,164)

$$\eta = C \cdot \exp \left( - \frac{E}{RT} \right) \quad ( 2.63 )$$

where

$\eta$  = viscosity of polymer

$C$  = a constant characteristic of polymer at a given frequency or shear rate

$R$  = gas constant

$T$  = temperature in degree Kelvin (°K)

$E$  = the slope of  $\log \eta$  vs.  $1/RT$ , it is the activation energy for the flow process

Quantitative estimations of matrix-filler interactions in a filled polymer have been attempted through dynamic viscoelastic melt studies (165). The existence of a correlation between the interaction parameter in the melt state and that in the solid state at the comparable frequency of deformation has been shown by Shenoy and Saini (165) so that the matrix-filler affinity at any temperature of interest can be estimated. A linear reciprocal temperature dependence of matrix-filler affinity was observed (165).

#### 2.6 Dispersion of Filler Particles in Polymer Matrices

The mechanical and rheological properties of polymer composites depend not only on the interfacial bonding, but also on the dispersion of filler particles in the polymer matrix. However, as discussed in section 2.4, the ability to disperse the silica filler particles in the polymer matrix is also affected by the interfacial characteristics of polymer and filler particles (34).

Dispersion is usually achieved through a combination of three mechanisms: (a) initial wetting, (b) size reduction and (c) intimate wetting. Without correctly controlling the interfacial bonding and the mixing process of polymer and filler particles, an optimum dispersion of filler particles in the polymer matrix cannot be achieved (8,103,139,140,148-151).

Dispersion of particulate filler particles in polymer matrices is dependent on several factors: (a) filler particle size, (b) interfacial bonding, and (c) mixing processing, including mixing temperature and mixing torque force.

Particle sizes less than 1  $\mu\text{m}$  in diameter exhibit a very strong tendency toward agglomeration and network formation (12,103,166). Nielsen and Lewis (151) pointed out that agglomerates reduced the maximum packing fraction, thereby increasing the viscosity of the composite. Good dispersion allows higher solid loading to be achieved, while the mix still maintains reasonably low viscosity.

Bigg showed that the status of the polymer-particle interface affects the interparticle morphology and state of dispersion in the high solid loading system (148,149). He proposed several mechanisms: (a) The polymer may have a tendency to wet the filler, in which case it merely surrounds the particle but does not adhere to it. (b) The polymer may fully wet the filler. Certain polymers form weak bonds with selected filler. These bonds may be due to van der Waals, polar or hydrogen bond forces. (c) The polymer may partially wet the filler particles (or fully wet a fraction of the particles). This situation occurs when there is some degree of particle agglomerate and the polymer cannot penetrate among the adherent particles. (d) With the use of a coupling agent, the polymer may be

chemically bonded to the filler particles through bifunctional coupling molecules. Each of these situations influences the interparticle network and rheological behavior of the system.

Sacks et al. (167,168) studied the effect of mixing temperature on particulate dispersion in a polymer matrix. They investigated the steady shear flow curves (ie., shear stress versus shear rate) of high solid loading polymers mixed at two different temperatures. Samples prepared at higher temperatures showed a high yield stress and extensive hysteresis in the flow curve, which was indicative of relatively poor dispersion of particles in the polymer, which in turn resulted in a higher viscosity. In contrast, the flow curve for samples mixed at lower temperature showed a low yield stress and very little hysteresis, indicating that the particulate dispersion was much improved, which resulted in a lower viscosity (167).

## 2.7 Friction in a Filled Polymer System

### 2.7.1 Coefficient of Friction

The frictional behavior of polymers is important in many practical situations involving abrasion, wear, and scratching. For example, it is desirable to have high friction of a tire against a road surface, while low friction is expected in plastic bearings or for plastic coated skis against snow. Friction also plays a role in the first section of extruders where the granulated polymer

must be moved into the section where the polymer becomes molten.

Friction is a measure of the force resisting the motion of one surface of a solid against another surface of a solid. The coefficient of friction,  $\mu$ , between two solid surfaces is defined by

$$\mu = F/W \quad ( 2.64 )$$

where  $F$  denotes the frictional force and  $W$  is the load or force normal to the surface (169,170). In other words,  $F$  is the tangential force required to produce motion at the interface between two surfaces when they are pressed together by a normal load  $W$ .

Friction (169,170) can be divided into three classes: (a) static, (b) dynamic, and (c) rolling. These different classes of friction generally have different values of coefficient for the friction. The coefficient of friction depends on many factors such as temperature, velocity of sliding, load, nature of the surface roughness, surface adhesion, and presence or absence of lubricants.

Furthermore, when particles are manipulated by mechanical means, and adhesive and frictional forces act between the solid particles, it has been observed that friction appears to increase for small particles. This apparent increase in friction is explained by considering

the results of the contact of loaded, adhesive, and elastic spheres (171-174).

#### 2.7.1.1 Effect of polar functional groups on the coefficient of friction

Molecular adhesion is an important factor in determining the friction between two phases. Studies of polymer friction and adhesion has been carried out between bulk or thin films of polymers and the contact of rigid materials. The effect of chemical structures, such as polar groups in polymer molecular chains, on the friction and wear of polymers has been shown to be important (175-177). Nonpolar polymers tend to have lower coefficients of friction against metal than polar polymers. It has been shown, from friction results of various polyimides, that the higher the coefficient of friction of the polymer, the higher the density of the polar functional groups in the polymer molecular chains will be (175-177).

#### 2.7.1.2 Effect of temperature on the coefficient of friction

The effect of temperature on the friction and wear of heat-resistant polymers has been studied (178-181). It has been shown that polyimide carried out a transition from high friction, high wear to low friction, low wear as the temperature is increased. Friction of heat resistant polymers generally varies markedly with the temperature. A thick transferred polymer layer on a steel sphere is

generally produced at high temperature, decreasing the friction and wear of the polymer (178).

### 2.7.2 Friction Factor

The friction factor is the coefficient of friction between a solid surface and a fluid.

Considering the steady flow of a small molecular fluid (33,182) with constant density in one of two systems:

(a) the fluid flows in a straight conduit of uniform cross section; and (b) the fluid flows around a submerged object which has either an axis or a plane of symmetry parallel to the direction of the velocity of the approaching fluid. The fluid will exert a force ( $F$ ) on the solid surfaces. This force may be conveniently split into two parts:  $F_s$ , the force which would be exerted by the fluid even if it was stationary, and  $F_k$ , which is the additional force associated with the kinetic behavior of the fluid. In systems of type (a),  $F_k$  points in the same direction as the average velocity in the conduit, and in systems of type (b),  $F_k$  points in the same direction as the approach velocity.

For both systems, the magnitude of the force  $F_k$  may be arbitrarily expressed as the product of a characteristic area  $A$ , a characteristic kinetic energy per unit volume  $K$ , and the dimensionless quantity ( $f$ ), known as the friction factor (32,33)

$$F_k = AKf \quad ( 2.65 )$$

This is not a law of fluid mechanics but just a definition for  $f$ ; clearly, for any given flow system  $f$  is not defined until  $A$  and  $K$  are specified. This is a useful definition because the dimensionless quantity  $f$  can be given as a relatively simple function of the Reynolds number ( $N_{Re}$ ) (183).

For example, considering the laminar flow process of fluid with low molecular weight in a circular duct, Bird et al. (33) have shown that the surface friction factor can be related by

$$f = \frac{64}{N_{Re}} \quad ( 2.66 )$$

where Reynolds number ( $N_{Re}$ ), can be described as the ratio of momentum transfer by the turbulence mechanism to momentum transfer by molecular transport (183). The Reynolds number can be expressed as

$$N_{Re} = \frac{\delta VD}{\eta} \quad ( 2.67 )$$

where

$\delta$  = the density of fluid

$V$  = the velocity of fluid far away from the filler surface

$D$  = the diameter of circular duct

$\eta$  = the viscosity of fluid

From equations ( 2.66 ) and ( 2.67 ), it is seen that the friction factor will be in reciprocal proportion to the velocity of fluid.

#### 2.7.2.1 Types of friction factor in a polymer system

The friction factor in a polymer system is complex. The entanglements of a polymer melt cause the internal friction between macromolecular chains (184,185). A filled polymer melt, in addition to the internal friction, also involves the friction factor at the contact surface of filler and polymer melt (32,33).

#### 2.7.2.2 Segmental friction of an unfilled polymer matrix

The viscosity of a fluid represents an internal friction which resists flow. This internal friction becomes important in polymers since macromolecules can form entanglements. It is known from Bueche's theory that the internal friction of an unfilled polymer melt comes from segmental friction ( $f_{se}$ ) (184,185). The interactions of entanglements of polymer molecules are the source of internal friction when the polymer melt is under a shear force. The friction factor ( $f$ ) of a polymer melt, which is greatly increased by increasing entanglements, is a measure of the force required to pull a polymer chain through its surroundings at unit speed.

### 2.7.2.3 Surface skin and form friction on particulate filled polymer melts

Filler particles incorporated with polymer melts make the system complex. It is known that the links of polymer molecular chains in a filled polymer consist of three catalogs: (a) direct linkage with the interparticle adsorbed polymer chains between different silica particles, (b) entanglement with the molecular chains adsorbed on the adjacent filler particles, and (c) the conventional chain entanglements in the polymer which are not bonded and/or adsorbed on the silica filler (16).

In addition to segmental friction, the frictions between the contact surfaces of filler particles and the polymer melt are involved and must be considered. There are two kinds of surface friction (32), that is, the skin friction ( $f_{sk}$ ) and the form fraction ( $f_{fr}$ ).

When any surface is in contact with a fluid, and when a relative motion exists between the fluid and the surface, a skin friction ( $f_{sk}$ ) will exist between the surface and the fluid. Skin friction is thus dependent on the size or contact surface area of the solid. Skin friction is associated with a tangential force on a smooth surface that is oriented parallel to the flow direction (32).

The acceleration or deceleration effects occur when the fluid changes paths to pass around a solid body in the flow path. This phenomenon is called form drag, and the

coefficient is form friction ( $f_{fr}$ ). Form friction is dependent on shape of the solid material. Form friction is a non-tangential force and depends on the shape of the immersed material (32). One example of form friction is evidenced in the existence of a finite velocity at which a particle settles in a fluid.

CHAPTER 3  
MATERIALS AND METHODS

3.1 Materials

3.1.1 Filler

The filler particles used in the experimental composite materials were either Stöber silica (186) or Cab-O-Sil silica (187).

3.1.1.1 Stöber silica

Stöber silica were spherical particles with a narrow size distribution being prepared from a precipitation method developed by Stöber (186). By standardizing processing constants such as temperature and reactant ratio, the particle diameter could be kept below 1  $\mu\text{m}$  with a narrow particle size distribution (188).

3.1.1.2 Cab-O-Sil silica

In addition to Stöber silica, Cab-O-Sil silica (Cab-O-Sil Division, Cabot Corporation, Tuscola, IL) was also used (187). Particles of this type were prepared from a combustion process, by burning silicon tetrachloride vapor in a flame of hydrogen and oxygen gas to produce the spherical particles. While still semi-molten, the primary particles fused irreversibly into aggregates. During further cooling, these aggregates became physically

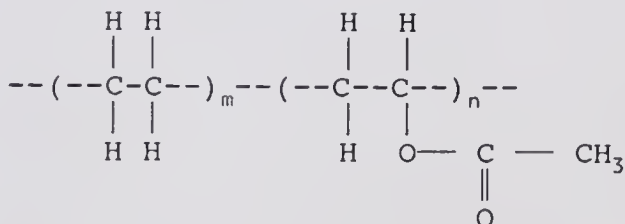
entangled to form agglomerates, a process which can be reversed by proper dispersion in a suitable medium. Cab-O-Sil fumed silica is available in several grades. The MS-7 grade of Cab-O-Sil silica with a mean particle size of 140 Å and with a surface area of  $200 \pm 25 \text{ m}^2/\text{g}$  was used in this study.

### 3.1.1.3 Quartz plates

Amorphous fumed quartz plates (Quartz Scientific, Inc., Fairport Harbor, OH) were used as a model material to characterize the surface properties of silica. It was assumed that the surface properties of the plates would be similar to the surface properties of silica fillers. After modifying the surface of the quartz plates, the contact angles of liquid drops on the quartz plates could be obtained and used to evaluate the surface properties of the silica powders.

### 3.1.2 Polymer

Ethylene-vinyl acetate (E-Va, 72% wt.-28% wt., Scientific Polymer Products, Inc., Ontario, NY) is a random copolymer which is in a rubber state at 25°C. The structure of the ethylene-vinyl acetate copolymer is



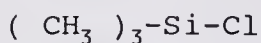
where the polar carbonyl group of E-Va copolymer can form hydrogen bonds with hydroxyl groups on the silica surfaces.

Salyer and Kenyon (189) showed that the crystallinity of the ethylene-vinyl acetate copolymer gradually decreases with an increase in vinyl acetate content. The E-Va copolymer is amorphous due to high weight percentage of vinyl acetate (189).

According to the information provided by Scientific Polymer Products, Inc., the E-Va (72% wt.-28% wt.) copolymer pellets are soluble in benzene, toluene and tetrahydrofuran (THF). The weight average molecular weight (M.W.) is approximately 285,000 when determined by gel permeation chromatography (GPC), using a polystyrene standard for calibration. Inherent viscosity is 0.82, density is 0.950 g/cm<sup>3</sup> and melt index is 20. The melt index is defined as the mass rate of flow of polymer through a specified capillary under controlled conditions of temperature and pressure.

### 3.1.3 Chemical for Surface Modification

Trimethylchlorosilane (TMCS, Fisher Scientific Co.) was used to modify the surface of silica. The methyl groups of TMCS made the surface more hydrophobic. The structure of TMCS is



Thus, the surface of silica should become hydrophobic when TMCS was bonded on its surface.

## 3.2 Techniques

### 3.2.1 Preparation of Stöber Silica

The silica particles were prepared by controlled hydrolysis and condensation reaction of tetraethylorthosilicate (TEOS, Fisher Scientific Co.) in a solution of ethanol and ammonium hydroxide (186,188).

The preparation of a batch (about 40 grams) of Stöber silica, was initiated by stirring 850 ml ammonium hydroxide with 4500 ml ethanol for 15 minutes at room temperature to avoid concentration gradients and to promote homogeneous nucleation. Following this initial step, 250 ml TEOS were then added to the mixture, yielding the final solution.

Within 2 minutes after the addition of TEOS, amorphous hydrated silica particles began to precipitate. After the initial precipitation, stirring was continued for 20 minutes in order to achieve equilibrium. The silica particles were then filtered, using a Millipore filtration unit (Millipore, Inc., Bedford, MA), washed by deionized water and dried at 70°C for 24 hours to remove adsorbed ammonium hydroxide. The obtained particles were purified by washing in the deionized water for 10 minutes to remove any supernatant and then dried again at 70°C for 12 hours. The particles were subsequently cooled to room temperature and transferred into an air-tight polyethylene bottle which was kept in a vacuum desiccator.

Nearly monodisperse, 0.6  $\mu\text{m}$ , spherical silica particles were obtained according to the procedure described above. Different particle sizes of Stöber silica have been reported in the literature. Thus, by controlling the reactant concentrations, averaging in diameter from 0.02  $\mu\text{m}$  to 2.0  $\mu\text{m}$  can be produced (186). By using TEOS along with a short chain alcoholic solvent (ethanol or n-propanol), and by simply varying the reaction temperature, it is possible to produce uniform silica spheres of the same size range (188).

### 3.2.2 Surface Modification on Silica Particle

The surface concentrations of hydroxyl groups on the fresh silica powders are high but can be modified. Two kinds of surface treatments of the silica particles were used: heat and chemical treatments. Both heat and/or chemical treatments will reduce the surface concentrations of hydroxyl groups on silica powders.

#### 3.2.2.1 Heat treatment

The surface concentrations of hydroxyl groups can gradually be reduced when silica particles are treated at higher temperature. In this study the silica particles were heat treated at either 110°C, 500°C, or 750°C for 24 hours at atmospheric pressure. The temperature was kept below 800°C to prevent sintering. Following this heat treatment the particles were cooled to room temperature inside the furnace. The silica particles were reheated at 110°C under vacuum for 12 hours and then kept at 25°C for another 12

hours before being stored in the vacuum desiccator for further use.

#### 3.2.2.2 Chemical treatment by trimethylchlorosilane (TMCS)

Surface concentrations of hydroxyl groups can also be reduced when silica surfaces react with TMCS. Silica particles were completely immersed in a 10% by volume solution of TMCS in hexane to give a ratio between TMCS and silica equal to 0.4% mole TMCS per gram of silica (190,191). This silica suspension was stirred by a magnetic stirrer for 1 hour. The silica particles were then collected and dried at 25°C after the solvent containing TMCS had been removed. The TMCS-treated silica was then heated at 110°C under vacuum for 12 hours and kept at 25°C for another 12 hours before being stored in a vacuum desiccator for further use.

#### 3.2.3 Contact Angle Measurement

The surface properties of amorphous fumed quartz plates are similar to those of silica powders. Amorphous fumed quartz plates were used as model surfaces to evaluate the surface characteristics of silica after heat and/or chemical treatments.

Cerium oxide ( $\text{CeO}_2$ , Fisher Scientific Co.) powders mixed with water were used to polish the surfaces of the amorphous quartz plates to get fresh surfaces before any treatment.

Similar processes of surface modification on the silica particles were also applied to the amorphous fumed quartz plates. Heat and/or chemical treatments were used. The

chemically hydrophobic treatment was conducted by placing the plate in a 10% by volume solution of TMCS in hexane for 15 minutes, followed by drying in nitrogen gas after removal from solution.

The contact angles of distilled water and methylene iodine (MI, Fisher Scientific Co.) were measured immediately, after the surface of plate was treated, by using a goniometer (NRL Model 100, Rame-Hart, Inc., Mountain Lakes, NJ). Water and MI were chosen because the former is a polar liquid, while the latter is a non-polar liquid.

The method used for measuring the contact angle in this study was by a direct observation of the profile of a liquid drop resting on a plane solid surface in an ambient environment. The contact angle was obtained by measuring the angle made between the tangent to the profile at the point of contact with the solid surface. This was measured by using a telescope fitted with a goniometer eyepiece. For each contact angle measurement, a drop of approximately  $5 \mu\text{l}$  was placed on a solid surface by means of a microsyringe. For such a small drop, the distorting effect of gravity is negligible (192,193), and the drop takes the shape of a spherical segment. Contact angles accurate to  $\pm 1$  or  $2^\circ$  were readily obtained. The uncertainties are higher for small angles (less than  $10^\circ$ ) and large angles (large than  $160^\circ$ ), because of the difficulties in locating the point of contact for constructing a tangent.

#### 3.2.4 Titration by Indicator Dye

The surface concentrations of hydroxyl groups on silica particles can be evaluated by a titration technique using an indicator dye. The surface concentrations of hydroxyl groups are determined from color changes of indicator dye.

For titration measurement, 1.5 gram neutral red (Pfaltz & Bauer, Inc., Stamford, CT) dissolved in 40 ml benzene (Fisher Scientific Co.) was used as indicator dye. The 0.1 M n-butylamine (Fisher Scientific Co.) in benzene was used to titrate the hydroxyl groups on the silica surface.

A technique, originally developed by Johnson (194) and modified by Benesi (195,196), was used to determine the surface concentration of hydroxyl groups. The indicator dye was added to the silica solution after the hydroxyl groups on the silica surface had been equilibrated with n-butylamine. The end-point was determined by a series of successive approximations.

Since the surface area per gram of silica differs between Stöber and Cab-O-Sil silica, amount of these two types of silica used for titration study is then different.

Approximately 10 grams of the desired heat and/or chemically-treated Stöber silica (or 1 gram of Cab-O-Sil silica) were prepared. About 0.1 gram of Stöber silica (or 0.01 gram of Cab-O-Sil silica) was transferred to a series of bottles and each bottle was heated at 110°C for 12 hours under vacuum and then kept at 25°C for another 12

hours. The silica was reweighed to get the exact weight. The 4 ml (or 6 ml) dry benzene was added to each of the silica samples immediately after weighing.

The 0.1 M n-butylamine in benzene was then added from a buret to each weighed silica sample so as to bracket the expected titer by the approximate number of millimoles of n-butylamine per gram of silica (195,196). The tightly capped silica was then equilibrated and rotated overnight at room temperature. The 0.01 ml prepared neutral red was then added to each silica sample.

After arranging the test tubes in order of increasing n-butylamine content, it was easy to determine at which stage enough n-butylamine had been added to neutralize the hydroxyl groups on the silica surface. This was easy since the neutral red was red in the acidic environments and became yellow in the basic environments.

Using smaller stepwise increases in n-butylamine content between the established border zone in the previous trial, the number of hydroxyl groups on the silica surface could be determined more accurately.

### 3.2.5 Diffuse Reflectance Infrared Fourier Transform (DRIFT) Spectrometry

A Nicolet 60SX Fourier Transform Infrared (FTIR) spectrometer (Nicolet Analytical Instruments, Madison, WI) purged with dry air and equipped with a wide-band liquid-nitrogen-cooled mercury-cadmium telluride detector

was used. Diffuse Reflectance Infrared Fourier Transform (DRIFT) spectra were acquired at a nominal resolution of  $4\text{ cm}^{-1}$ . A diffuse reflectance accessory (Model DRA-350, Harrick Scientific Corp., Ossining, NY) was used. It consisted of two 6:1  $90^\circ$  off-axis ellipsoidal mirrors for focusing the radiation onto the sample and collecting the diffusely reflected radiation. The four mirrors in the accessory were aligned for maximum throughput using the alignment mirror at  $30.75^\circ$  tilt. This mirror was later replaced by the sample cup containing KBr powder to obtain a reference spectrum. A hot stage was used and replaced the sample cup when the sample was studied at different temperatures in the heating/cooling process.

Blitz et al. (197) have demonstrated that the employing simple sample preparation step, involving the mixing of silane-modified Cab-O-Sil silica with KCl to obtain diffuse reflectance infrared Fourier transform (DRIFT) spectra, is superior to using pressed pellets of the sample for transmission studies. For example, in the case of transmission FTIR spectrometry, Cab-O-Sil pressed pellets can react with trimethoxymethylsilane (TMMS) from a toluene medium. Therefore, such pellets are unsuitable for quantitative work because the pressure applied to prepare the pellet could increase the hydrolysis of the methoxy groups by releasing water from the silica (197).

However, silica particle size and size distribution are also important variables for quantitative study with the diffuse reflectance technique even after dilution with a non-absorbing matrix. A detailed study the effect of silica particle size on the intensity of the strong Si-O stretch band at  $1100\text{ cm}^{-1}$  and other weak bands, such as the Si-O combination band at  $1870\text{ cm}^{-1}$  or the Si-O stretch band at  $810\text{ cm}^{-1}$ , has been published by Benesi and Jones (198). It has shown that a change in particle size affects the intensity of some bands differently from other bands (199).

DRIFT spectrometry, therefore, seemed to be the most suitable technique to quantify the surface properties of silica (200-205) and its surface modification.

In spite of its popularity, the use of DRIFT to obtain (a) quantitative data and (b) spectra of a dynamically changing sample either by heating or by chemical reaction has not yet received adequate attention (199,204,206).

The investigation of temperature effects on the dynamic change of interfacial bonding strength from the polymer adsorption onto the surface of silica particles was also carried out by DRIFT technique combined with the use of the hot stage.

### 3.2.6 Thermogravimetric Analysis (TGA)

Thermogravimetric analysis (207-210) was carried out with a thermal analyzer (STA409, Netzsch Brothers, Inc., Exton, PA) using a PtRh 10% - Pt thermocouple. The

measurements were done in air under atmosphere pressure. The temperature range for studying the weight loss of silica was from 30°C to 1000°C, with a heating rate 5° C/min. The data were collected with a Hewlett-Packard 86B computer using the standard Netzsch software.

### 3.2.7 Polymer Adsorption on the Silica Surface

Adsorption of polymer on a solid surface from different concentrations of polymer solutions was studied (211-215).

Each Cab-O-Sil silica sample of MS-7 grade weighing by 0.30 grams, which was previously heat treated (110°C, 500°C or 750°C) or heat/chemically treated (750°C/TMCS, 500°C/TMCS or 110°C/TMCS), was used to study polymer adsorption.

Different concentrations of the ethylene-vinyl acetate copolymer (E-Va) were prepared by dissolving in benzene solvent for polymer adsorption. Each 0.30 grams Cab-O-Sil silica adsorbed the E-Va copolymer onto its surface from 0.5%, 2% and 6% volume concentrations (ethylene-vinyl acetate versus Cab-O-Sil) of 100 ml polymer solution.

After the silica particles in polymer solution were stirred for one hour, the polymer-absorbed silica particles were separated from the polymer solution by centrifuge for 5 minutes at 5000 rpm and then dried in air.

The amount of polymer adsorbed from different polymer solutions was measured by DRIFT technique. The relative peak intensity (carbonyl groups of polymer versus siloxane groups of silica), measured from the area under the peak of

specific groups, was used to evaluate the relative amount of polymer adsorbed onto the silica surface.

The characteristic properties of the E-Va copolymer were also studied. The E-Va copolymer was first dissolved in benzene. One drop of the E-Va polymer solution from pipette was added on the sample cup of DRIFT filled with non- or low-infrared-adsorbing powders such as KBr. The carbonyl groups of the E-Va copolymer were characterized by DRIFT technique after the solvent had been evaporated.

The effect of heating and/or cooling on a thin layer of silica-surface-adsorbed polymer was also examined by the DRIFT techniques. This was done with the hot stage to investigate the effect of temperature on the interfacial bonding. The heating rate was  $5^{\circ}\text{C}/\text{min}$ . The effect of cooling was studied when the sample was cooled down in the sample chamber from a high temperature.

### 3.2.8 Preparation of Polymer Composites

Polymer composites of different volume fractions of filler (Stöber silica and Cab-O-Sil silica, respectively) with various surface modifications ( $110^{\circ}\text{C}$ ,  $500^{\circ}\text{C}$ ,  $750^{\circ}\text{C}$ ,  $750^{\circ}\text{C}/\text{TMCS}$ ,  $500^{\circ}\text{C}/\text{TMCS}$  and  $110^{\circ}\text{C}/\text{TMCS}$ , respectively) were cast from polymer solutions. Forty grams of E-Va copolymer were completely dissolved in 800 ml benzene at  $40^{\circ}\text{C}$ . Silica filler volume fractions ranging from 5% to 20% (silica vs. polymer) were then incorporated into the polymer solution. A magnetic stirrer was applied to disperse the silica filler

particles in the polymer solution. In addition, sonication (Model W-375, Heat Systems-Ultrasonic, Inc., Plainview, NY) was used for the Cab-O-Sil silica solutions for 15 minutes at 20KHZ frequency to increase the Cab-O-Sil silica particle dispersion in the polymer solution. Benzene was chosen as the solvent because it is non-polar and is a good solvent for E-Va copolymer. The filler particles were expected to disperse and stabilize in the polymer solution since the solvent had induced the polymer chains to expand to their optimum lengths.

The polymer composite solution was then spread over a large teflon pan and rapidly evaporated to prevent an uneven filler precipitation and to avoid the polymer sticking to the pan when benzene was vaporized. The polymer composite was then made into a 12cm\*12cm composite sheet with a thickness of 0.65 cm by compression molding,

### 3.2.9 Mechanical and Rheological Measurements

Tensile specimens were prepared according to ASTM 1822 from the compression-molded sheets. Before the tensile test, the Stöber silica and Cab-O-Sil silica filled E-Va copolymers were annealed at 100°C and 130°C, respectively, for Three hours and then conditioned at 25°C for 3 days. The composites were tested at a crosshead speed of 2 in/min at 25°C using an Instron model 1122 (Instron Corporation, Atlanta, GA). At least six specimens were used for each

data point. The Young's modulus and the tensile strength of silica filled composites were measured.

The rheological properties of silica filled E-Va copolymer were studied by dynamic spectrometer since the results of the dynamic mode can be directly related to the structure of the materials. The dynamic viscosity and the shear modulus (216,217) were measured by a Rheometrics Dynamic Spectrometer (Model RDS-II, Rheometrics, Inc., Piscataway, NJ).

In dynamic measurements of polymer melts, the angular frequency becomes analogous to the shear rate in the usual rheological measurements (163,164,216,217).

The volume fractions ranged from 5% to 20% for the Stöber silica and 5% volume of Cab-O-Sil silica filled E-Va were measured by dynamic model with the parallel plates. Dynamic rate sweeps from frequencies of 0.1 to 100 rad/sec with 100% strain were used. The rheological tests of Stöber filled composites were measured at 150°C with a 0.6 mm gap between the parallel plates. The Cab-O-Sil silica filled composites had higher glass transition and softening temperature than the Stöber silica filled composite based on the same volume fraction of filler particle. This was related to the high surface area of the Cab-O-Sil silica. The Cab-O-Sil silica filled composites were therefore measured at 210°C with a 2.0 mm gap between the parallel plates.

### 3.2.10 Scanning Electron Microscopy (SEM) and Scanning Transmission Electron Microscopy (STEM) Studies

Observation of spherical particles of Stöber silica with a narrow size distribution was accomplished by scanning electron microscopy (SEM) (Model JSM-35CF, Japan Electron Optics Co. Ltd., Tokyo, Japan).

The dispersion of filler particles in the polymer matrix can be studied from the fracture surface of composites. The fracture surface is prepared at liquid nitrogen temperature to keep the original positions of silica particles in the polymer matrix without any disturbance from plastic deformation in the polymer during sample preparation.

The dispersion of silica particles in the polymer matrix was studied by SEM and scanning transmission electron microscopy STEM (Model JSM-200CX, Japan Electron Optics Co. Ltd., Tokyo, Japan). The samples of silica filled E-Va copolymer were immersed in liquid nitrogen for 30 minutes, the silica filled composites were then broken by impact force with a hammer. The brittle fracture surface of composite samples was thus obtained. Examination of dispersion of either Stöber or Cab-O-Sil silica particles in the E-Va matrix was carried out on these brittle fracture surfaces by SEM. Since the particle size of Cab-O-Sil silica is very small, the Cab-O-Sil silica filled E-Va copolymer samples were prepared by a microtome (Model MT-2, Ultra-Microtome, DuPont Company, Newtown, CT) at liquid

nitrogen temperature for a further dispersion study by STEM. The adhesion between polymer matrix and Stöber silica particles treated by heat and/or chemical was also examined by SEM on the tensile fractured surfaces of samples being forced in tension in the Instron testing machine.

CHAPTER 4  
CHARACTERIZATION AND SURFACE MODIFICATION  
OF SILICA PARTICLES

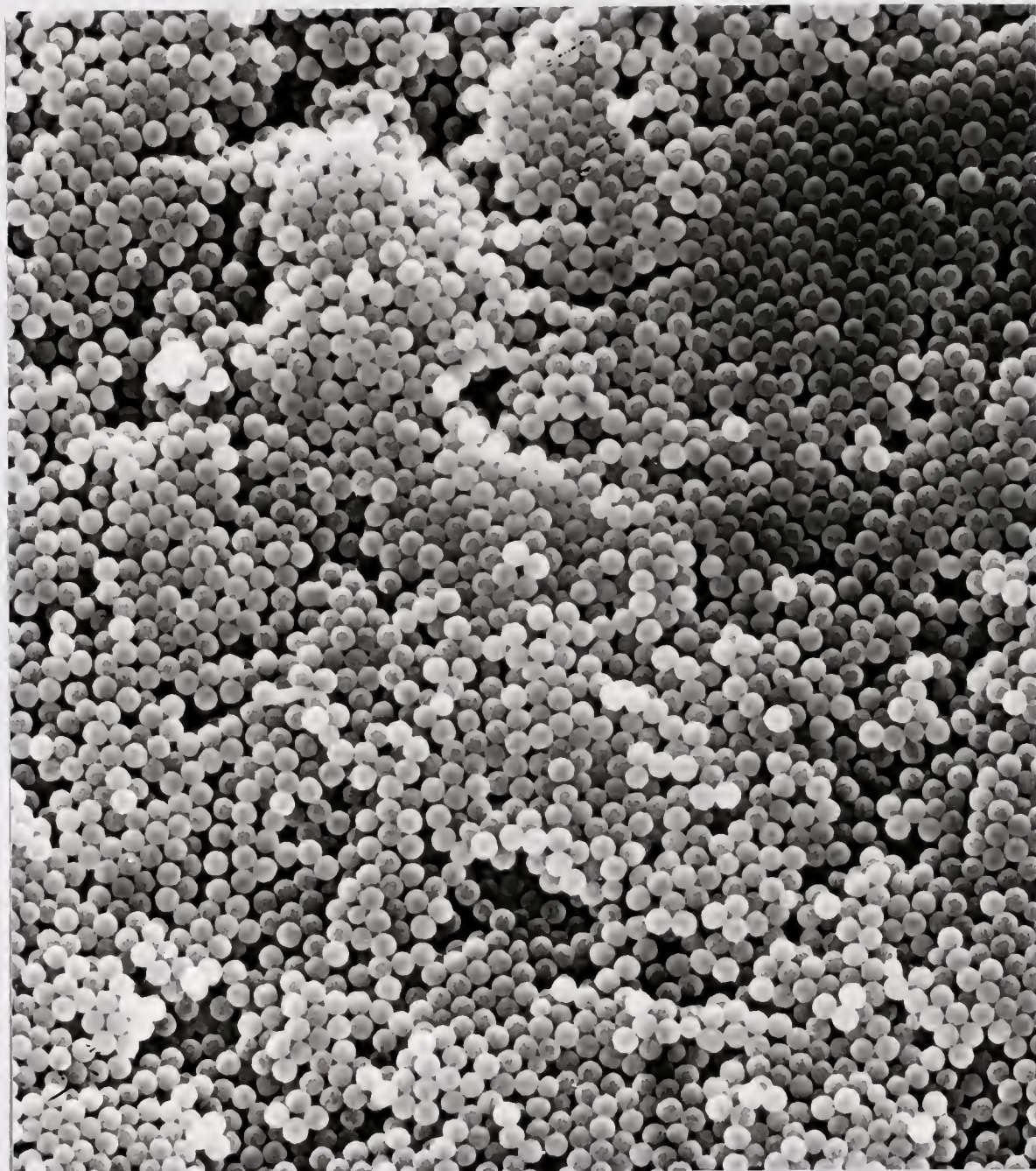
4.1 Characterization of Silica Particles

The characteristic properties of Stöber silica and Cab-O-Sil silica have been extensively studied and the information is readily available in the literature (186, 187, 188, 218-226).

4.1.1 Stöber Silica

Stöber silica particles with an average diameter of 0.6  $\mu\text{m}$  are synthesized by mixing of 3.0 moles of  $\text{NH}_3$  per liter of ethanol, 6.6 moles of  $\text{H}_2\text{O}$  per liter of ethanol, and 0.25 moles of TEOS per liter of ethanol, as described in the materials and methods section. The scanning electron micrograph (SEM) in Figure 4.1 shows that the silica particles are spherical and have a narrow size distribution (186, 188, 218-222).

Stöber silica particle size increases as the  $\text{NH}_4\text{OH}$ /ethanol ratio increases when the TEOS/ethanol ratio is fixed, or if from a given  $\text{NH}_4\text{OH}$ /ethanol ratio, as the TEOS/ethanol ratio decreases (186). Regardless of which alcoholic solvent is used, the mean diameter of the silica decreases with an increase in reaction temperature (188). However, in all the cases, the size distribution (standard



—  
1.0  $\mu\text{m}$

Figure 4.1 Shape and Size of Stober Silica by SEM

deviation) becomes gradually nonuniform and occasionally non-spherical when the mean particle size deviates significantly from half a micron (186,188).

The average density of Stöber silica particles formed at room temperature is below  $2.10 \text{ g/cm}^3$ . Particle shows a slight increase in density with an increase in calcination temperature. The density of Stöber silica calcined at  $800^\circ\text{C}$  is approximately  $2.20 \text{ g/cm}^3$ , usually reported for fused silica (218,223). Furthermore, the surface areas (approximately  $7 \text{ m}^2/\text{g}$ ) measured by BET are in good agreement with values ( $6 \text{ m}^2/\text{g}$ ) calculated by assuming that the particles are perfectly spherical with smooth surfaces (218,223). The specific surface areas are found to be independent of calcination temperature up to  $800^\circ\text{C}$ . This suggests that the silica particles are free of micropore formation during the heat treatment (218).

Porosity of the silica particles is studied using a mercury porosimeter (223). The change in surface pore volume as a function of calcination temperature is insignificant because the BET surface area is found to be constant and independent of calcination temperature (223).

The X-ray diffraction pattern of Stöber silica confirms that very little change occurred up to  $1000^\circ\text{C}$  for particles calcined in a loose-stack arrangement (218,223). The observed band, which was extensive, broad, and centered at

$2\theta = 22^\circ$ , is characteristic of amorphous silica. This suggests that all the silica particles being heat treated below  $1000^\circ\text{C}$  are in the amorphous state (218,223).

#### 4.1.2 Cab-O-Sil Silica

The characterization of Cab-O-Sil silica is obtained from the bulletin provided by the Cabot Corporation (187). Cab-O-Sil silica is known as a fumed silica because of its smoke-like appearance as it forms in the flame. The fine, particulate nature of Cab-O-Sil silica can be seen in high magnification electron micrographs. The electron micrographs of gold-shadowed Cab-O-Sil samples in Figure 4.2 gives an impression of the three-dimensional branching of the aggregates. Figure 4.3 shows a typical electron micrograph of Cab-O-Sil, well dispersed in collodion to show the branched chain aggregates. There is virtually no mechanical entanglement (agglomeration) of the Cab-O-Sil aggregates in this micrograph. Figure 4.4 is a much higher magnification of a single aggregate. These three figures are all from a bulletin of Cabot Corporation which shows that the aggregate chain consists of many primary particles which have fused together. The maximum lengths of the aggregates are a few tenths of a micron. The true density of the aggregate is  $2.20 \text{ g/cm}^3$ , but the bulk density of uncompressed Cab-O-Sil is much lower, being approximately  $0.032 \text{ g/cm}^3$  in the standard form.



---

0.1 $\mu$ m

Figure 4.2 The Three Dimensional Random Branching of the Aggregates of Cab-O-Sil Silica



1000Å

Figure 4.3 The Isolated Individual Aggregates of Cab-O-Sil Silica



500Å

Figure 4.4 The Individual Particles in the Aggregates of Cab-O-Sil Silica

Gas adsorption studies of Cab-O-Sil show that the material is non-porous (187). Thus, adsorption processes are rapid since molecules are only held physically on the exterior surface, and not entrapped in pores. However, the clustered nature of the aggregates may make it difficult for large molecules, such as polymers, to gain access to all the surfaces which can be reached by the gas molecules used in the surface area measuring procedure.

The surface area of MS-7 grade Cab-O-Sil silica is  $200 \pm 25 \text{ m}^2/\text{g}$ . At temperatures above  $800^\circ\text{C}$ , the Cab-O-Sil silica starts to sinter, with a consequent loss in surface area. The amorphous nature of Cab-O-Sil silica is shown by the absence of lines in its X-ray diffraction pattern (187). The amorphous form is probably caused by the extremely rapid solidification and cooling of the silica aggregates, which takes place in only a few thousandths of a second.

## 4.2 Modification of the Silica Surface

### 4.2.1 Contact Angles on Amorphous Fused Quartz Plates

The surface chemistry of the silica particles (Stöber silica or Cab-O-Sil silica) is modified using heat and/or surface hydrophobic agent (TMCS) treatments. TMCS, with only one reactive site, cannot polymerize under the studied reaction conditions (190,191,227-230). Similar processes are also applied to amorphous fused quartz plates to simulate the surface modification on silica particles.

A range of contact angles of water on the solid plates are obtained from  $0^\circ$  to  $42^\circ$  by increasing the heat treatment temperature from  $25^\circ\text{C}$  to  $1250^\circ\text{C}$ , as shown in Figure 4.5. The surface changes gradually from being hydrophilic to hydrophobic as a result of the heat treatment because of the condensation of surface hydroxyl groups.

The surface reaction with the surface hydrophobic agent, TMCS, makes the silica even more hydrophobic since polar surface hydroxyl groups are replaced by non-polar trimethylsilane groups (190,227-230). The highest water contact angle is  $86^\circ$ , which is achieved with the  $110^\circ\text{C}/\text{TMCS}$  treatment, as shown in Figure 4.5.

The contact angles of distilled water and methylene iodine (MI), respectively, on the amorphous fumed quartz plates being treated by either heat and/or TMCS are shown in Table 4.1.

#### 4.2.2 Fourier Transform Infrared (FTIR) and Thermogravimetry Analysis (TGA) Studies of Silica Particles

##### 4.2.2.1 Heat treatment

The surface modification of the silica particles due to the different treatments can be identified by the DRIFT technique. Figure 4.6 illustrates Stöber silicas which have been treated at  $110^\circ\text{C}$ ,  $500^\circ\text{C}$  or  $750^\circ\text{C}$  for 24 hours, respectively, and examined at room temperature by DRIFT. Figure 4.7 shows MS-7 grade Cab-O-Sil silicas which have

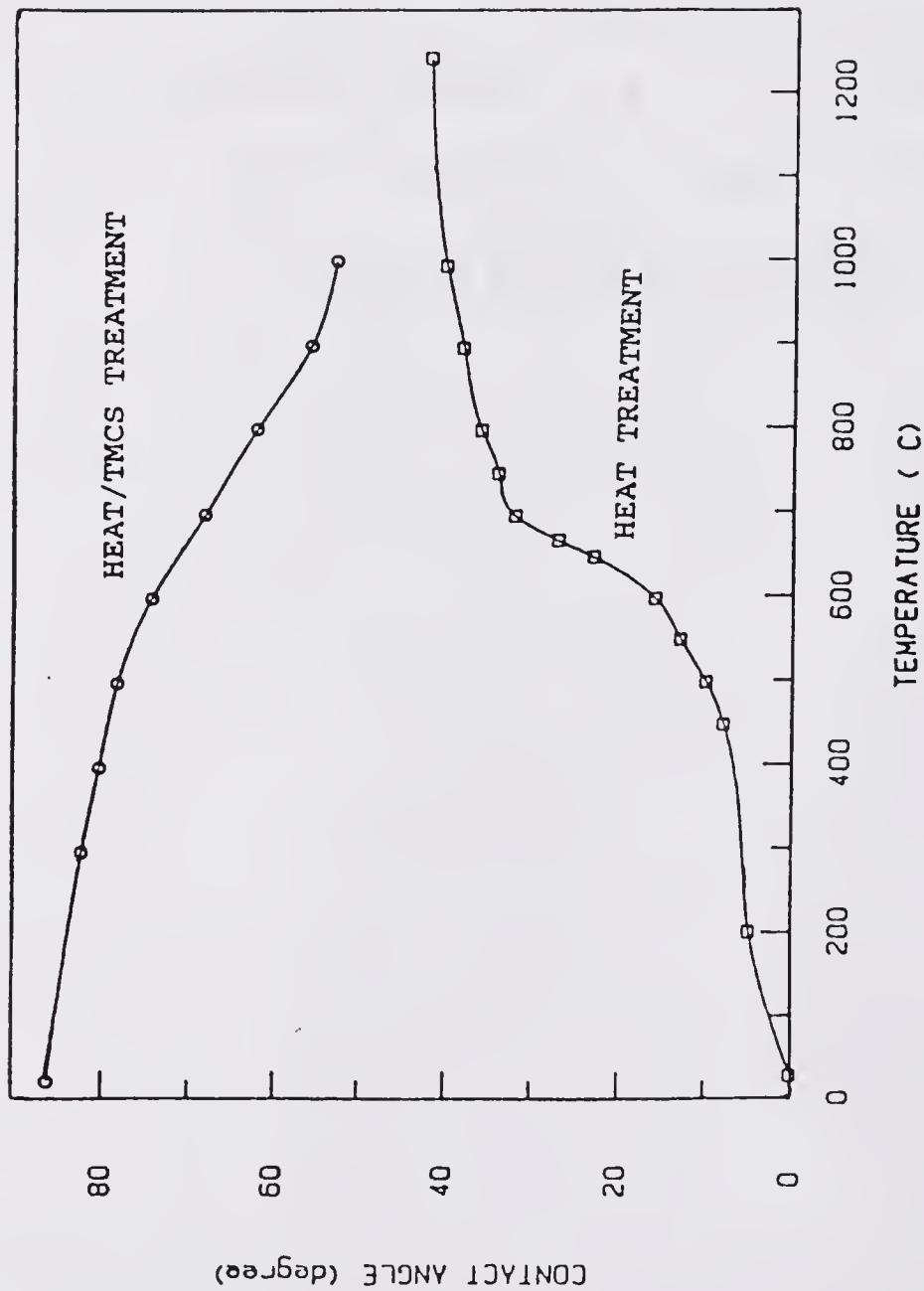


Figure 4.5 Contact Angles of Water on the Surface of the Fused Quartz Plates Treated by Heat or Heat/TMCS

TABLE 4.1

CONTACT ANGLES VERSUS SURFACE MODIFICATION  
ON AMORPHOUS FUMED QUARTZ PLATES

Treatment	Water ( contact angle )	Methylene Iodide ( contact angle )
110°C	0	39±3
500°C	10±2	35±2
750°C	36±2	30±3
750°C/TMCS	66±2	48±2
500°C/TMCS	76±2	54±2
110°C/TMCS	86±1	63±2

STOBER SILICA  
HEAT TREATMENTS

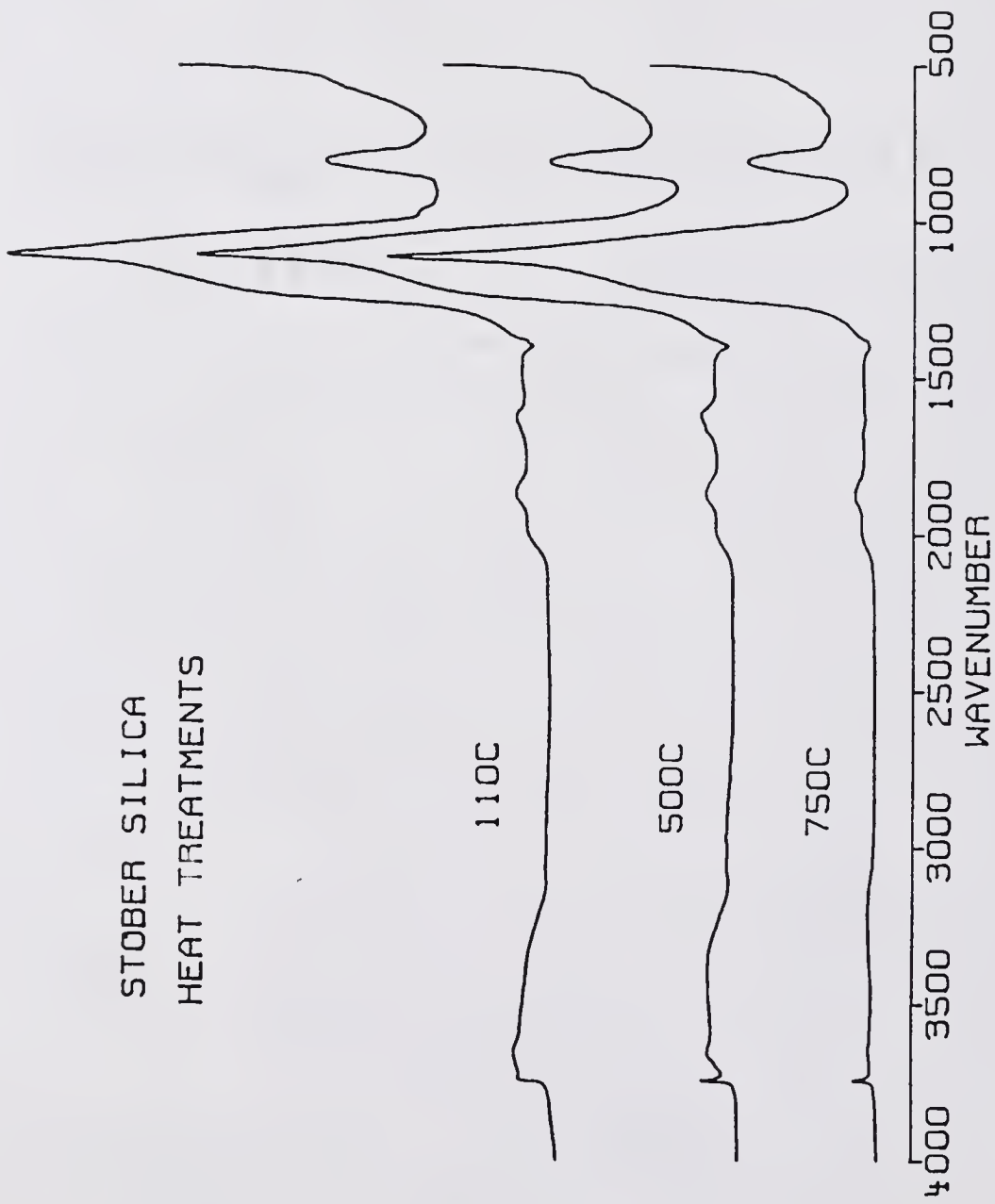


Figure 4.6 FTIR Spectrum of Stober Silica Heat Treated at Different Temperatures

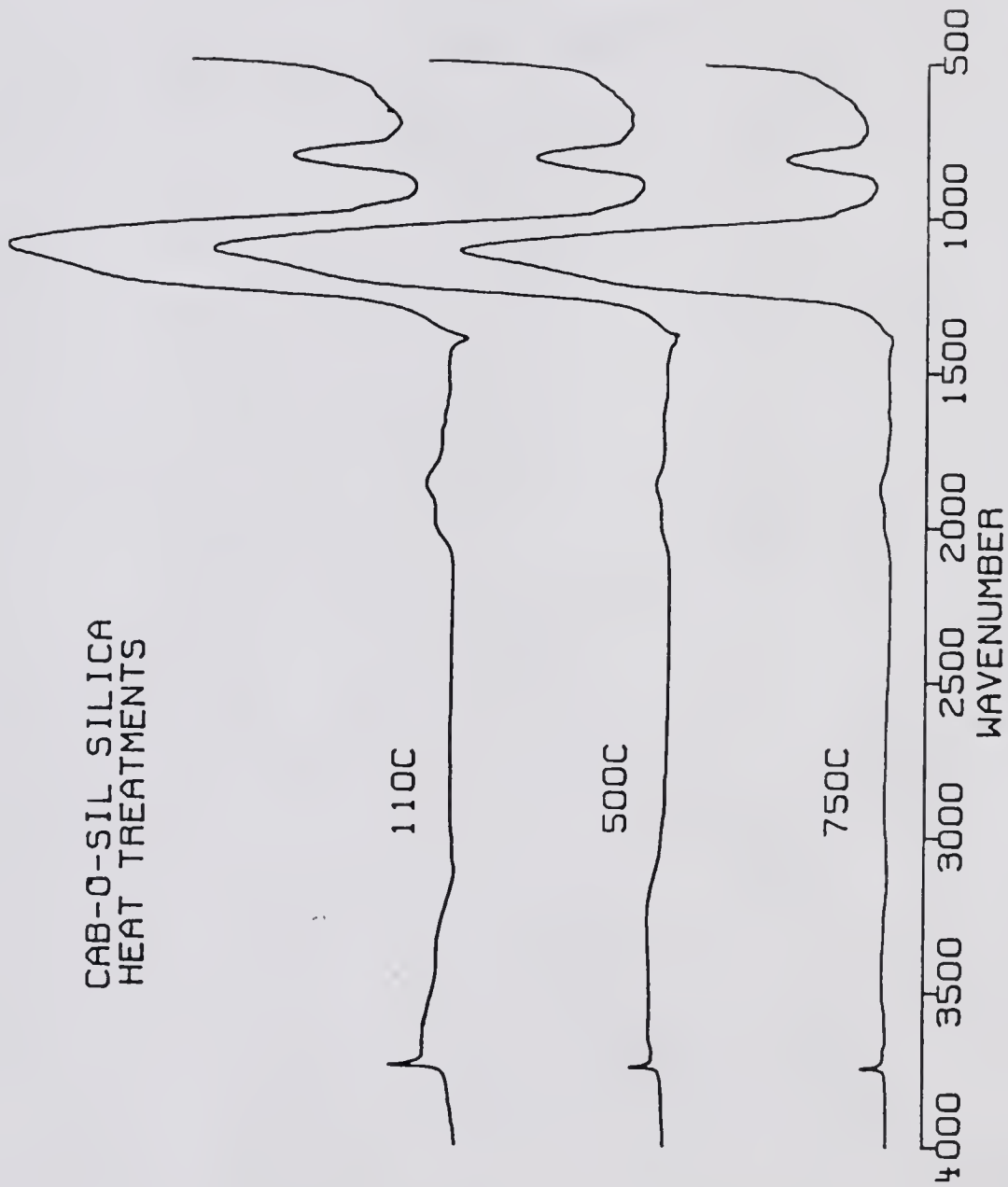


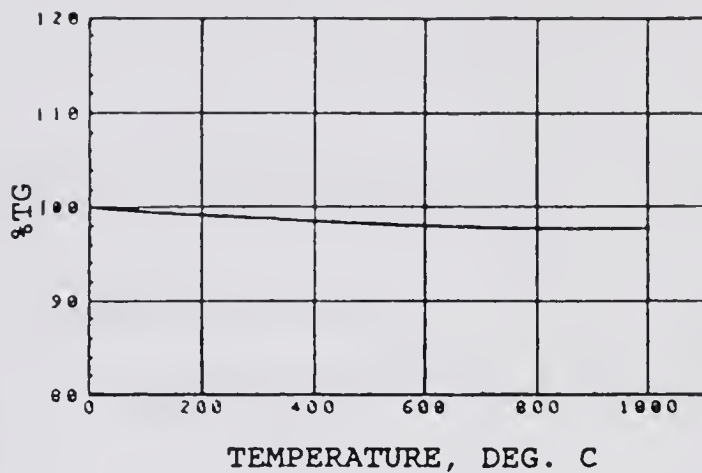
Figure 4.7 FTIR Spectrum of Cab-O-Sil Silica Heat Treated at Different Temperatures

been treated as described previously and examined at room temperature by DRIFT.

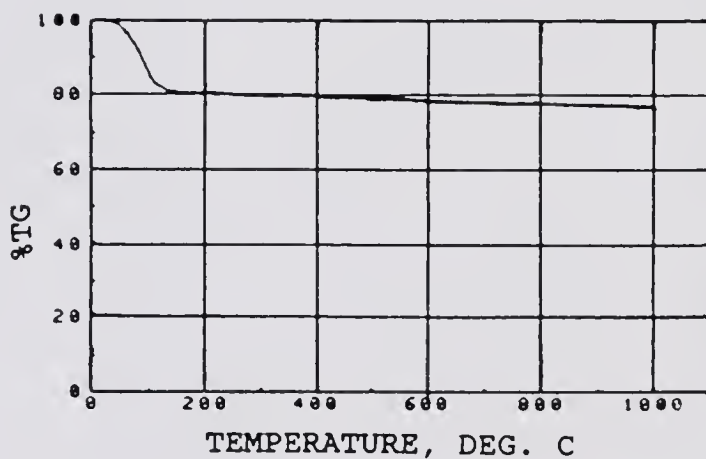
The peak at  $1100\text{ cm}^{-1}$  is assigned to the siloxane (Si-O) groups on silica surfaces (227,228). The peak at  $3746\text{ cm}^{-1}$  is assigned to the isolated hydroxyl groups (227,228). The peak around  $3660\text{ cm}^{-1}$  is assigned to hydrogen-bonded hydroxyl groups. The broad peak around  $3500\text{ cm}^{-1}$  is assigned to physically adsorbed molecular water (227,228).

The peak intensities of the molecular water and the hydrogen-bonded hydroxyl group are gradually reduced with an increase in heat treatment temperature, and finally disappear at high temperatures. The intensity of the isolated hydroxyl group is also gradually reduced at even higher temperatures (227,228).

In the FTIR spectra of silica which have been heat treated at  $110^{\circ}\text{C}$ , Stöber silica shows more physically adsorbed molecular water on the surface than Cab-O-Sil silica. This result is also confirmed by thermogravimetric analysis (TGA). Both Stöber silica and Cab-O-Sil silica were exposed to ambient conditions in the laboratory for one day. The total weight loss of Stöber silica is 23% when temperature increases from  $30^{\circ}\text{C}$  to  $1000^{\circ}\text{C}$ . However, the Cab-O-Sil silica loses 3% in the same temperature range, as shown in Figure 4.8.



WEIGHT LOSS OF CAB-O-SIL SILICA IS  
2.3 % BETWEEN 30°C AND 1000°C

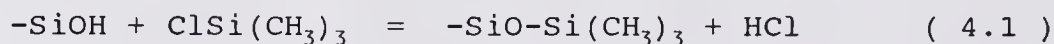


WEIGHT LOSS OF STOBER SILICA IS  
19.5 % BETWEEN 30°C AND 200°C,  
3.2 % BETWEEN 200°C AND 1000°C

Figure 4.8 TGA Spectrum of the Weight Loss of Cab-O-Sil and Stober Silica by the Heating Process

#### 4.2.2.2 Chemical treatment

Methylated chlorosilanes have been found to be extremely efficient in their ability to dehydroxylate surfaces, and many spectroscopic studies on the nature of these reactions have been investigated (227-232). In a typical reaction, the silica releases the adsorbed water by evacuation at 110°C and then reacts with TMCS in hexane solution. The reaction proceeds as follows



The infrared spectrum of this silica surface which has reacted with TMCS exhibited a characteristic strong absorption peak at 2968  $\text{cm}^{-1}$ , which is characteristic of the asymmetric stretching vibration of the C-H bond in the methyl groups.

Complete dehydroxylation of the surface has not been achieved by this chemical reaction. Whether this is due to an equilibrium condition or whether the bulky trimethyl chlorosilane molecules are sterically hindered in reaching some surface hydroxyl groups has not been established (227).

Hair noted that the ability of hydroxyl groups on silica surface to absorb and react with the other molecules was dependent on whether the hydroxyl groups existed as isolated groups on the surface or as hydrogen-bonded

hydroxyl groups (228). In studying the silane reaction with silica, the reaction of  $\text{ClSiMe}_3$  with the silica surface followed first order kinetics. The reaction of  $\text{Cl}_2\text{SiMe}_2$ ,  $\text{Cl}_3\text{SiMe}$  and  $\text{SiCl}_4$  followed 1.6 order kinetics (229). This implied that 40% of the freely vibrating surface hydroxyl groups reacted monofunctionally, but 60% must be presented in a position sufficiently close to each other so that they could react in a bifunctional manner (228,229). Furthermore, it was emphasized that these hydroxyl groups reacting with silane would not be hydrogen-bonded to each other (228,229).

#### 4.2.2.2.1 Cab-O-Sil silica

It is shown in Figure 4.9 that the isolated hydroxyl groups on the Cab-O-Sil silica surface have reacted with TMCS. This is confirmed by the almost complete disappearance of the isolated hydroxyl group peak at  $3746\text{ cm}^{-1}$ , and the appearance of a peak around  $2850\text{ cm}^{-1}$ , which is characteristic of methyl groups. This indicates that TMCS is adsorbed and replaces the hydroxyl groups on silica surface.

When Cab-O-Sil silica reacts with 10% by volume of TMCS in hexane solution, it is found from FTIR spectroscopy that silica surfaces which have been pretreated at  $110^\circ\text{C}$  ( $110^\circ\text{C}/\text{TMCS}$ ) have the highest intensity ratio of methyl groups/siloxane groups. This finding also corresponds to the highest contact angle of water after a similar

CAB-O-SIL SILICA  
CHEMICAL TREATMENTS

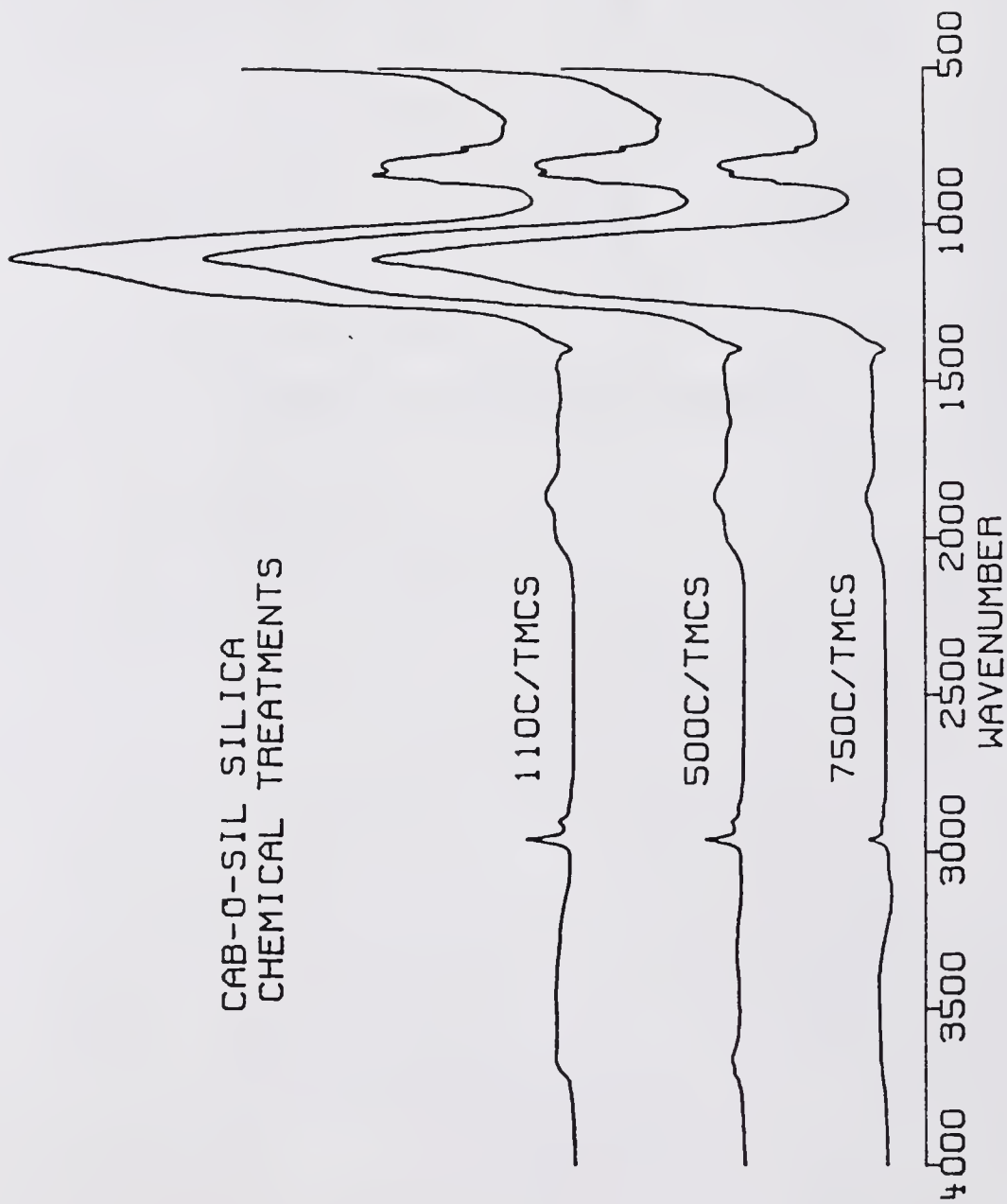


Figure 4.9 FTIR Spectrum of cab-O-sil silica at Different Heat/TMCS Treatments

treatment of a solid fused quartz plate, which is explained as a result of more methyl groups existing on the silica surface.

#### 4.2.2.2.2 Stöber silica

When Stöber silica reacts with the same concentration of TMCS solution as Cab-O-Sil does, the peak intensity of the methyl group is much less for the Stöber silica, as shown in Figure 4.10. This is explained as a result of the larger particle size of Stöber silica. Several reasons have been proposed to explain why the DRIFT spectrum has a low peak intensity of methyl groups in the TMCS treated Stöber silica.

One explanation is that the surface curvature is different between Stöber silica and Cab-O-Sil silica. Stöber silica has a lower surface curvature, and might sterically prevent the large TMCS molecules from bonding to its surface. In Figure 4.10, an isolated hydroxyl group peak is seen. This finding may indicate that bulky TMCS molecules are sterically prevented from reaching some of the isolated hydroxyl groups on the surface of the Stöber silica. However, the steric hindrance is less pronounced in Cab-O-Sil silica due to a higher surface curvature of this silica.

Another explanation of a low peak intensity of the methyl groups in Stöber silica is that Stöber silica, of the same weight as Cab-O-Sil silica, has less surface area

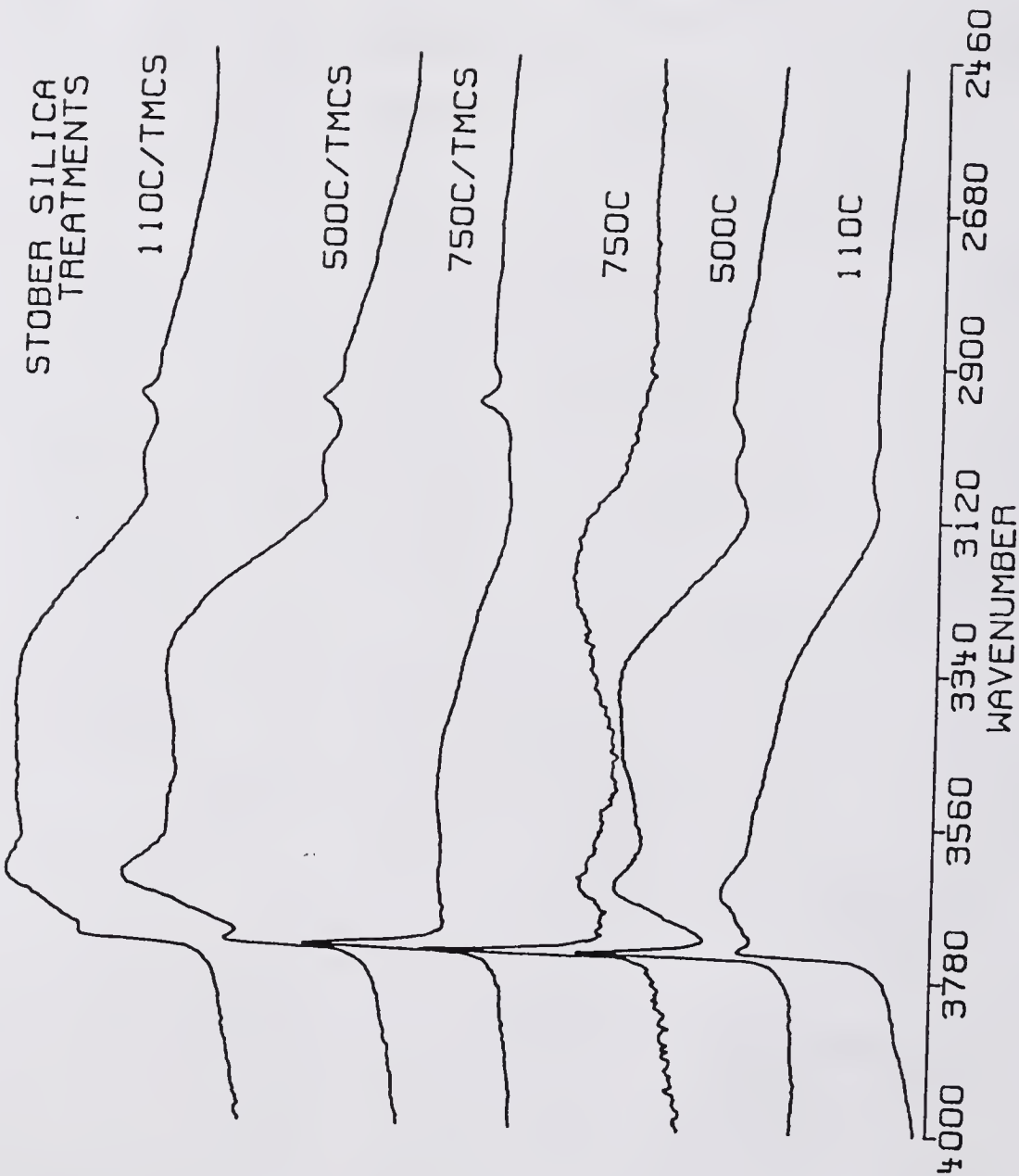


Figure 4.10 FTIR Spectrum of Stober Silica at Different Heat/TMCS Treatments

which is available to react with TMCS. The total amount of TMCS, which has reacted and bonded on the Stöber silica surface is, therefore, less than that on the Cab-O-Sil silica surface.

The particle size effect of silica on the DRIFT spectrum is another possible reason for these differences. This difference have been studied by Murthy and Leyden (199). Looking at the spectra of 3-amino-propyl-triethoxy-silane (APTS) treated silica gel samples, silica particles less than 5  $\mu\text{m}$  in size showed an obvious CH peak, but silica having a 150  $\mu\text{m}$  particle size showed a much smaller intensity of this peak (199). These results were attributed to the effect of silica particle size.

Fuller and Griffiths (202) studied the matrix particle size effect. The effect of particle size of non- or low-absorbing powders, such as KBr or KCl, on the diffuse reflectance spectra of a pure compound, such as azobenzene, was discussed (202). They showed that the bandwidth of all bands of azobenzene decreased and their intensity generally increased with a decrease in the particle size of KCl or KBr (202). However, it was interesting to note that the intensity of certain bands appeared to change more dramatically with particle size than others (202).

#### 4.3. Concentrations of Hydroxyl Groups on the Silica Surface

It is well known that on a fully hydroxylated silica surface, the number of silanol (also called hydroxyl) groups per square nanometer lies within the range of 4.2 and 5.7. This is true even though the samples are prepared in different ways and have different structural characteristics (233,234). The average number of the silanol groups is 4.9 hydroxyl groups per square nanometer for the fully hydroxylated state, which includes both isolated and adjacent silanol groups. This value is independent of the origin and structural characteristics of the silica (223).

The number of hydroxyl groups per unit square nanometer on the surface of silica (Stöber silica and Cab-O-Sil silica) achieved with different surface modification is listed in Table 4.2. The number of silanol groups of either Cab-O-Sil or Stöber silica treated at 110°C is close to the reported average value. Basically, the concentrations of surface hydroxyl groups on either Stöber silica or Cab-O-Sil silica are approximately equal.

The number of hydroxyl groups is measured by titration of n-butyl-amine on the surface modified silica particles using neutral red as an indicator. Table 4.2 shows that the heat and/or chemical reaction treatments used for the surface modification cover a wide range of concentrations

TABLE 4.2

## SURFACE HYDROXYL GROUPS PER UNIT AREA

indicator dye method / titrating with 0.1 M n-butylamine

indicator dye: neutral red

Treatment	Cab-O-Sil silica ( OH/100 Å <sup>2</sup> )	Stöber silica ( OH/100 Å <sup>2</sup> )
110°C	4.39 ± 0.12	4.55 ± 0.04
500°C	2.86 ± 0.08	2.96 ± 0.05
750°C	1.88 ± 0.11	1.95 ± 0.05
750°C/TMCS	0.13 ± 0.02	
500°C/TMCS	0.27 ± 0.04	
110°C/TMCS	0.39 ± 0.04	

of surface hydroxyl groups. The lowest concentration (750°C/TMCS) of hydroxyl groups is less than 3% of the highest concentrations of hydroxyl groups (110°C).

Silica treated by 750°C/TMCS has the lowest surface concentration of the hydroxyl groups. This is because most hydrogen-bonded hydroxyl groups are condensed and removed at this high temperature and that the remaining isolated hydroxyl groups react readily with TMCS.

However, the highest contact angle of water (86°) is achieved on the fused quartz plate with 110°C/TMCS treatment due to a greater number of methyl groups on the silica surface. These methyl groups are more hydrophobic (lower surface free energy) than the siloxane groups on the silica surface. Furthermore, as shown in Table 4.2, the 110°C/TMCS treated silica retains more surface hydroxyl groups on the silica surface than the 750°C/TMCS treated silica. This is because most of hydrogen-bonded hydroxyl groups are not condensed and removed from the silica surface at 110°C. These hydrogen-bonded hydroxyl groups also do not react with TMCS (227-232). Therefore, the 110°C/TMCS treated silica, having a higher number of surface hydroxyl groups, shows a higher contact angle of water than the 750°C/TMCS treated silica.

#### 4.4 Polymer Adsorption on Silica Surface

E-Va copolymer is adsorbed from its polymer solution onto Cab-O-Sil silica particles which have been previously

treated by heat and/or chemical processes. The hydrogen and/or polar bonding at the interface between the silanol groups on the silica surface and the carbonyl groups of the E-Va copolymer is examined by DRIFT.

Adsorption of polymer onto the silica surface is obtained from 0.5% to 6% volume concentrations (E-Va copolymer versus Cab-O-Sil Silica) of polymer solution. The 6% volume polymer solution has more polymer available for the silica to adsorb polymer onto the silica surface, and therefore has the highest amount of polymer bonded and/or adsorbed on the Cab-O-Sil silica surfaces.

#### 4.4.1 Evidence of Hydrogen Bonding Studied by FTIR

The carbonyl groups of the E-Va copolymer being bonded and/or adsorbed on the surface of Cab-O-Sil silica are studied by FTIR. The E-Va copolymer bonded and/or adsorbed on silica after treatment at 110°C is shown in Figure 4.11. The carbonyl groups of the E-Va copolymer can be identified as the small peak at 1739  $\text{cm}^{-1}$  and the large peak at 1704  $\text{cm}^{-1}$ , where both peaks are characteristic of the carbonyl groups on the polymer-adsorbed-silica surfaces (28,95).

The peak at 1739  $\text{cm}^{-1}$  is assigned to the unbonded carbonyl group of the E-Va copolymer. The carbonyl group of E-Va copolymer resin is also shown in Figure 4.11 for comparison. The peak at 1704  $\text{cm}^{-1}$  is assigned to the carbonyl group which is hydrogen and/or polar bonded with the hydroxyl group of the silica surface (28,95).

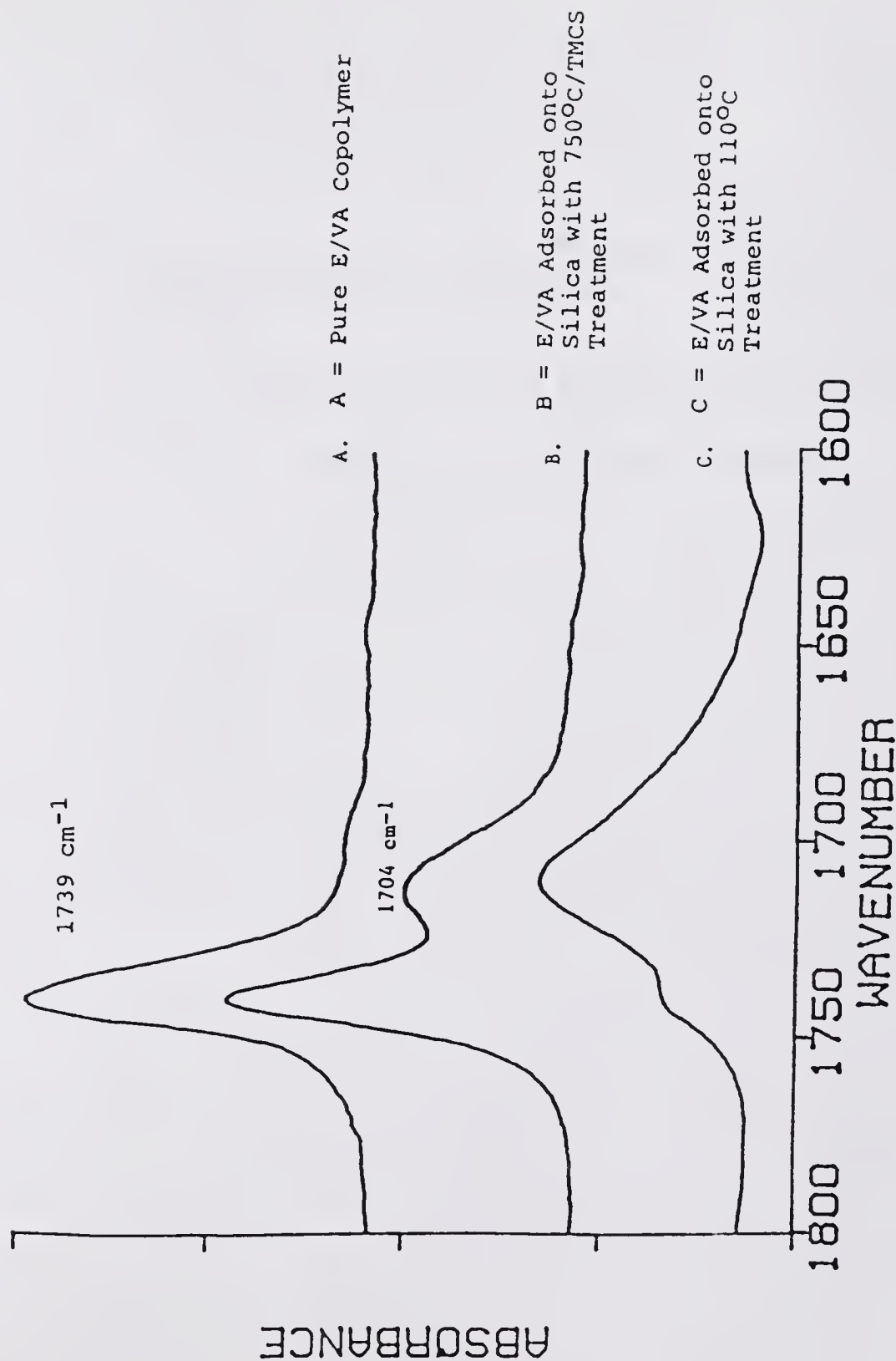


Figure 4.11 The Wavenumber Shift of the Carbonyl Groups of the E-Va Copolymer after Hydrogen Bonding with the Hydroxyl Groups on the Silica Surface

However, for the 750°C/TMCS treatment, there is a small peak at 1704  $\text{cm}^{-1}$  and also a large peak at 1739  $\text{cm}^{-1}$ , as shown in Figure 4.11.

It is concluded that more hydrogen and/or polar bonding exists at the interface when the silica surface has more silanol groups.

The wavenumber shift of the carbonyl group gives information for evaluating the energy of the hydrogen and/or polar bonding at the interface between the silanol group and the carbonyl group. It is important information which is used to evaluate work of adhesion between silica filler and polymer matrix.

#### 4.4.2 Effect of Hydrogen Bonding on Polymer Adsorption

The spectrum of [ 0.56%, (A) ] in Figure 4.12 shows the adsorption of E-Va copolymer from 0.56% volume of polymer solution onto the Cab-O-Sil silica being previously treated at 110°C. It indicates that some of the isolated hydroxyl groups (3747  $\text{cm}^{-1}$ ) form hydrogen and/or polar bonds with the carbonyl group, and therefore the wavenumber of carbonyl groups is shifted to a lower frequency (1704  $\text{cm}^{-1}$ ) (28,95). The other isolated hydroxyl groups (3747  $\text{cm}^{-1}$ ), which are not covered and bonded by polymers, can be detected and identified by DRIFT spectroscopy. However, these unbonded hydroxyl groups eventually form hydrogen bonds with the carbonyl groups when more polymers are available in the polymer solution. This is confirmed by

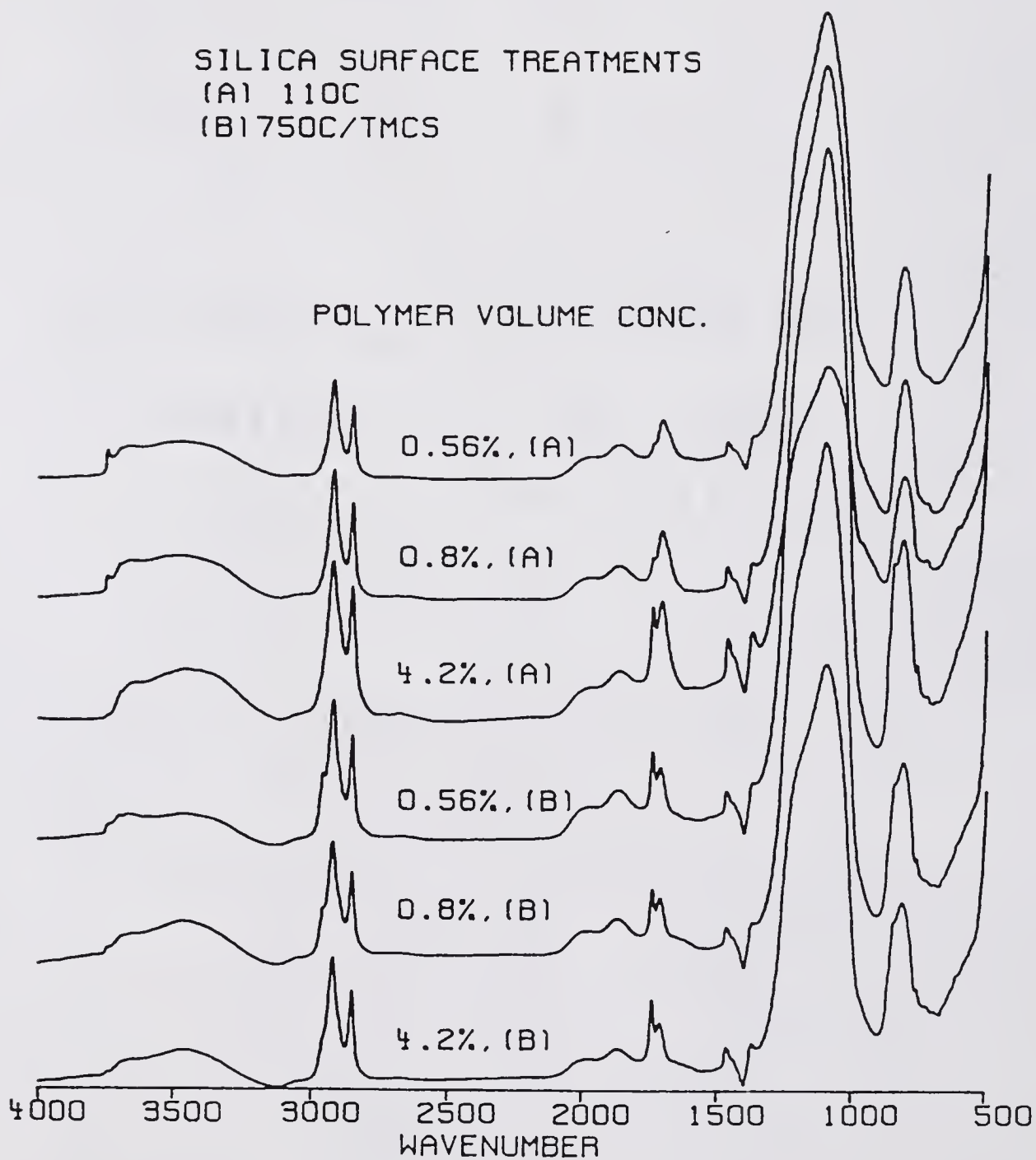


Figure 4.12 Effect of Volume Concentrations of Polymer Solution on the Extent of Polymer Adsorbed on 110°C and 750°C/TMCS Cab-O-Sil Silica Surfaces

the spectrum of [ 4.2%, (A) ], where the peak at  $3747\text{ cm}^{-1}$  forms hydrogen bonds with carbonyl groups and then completely disappears when enough polymer is adsorbed and coated on the silica surface.

When silica is  $750^{\circ}\text{C}/\text{TMCS}$  treated, most hydroxyl groups react with TMCS, with only few hydroxyl groups remaining on the silica surface available for the formation of hydrogen bonds with the carbonyl groups of the E-Va copolymer.

The relative amount of polymer adsorbed on the unit surface area of Cab-O-Sil silica (i.e., polymer adsorbed on silica surface/surface area of silica) is evaluated by the DRIFT technique and listed in Table 4.3. The amount of adsorbed polymer is estimated from the areas under the peaks of both hydrogen and non-hydrogen bonded carbonyl groups by FTIR spectroscopy. The amount of silica was determined from the area under the siloxane (Si-O) peak.

As shown in Table 4.3, when polymer is adsorbed on  $110^{\circ}\text{C}$  treated silica, the amount of polymer adsorbed on silica surface from a 4.2% volume polymer solution corresponds to the 0.086 percentage of adsorbed polymer per unit of surface area of silica, and the 0.56% volume polymer solution corresponds to the 0.025 percentage. The amount of bonded and/or adsorbed polymer per unit of surface area is increased (i.e., exhibits a thicker coating) when more polymer is available in polymer solution to allow bonding and/or adsorption onto the silica surface.

TABLE 4.3

AMOUNT OF POLYMER ADSORBED ON UNIT AREA OF SILICA SURFACE  
( ADSORBED POLYMER ON SILICA SURFACE/SILICA SURFACE AREA )

DATA WAS EVALUATED FROM FTIR SPECTROSCOPY  
BY DRIFT TECHNIQUE

POLYMER VOLUME CONC. FOR SILICA TO ADSORB POLYMER ON ITS SURFACE	SILICA TREATMENT	
	110°C	750°C/TMCS
4.2% VOL.*	0.086	0.054
0.8% VOL.	0.030	0.021
0.56% VOL.*	0.025	0.019

\*

4.2% VOL.: thick coating of polymer  
0.56% VOL.: thin coating of polymer

From Table 4.3, it is seen that with the same volume concentration of polymer solution available for polymer adsorbed on the silica surface, less polymer is adsorbed on silica subjected to heat/chemical treatments, especially when there is enough polymer available for adsorption. For example, in the case of the 4.2% volume polymer solution, the amount of polymer adsorbed on heat treated silica is about 1.6 times higher than the amount of polymer adsorbed on heat/chemically treated silica. This is very important information because it shows the impact of hydrogen bonding at the interface. It is inferred that the hydrogen bonding at the interface will play an important role on the mechanical and rheological properties of filled polymer composites being investigated in this study.

Therefore, it is interesting to study the polymer adsorption from the same volume concentration of polymer solution on the Cab-O-Sil silica subjected to different surface modifications. Figure 4.13 shows the polymer adsorbed from a 6.0% volume concentration of polymer solution on the heat and/or chemically treated Cab-O-Sil silica. Figure 4.14 shows Cab-O-Sil silica adsorbing polymer from a 2% volume concentration of polymer solution. The polymer bonded and/or adsorbed from different volume concentrations of polymer solution onto the Cab-O-Sil silica subjected to various surface modifications is shown in Figure 4.15.

6% VOL. OF POLYMER  
ONTO SILICA SURFACE

SURFACE TREATMENTS

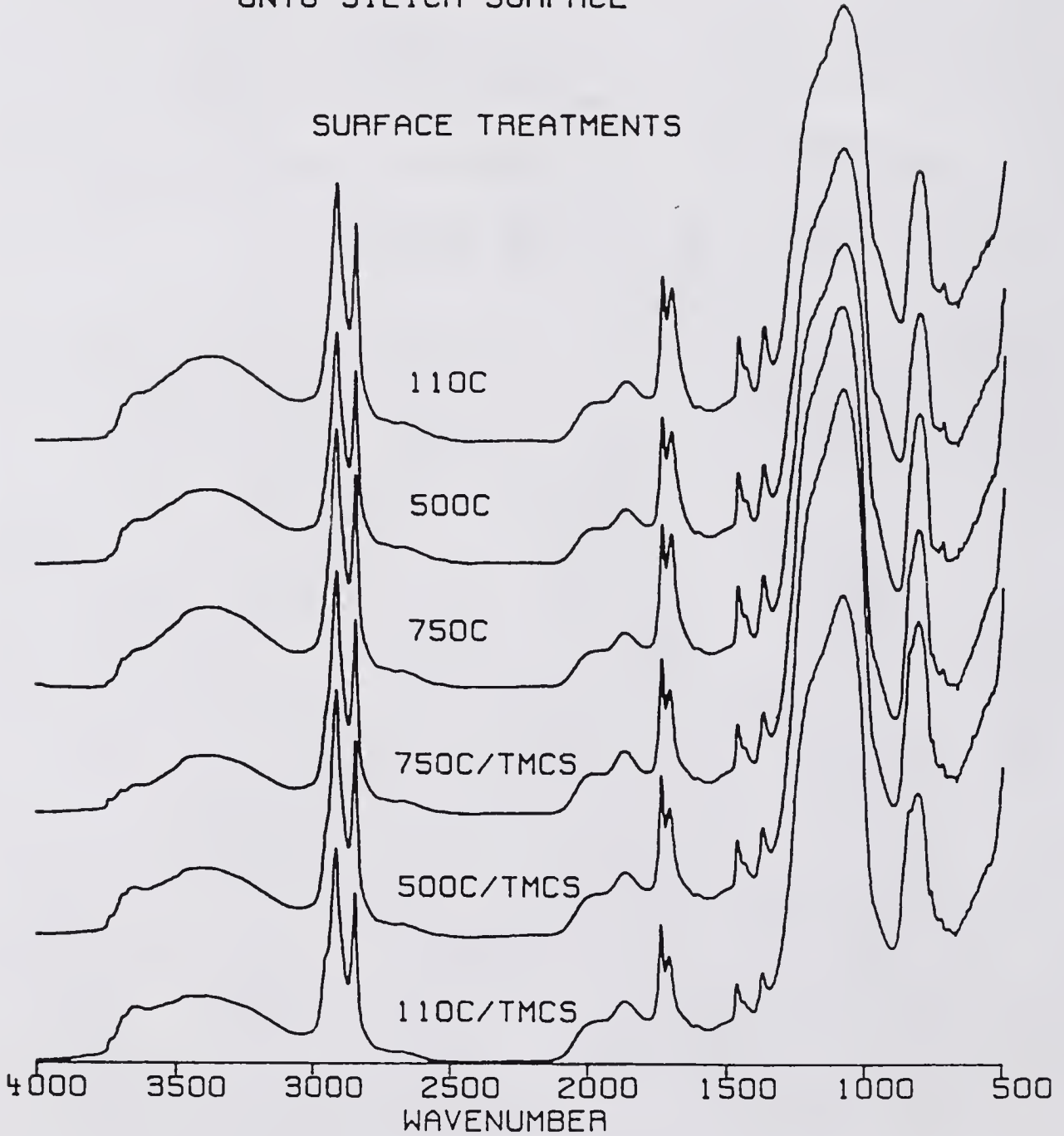


Figure 4.13 Effect of Silica Surface Properties on Polymer Bonded and/or Adsorbed on the Cab-O-Sil Silica Surface from 6% Volume of Polymer Solution

2% VOL. OF POLYMER  
ONTO SILICA SURFACE

## SURFACE TREATMENTS

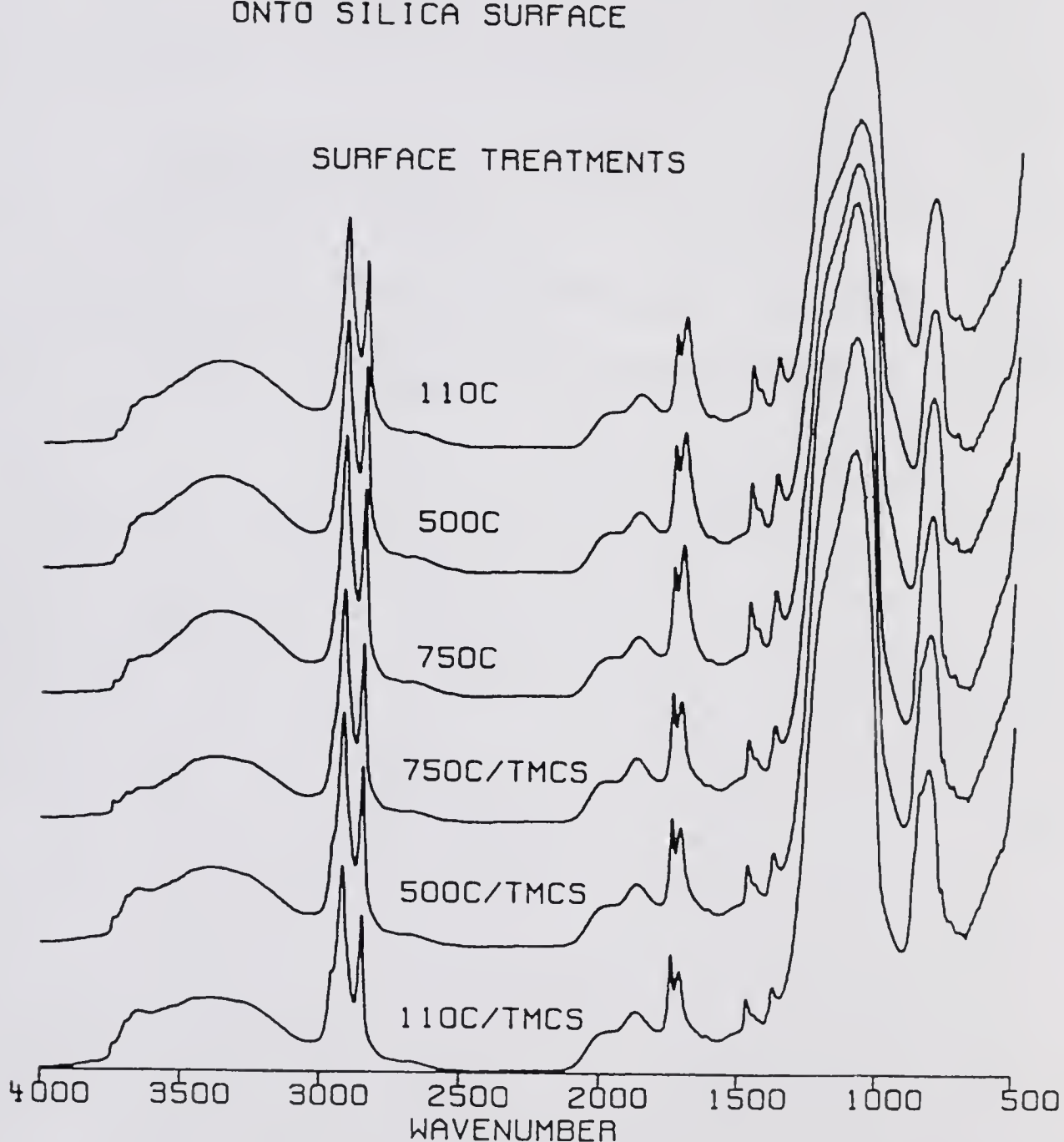


Figure 4.14 Effect of Silica Surface Properties on Polymer Bonded and/or Adsorbed on the Cab-O-Sil Silica Surface from 2% Volume of Polymer Solution

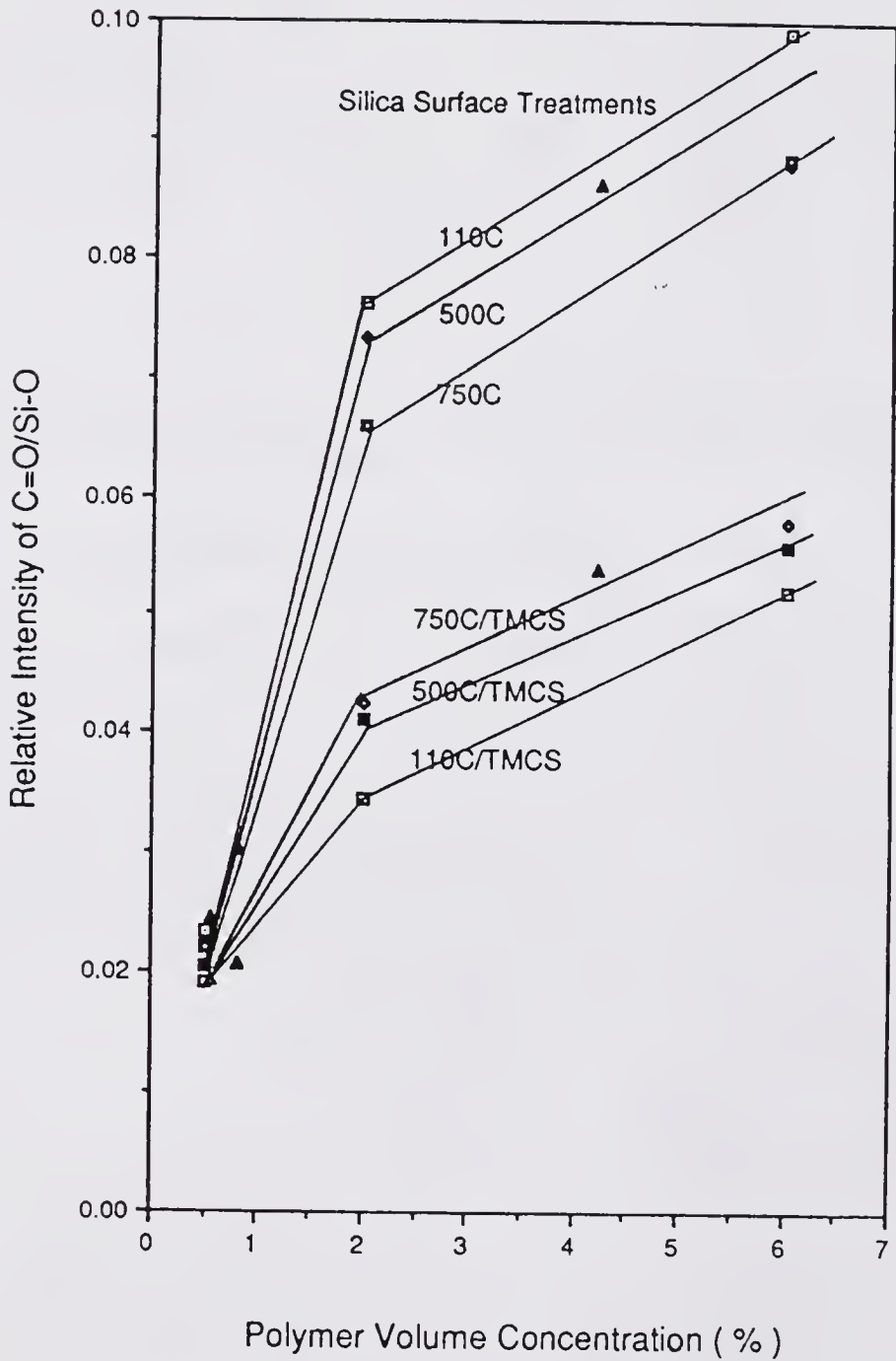


Figure 4.15 Effect of Silica Surface Properties and Volume Concentration of Polymer Solution on the Extent of Adsorbed Polymer per Unit Silica Surface

Two conclusions can be drawn from Figure 4.15. One is that the amount of bonded and/or adsorbed polymer is increased when polymer volume concentration is increased. Another is that the bonded and/or adsorbed polymer per unit of Cab-O-Sil silica surface area is gradually increased when the silica has more hydroxyl groups available to provide polymer to be bonded and/or adsorbed onto the silica surface. For example, the polymer adsorbed from 6% polymer volume concentration is about two times higher for the 110°C sample than in 110°C/TMCS. Figure 4.15 also indicates that the amount of polymer adsorbed on the silica surface shows a slow increase with the polymer volume concentration when it is above 2% polymer volume concentration.

Furthermore, it is interesting to study the extent of polymer bonded and/or adsorbed on the Cab-O-Sil silica surface versus the calculated work of adhesion, which is listed in Table 5.2. An exponential result is obtained in Figure 4.16. This indicates that the amount of polymer bonded and/or adsorbed onto the Cab-O-Sil silica surface from polymer solution exponentially increases with a linear increase in work of adhesion.

#### 4.4.3 Ratio of Hydrogen-Bonded to Non-Hydrogen-Bonded Carbonyl Group

The ratio of the area under the peak of the hydrogen-bonded carbonyl group to that of the non-hydrogen-bonded

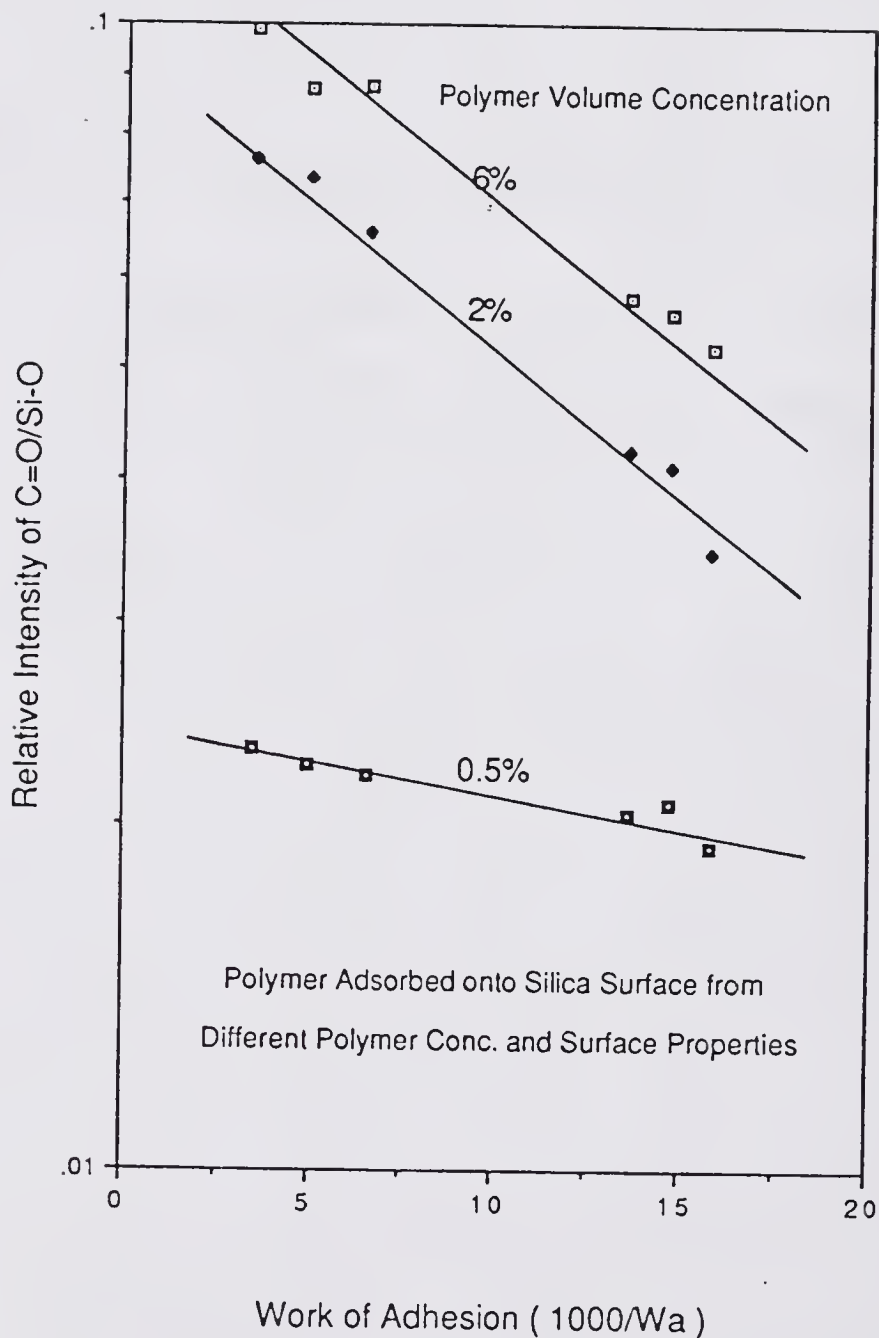


Figure 4.16 The Extent of Polymer Bonded and/or Adsorbed on the Silica Surface versus Work of Adhesion from Different Solution Concentrations

carbonyl group can be evaluated from Figure 4.11 using the deconvolution function within the FTIR software. The original overlapped peak of the non-hydrogen-bonded ( $1739\text{ cm}^{-1}$ ) and the hydrogen-bonded ( $1704\text{ cm}^{-1}$ ) carbonyl groups, is deconvoluted. The area under each of the deconvoluted peaks of the hydrogen and the non-hydrogen-bonded carbonyl groups is measured. The ratio between two carbonyl groups on the Cab-O-Sil silica treated at  $110^{\circ}\text{C}$ , which has more silanol groups on its surface, is expected to be higher than that on the silica treated by  $750^{\circ}\text{C}/\text{TMCS}$ , as determined from Figure 4.11.

Therefore, Figure 4.17 shows the relative amount of bonded and/or adsorbed polymer on the Cab-O-Sil silica treated at  $110^{\circ}\text{C}$ . By the deconvolution technique, the relative area ratios of hydrogen-bonded carbonyl to non-hydrogen-bonded carbonyl groups are 38.5, 16.5 and 2.8 corresponding to the polymer adsorbed from 0.56%, 0.8% and 4.2% volume concentration of polymer solution, respectively. In Figure 4.18, illustrating the adsorbed polymer on the silica with  $750^{\circ}\text{C}/\text{TMCS}$  treatment, the relative ratios are 1.25, 1.02 and 0.72 respectively. These ratios are listed in Table 4.4.

The ratio of hydrogen-bonded carbonyl to non-hydrogen-bonded carbonyl groups is decreased in either silica surface treatment when polymer volume concentration is increased. For polymer adsorption on the silica surfaces

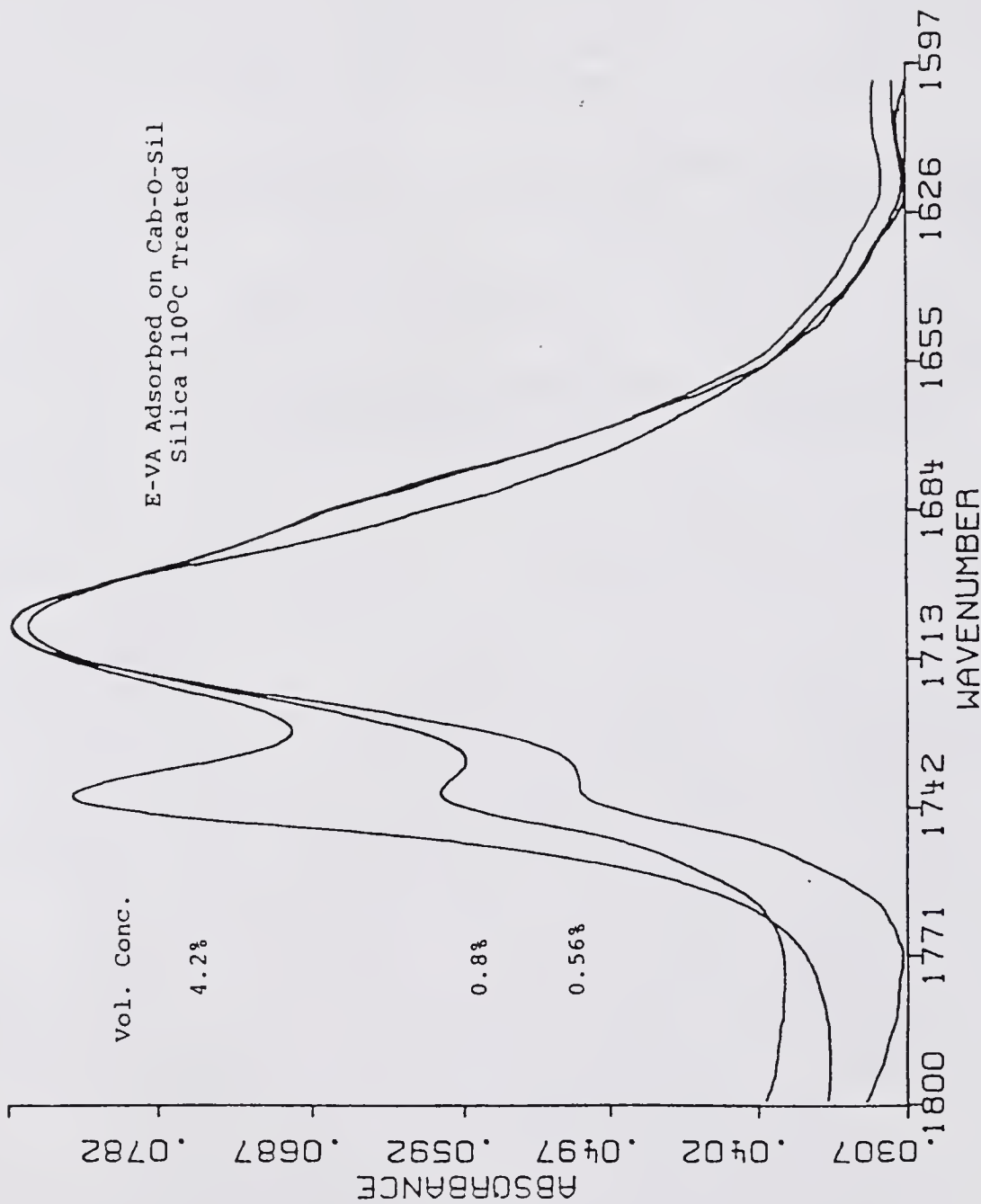


Figure 4.17 Effect of Concentrations of Polymer Solution on the Ratio of Hydrogen-Bonded to Non-Hydrogen-Bonded Carbonyl Groups of 110°C Treated Silica

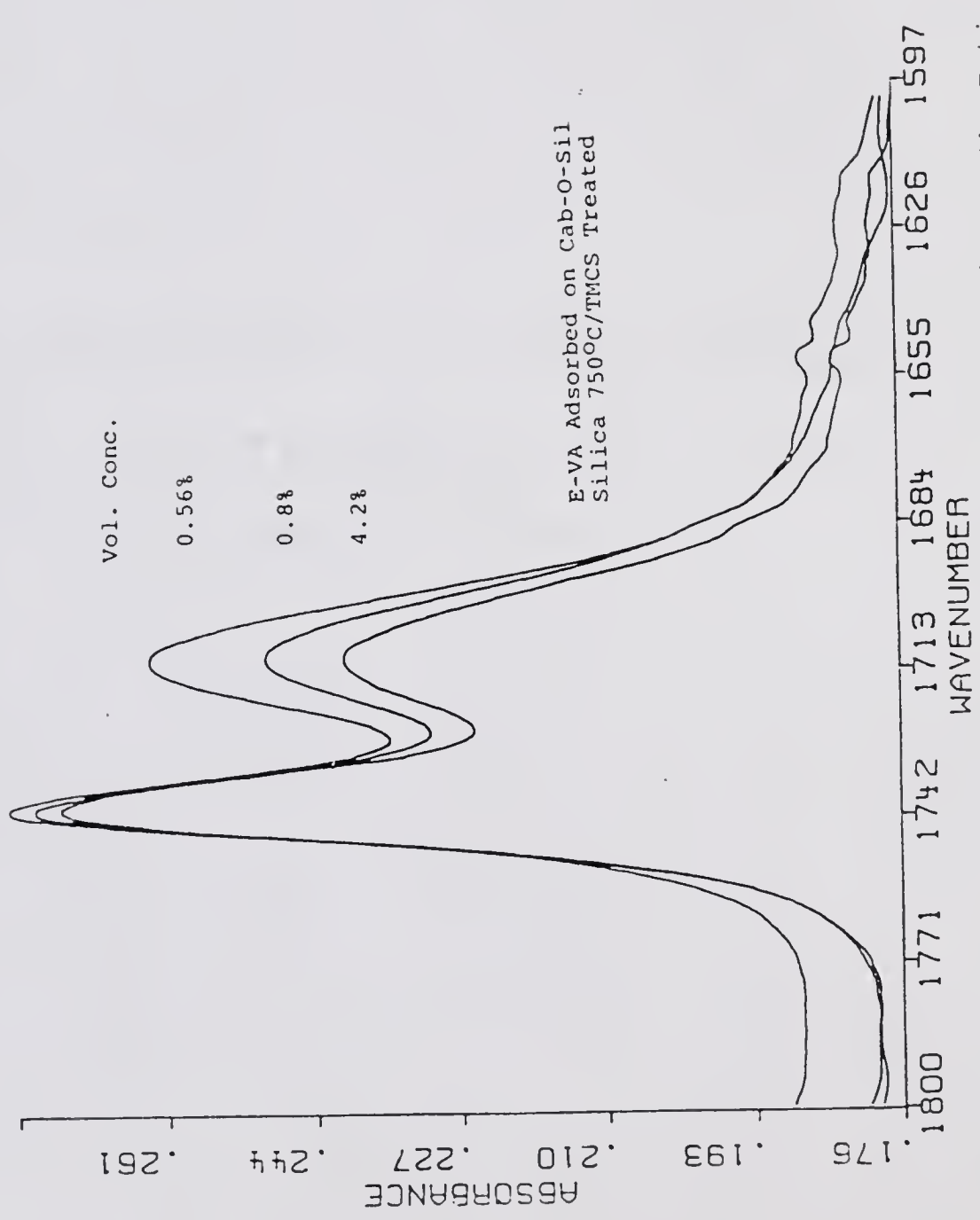


Figure 4.18 Effect of Concentrations of Polymer Solution on the Ratio of Hydrogen-Bonded to Non-Hydrogen-Bonded Carbonyl Groups of 750°C/TMCS Silica

TABLE 4.4

RATIO OF HYDROGEN-BONDED TO NON-HYDROGEN-BONDED  
CARBONYL GROUPS

DATA WAS MEASURED BY DRIFT TECHNIQUE AND EVALUATED BY  
DECONVOLUTION TECHNIQUE USING FTIR SOFTWARE PROGRAM

POLYMER VOLUME CONC. FOR SILICA TO ADSORB POLYMER ON ITS SURFACE	SILICA TREATMENT	
	110°C	750°C/TMCS
4.2% VOL.*	2.74	0.72
0.8% VOL.	16.45	1.02
0.56% VOL.*	38.50	1.25

\*

4.2% VOL.: thick coating of polymer

0.56% VOL.: thin coating of polymer

from a polymer solution, the higher concentration of polymer solution results in more polymer adsorbed per volume unit on the silica surfaces and, therefore, more non-hydrogen-bonding carbonyl contribution to the ratio.

This is confirmed by examining the silanol peak at  $3746\text{ cm}^{-1}$  in Figure 4.12: the spectrum of the E-Va adsorbed on silica treated at  $110^{\circ}\text{C}$  from a 0.56% polymer volume concentration [ 0.56%, (A) ] shows the silanol group peak at  $3746\text{ cm}^{-1}$ . However, when adsorbed from 4.2% volume concentration [ 4.2%, (A) ], the silanol groups are completely bonded and covered by polymer, i.e., have more multilayers of polymer adsorbed. Therefore, the 4.2% volume concentration has more non-hydrogen-bonded carbonyl contribution to the relative intensity ratio since the hydrogen bonding exists only on the contact surface of silica.

Combining the information available from Figures 4.17, 4.18 and Table 4.4, one can see that the order of the ratios of the hydrogen bonded carbonyl to non-hydrogen-bonded carbonyl group is different after different surface treatments.

Silica heated at  $110^{\circ}\text{C}$  has more hydrogen and/or polar bonding at the interface than silica with  $750^{\circ}\text{C}/\text{TMCS}$  treatment. The molecular packing of the polymer at the surface of the silica particles thus differs with varying surface properties of the silica. This results in

different densities and thicknesses of the interphase region. The dewetting mechanism and dewetted process under tensile testing, as well as the effective particle size of silica under rheological testing, are also different.

#### 4.5 Temperature Dependence of the Interfacial Bonding

The effect of temperature on the amount and strength of interfacial bonding is examined by the DRIFT technique. The E-Va copolymer is adsorbed from polymer solution on the surface of Cab-O-Sil silica at room temperature, leading to the formation of a thin layer of polymer molecules on the silica surface.

##### 4.5.1 Heating Effect on the Silica-Surface-Adsorbed Polymer

Figure 4.19 gives the spectra of the temperature effect on the polymer adsorbed on the 110°C treated silica particles. These spectra show that the peak intensity of the hydrogen-bonded C=O at 1704  $\text{cm}^{-1}$  is gradually reduced with increasing temperature. However, the peak intensity of the non-hydrogen-bonded C=O at 1739  $\text{cm}^{-1}$  simultaneously slowly increases with increasing temperature. Higher temperature increases the mobility of the polymer molecular chain, and thus both the extent and interaction energy of the interfacial bonding are changed. The hydrogen bonding strength at the interface is then varied when the environmental temperature is increased.

The peak wavenumber of the hydrogen-bonded C=O becomes higher with increasing temperature as shown in Figure 4.19.

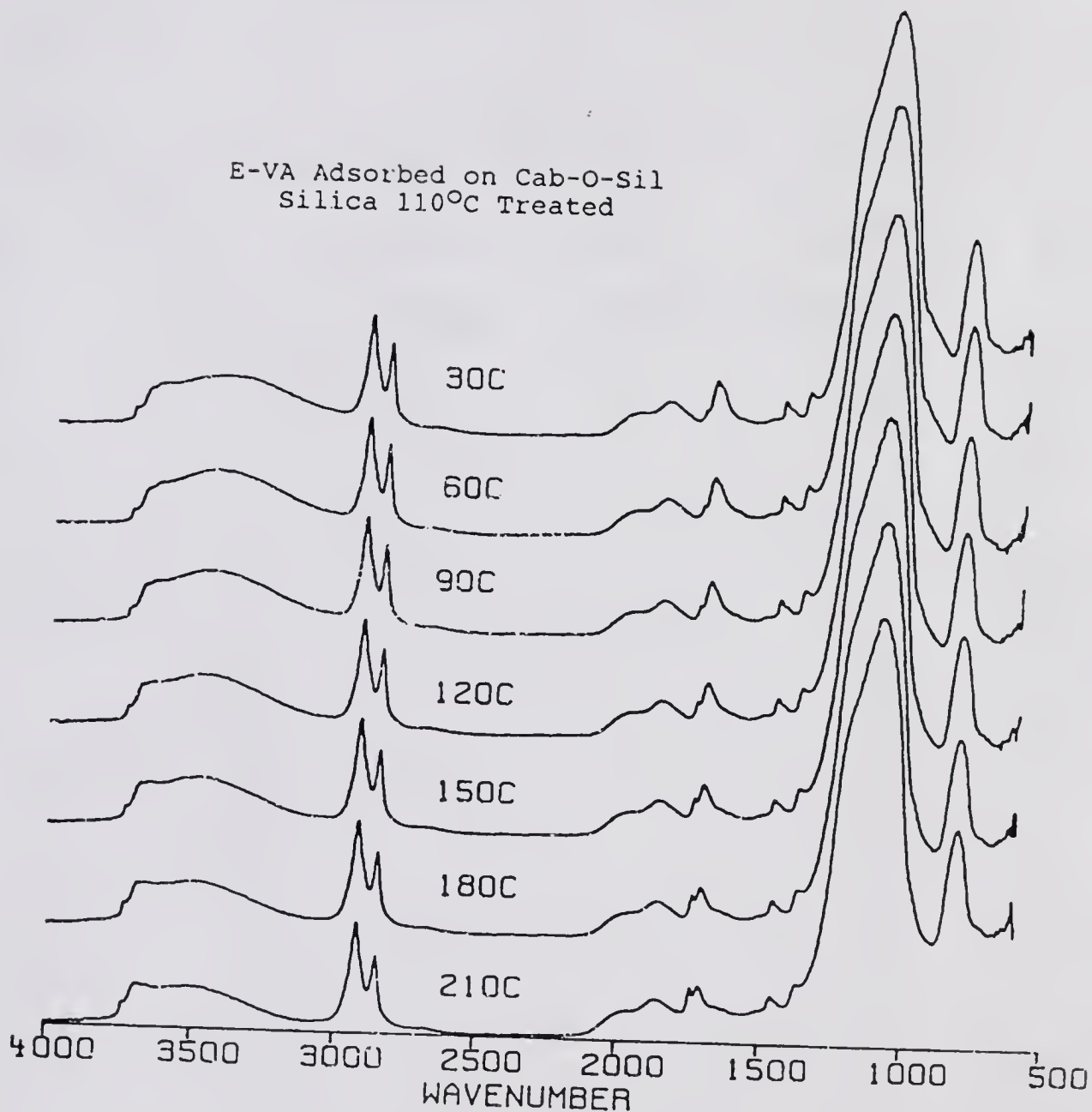


Figure 4.19 Effect of Environmental Temperature on the Carbonyl Groups Bonded/Adsorbed on the Cab-O-Sil Silica Treated at 110°C

However, the peak wavenumber of the free C=O peak does not change with temperature. This provides further evidence that the peak at  $1704\text{ cm}^{-1}$  is hydrogen-bonded C=O since the bonding energy and peak wavenumber do change in the range of temperature studies. Combining the information of peak wavenumber shift and peak intensity change illustrates that both interaction energy and extent of hydrogen bonding at the interface decrease with an increase in temperature.

Furthermore, some of the originally hydrogen-bonded carbonyl groups at the interface become debonded from silica surface at high temperature. The number of hydroxyl groups on the silica surface, unbonded by E-Va copolymer, will gradually increase and can be detected and identified by infrared spectroscopy. This is confirmed by Figure 4.20 which shows that the peak intensities of the isolated ( $3746\text{ cm}^{-1}$ ) and the hydrogen-bonded ( $3660\text{ cm}^{-1}$ ) hydroxyl groups gradually increase as the temperature increases.

The E-Va copolymer adsorbed on the  $750^{\circ}\text{C}/\text{TMCS}$  treated silica is also studied for comparison and this is shown in Figure 4.21. The temperature effect on the hydrogen bonding at this interface is similar to the case with the polymer adsorbed on the  $110^{\circ}\text{C}$  treated silica, except that the peak at  $1704\text{ cm}^{-1}$  due to hydrogen-bonded C=O is much smaller. The increase in the intensity of hydroxyl groups on the  $750^{\circ}\text{C}/\text{TMCS}$  treated silica surface due to an increase in temperature is shown in Figure 4.22. The increase in

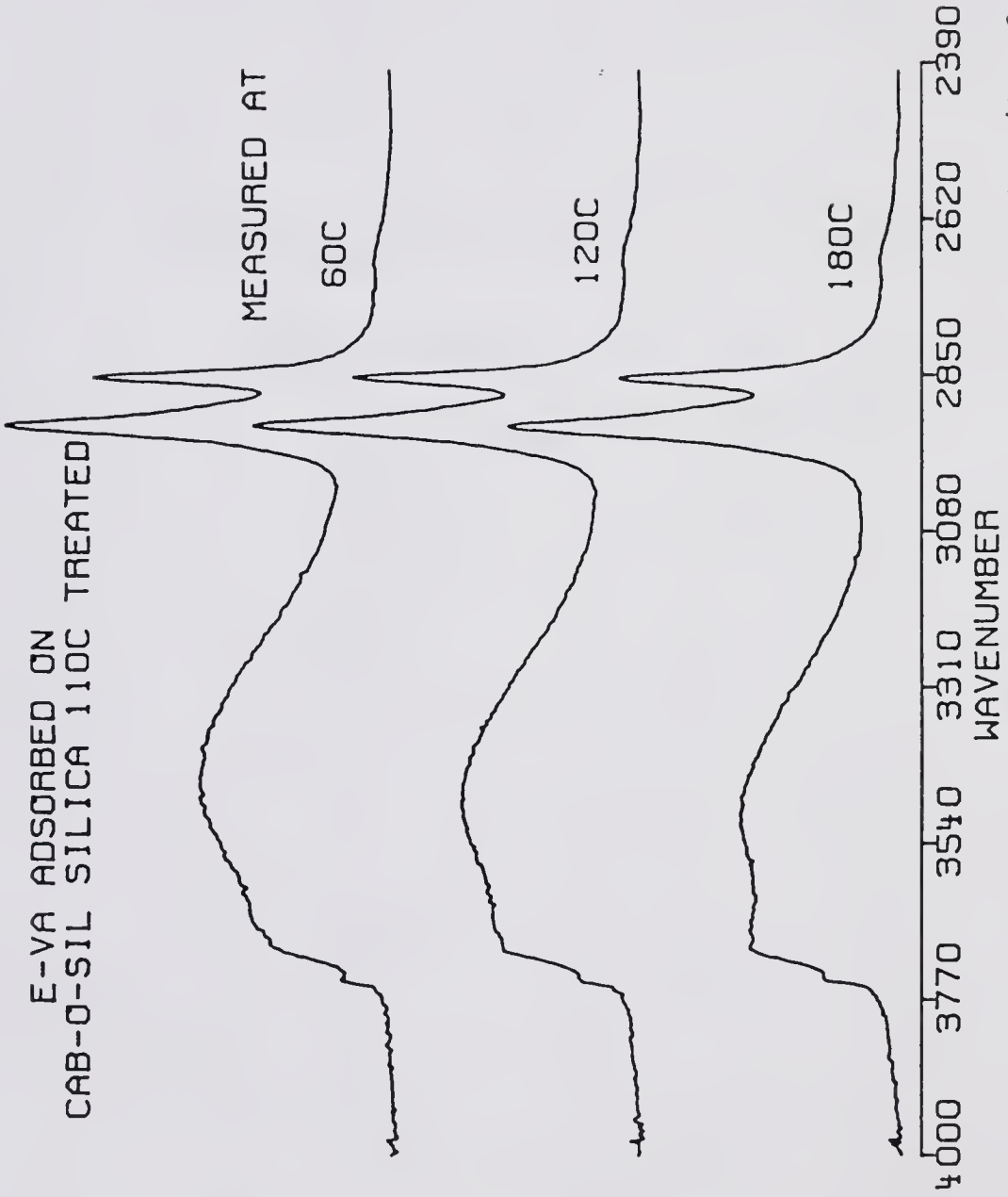


Figure 4.20 Effect of Environmental Temperature on the Intensity of Hydroxyl Groups of the Cab-O-Sil Silica Treated at 110°C

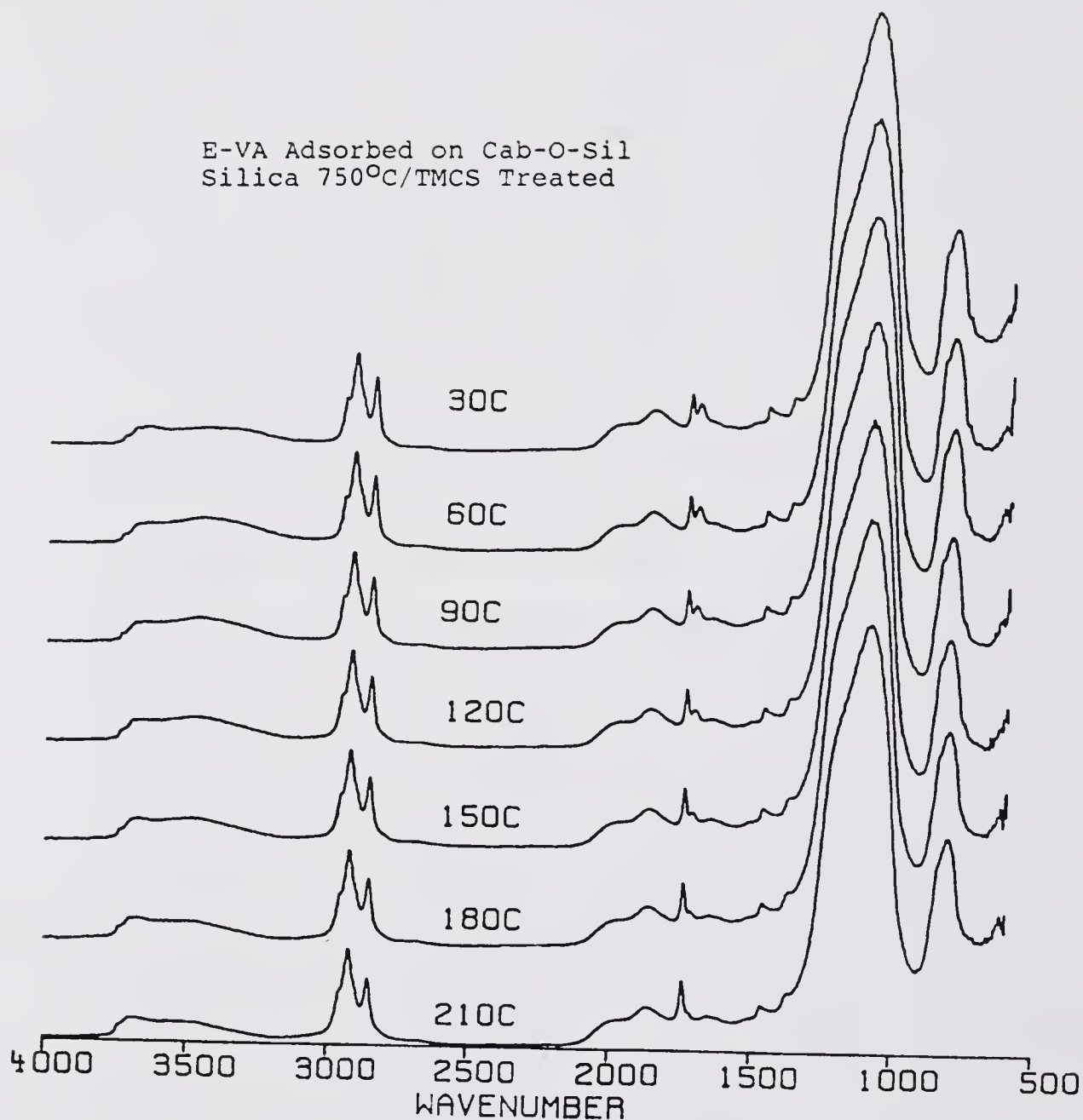


Figure 4.21 Effect of Environmental Temperature on the Carbonyl Groups Bonded/Adsorbed on the Cab-O-Sil Silica Treated by 750°C/TMCS

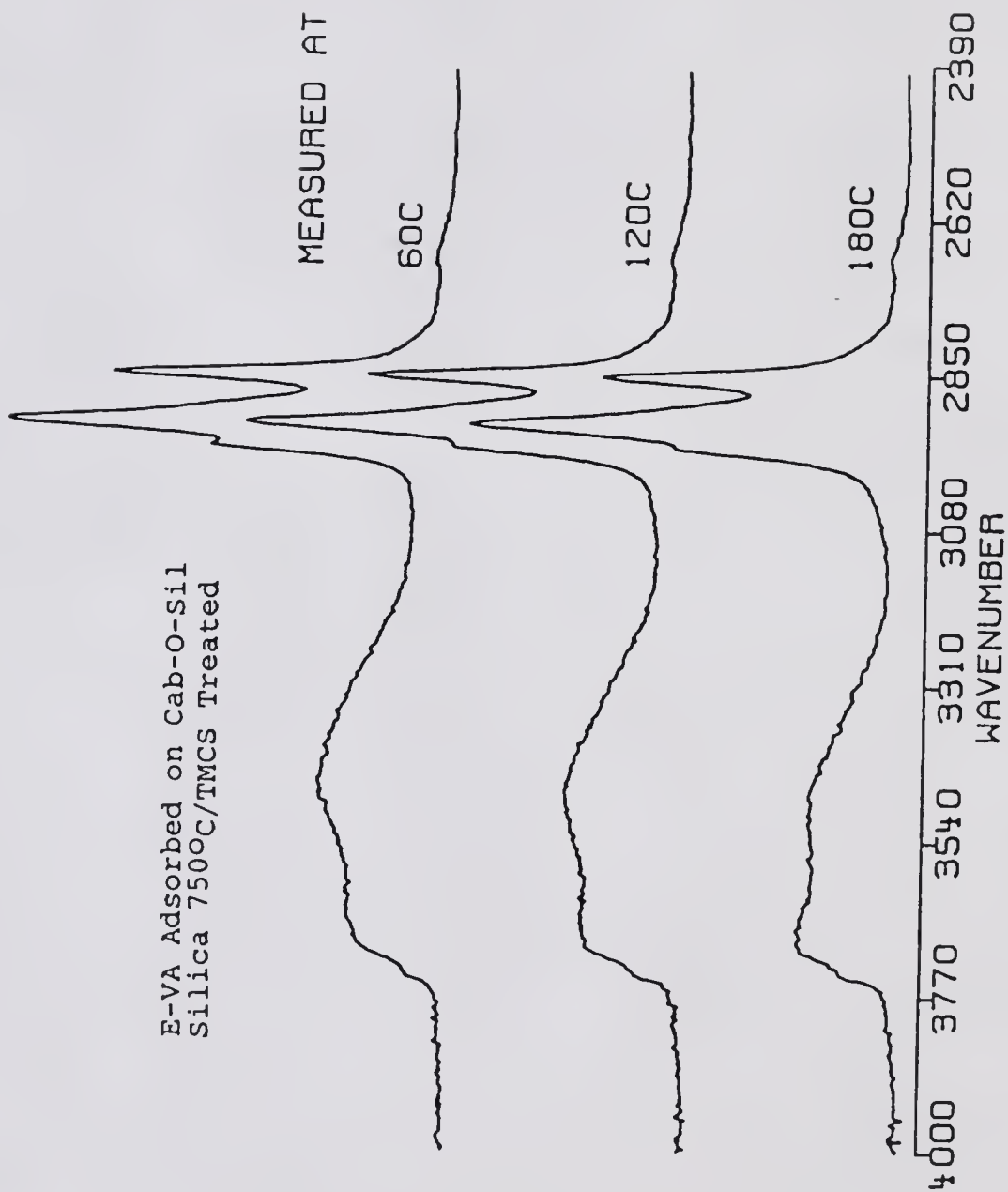


Figure 4.22 Effect of Environmental Temperature on the Intensity of Hydroxyl Groups of the Cab-O-Sil Silica Treated by 750°C/TMCS

the number of hydroxyl groups is few since there are originally not many hydrogen bonds at the interface. Thus, the information from Figures 4.20 and 4.22 suggests that both the isolated and the hydrogen-bonded hydroxyl groups on the silica surface may form hydrogen bonds with the carbonyl groups of the E-Va copolymer.

#### 4.5.2 Cooling Effect on the Silica-Surface-Adsorbed Polymer

Polymer adsorbed onto the silica particles is prepared from polymer solution at room temperature. The cooling processes of this silica-surface-adsorbed E-Va copolymer from a high temperature to a low temperature are interesting. The results of cooling the E-Va polymer adsorbed on 110°C treated silica are shown in Figure 4.23. The peak of hydrogen-bonded C=O returns to its original peak intensity and wavenumber when the temperature is brought back down to room temperature. This indicates that the hydrogen bonding between the silica surface and the E-Va copolymer is a reversible process. However, the studied high temperature can not be higher than the thermal degradation temperature of polymer.

Figure 4.24 shows the cooling processes of the E-Va copolymer adsorbing on the Cab-O-Sil silica treated by 750°C/TMCS. The trends of cooling processes are similar to those in the system with good interfacial bonding. In Figure 4.24, the hydrogen bonding also returns to its original peak intensity and wavenumber when the temperature

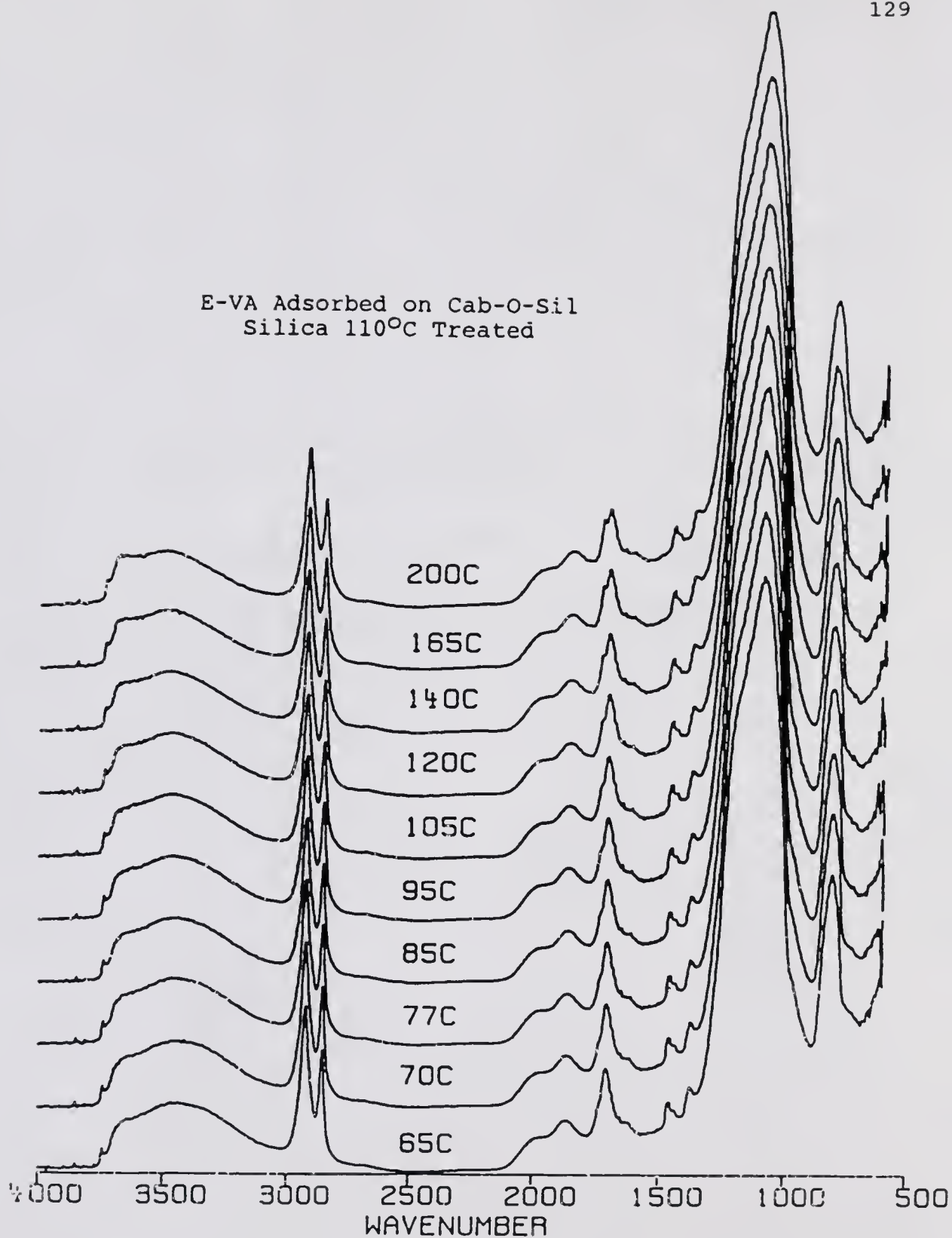


Figure 4.23 FTIR Spectrum of Temperature Cooling Process on the Hydrogen-Bonded Carbonyl Groups Adsorbed on the Cab-O-Sil Silica Treated at 110°C

E-VA Adsorbed on Cab-O-Sil  
Silica 750°C/TMCS Treated

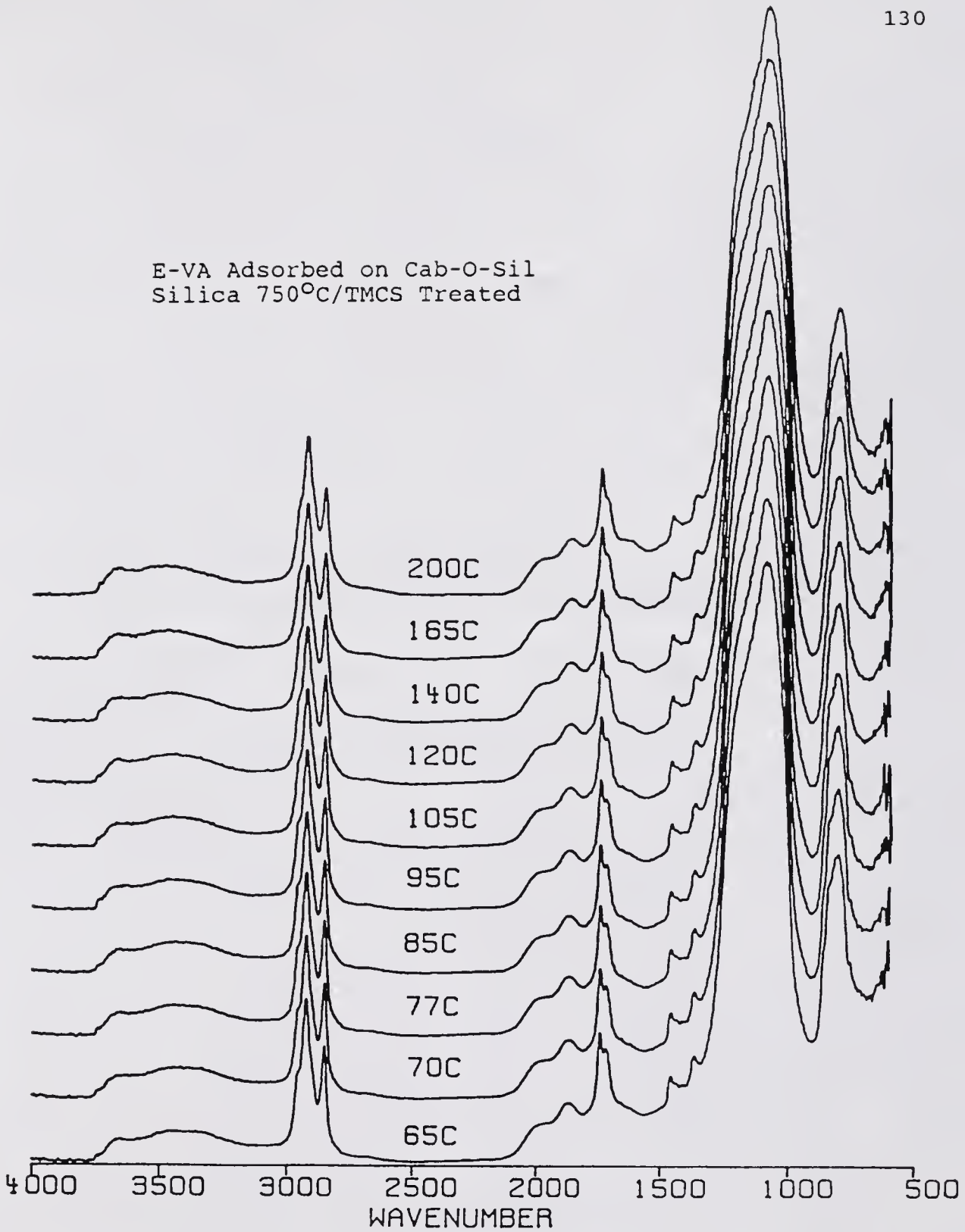


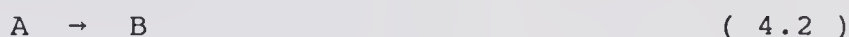
Figure 4.24 FTIR Spectrum of Temperature Cooling Process on the Hydrogen-Bonded Carbonyl Groups Adsorbed on the Cab-O-Sil Silica Treated by 750°C/TMCS

drops from a high temperature to a low temperature, but the peak intensity of the hydrogen-bonded C=O group is smaller than that of the silica treated at 110°C.

#### 4.5.3 Quasi-Equilibrium Constant of Hydrogen Bonding

##### 4.5.3.1 Thermodynamic approach

From a thermodynamic approach, the equilibrium constant of a reaction can be expressed as



$$K = \frac{[ B ]}{[ A ]} \quad ( 4.3 )$$

where

$K$  = is the equilibrium constant

$[ A ]$  = is the concentration of reactant A

$[ B ]$  = is the concentration of product B

The equilibrium constant can vary with temperature according to the Gibbs-Helmholtz equation (235)

$$\frac{d \ln K}{dT} = \frac{\Delta H}{RT^2} \quad ( 4.4 )$$

where

$K$  = is the equilibrium constant of reaction

$\Delta H$  = is the heat of reaction

$R$  = is the gas constant

$T$  = is the absolute temperature (K)

The relationship between equilibrium constant and temperature is dependent on the heat of reaction.

$$\Delta H = \int \Delta C_p \, dT + \Delta H_0 \quad ( 4.5 )$$

where

$\Delta C_p$  = is the heat capacity (cal mole<sup>-1</sup> degree<sup>-1</sup>)

$\Delta H_0$  = is the heat of reaction at a reference temperature (cal mole<sup>-1</sup>)

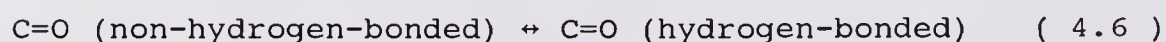
In other words, the relationship between equilibrium constant and temperature is dependent on the relative magnitudes of  $\Delta C_p$  and  $\Delta H_0$ .

The logarithm of the equilibrium constant will be linearly proportional to the reciprocal of the temperature if  $\Delta H$  is insensitive to the temperature in the range of study.

However, the linear relationship may not hold if the heat of reaction is temperature dependent.

#### 4.5.3.2 Temperature dependence of the quasi-equilibrium constant of hydrogen bonding at the interface

The change of equilibrium constant of hydrogen bonding at the interface with temperature can be expressed as



$$K = \frac{[ \text{C=O (hydrogen-bonded)} ]}{[ \text{C=O (non-hydrogen-bonded)} ]} \quad ( 4.7 )$$

where

$K =$  is the quasi-equilibrium constant of hydrogen bonding.

$[ \text{C=O (hydrogen-bonded)} ] =$  is the concentration of hydrogen-bonded carbonyl groups.

$[ \text{C=O (non-hydrogen-bonded)} ] =$  is the concentration of non-hydrogen-bonded carbonyl groups.

The numerator and denominator of the right-hand side of Equation 4.7 are concentrations, which are evaluated by the deconvolution technique and measured from the area under each peak from the FTIR software program. The values of concentrations of hydrogen-bonded and non-hydrogen-bonded carbonyl groups are evaluated at several different temperatures for study of the equilibrium constant.

The logarithm values of the ratio of hydrogen-bonded C=O to non-hydrogen-bonded C=O are plotted against reciprocal temperatures. Figure 4.25 shows these logarithm values of the equilibrium constant of hydrogen bonding versus reciprocal temperature for the cases of silica treated at 110°C and 750°C/TMCS. Obviously, the slopes are linear and parallel each other when temperature is below 120°C. The linear relationship does not hold at high temperatures, with the experimental points being localized below the extrapolated lines. This means that the decrease in the number of hydrogen bonds at the interface is faster at high temperatures than at low temperatures.

The temperature dependence of heat of reaction may be one of reasons for this phenomenon. The conformation and

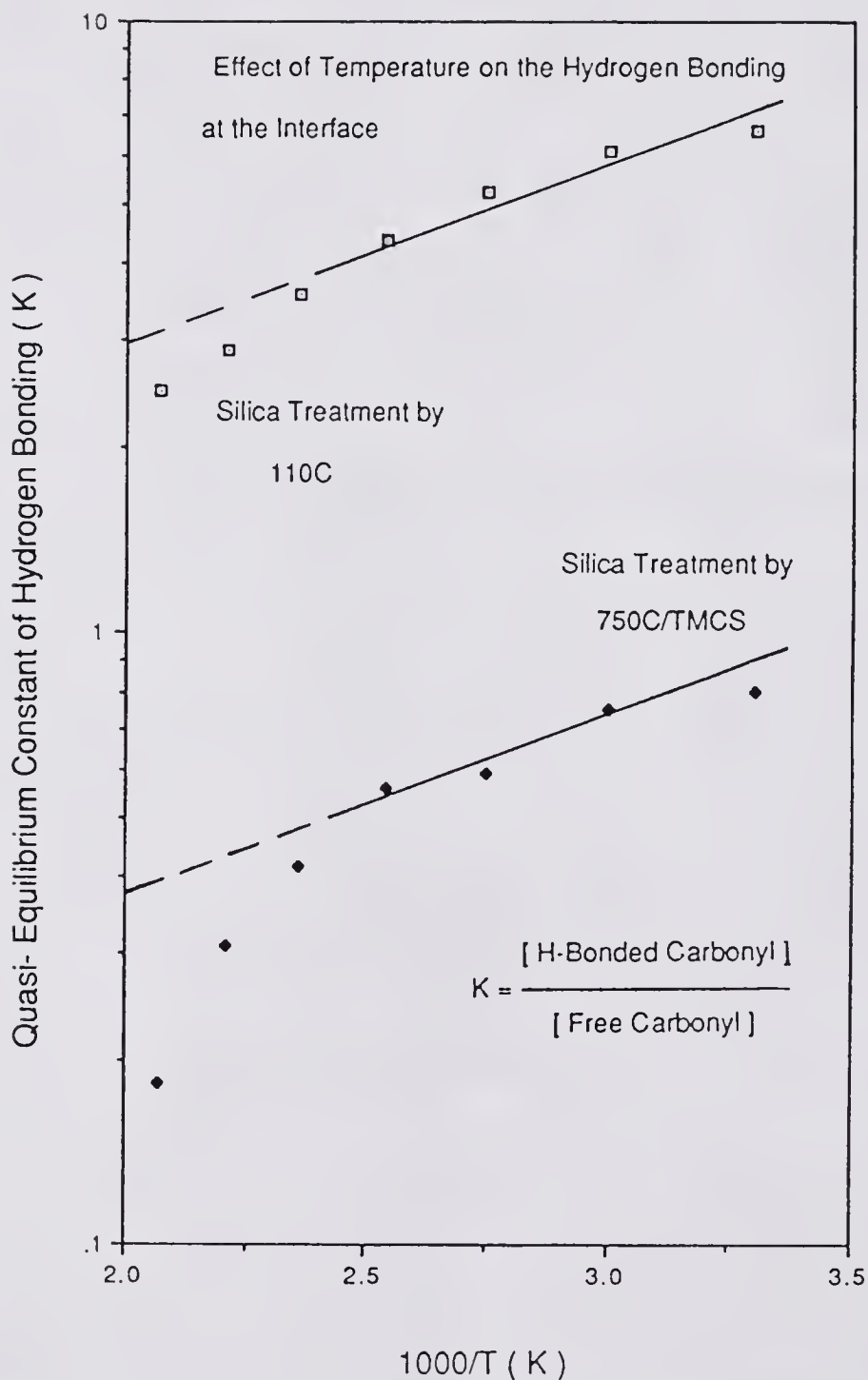


Figure 4.25 Quasi-Equilibrium Constant between Hydrogen-Bonded and Non-Hydrogen-Bonded Carbonyl Groups at the Interface

mobility of polymer molecules are also affected by temperature, which may influence the hydrogen bonding at the interface. The heating rate used to study temperature effect, especially at high temperatures, may cause local hot spots around the silica surface, and true equilibrium of hydrogen bonding at the interface may never be reached. Meanwhile, the carbonyl groups on the adsorbed layers, which do not really come into contact with silica surface, may also contribute to the peak intensity of non-hydrogen-bonded carbonyl groups.

Due to these reasons, the equilibrium constant obtained by DRIFT, combining with deconvolution technique from FTIR software, may not be the true equilibrium constant. Thus, in this study the quasi-equilibrium constant may be the correct term to describe the temperature effect of the hydrogen bonding equilibrium at the interface.

Since Figure 4.26 showed the change in quasi-equilibrium constant with temperature, it seems that the quasi-equilibrium constant is linearly proportional to reciprocal temperature. The number of hydrogen bonds at the interface is reduced when the temperature is increased, and the ratio is a linear relationship to the temperature. Shenoy and Saini in their studies of polymer-filler interaction also found that there was a linear relationship between the extent of polymer-filler interaction and reciprocal temperature (165).

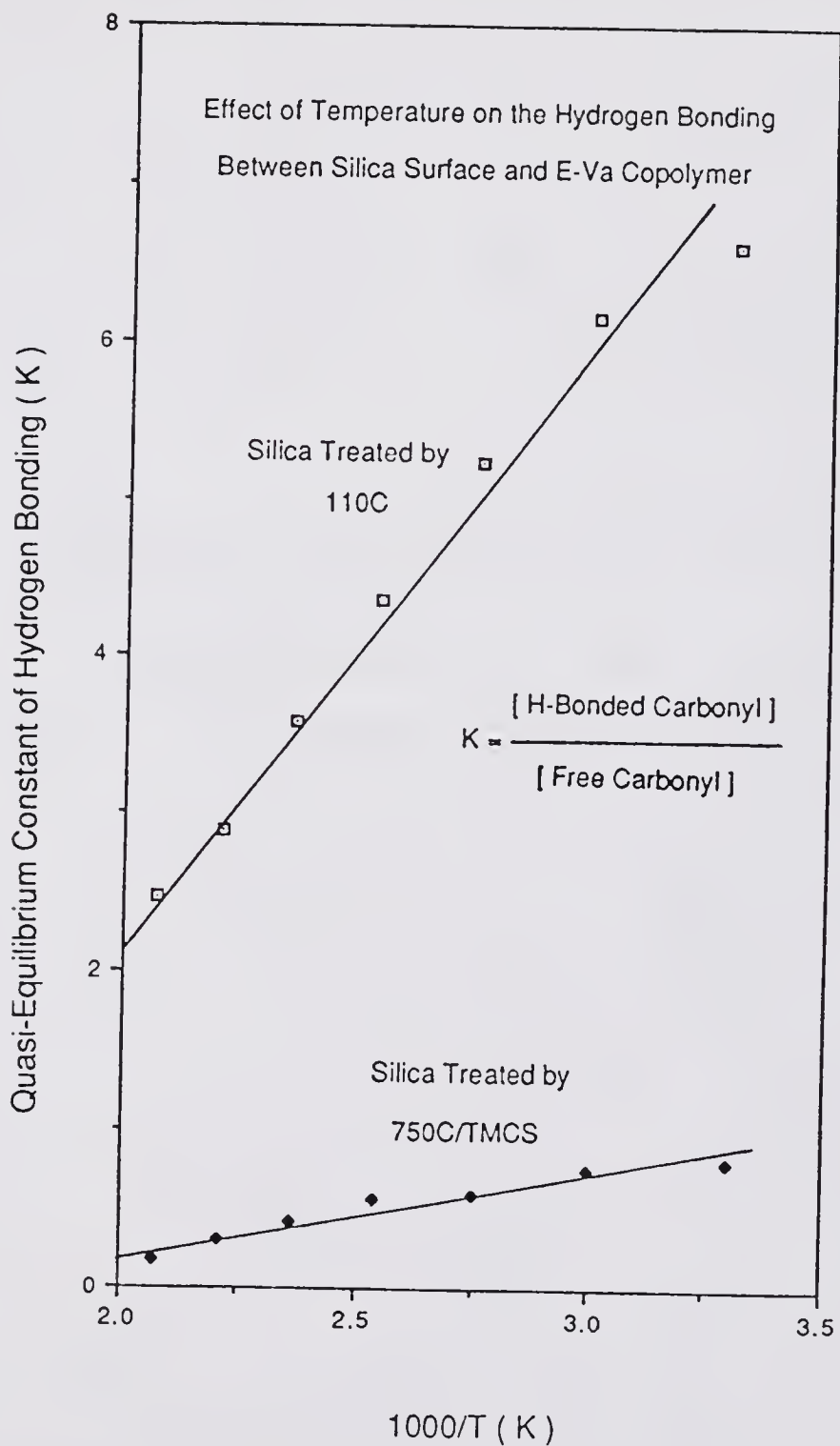


Figure 4.26 Effect of Temperature on the Quasi-Equilibrium Constant bet. Hydrogen-Bonded and Non-Hydrogen-Bonded Carbonyl Groups at the Interface

## CHAPTER 5 RESULTS

### 5.1 Work of Adhesion between Silica Particles and E-Va Copolymer

The bonding strength across an interface between silica surface and E-Va copolymer can be evaluated by work of adhesion ( $W_a$ ),

$$W_a = W_a^d + W_a^h \quad ( 5.1 )$$

The  $W_a^h$  is mainly contributed from hydrogen bonding at the interface between silica and E-Va copolymer. Thus, the  $W_a^h$  is used to replace the  $W_a^p$  which is used in Chapter 2.

The dispersion component of the work of adhesion in this study is evaluated from the dispersion component of the surface energy of each phase via contact angle measurements (18,29,80). However, the evaluation of the hydrogen and/or polar component of the work of adhesion is either from a combination of the DRIFT technique and titration measurements or from contact angle measurements, depending on the strength of the interfacial bonding.

#### 5.1.1 Work of Adhesion of Weak Interfacial Bonding

For those composites in which there is little or no hydrogen and/or polar bonding between silica and E-Va

copolymer,  $W_a$  is determined using the following equations

$$W_a^d = 2( \tau_f^d \tau_p^d )^{1/2} \quad ( 5.2 )$$

$$W_a^h = 2( \tau_f^h \tau_p^h )^{1/2} \quad ( 5.3 )$$

Where  $\tau$  is surface free energy, d refers to the dispersion component and h refers to the hydrogen and/or polar component. Subscripts f and p represent the silica filler particles and the E-Va copolymer, respectively.

The contact angles of distilled water and methylene iodide on amorphous quartz plates with different surface modifications are shown in Table 4.1. The  $\tau_s^d$  and  $\tau_s^h$  of heat and/or chemical treatments on the amorphous quartz plates are calculated by substituting these contact angles in equation (2.26) and are shown in Table 5.1. There is little change in  $\tau_s^d$ , but the change in  $\tau_s^h$  is much greater, since most of the hydroxyl groups are replaced by non-polar methyl groups. The values of surface energy ( $\tau_s$ ) are obtained by adding each component of the surface energy and are also listed in Table 5.1. The same procedures are also applied to the E-Va copolymer to obtain each component of surface energy and these data are also shown in Table 5.1.

$W_a^d$  and  $W_a^h$  are calculated from the components of surface energy of the silica and the E-Va copolymer by equations ( 5.2 ) and ( 5.3 ), respectively. The work of

adhesion and its components for the weak hydrogen bonding systems (110°C/TMCS, 500°C/TMCS, and 750°C/TMCS) at the interface are shown in Table 5.2.

### 5.1.2 Work of Adhesion of Strong Interfacial Bonding

For systems which exhibit strong hydrogen and/or polar bonding,  $W_a^d$  is also evaluated by equation ( 5.2 ); however, a different model is used to calculate  $W_a^h$ . The model was proposed by Fowkes (24,28) and yielded the following equation

$$W_a^h = f \cdot \Delta H^{ab} \cdot \text{moles of acid-base pairs/unit area} \quad ( 5.4 )$$

$$\Delta H^{ab} \text{ ( KJ/mole )} = 1.00 \cdot \Delta \nu_{c=O} \text{ ( KJ/mole/cm}^{-1} \text{ )} \quad ( 5.5 )$$

When Fowkes's equation is used in this system,  $\Delta H^{ab}$  is the interfacial bonding energy of one mole of acid-base pairs between hydroxyl groups and carbonyl groups. Acid-base pairs per unit area is the extent of the hydroxyl groups on the silica surface which forms hydrogen bonds with the carbonyl groups of polymer.  $f$  is a conversion factor, which usually equals 1.

The  $\Delta \nu_{c=O}$  is the wavenumber shift of the carbonyl stretching band of the polymer which occurs upon hydrogen bond formation (24,28). In Figure 4.11, this wavenumber shift is 35  $\text{cm}^{-1}$ . According to equation ( 5.5 ), it indicates that  $\Delta H$  is equal to 8.3  $\text{Kcal mole}^{-1}$  of acid-base pairs.

TABLE 5.1

SURFACE ENERGY OF SILICA AND E-VA COPOLYMER  
EVALUATED BY CONTACT ANGLES

	Surface Energy ( dyne cm <sup>-1</sup> )					
	110°C	500°C	750°C	750°C TMCS	500°C TMCS	110°C TMCS
$\tau_s$	74±1	72±1	60±2	40±1	33±2	27±1
$\tau_s^h$	60	56	38	17	10	06
$\tau_s^d$	14	16	22	23	23	21
	E-Va Copolymer			H <sub>2</sub> O	MI	
$\tau_s$	35±1			72.8	50.8	
$\tau_s^h$	07			50.7	6.7	
$\tau_s^d$	28			22.1	44.1	

TABLE 5.2

CALCULATED WORK OF ADHESION ( erg cm<sup>-2</sup> )

## Cab-O-Sil Silica / E-Va Copolymer

	110°C	500°C	750°C	750°C TMCS	500°C TMCS	110°C TMCS
Wa	292±3	205±2	154±2	73±2	68±3	63±2
Wa <sup>h</sup>	251	163	105	20	17	13
Wa <sup>d</sup>	41	42	49	53	51	50
Wa <sup>h</sup> /Wa	0.86	0.79	0.68	0.27	0.25	0.20

## Stöber Silica / E-Va Copolymer

	110°C	500°C	750°C	750°C TMCS	500°C TMCS	110°C TMCS
Wa	301±3	210±2	158±3	73±2	68±3	63±2
Wa <sup>h</sup>	260	168	109	20	17	13
Wa <sup>d</sup>	41	42	49	53	51	50
Wa <sup>h</sup> /Wa	0.86	0.80	0.69	0.27	0.25	0.20

The number of hydroxyl groups per unit square nanometer on the surface of both Cab-O-Sil and Stöber silica achieved with various surface modifications is shown in Table 4.2. The concentration of surface hydroxyl groups obtained by heat treatment on either the Stöber silica or the Cab-O-Sil silica is approximately the same. It is reported that a polymer with only 0.2 to 0.5% by weight carbonyl groups will occupy all the available surface sites, if the surface contains one hydroxyl group per square nanometer and the conditions permit sufficient time and mobility for carbonyl groups to be able to migrate to the preferred adsorption sites (236).

The  $W_a^h$  of the strong hydrogen bonding is obtained after the acid-base interaction energy and the surface concentration of the hydroxyl groups are substituted into equations ( 5.4 ) and ( 5.5 ). The values of  $W_a^h$  of the strong interfacial bonding (110°C, 500°C, 750°C) are also shown in Table 5.2.

### 5.1.3 Work of Adhesion and Surface Energy of Silica Particles

It is seen from Tables 5.1 and 5.2 that the value of the work of adhesion is increased when the surface energy of silica is increased. The relationship between the work of adhesion and the surface energy of silica is shown in Figure 5.1. The  $W_a$  increases rapidly when  $\gamma_s$  increases.

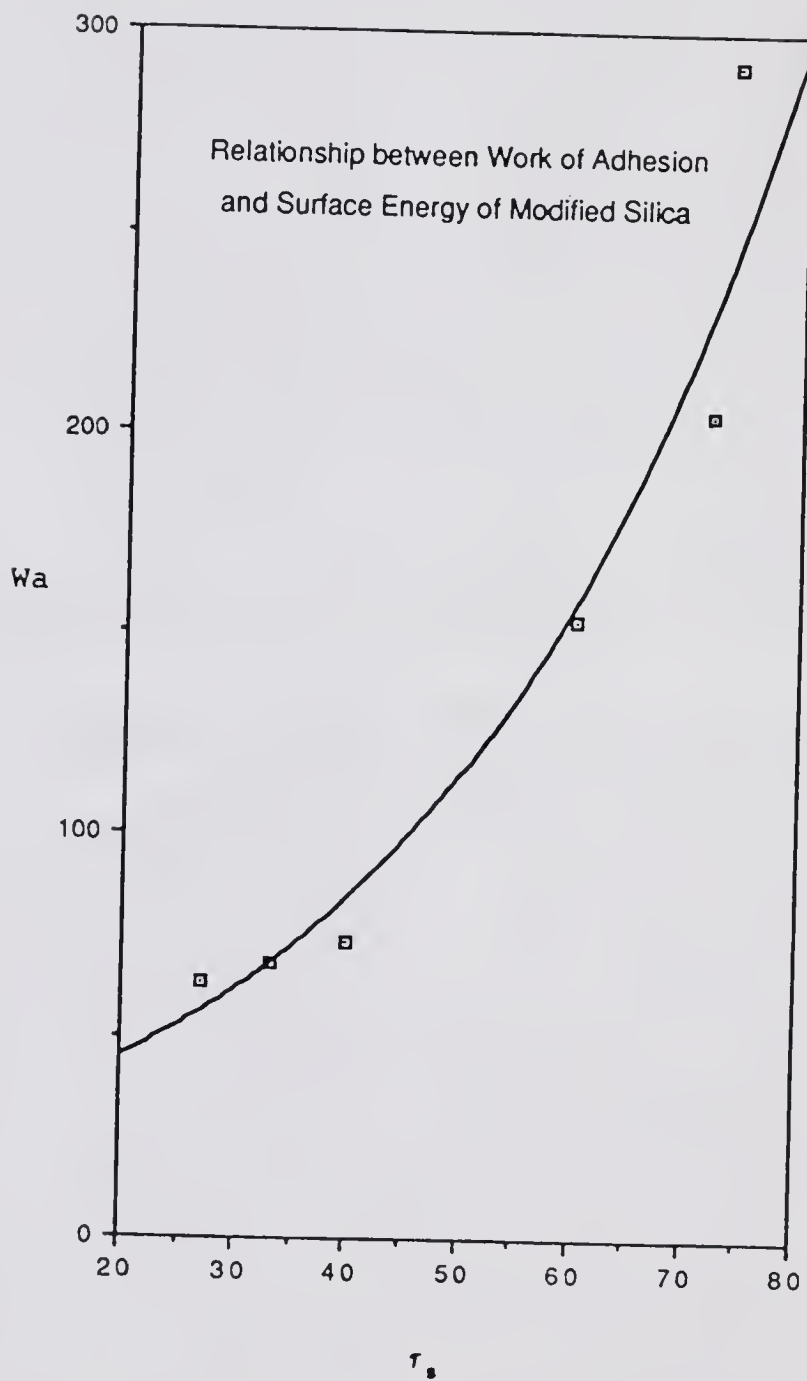


Figure 5.1 Work of Adhesion versus Surface Energy of Silica

Table 5.1 shows that the hydrogen bonding component of surface energy in the 110°C/TMCS treated silica surface is only 6 dyne cm<sup>-1</sup>. The  $\tau_s^h$  of silica surface may be reduced to an even lower value than that value by other methods of surface modification, and thus the  $\tau_s$  is also reduced. According to equation ( 5.3 ), the work of adhesion will, therefore, become lower if the  $\tau_s$  decreases.

The relationship between the work of adhesion and the surface energy of silica is, therefore, a monotonic function. That is, there is no inversion point of the work of adhesion between the maximum and minimum of the surface energies of silica in this system. In other words, the work of adhesion increases whenever the interfacial bonding is stronger.

When the numerical values of interfacial bonding strengths are available, the effect of interfacial bonding strength on the mechanical and rheological properties of polymer composites can be quantitatively studied.

#### 5.1.4 The Hydrogen Bonding Component of Work of Adhesion

The magnitude of  $W_a$  is strongly dependent on the surface properties of silica. From Table 5.2, it is seen that the values of  $W_a$  ranged from 63 erg cm<sup>-2</sup> to 301 erg cm<sup>-2</sup>. The values of  $W_a^h$  do vary significantly when the silica surfaces are treated by heat and/or chemical. However, the values of  $W_a^d$  vary only slight with these treatments. The reason for this is that the OH groups are

replaced by siloxane groups due to heat treatment and by methyl groups due to TMCS treatment.

Figure 5.2 shows the relationship between  $W_a^h$  and  $\tau^h$ . Comparing Figures 5.1 and 5.2 indicates that the trend for the dependence of  $W_a^h$  on  $\tau^h$  is similar to the dependence of  $W_a$  on  $\tau$ . In other words, the  $W_a^h$  is the main contributor to the magnitude of  $W_a$  since the  $W_a^d$  does not vary much in these treatments.

The percentage of  $W_a^h$  in  $W_a$  is also listed in Table 5.2. In the heat treatments, the percentage is more than 68% of the fully hydroxylated silica surface, however, it is less than 27% in the heat/TMCS treatments.

From this discussion, it can be seen that the  $W_a^h$  plays a very important role in the interfacial bonding which determines the mechanical and rheological properties of the silica filled E-Va polymer composites.

## 5.2 The Mechanical Properties of Silica Filled Composites

The Young's modulus ( $E$ ) and tensile strength ( $\sigma$ ) of silica filled E-Va copolymers, ranging from 5% to 20% volume fraction, are obtained from stress-strain curves (1,9,30,31,101,143,144)

### 5.2.1 Effects of Particle Size and Volume Fraction of Silica Filler

In Figures 5.3 and 5.4, the Young's moduli of the Stöber silica and the Cab-O-Sil silica filled polymer composites increase with an increase in the volume fraction

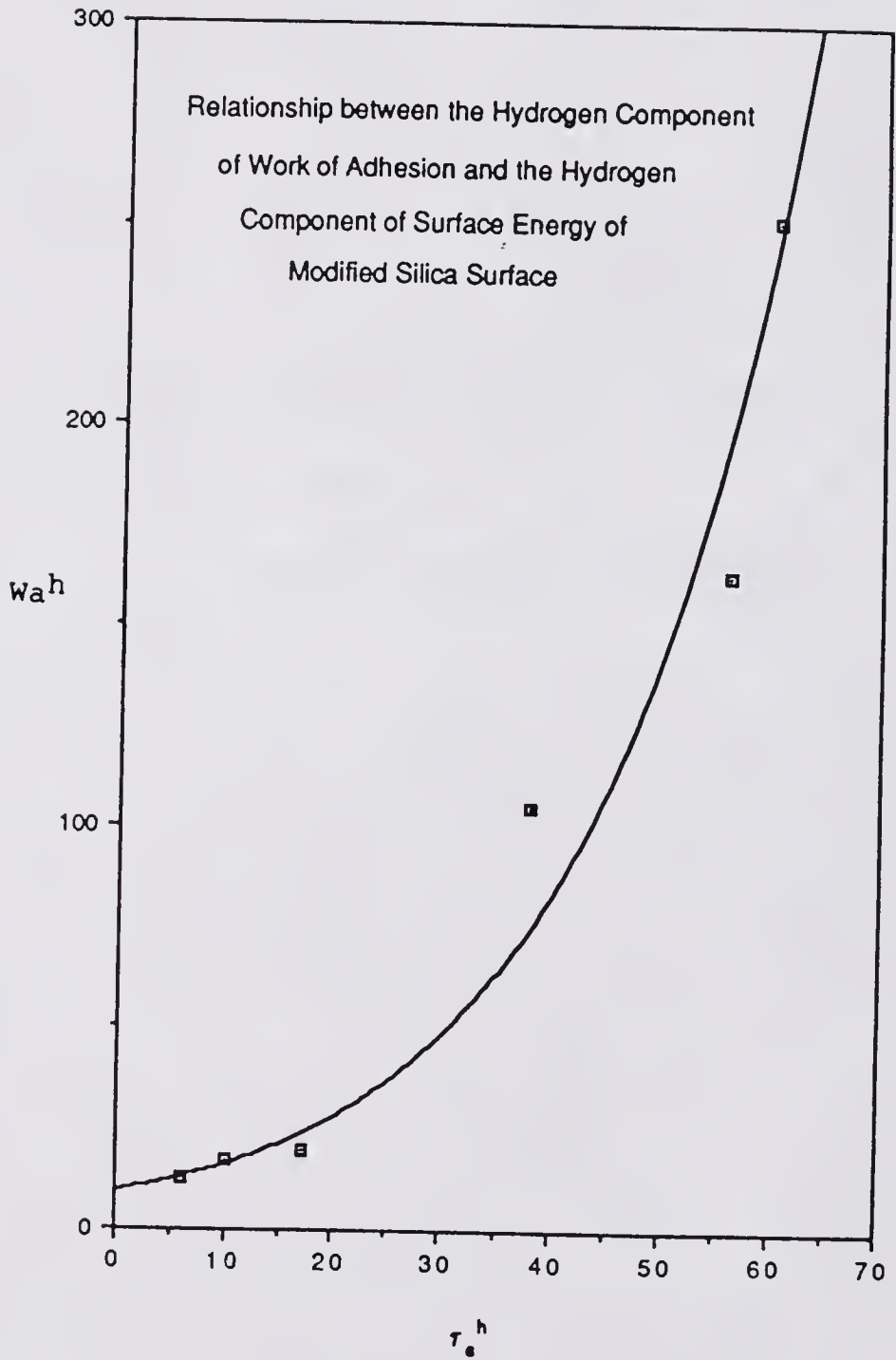


Figure 5.2 Hydrogen Component of Work of Adhesion versus Hydrogen Component of Surface Energy of Silica

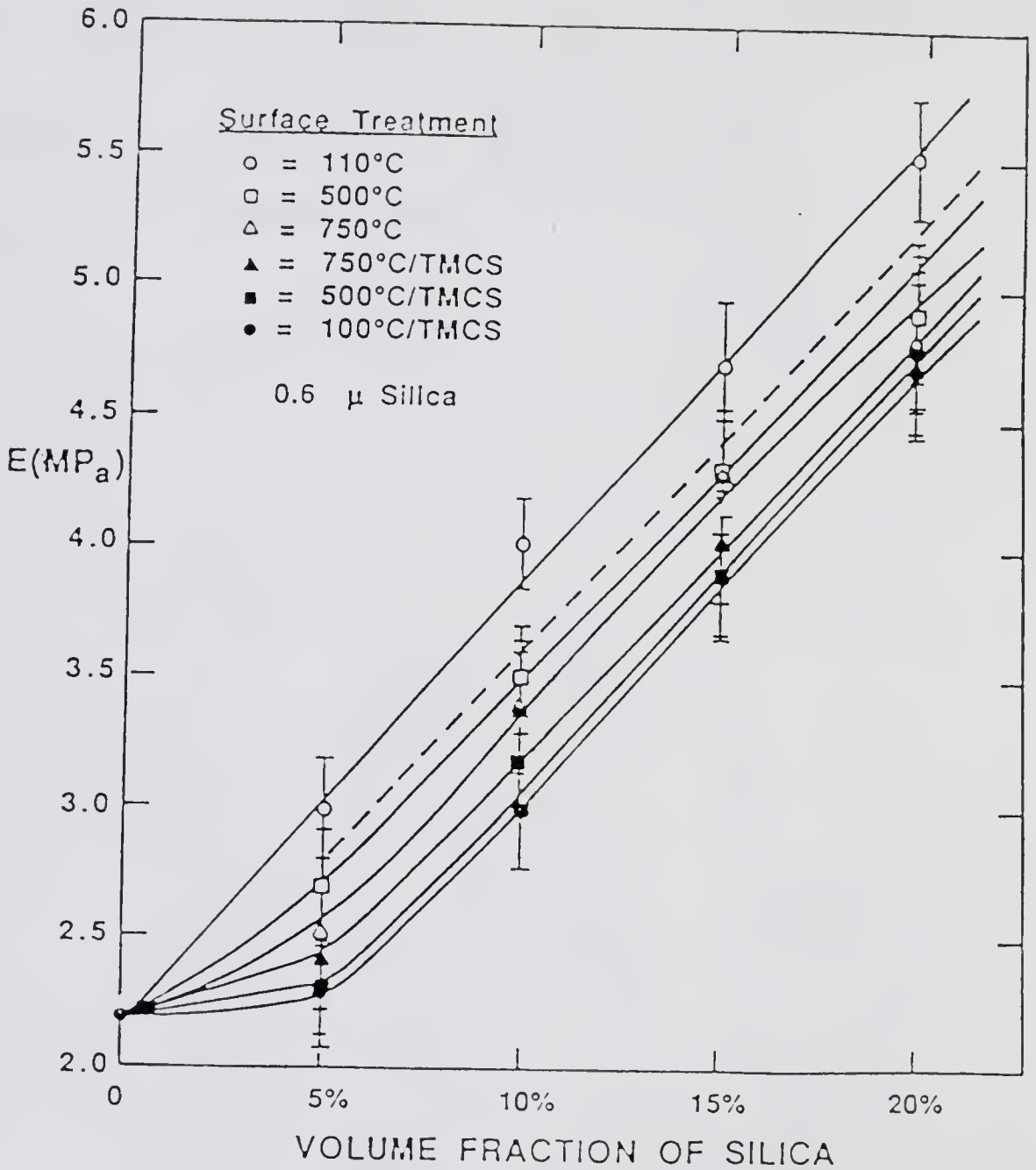


Figure 5.3 Effect of Volume Fraction and Surface Properties of Stober Silica Filler Particles on the Modulus of Polymer Composites

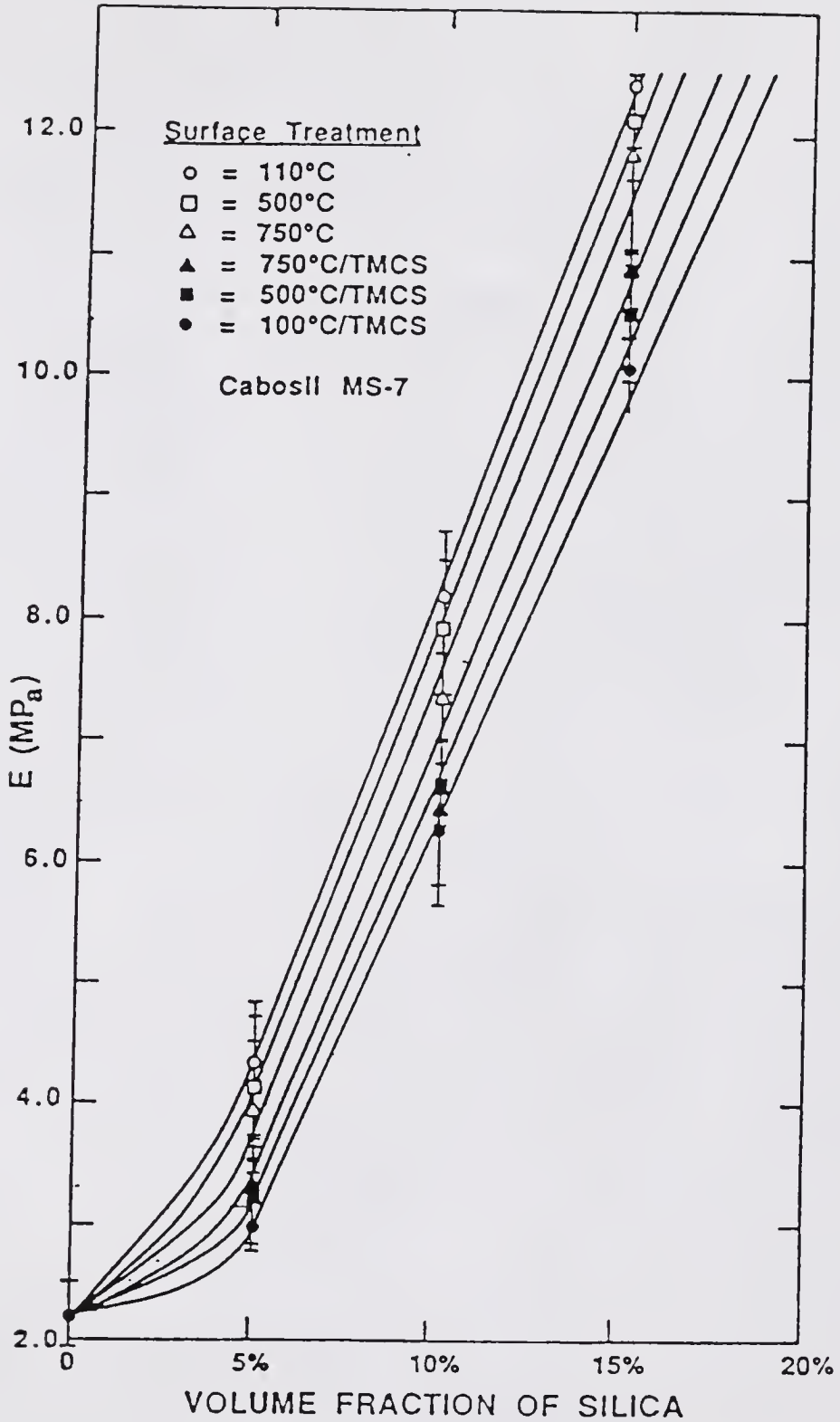


Figure 5.4 Effect of Volume Fraction and Surface Properties of Cab-O-Sil Silica Filler Particles on the Modulus of Polymer Composites

of silica filler particles, respectively. With the same volume fraction of silica in the polymer matrix, the modulus of the Cab-O-Sil silica filled composite is higher than that of the Stöber silica filled composite. In other words, the increase in modulus with filler concentration is faster in the Cab-O-Sil silica filled composite than in the Stöber silica filled composite.

The tensile strengths of the Stöber silica and Cab-O-Sil silica filled composites are shown in Figures 5.5 and 5.6, respectively. The composite filled by the Stöber silica has a lower tensile strength than the unfilled E-Va copolymer, but the composite filled by the Cab-O-Sil silica has a higher tensile strength than the unfilled polymer in the range of study (237-246).

At the low filler concentration in Figure 5.6, the tensile strength of the composite increases with an increase in volume fraction of filler. However, the tensile strength reaches a maximum at a volume fraction around 4%. After this the tensile strength of the composite decreases with increasing volume fraction of Cab-O-Sil silica. This behavior has also been seen in the carbon black filled rubber (104).

### 5.2.2 Effect of Work of Adhesion

#### 5.2.2.1 Young's modulus

In Figures 5.3 to 5.6, when the interfacial bonding increases, both the modulus and tensile strength of silica

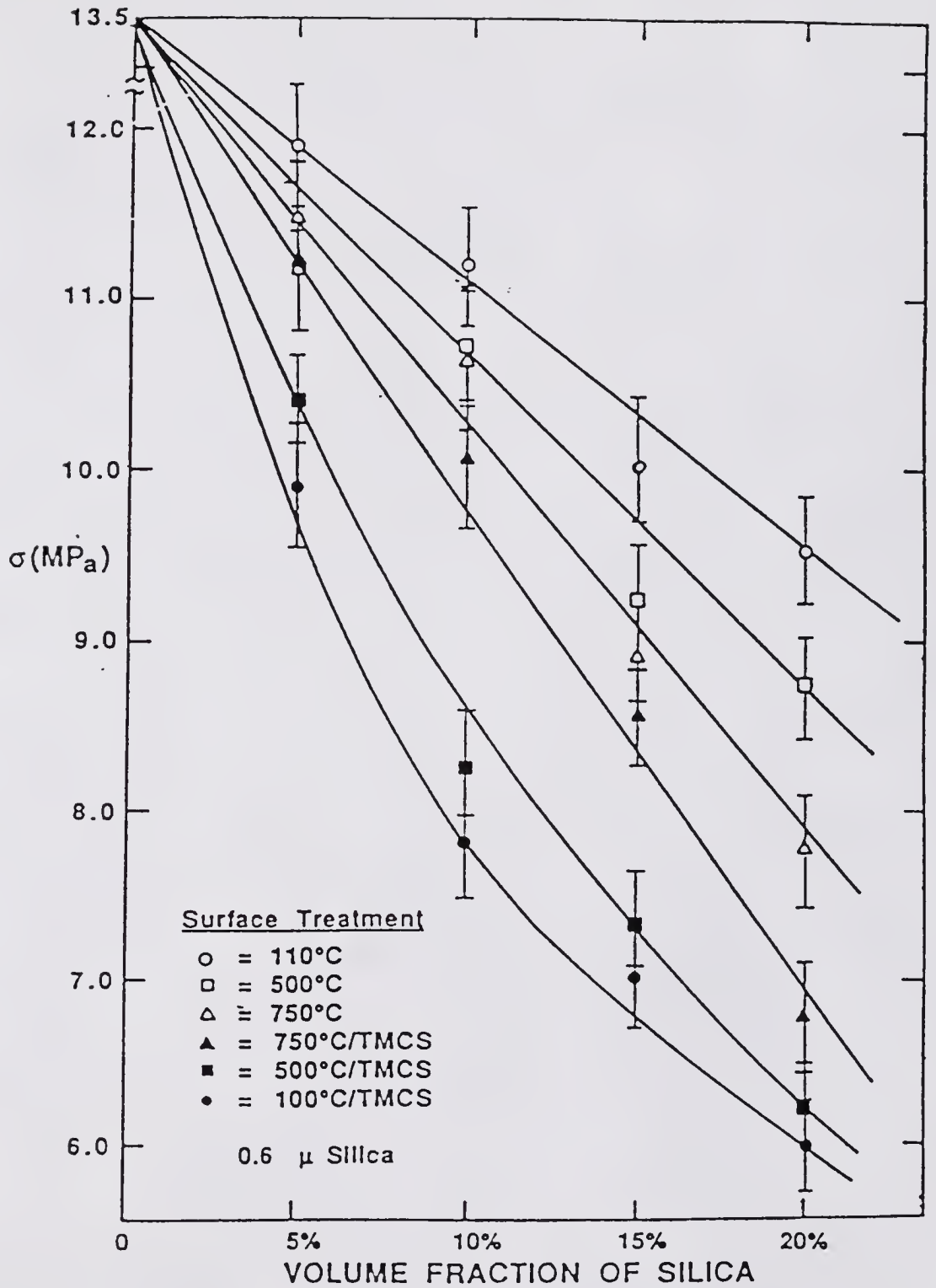


Figure 5.5 Effect of Volume Fraction and Surface Properties of Stober Silica Filler on the Tensile Strength of Polymer Composites

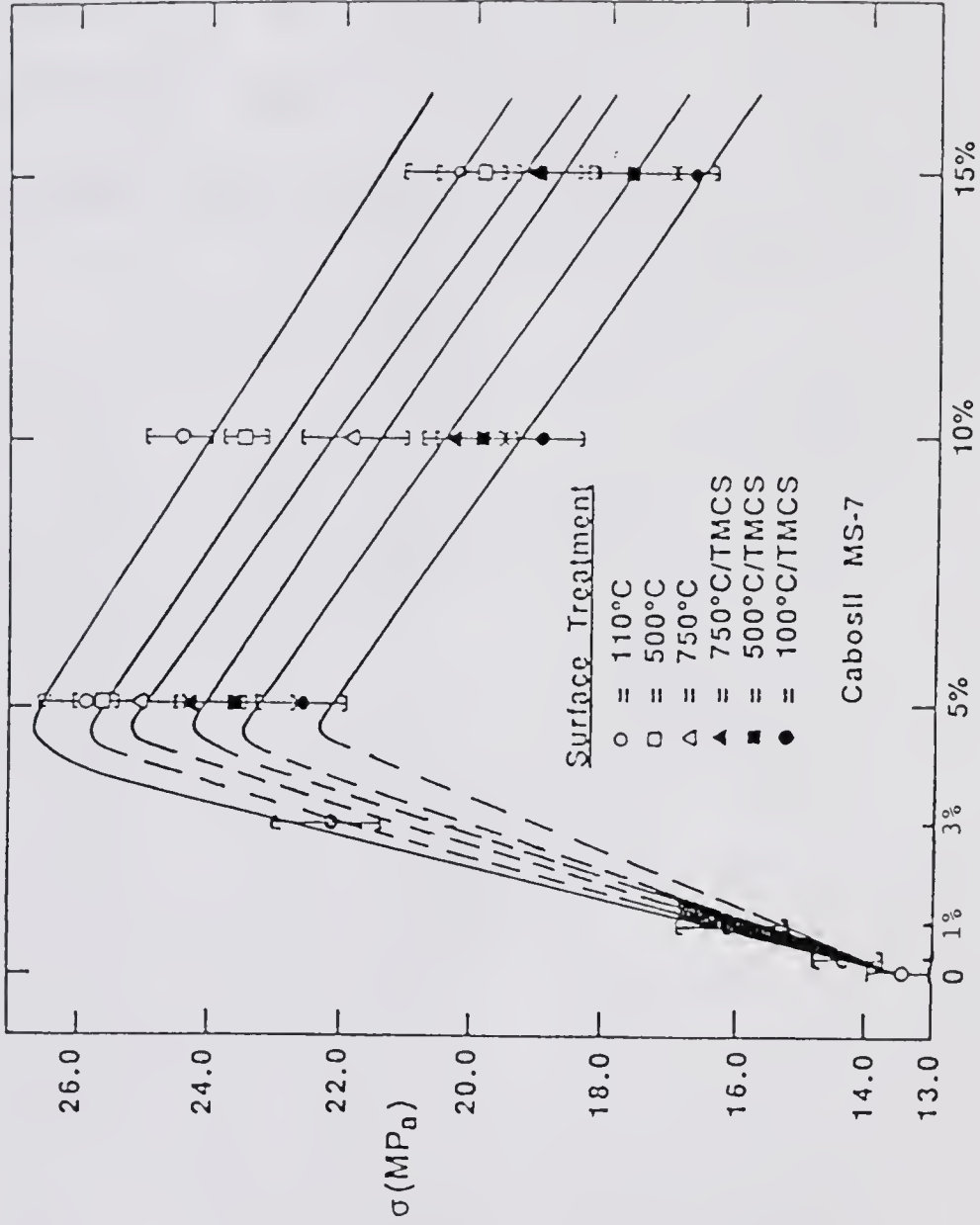


Figure 5.6 Effect of Volume Fraction and Surface Properties of Cab-O-Sil Silica on the Tensile Strength of Polymer Composites

filled polymer composites increase. The interfacial bonding is characterized in terms of the work of adhesion ( $W_a$ ). For a plot of the Young's moduli of composites versus the work of adhesion, a quantitative relationship can be obtained. In Figure 5.7, the logarithm of Young's modulus ( $\log E$ ) is plotted against the reciprocal of  $W_a$  ( $1000/W_a$ ) for the two various sizes of silica fillers at different volume fractions. There is an exponential relationship between Young's modulus and the reciprocal of  $W_a$  at a constant volume fraction of silica filler (30,31). The results depicted in Figure 5.7 can be described by

$$E_c = C e^{-K \left( \frac{1}{W_a} \right)} \quad ( 5.6 )$$

where  $E_c$  is the modulus of the composite and  $C$  and  $K$  are constants.

The constant  $C$  can be removed if the ratio of two moduli is taken at the same volume fraction of filler, but with different silica surface properties.

$$\frac{E_c}{E_{c0}} = e^{-K \left( \frac{1}{W_a} - \frac{1}{W_{a0}} \right)} \quad ( 5.7 )$$

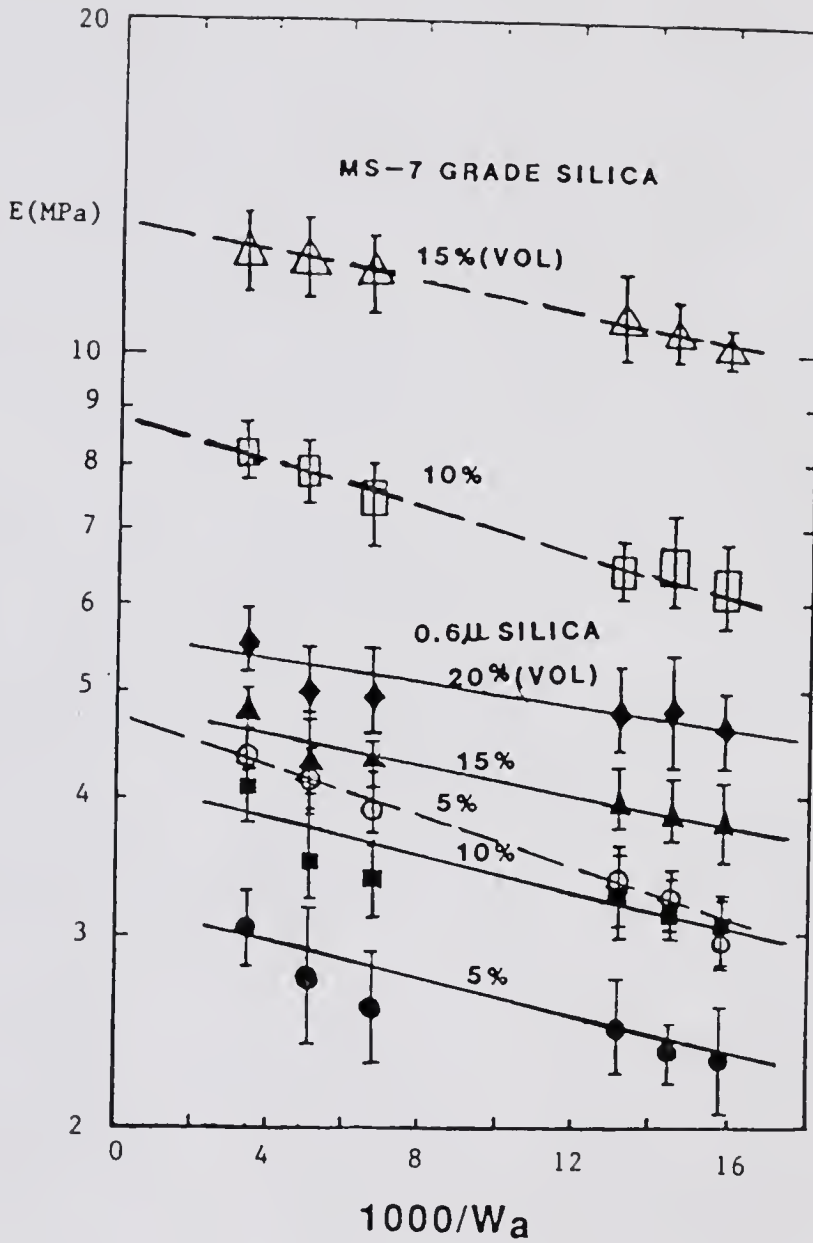


Figure 5.7 Effect of Work of Adhesion, Volume Fraction and Particle Size of Silica Filler on the Modulus of Polymer Composites

where  $E_{co}$  is the modulus of the polymer composite with the poorest interfacial bonding (110°C/TMCS treatment,  $Wao = 63 \text{ erg cm}^{-2}$ ). The  $Wao$  is the work of adhesion for the case of the poorest interfacial bonding.

The slope can be easily determined from experimental data. This slope will be defined in Chapter 6 as the apparent surface energy barrier of Young's modulus. When one Young's Modulus with its corresponding  $W_a$  is known, equation (5.7) can thus be used to predict the Young's Modulus of a composite with different interfacial bonding strengths at the same volume fraction of filler. The slopes of Young's Moduli of Stöber silica and Cab-O-Sil silica filled E-Va copolymer are listed in Table 5.3.

#### 5.2.2.2 Extension of Guth-Smallwood equation

There is an interesting result in the composites filled by Stöber Silica. The modulus of the Stöber silica filled composite with the poorest interfacial bonding is found to follow the Guth-Smallwood equation.

$$E_{110C/TMCS} = E_p ( 1 + 2.5 V_f + 14.1 V_f^2 ) \quad ( 5.8 )$$

where

$E_{110C/TMCS}$  = Modulus of composite filled by Stöber silica with the poorest interfacial bonding  
=  $E_{co}$  in equation ( 5.7 )

$E_p$  = Modulus of the unfilled E-Va copolymer

$V_f$  = Volume fraction of Stöber silica filler

Table 5.3

SLOPES OF THE YOUNG'S MODULUS  
OF SILICA FILLED E-VA COPOLYMERS

Volume Fraction of Silica Filler	( -slope * 1000, erg cm <sup>-2</sup> )	
	Stöber Silica	Cab-O-Sil Silica
5%	7.6	10.8
10%	7.9	10.7
15%	7.1	10.3
20%	7.2	

Equation ( 5.8 ) can be combined with equation ( 5.7 ) to yield

$$E_c = E_p \left( 1 + 2.5 V_f + 14.1 V_f^2 \right) e^{-K \left( \frac{1}{Wa} - \frac{1}{Wao} \right)} \quad ( 5.9 )$$

Equation ( 5.9 ) predicts the modulus behavior of the Stöber silica filled composites over the entire range of experimental data. Very good agreement is obtained for all values of  $Wa$  and  $V_f$  calculated from equation ( 5.9 ) except for the case of the highest interfacial bonding ( $Wa = 301$  erg/cm<sup>2</sup>). The predicted value in that case is lower than the experimentally obtained modulus value.

The Guth-Smallwood equation correctly predicts the relatively modest increases in modulus developed by the addition of inactive or non-reinforcing fillers, but has been found relatively unsatisfactory for highly reinforced systems, where large positive deviations occur. The reinforced system usually has very small filler particles. Therefore, for composites filled with very small Cab-O-Sil silica particles, equation ( 5.9 ) cannot be applied; however, equation ( 5.7 ) is still found to give very good agreement for all these composites.

#### 5.2.2.3 Tensile strength

Figure 5.8 shows a plot of the logarithm of tensile strength ( $\log \sigma$ ) versus the reciprocal of  $Wa$  (or  $1000/Wa$ )

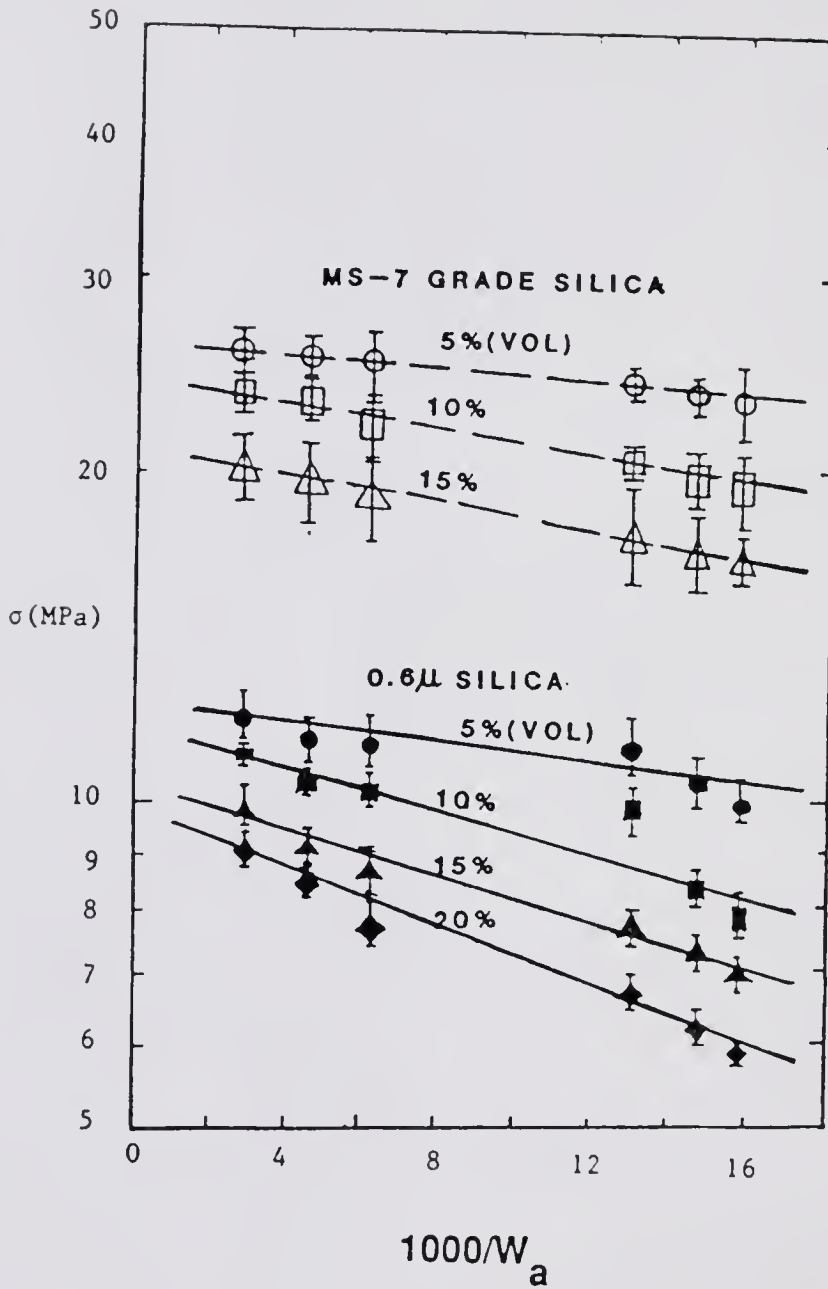


Figure 5.8 Effect of Work of Adhesion, Volume Fraction and Particle Size of Silica Filler on the Tensile Strength of Polymer Composites

for the composites at various filler concentrations. The results are similar to those obtained previously for Young's modulus in that there is an exponential relationship between the tensile strength and reciprocal work of adhesion. The relationship can be expressed as

$$\frac{\sigma_c}{\sigma_{co}} = e^{-K \left( \frac{1}{W_a} - \frac{1}{W_{ao}} \right)} \quad ( 5.10 )$$

where

$\sigma_c$  = Tensile strength of polymer composite with  $W_a$

$\sigma_{co}$  = Tensile strength of polymer composite with the poorest interfacial bonding ( $W_{ao} = 63 \text{ erg cm}^{-2}$ )

However, it is seen in Figure 5.8 that the slope of the tensile strength is dependent on both the particle size and volume fraction of filler. The slope will be defined in Chapter 6 as the apparent surface energy barrier of tensile strength. The slopes of the tensile strengths of Stöber silica and Cab-O-Sil silica filled E-Va copolymer are listed in Table 5.4. When compared at the same volume fraction of filler, the slope values of the Stöber silica filled polymer composites are higher than those of the Cab-O-Sil silica filled composites. The slope becomes steep with an increase in solid loading, especially in the case of the Stöber silica filled polymer composites (30,31).

Table 5.4

SLOPES OF THE TENSILE STRENGTH  
OF SILICA FILLED E-VA COPOLYMERS( -slope \* 1000, erg cm<sup>-2</sup> )

Volume Fraction of Silica Filler	Stöber Silica	Cab-O-Sil Silica
5%	6.4	4.6
10%	9.6	6.1
15%	12.1	7.3
20%	14.2	

### 5.3 The Rheological Properties of Silica Filled Composite

The shear storage modulus ( $G'$ ) and dynamic viscosity ( $\eta^*$ ) of filled polymer melts are obtained as the function of the materials characteristics (particle size and volume fraction of silica filler) and environmental testing conditions (frequency and temperature).

#### 5.3.1 Shear Storage Modulus of Polymer Composite

##### 5.3.1.1 Dependence of frequency and solid loading on the shear modulus

###### 5.3.1.1.1 Cab-O-Sil silica filled composites

Figure 5.9 shows a plot of  $\log G'$  of the 5% volume Cab-O-Sil silica filled E-Va copolymer versus frequency, which is measured at 210°C. The shear storage moduli of the E-Va copolymer and its composites increase with an increase in frequency (148,149,164).

In Figure 5.9, it is seen that a better interfacial bonding corresponds to a higher shear storage modulus. This is obvious at a low frequency, and the shear moduli of polymer melts filled by the heat treated silica particles form one group. These shear moduli are higher than those of the other group filled by heat/TMCS treated particles.

The shear moduli of the composites approximate a constant value as the frequency increases. This is shown in Figure 5.10 where the relative shear storage modulus ( $G'_c/G'_p$ ) versus frequency reaches a constant value and becomes independent of the frequency and the interfacial

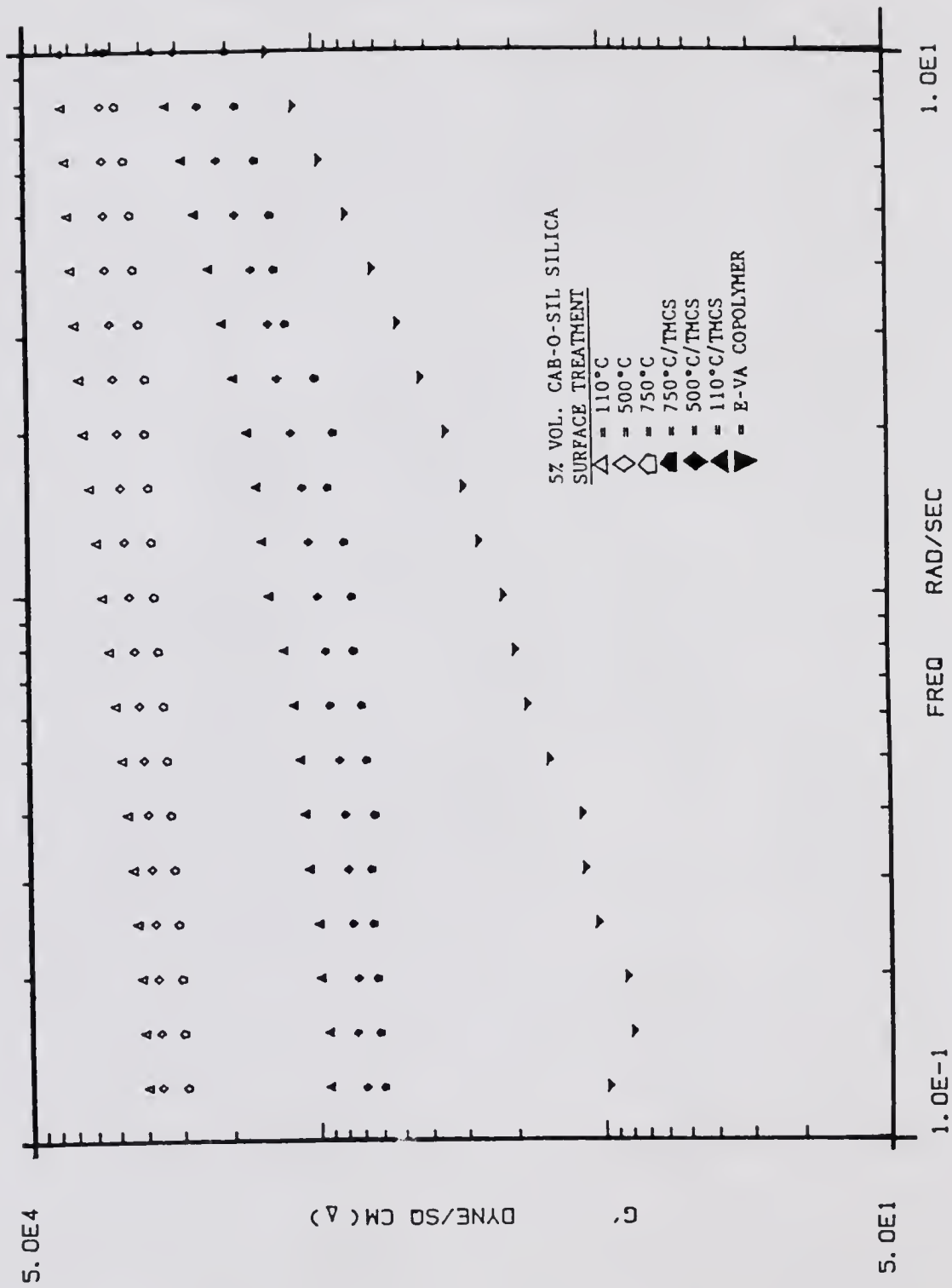


Figure 5.9 Effect of Frequency and Surface Properties of Silica on the Shear Modulus of 5% Volume Cab-O-Sil Filled E-Va Copolymer

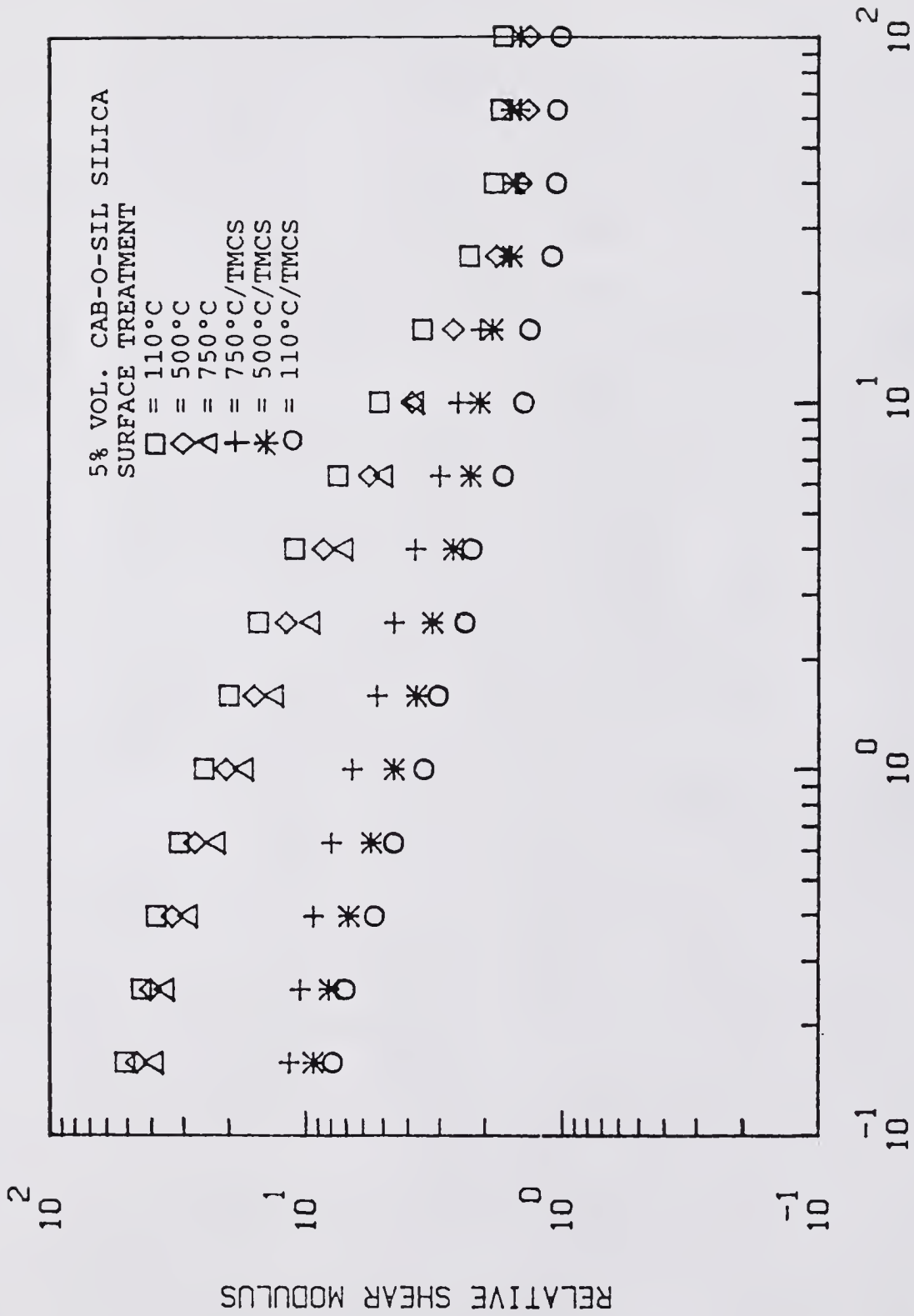


Figure 5.10 Relative Shear Storage Modulus versus Frequency of Various Surface Properties of 5% Volume Cab-O-Sil Filled Copolymer

bonding when the frequency increases. By introducing relative values, the matrix effect can be minimized.

#### 5.3.1.1.2 Stöber silica filled composites

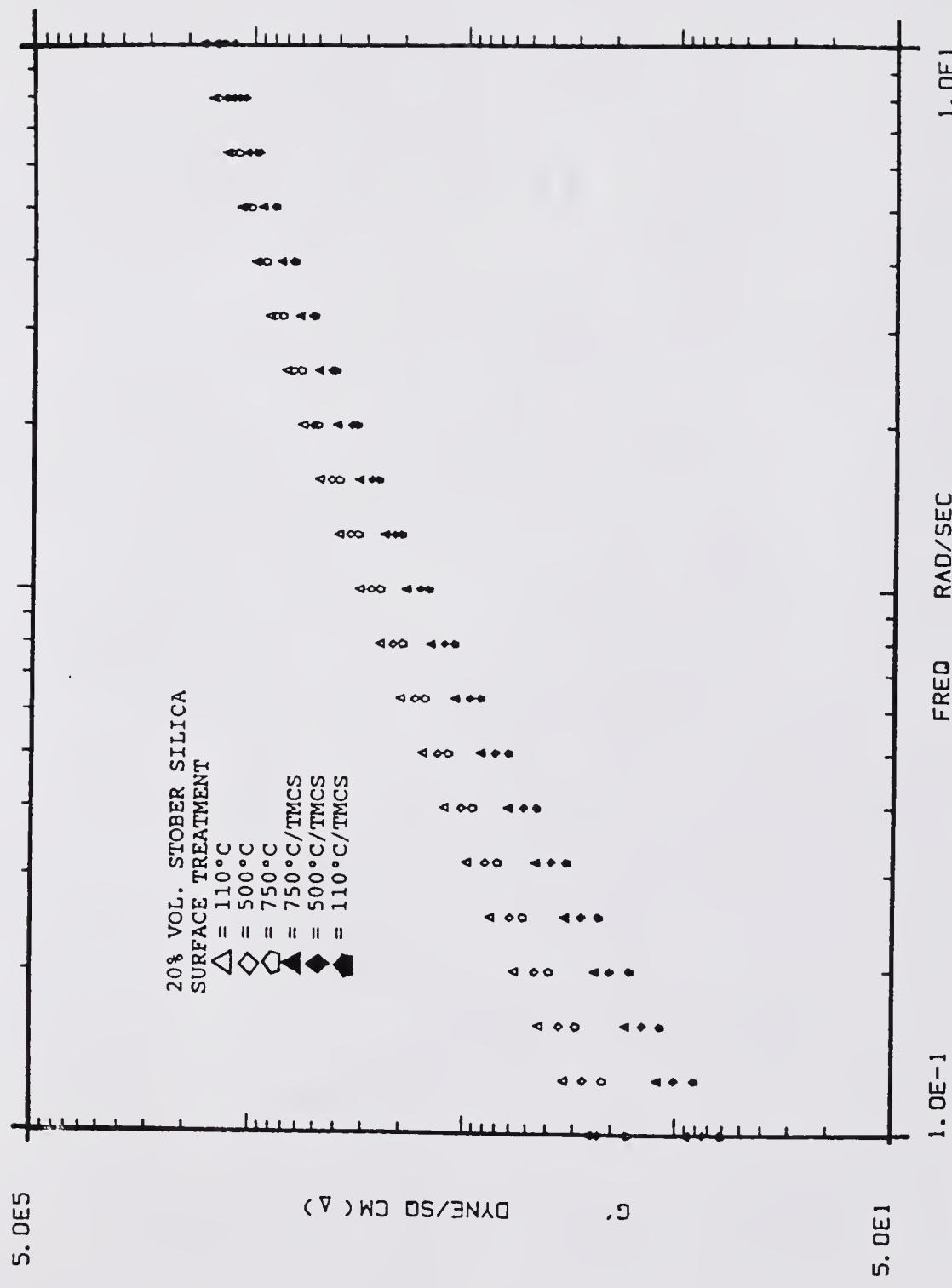
Figures 5.11 to 5.14 show plots of the  $\log G'$  of 20%, 15%, 10% and 5% volume fraction of Stöber silica versus frequency. All these filled polymer melts are measured at 150°C. A trend similar to that the Cab-O-Sil silica filled composites is also observed in the Stöber silica filled polymer melts. The  $\log G'$  of the Stöber silica filled polymer melts increases with an increase in frequency and in interfacial bonding. At a constant silica volume fraction, the shear moduli of polymer melts filled by the heat treated silica particles form one group at low frequencies. These shear moduli are higher than those of the other group filled by heat/TMCS treated particles.

The relative shear moduli ( $G'_c/G'_p$ ) of the Stöber silica filled composites at 20%, 15%, 10% and 5% volume fractions of filler versus frequency are plotted in Figures 5.15 to 5.18. The results show that the shear moduli of these polymer melts approach a constant value as the frequency increases and becomes independent of the frequency and the interfacial bonding strength.

#### 5.3.1.2 Dependence of work of adhesion on the shear modulus

##### 5.3.1.2.1 Cab-O-Sil silica filled composites

The effect of the work of adhesion ( $W_a$ ) on the relative shear storage modulus of the 5% volume fraction of



1.0E-1 1.0E1  
 Figure 5.11 Effect of Frequency and Surface Properties of Silica on the Shear Modulus of 20% Volume Stöber Silica Filled Copolymer

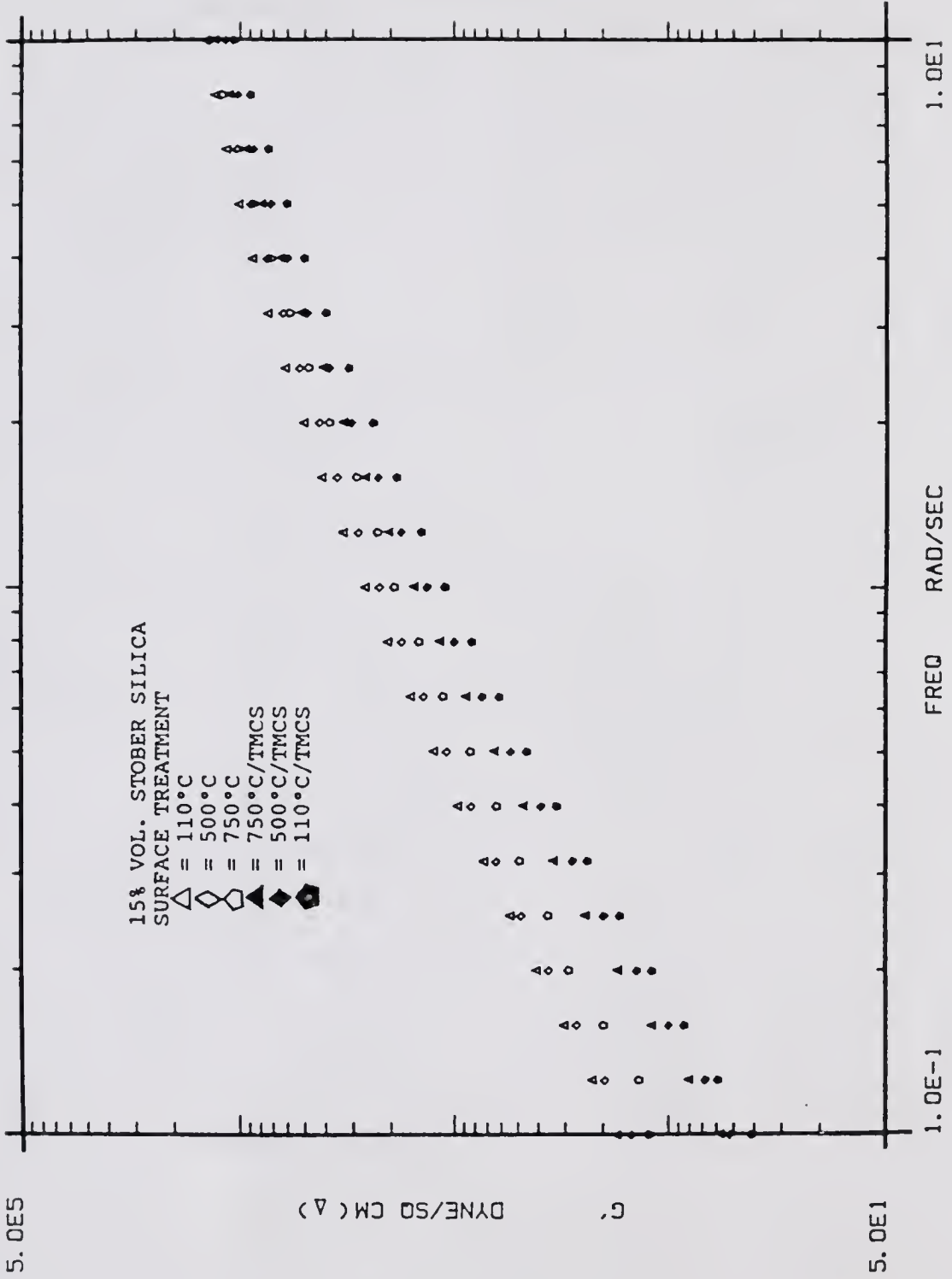


Figure 5.12 Effect of Frequency and Surface Properties of Silica on the Shear Modulus of 15% Volume Stöber Silica Filled Copolymer

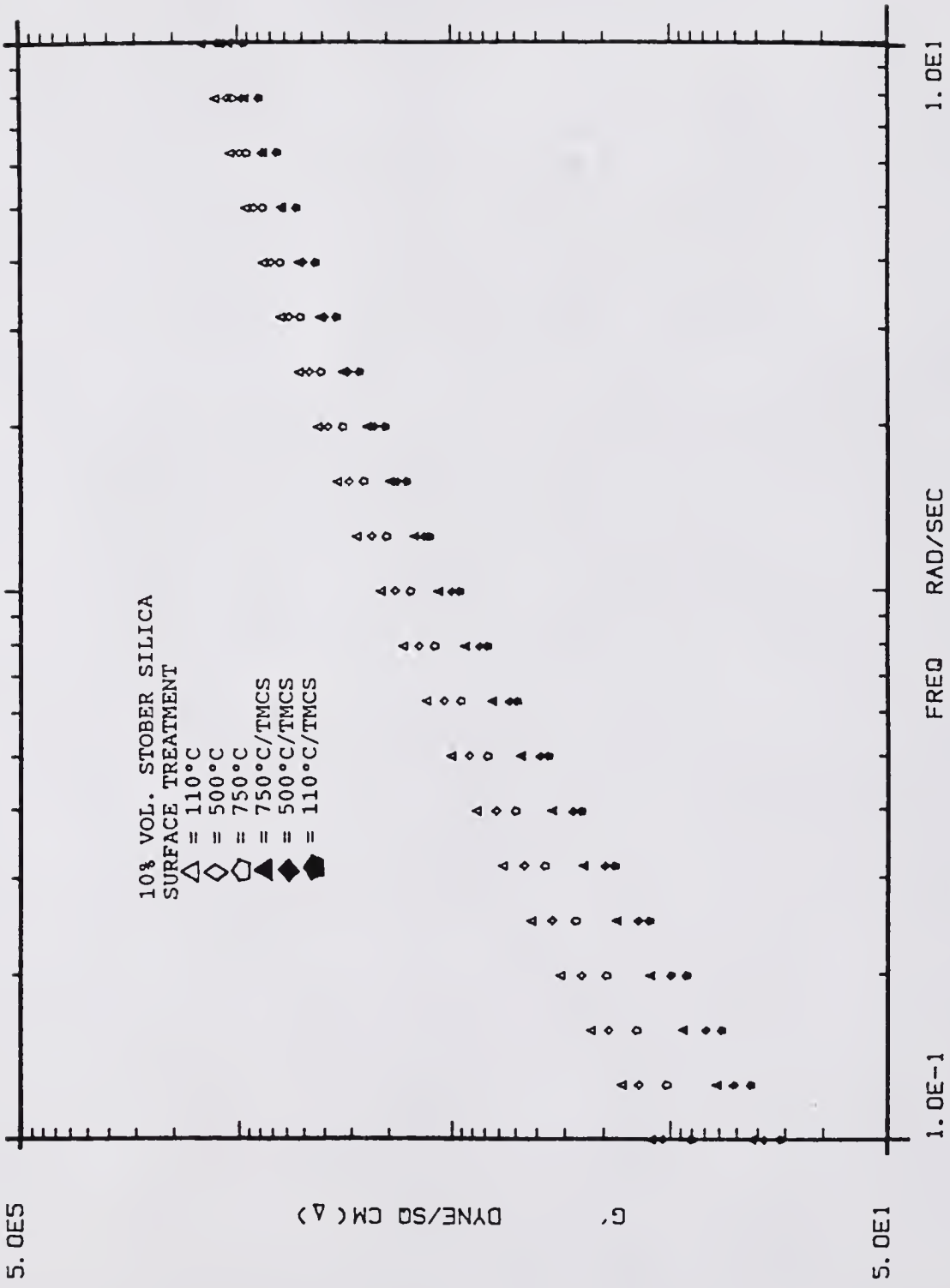


Figure 5.13 Effect of Frequency and Surface Properties of Silica on the Shear Modulus of 10% Volume Stöber Silica Filled Copolymer

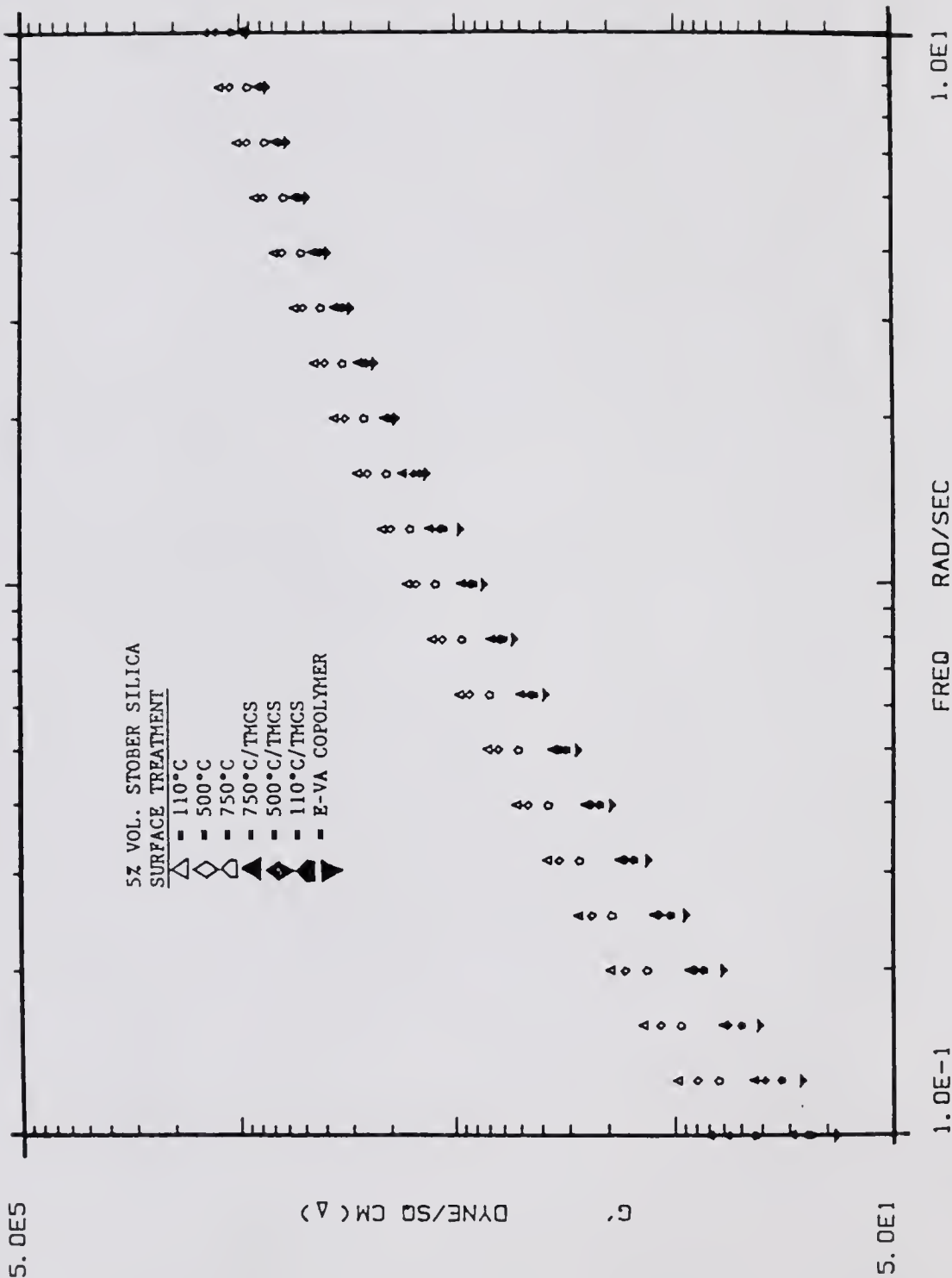


Figure 5.14 Effect of Frequency and Surface Properties of Silica on the Shear Modulus of 5% Volume Stöber Silica Filled Copolymer

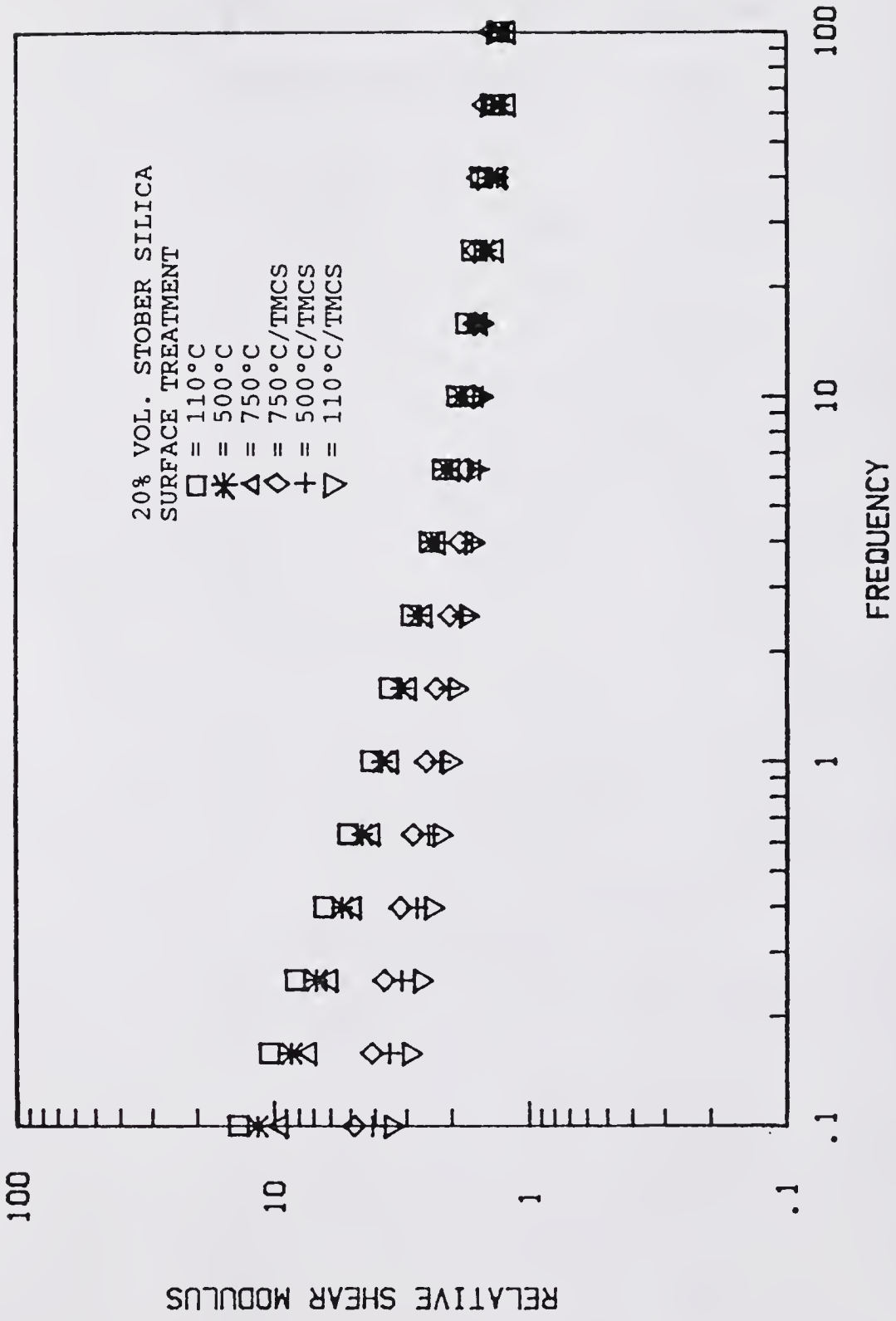


Figure 5.15 Relative Shear Modulus versus Frequency of Various Surface Properties of 20% Volume Stöber Silica Filled Copolymer

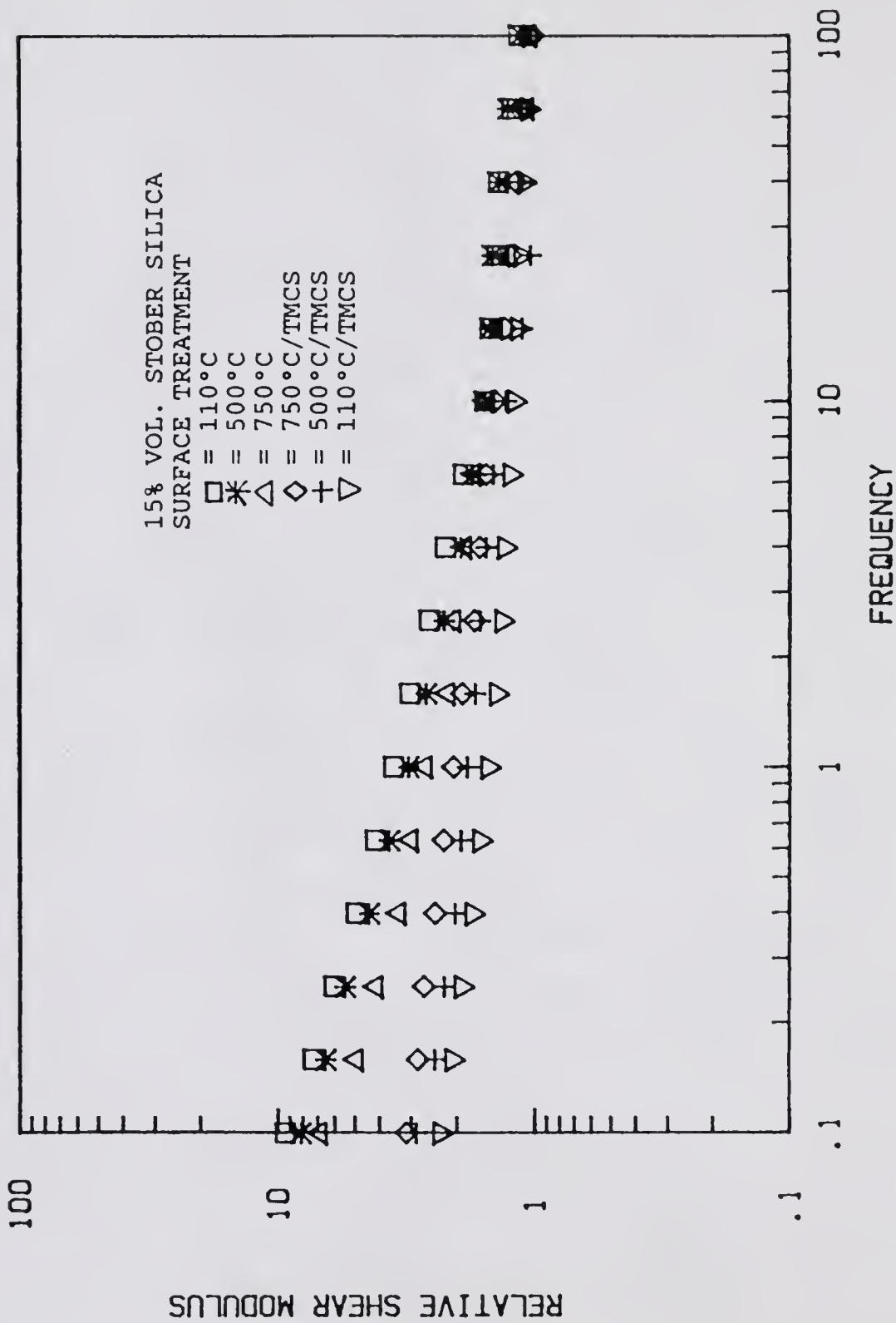


Figure 5.16 Relative Shear Modulus versus Frequency of Various Surface Properties of 15% Volume Stöber Silica Filled Copolymer

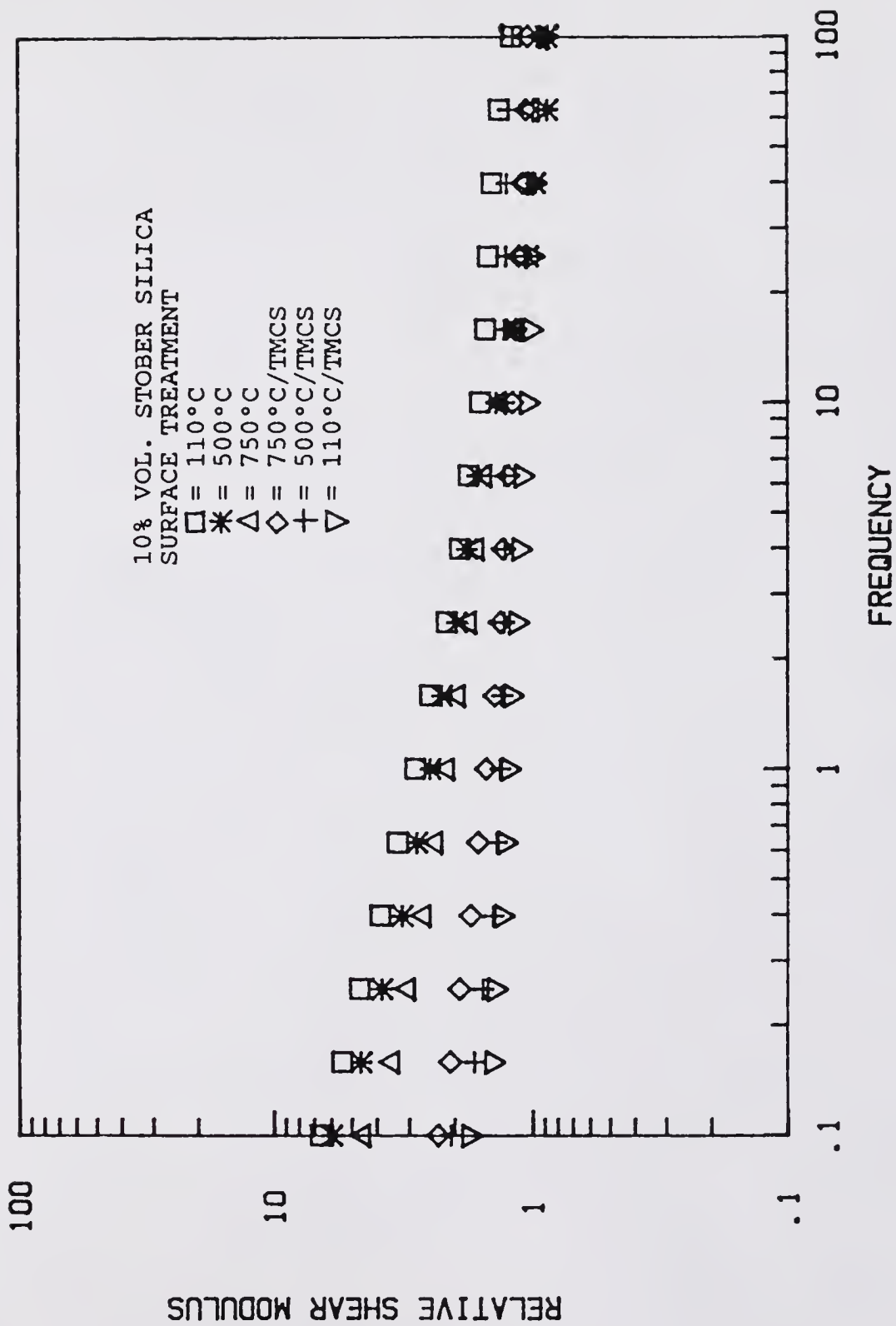


Figure 5.17 Relative Shear Modulus versus Frequency of Various Surface Properties of 10% Volume Stöber Silica Filled Copolymer

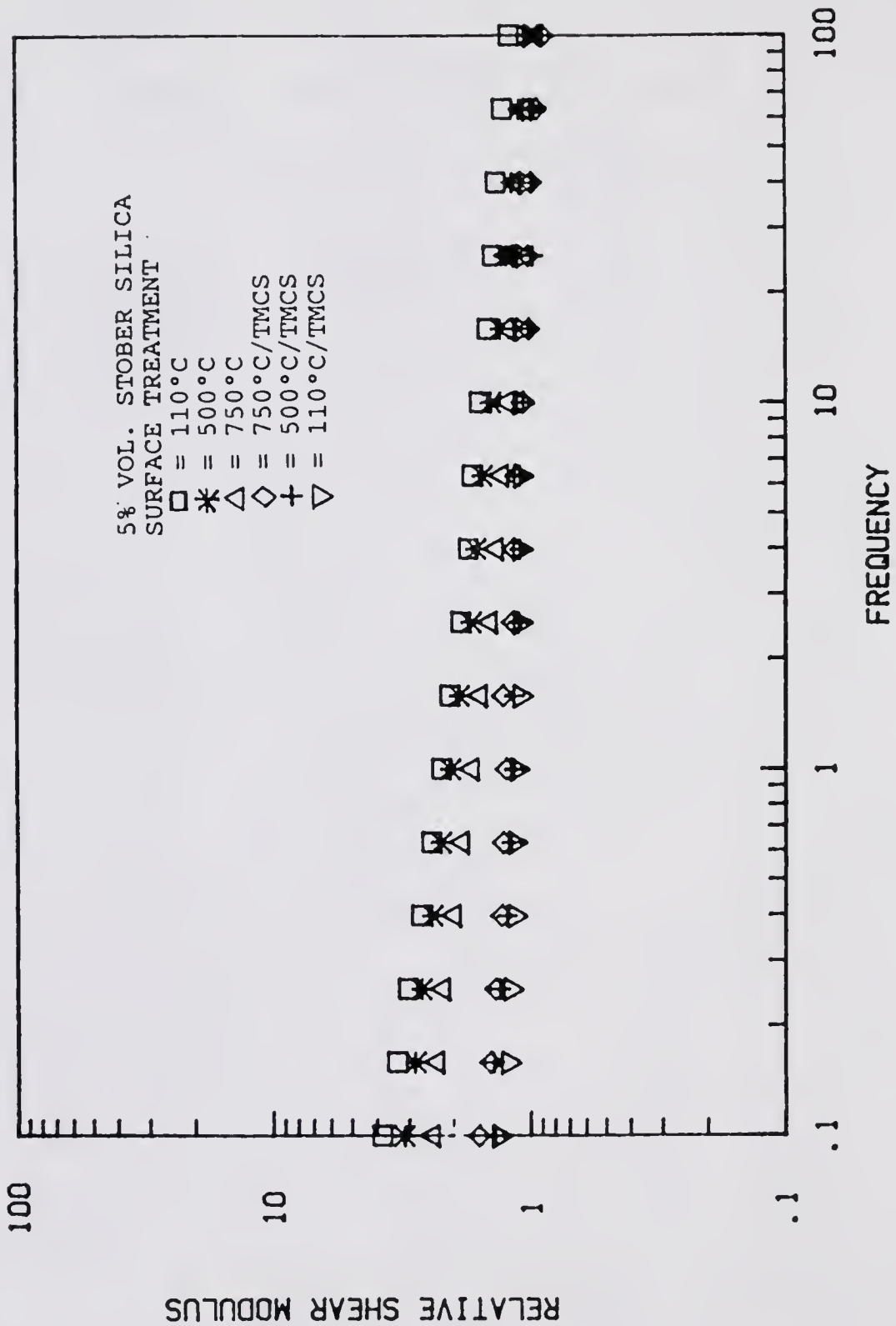


Figure 5.18 Relative Shear Modulus versus Frequency of Various Surface Properties of 5% Volume Stöber Silica Filled Copolymer

Cab-O-Sil silica filled E-Va copolymer is shown in Figure 5.19. Regardless of the frequencies studied, 0.1, 1.0 or 10 rad/sec, there exists an exponential relationship between the shear storage moduli of filled polymer melts and the reciprocal of work of adhesion (15,16,30,31).

As the work of adhesion is increased, there is a corresponding increase in the relative shear modulus. However, as seen in Figure 5.19, the slope is steep when the studied frequency is low. This slope will be defined in Chapter 6 as the apparent surface energy barrier of shear modulus. It indicates that work of adhesion has a greater effect on the shear storage modulus at a lower frequency. At a higher frequency, work of adhesion is not as effective in controlling properties as at a lower frequency. The Young's modulus of a 5% volume fraction of Cab-O-Sil filled E-Va measured at 25°C, which has a low slope value, is also plotted in Figure 5.19 for comparison.

#### 5.3.1.2.2 Stöber silica filled composites

The effect of work of adhesion on the relative shear storage modulus of the 20% volume fraction of Stöber silica filled E-Va copolymer is shown in Figure 5.20. At the studied frequencies, exponential relationships between the relative shear modulus and the reciprocal of work of adhesion are obtained.

The apparent surface energy barrier of shear modulus of Stöber silica filled composites is increased when the

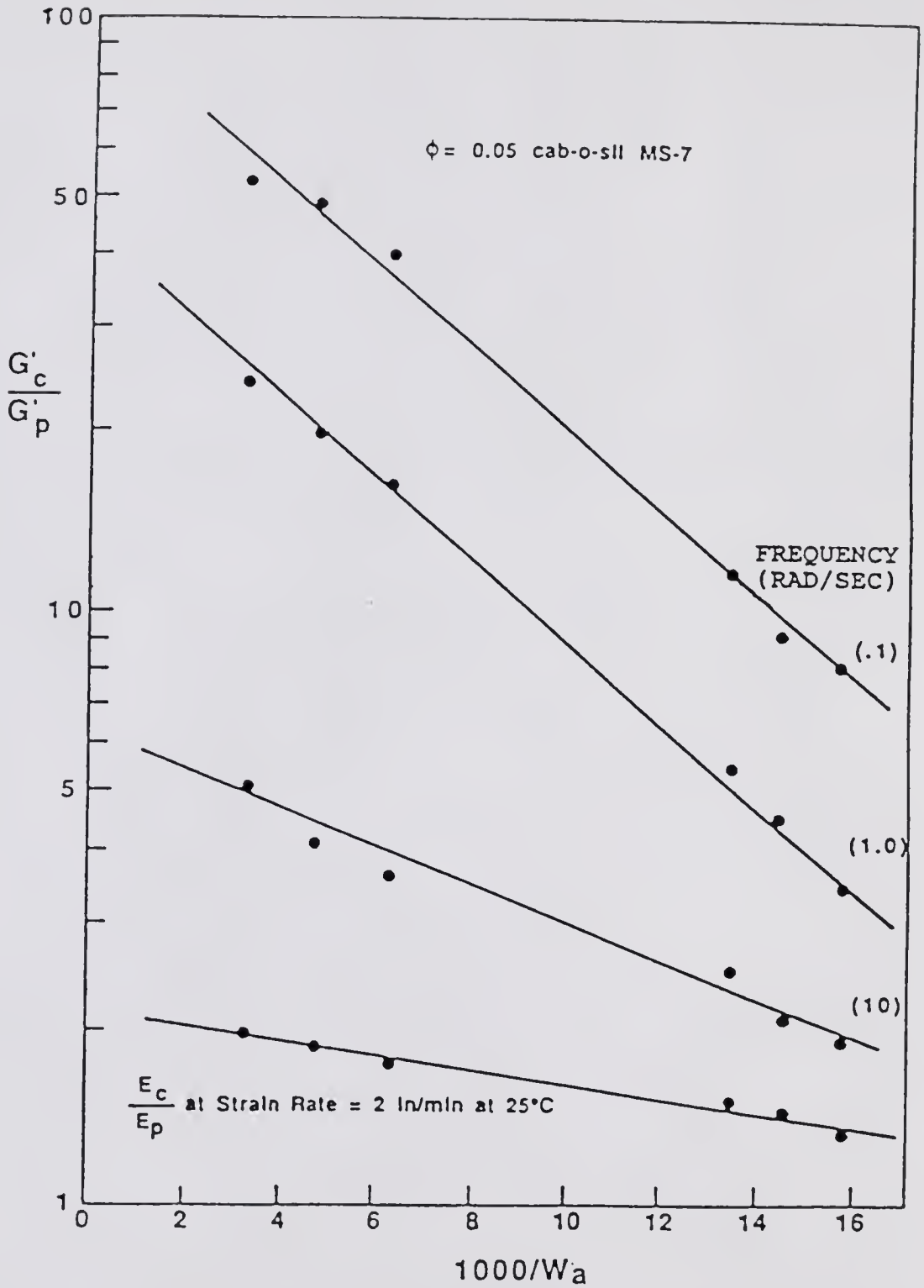


Figure 5.19 Effect of Work of Adhesion and Frequency on the Relative Shear Modulus of 5% Volume Cab-O-Sil Silica Filled E-Va Copolymer

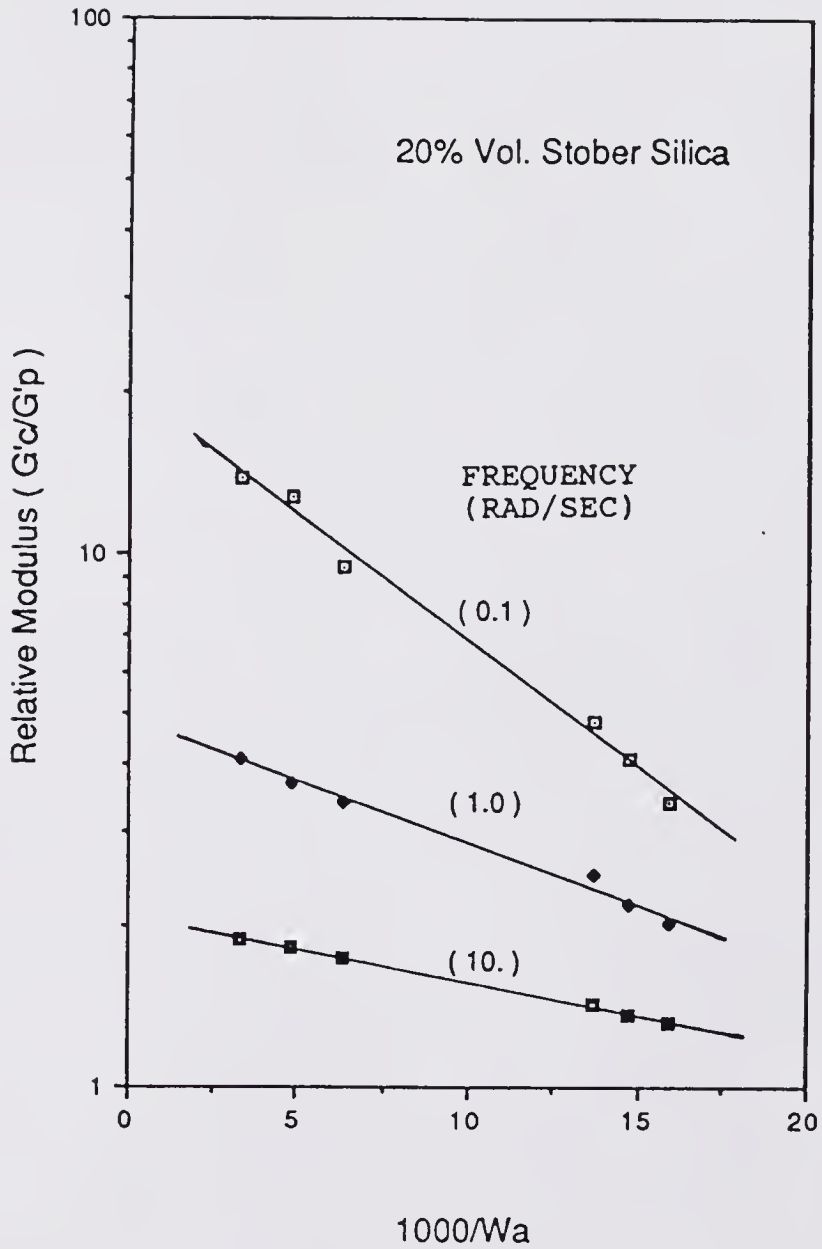


Figure 5.20 Effect of Work of Adhesion and Frequency on the Relative Shear Modulus of 20% Volume Stober Silica Filled E-Va Copolymer

frequency is decreased. It indicates that work of adhesion is more effective at a low frequency in controlling properties of filled polymer. The other polymer melts filled with volume fractions at 15%, 10% and 5% of the Stöber silica also show exponential relationships between the reciprocal of work of adhesion and relative shear modulus. These are shown in Figures 5.21 to 5.23.

One can also study at a given frequency, the effect of work of adhesion on the relative shear moduli at different volume fractions of Stöber silica. Figure 5.24 shows the relative shear moduli at various volume fractions of silica versus the reciprocal of work of adhesion at a frequency of 0.10 rad/sec. The relative shear modulus is higher with a higher value of volume fraction of silica. However, the apparent surface energy barrier of shear moduli of the studied volume fractions of silica is approximately the same.

This independence of volume fraction of the Stöber silica on the apparent surface energy barrier of the shear modulus is also observed for the apparent surface energy barrier of the Young's modulus in Figure 5.7. Furthermore, when the frequency studied is 1.0 or 10 rad/sec, as shown in Figures 5.25 and 5.26, respectively, the results also show that the apparent surface energy barrier of shear modulus is independent of volume fraction of silica.

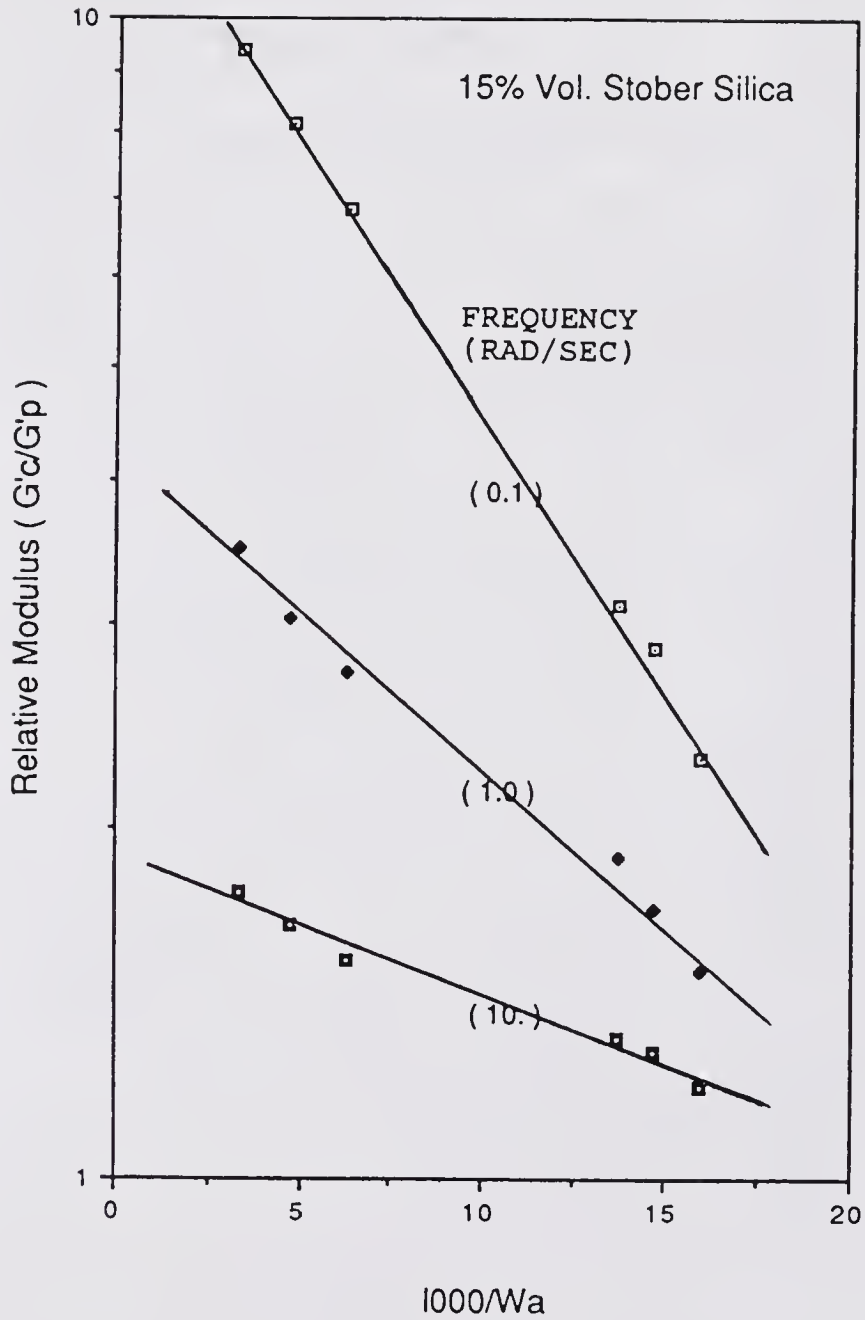


Figure 5.21 Effect of Work of Adhesion and Frequency on the Relative Shear Modulus of 15% Volume Stober Silica Filled E-Va Copolymer

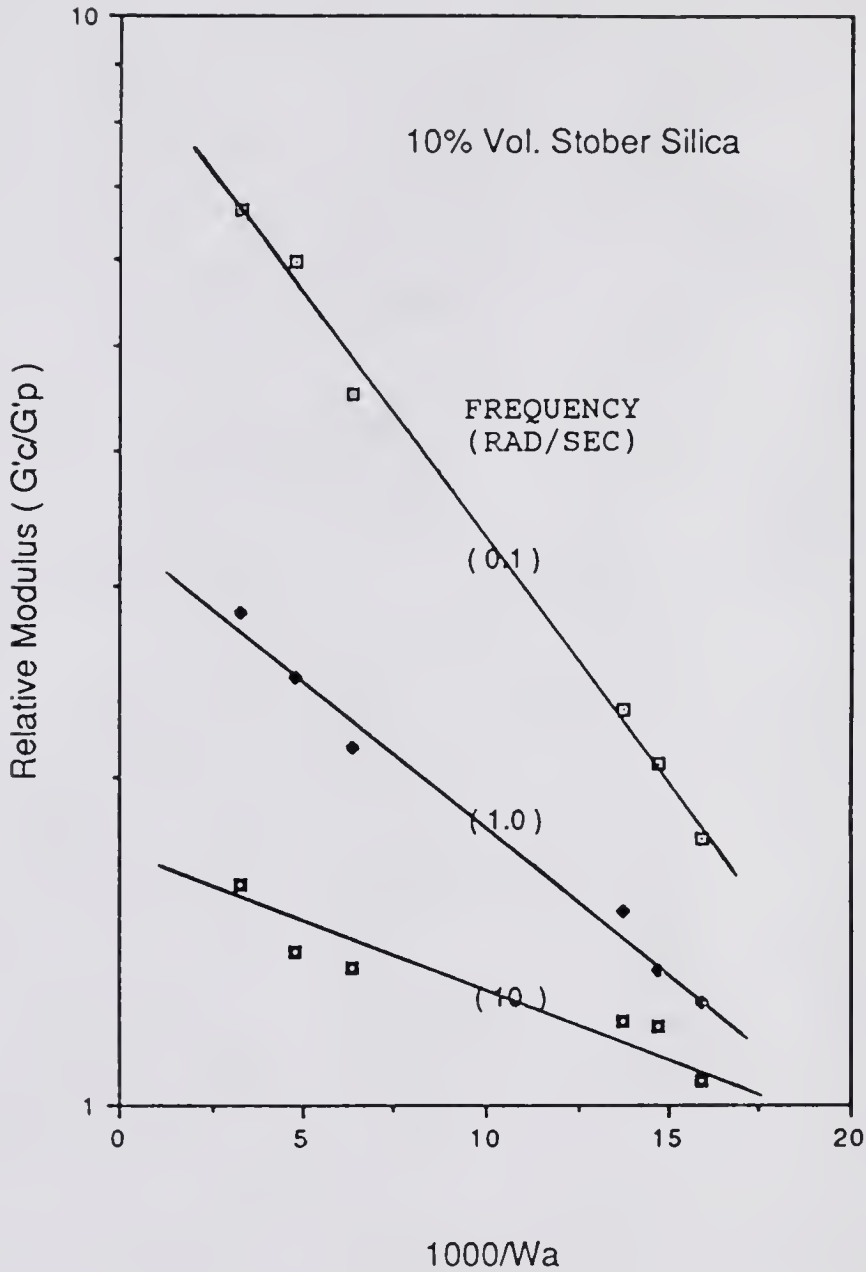


Figure 5.22 Effect of Work of Adhesion and Frequency on the Relative Shear Modulus of 10% Volume Stober Silica Filled E-Va Copolymer

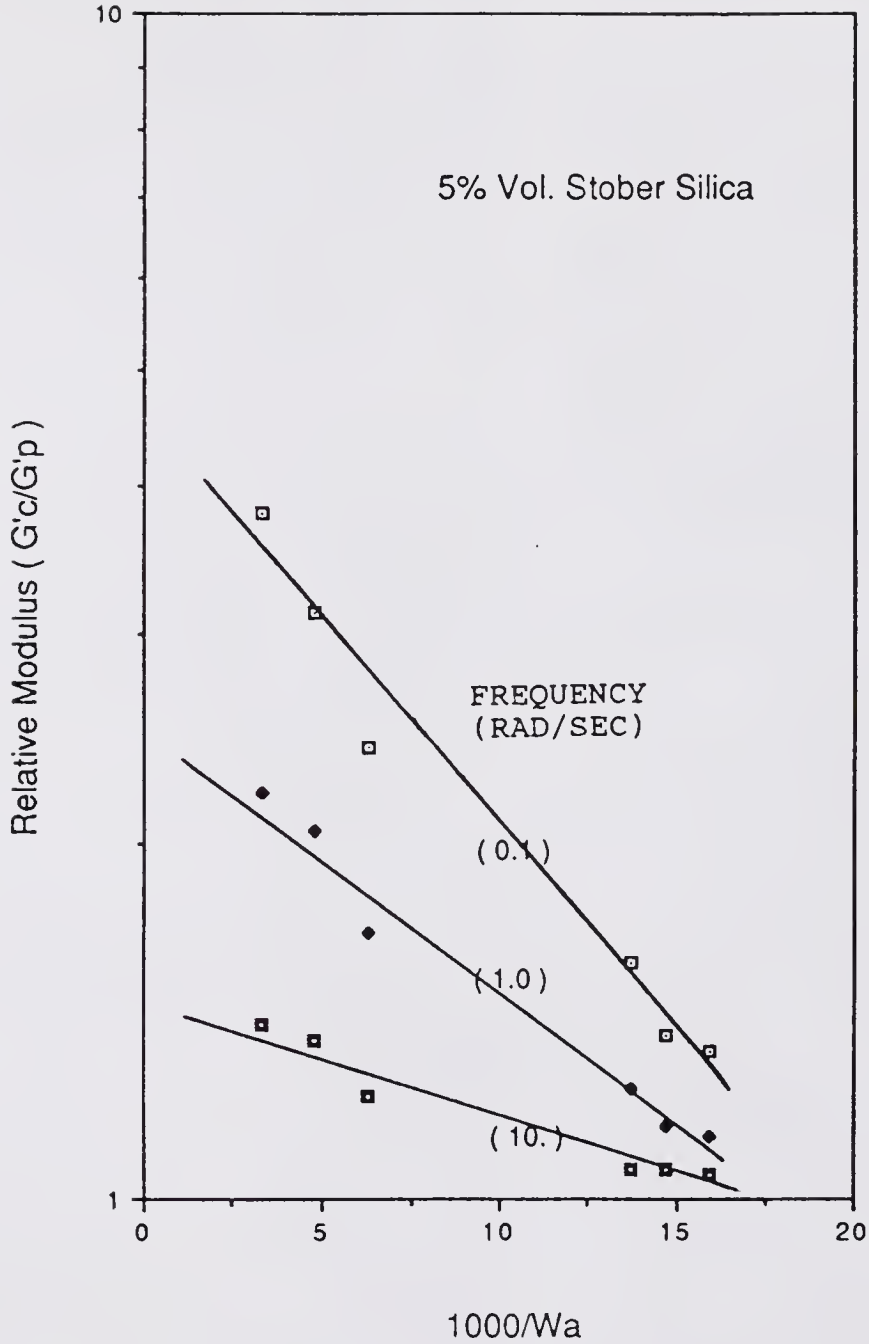


Figure 5.23 Effect of Work of Adhesion and Frequency on the Relative Shear Modulus of 5% Volume Stober Silica Filled E-Va Copolymer

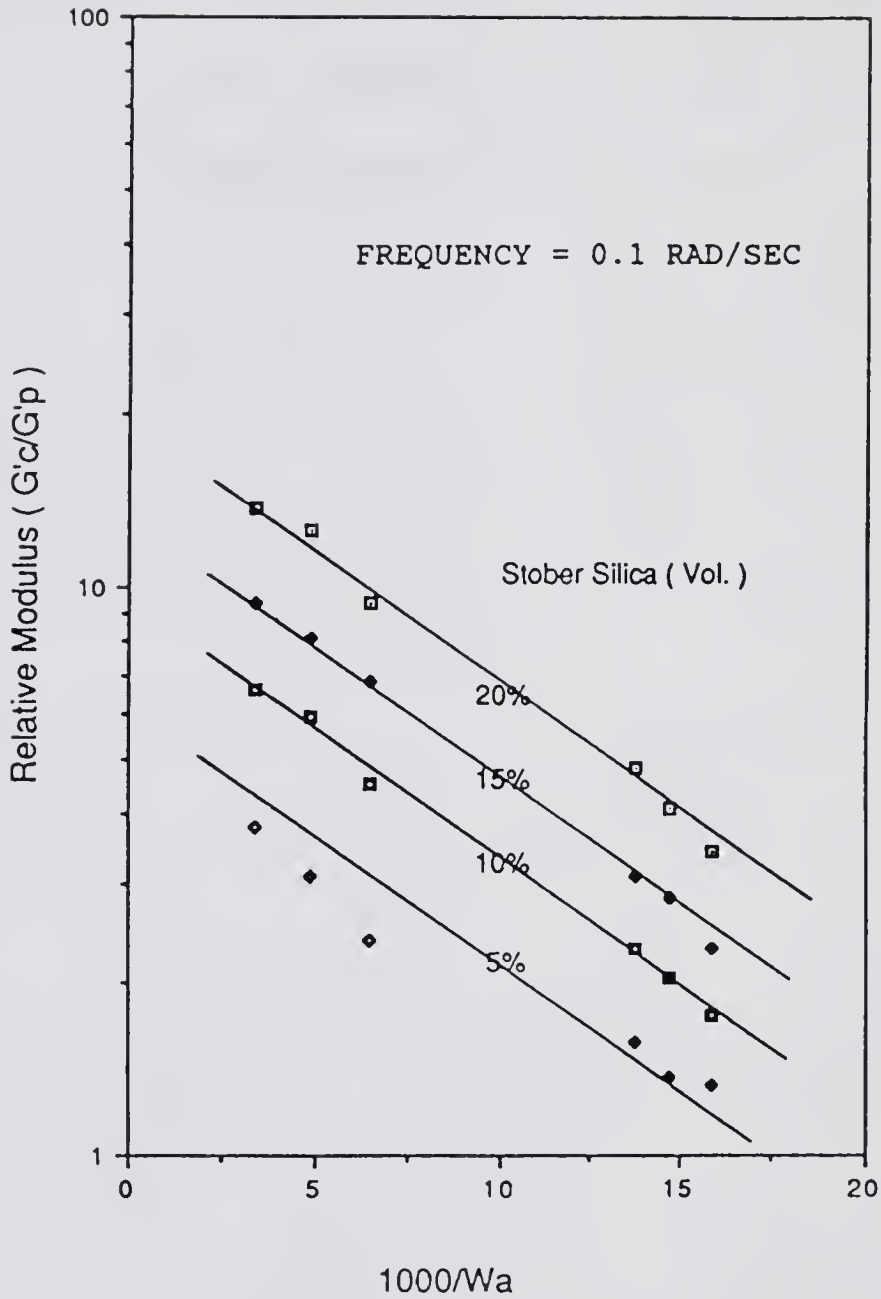


Figure 5.24 Effect of Work of Adhesion and Volume Fraction on the Relative Shear Modulus of Stöber Silica Filled E-Va Copolymer Measured at 0.1 rad/sec

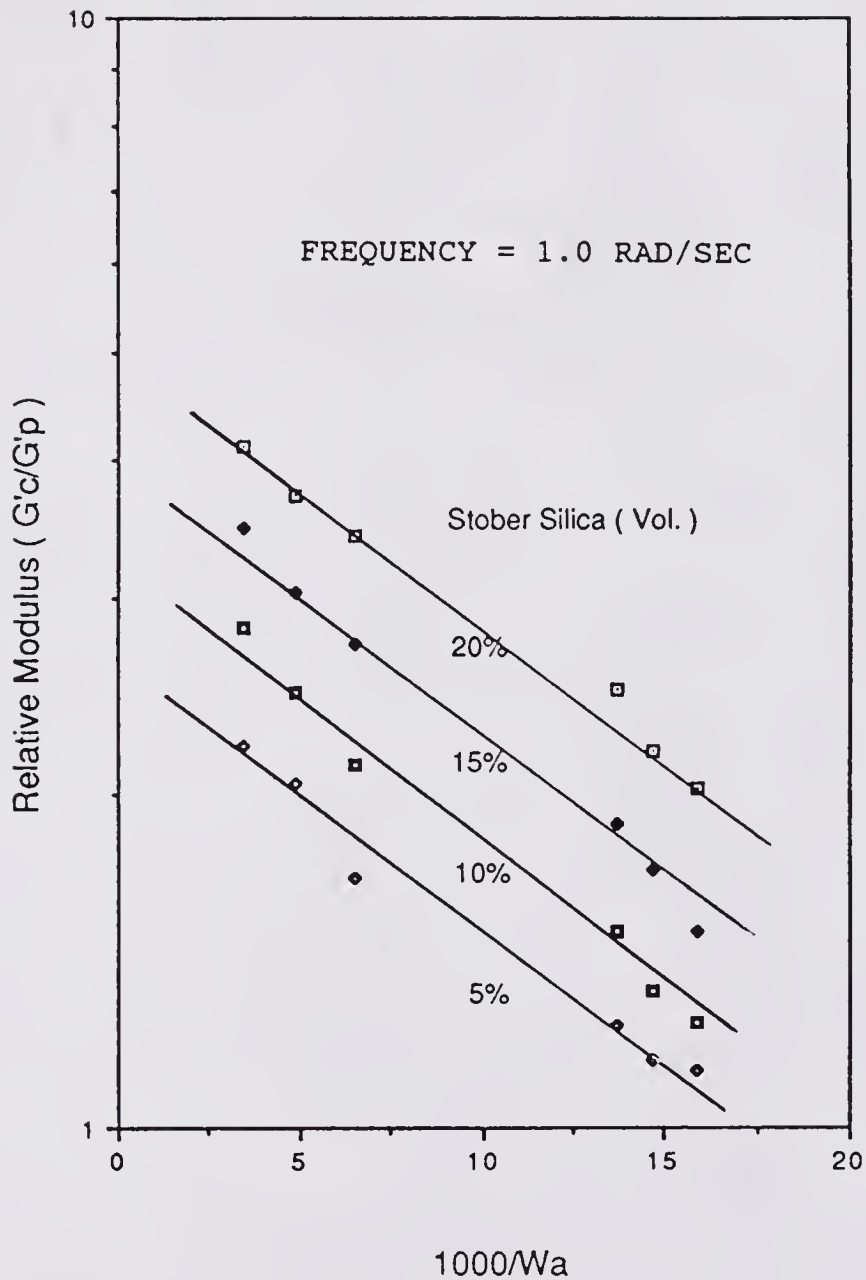


Figure 5.25 Effect of Work of Adhesion and Volume Fraction on the Relative Shear Modulus of Stober Silica Filled E-Va Copolymer Measured at 1.0 rad/sec

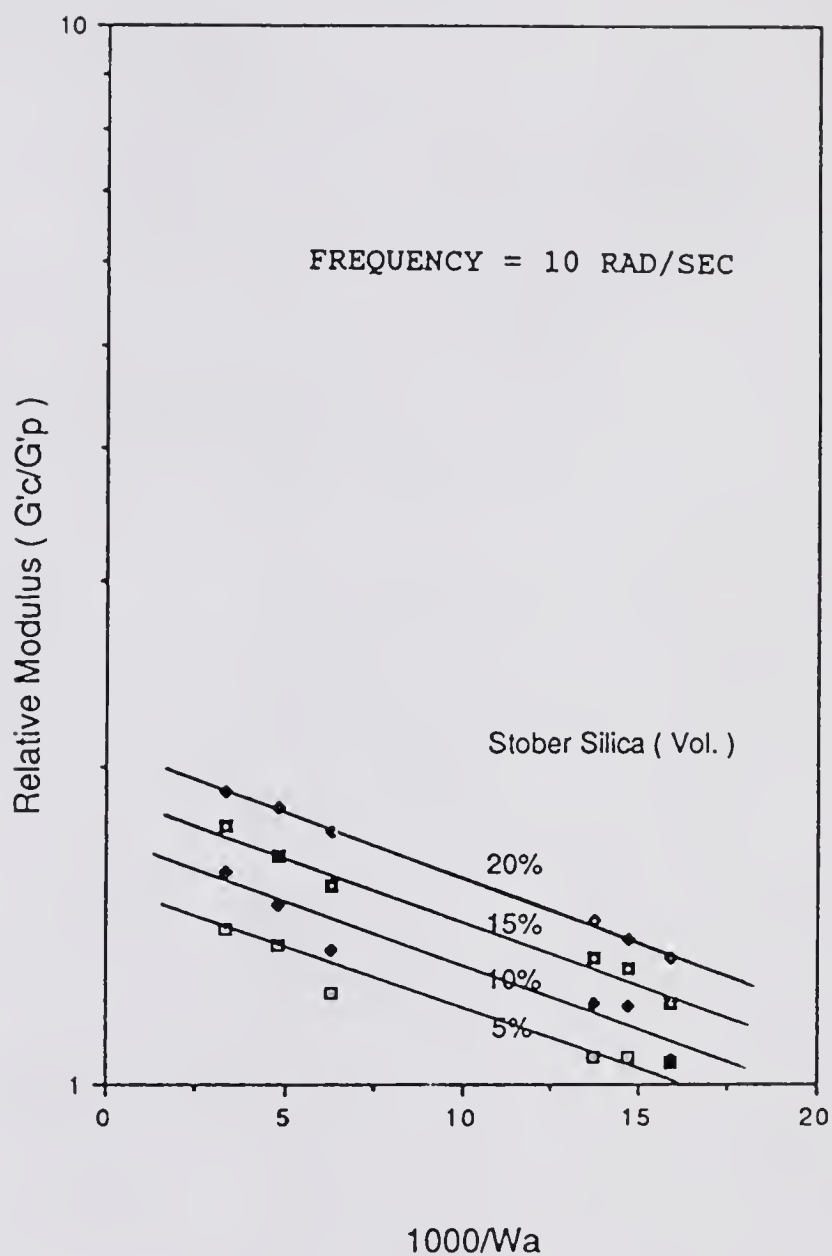


Figure 5.26 Effect of Work of Adhesion and Volume Fraction on the Relative Shear Modulus of Stober Silica Filled E-Va Copolymer Measured at 10 rad/sec

When the apparent surface energy barrier of relative shear modulus ( $G'_c/G'_p$ ) versus  $1000/Wa$  is plotted against the volume fractions of silica at a frequency of 0.1 rad/sec, the result is a horizontal line, as shown in Figure 5.27. When these energies are studied at other frequencies, such as 0.4, 1.0, 2.4 and 10 rad/sec, horizontal lines are also obtained. These data suggest that the apparent surface energy barrier of relative shear moduli is only dependent on frequency and is independent of volume fraction of silica in the range of study.

Figure 5.27 shows the effect of frequency on the Y-axis intercept of the horizontal lines [that is, the line formed from the apparent surface energy barrier of shear modulus (i.e., the slopes of  $G'_c/G'_p$  vs.  $1000/Wa$ ) against volume fraction of silica], which is relevant to the quantitative study of rheological properties. Each of the horizontal lines in Figure 5.27 has different intercepts at the Y-axis. When these values are plotted against the logarithm of frequency, a straight line is obtained, as shown in Figure 5.28. In other words, the intercept of the horizontal line in Figure 5.27 is linearly dependent on the logarithm of frequency.

The relationships discussed above between the work of adhesion and relative shear modulus ( $G'_c/G'_p$ ) of filled polymer melts can be described by a mathematical equation.

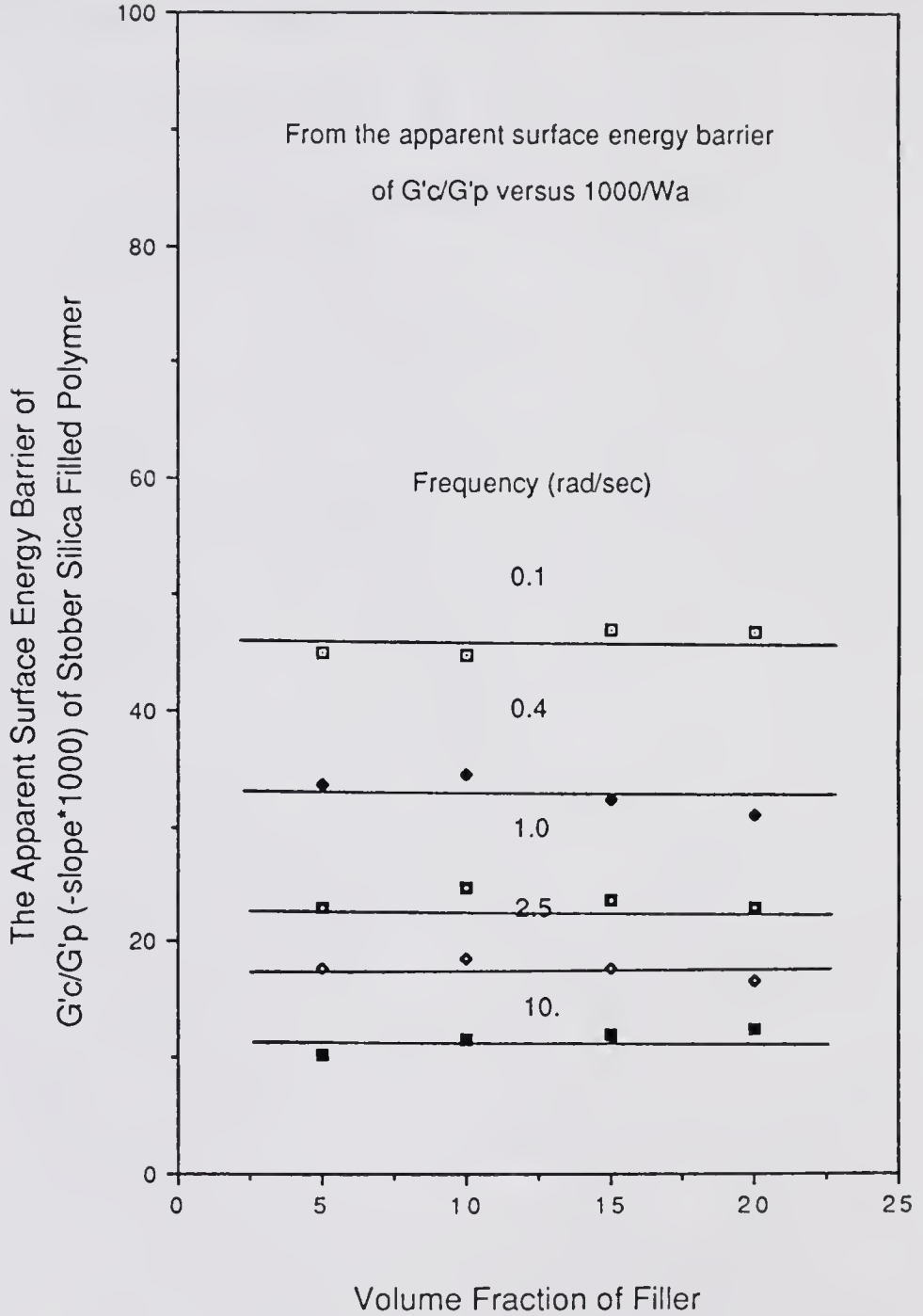


Figure 5.27 Effect of Volume Fraction of Stober Silica and Frequency on the Apparent Surface Energy Barrier of Shear Modulus

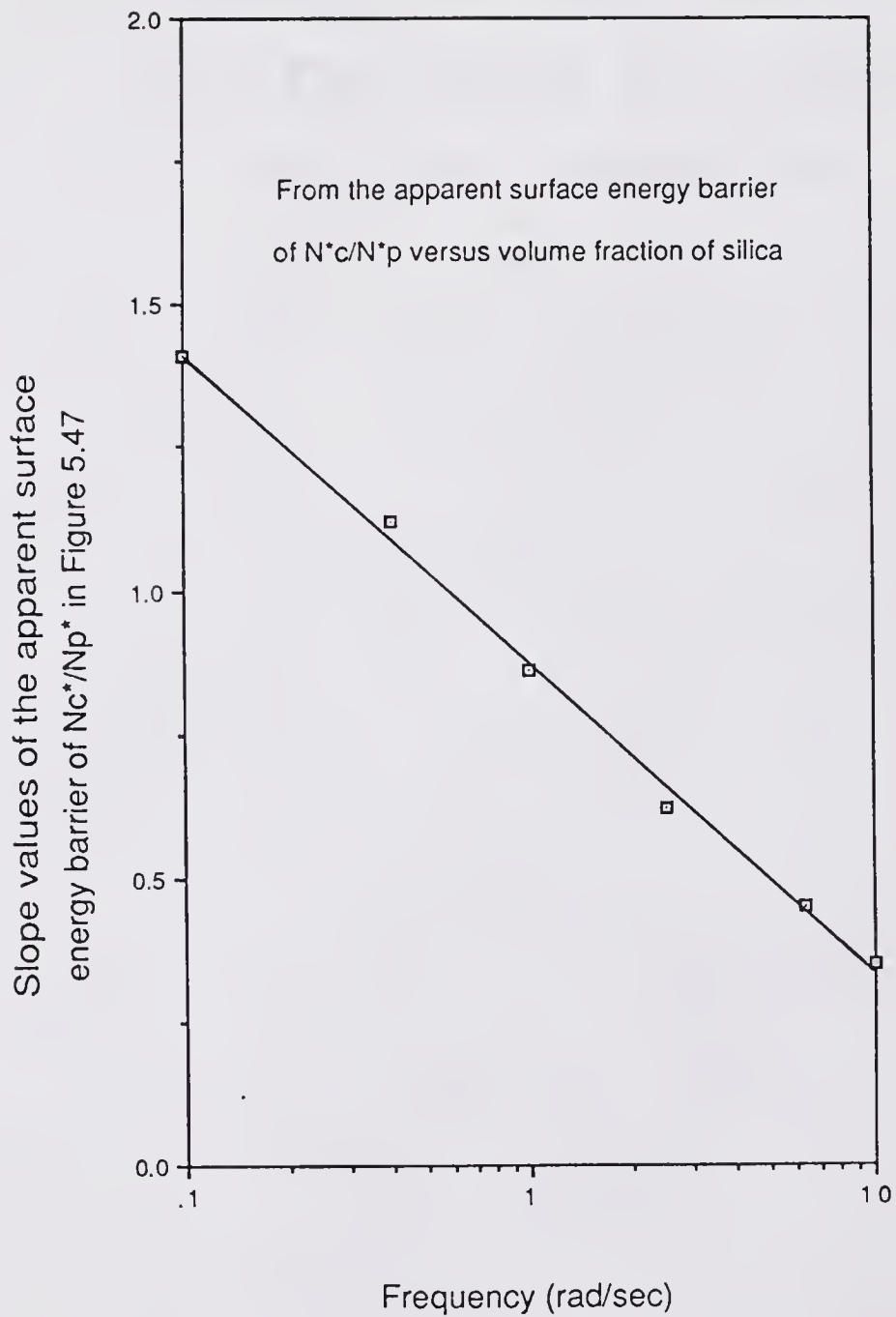


Figure 5.28 Effect of Frequency on the Intercept Values in Figure 5.27

In Figures 5.19 to 5.23, the relationship between the relative shear storage modulus and work of adhesion can be expressed as

$$\frac{G'_c}{G'_p} = C e^{-K \left( \frac{1}{Wa} \right)} \quad ( 5.11 )$$

where

$G'_c$  = shear modulus of silica filled polymer composite

$G'_p$  = shear modulus of the unfilled E-Va copolymer

$Wa$  = work of adhesion

$C$  = constant at a given filler concentration

$K$  = slope of  $G'_c/G'_p$  vs.  $1/Wa$ ; the apparent surface energy barrier of relative shear modulus

With different silica surface properties of a given filler concentration of polymer melts, the shear storage modulus can be expressed by

$$\frac{G'_c}{G'_{co}} = e^{-K \left( \frac{1}{Wa} - \frac{1}{Wao} \right)} \quad ( 5.12 )$$

where

$G'_{co}$  = shear modulus of a composite with the poorest interfacial bonding ( $Wao = 63 \text{ erg cm}^{-2}$  for  $110^\circ\text{C/TMCS}$ )

$Wao$  = Work of adhesion of the poorest interfacial bonding at the interface

K is a function of frequency and particle size, but not a function of volume fraction of filler.

At a constant frequency:

$$K \neq f( V_f ) \quad ( 5.13 )$$

$$K = A + B \cdot V_f \quad B=0 \quad ( 5.14 )$$

But with varying frequencies:

$$A = C + m \cdot \log w \quad ( 5.15 )$$

Therefore:

$$K = C - m \cdot \log w \quad ( 5.16 )$$

where w is frequency, and C and m are dependent on the particle size of filler.

### 5.3.2 Melt Viscosity of Silica Filled Polymer

#### 5.3.2.1 Dependence of frequency and solid loading on the melt viscosity

##### 5.3.2.1.1 Cab-O-Sil silica filled composites

The melt viscosity of the 5% volume fraction of Cab-O-Sil silica filled E-Va copolymer versus frequency, measured at 210°C, is plotted in Figure 5.29. The

viscosity decreases extend over many decades of change in frequency (8,148,149, 247-259).

The response of a polymer at high frequencies is limited to a small segment of polymer molecular chain since the polymer is a viscoelastic material (164). The characteristics of the entanglements of polymer molecular chains will be ignored and the viscosity then becomes small (164). The viscosity at a high frequency is several orders of magnitude smaller than the viscosity of the same polymer at a low frequency.

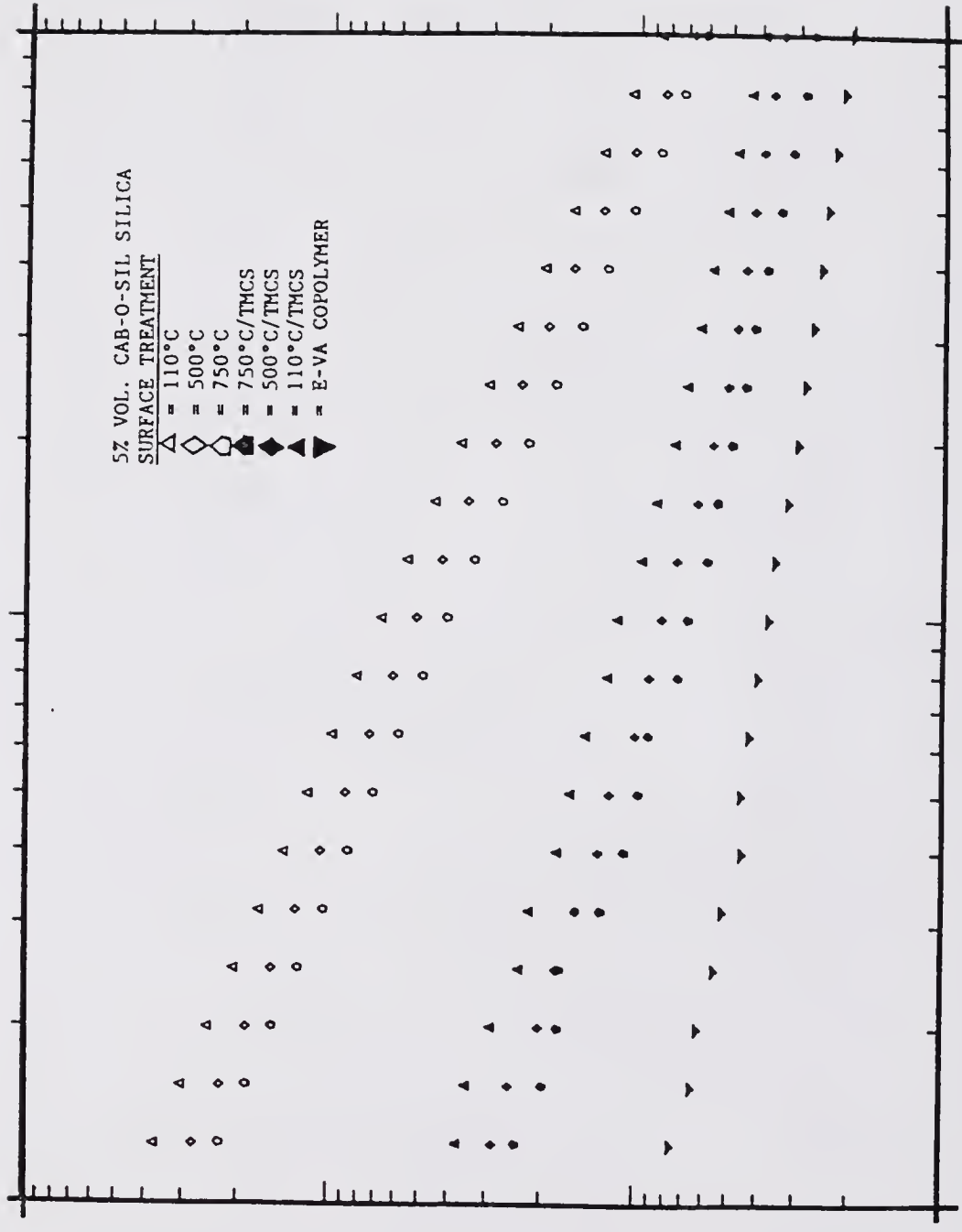
In Figure 5.29, it is seen that better interfacial bonding corresponds to a higher melt viscosity. At low frequencies, the viscosities of the heat treated Cab-O-Sil silica filled polymer melts form one group, which has higher viscosities than those of the other group filled by heat/TMCS treated silica.

The viscosities of these filled melts approach a constant value as frequency increases. Figure 5.30 shows the relative viscosity ( $\eta_c^*/\eta_p^*$ ) versus frequency. It indicates that relative viscosity reaches a constant value and becomes independent of frequency and interfacial bonding when the frequency increases.

#### 5.3.2.1.2 Stöber silica filled composites

The dynamic viscosities of the Stöber silica filled E-Va copolymers, measured at 150°C, are studied at 20%, 15%, 10% and 5% volume fractions of silica fillers.

1.0E6



1.0E3

1.0E-1

FREQ RAD/SEC

Figure 5.29 Effect of Frequency and Surface Properties of Silica on the Melt Viscosity of 5% Volume Cab-O-Sil Filled Copolymer

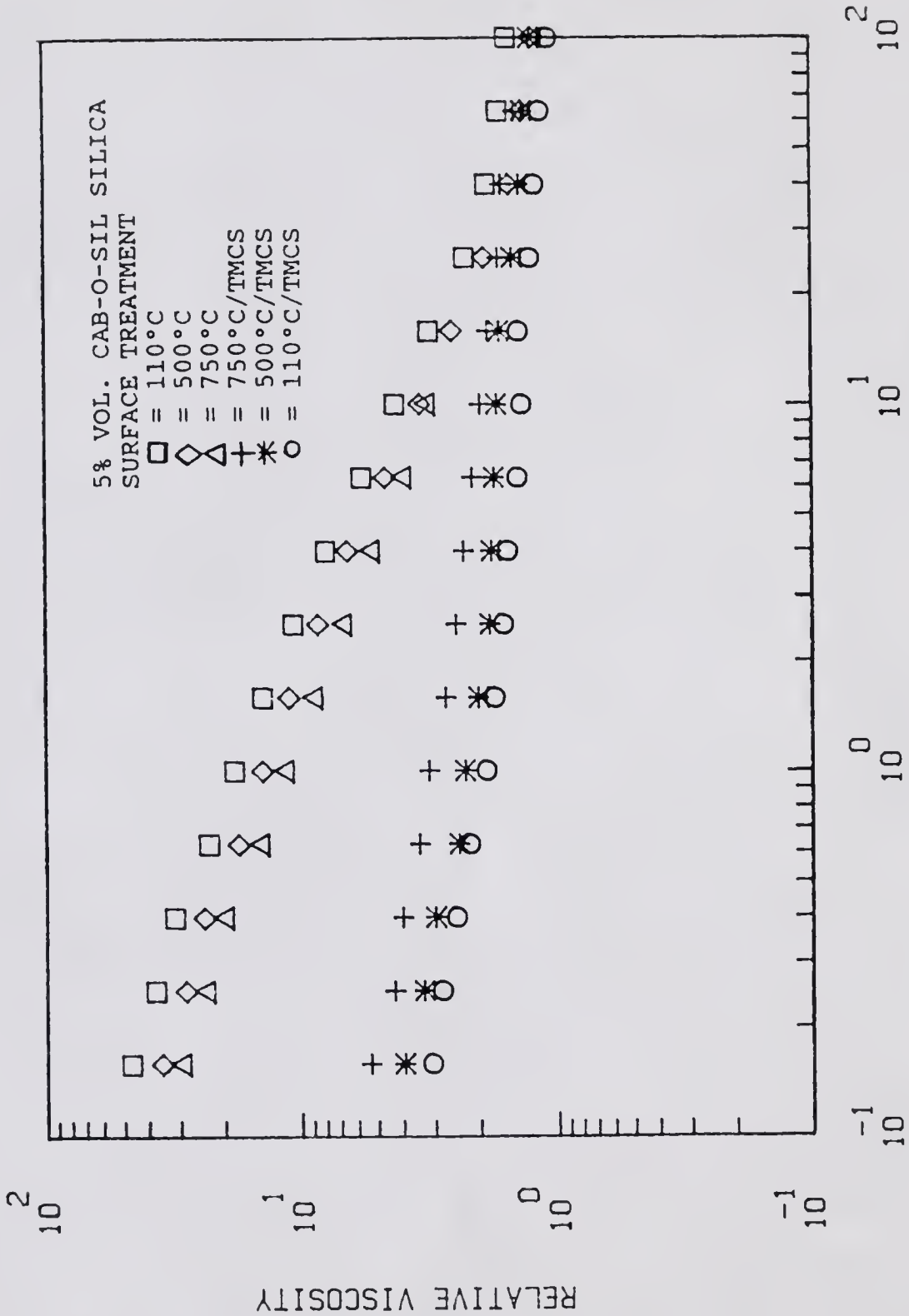


Figure 5.30 Relative Melt Viscosity versus Frequency of Various Surface Properties of 5% Volume Cab-O-Sil Filled Copolymer

Figures 5.31 to 5.34 show these plots of  $\log \eta^*$  of various volume fractions of silica filled polymer melts versus frequency. The results show a similar trend to those from the Cab-O-Sil silica filled polymer melts, the  $\log \eta^*$  of the Stöber silica filled polymer melts decreasing with an increase in frequency.

The polymer melt filled by the silica with good interfacial bonding has a higher viscosity than when filled with silica having poor interfacial bonding. At 20% volume fraction of Stöber silica filled polymer melts, the viscosities of the heat treated silica filled polymer melts form one group at low frequencies, which has higher viscosities than those of the other group filled by heat/TMCS treated silica. However, when the volume fraction of Stöber silica is reduced to 5%, the viscosity of each group is not much different. This result is different from the result seen with a 5% Cab-O-Sil silica filled polymer melt because the surface area of Cab-O-Sil silica is much higher even though the volume fraction of silica is the same.

The relative melt viscosity ( $\eta_c^*/\eta_p^*$ ), Figures 5.35 to 5.38, shows similar trends to the relative shear storage modulus of the Stöber silica filled E-Va copolymer. The relative viscosities approximate to a constant value at high frequencies regardless of the volume fractions of filler and surface properties of Stöber silica filler.

3.0E5

ETA\* POISE (Δ)

3.0E3

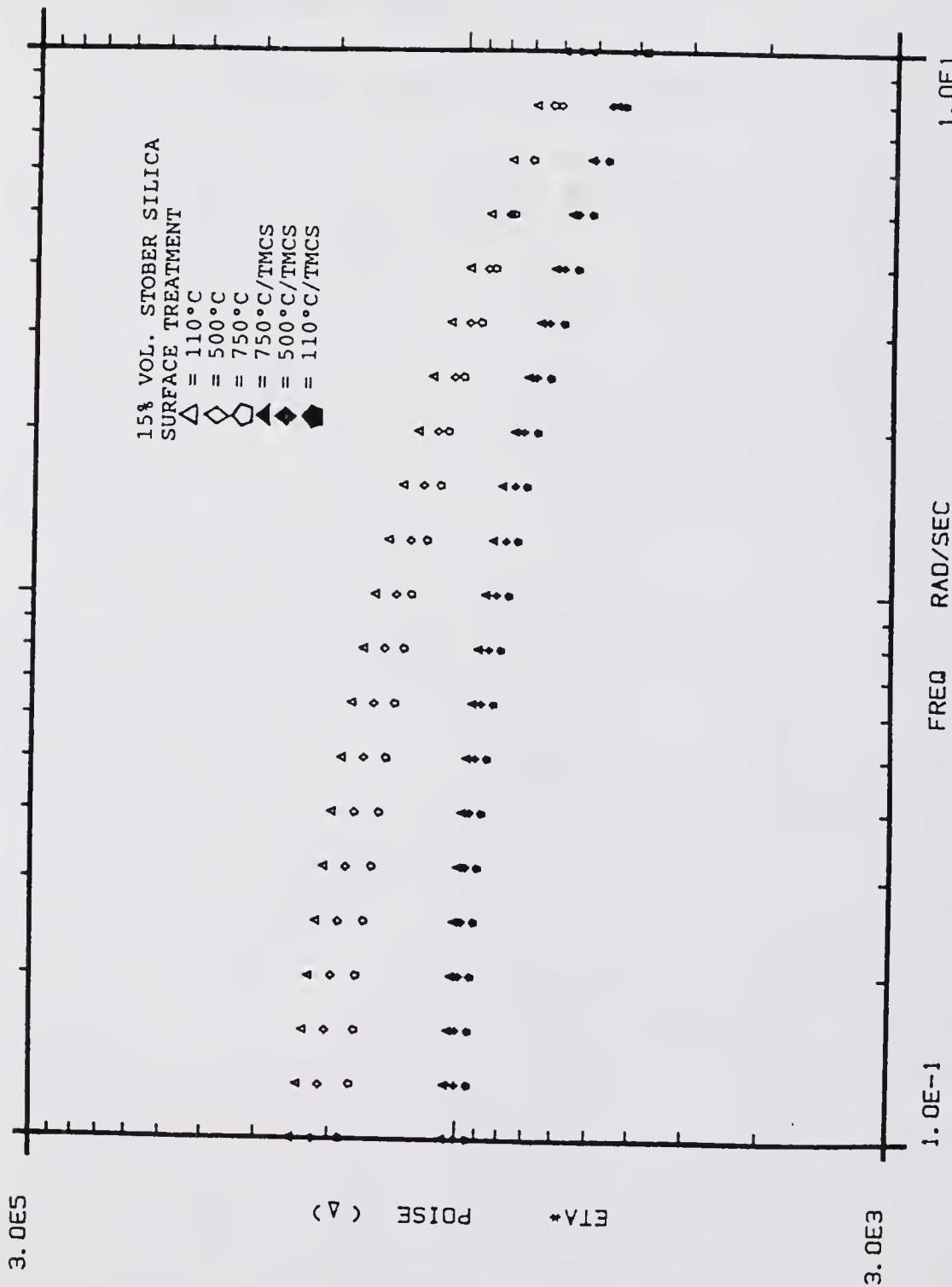
20% VOL. STÖBER SILICA  
 SURFACE TREATMENT  
 = 110°C  
 = 500°C  
 = 750°C  
 = 750°C/TMCS  
 = 500°C/TMCS  
 = 110°C/TMCS  
 = E-Va Copolymer

1.0E1

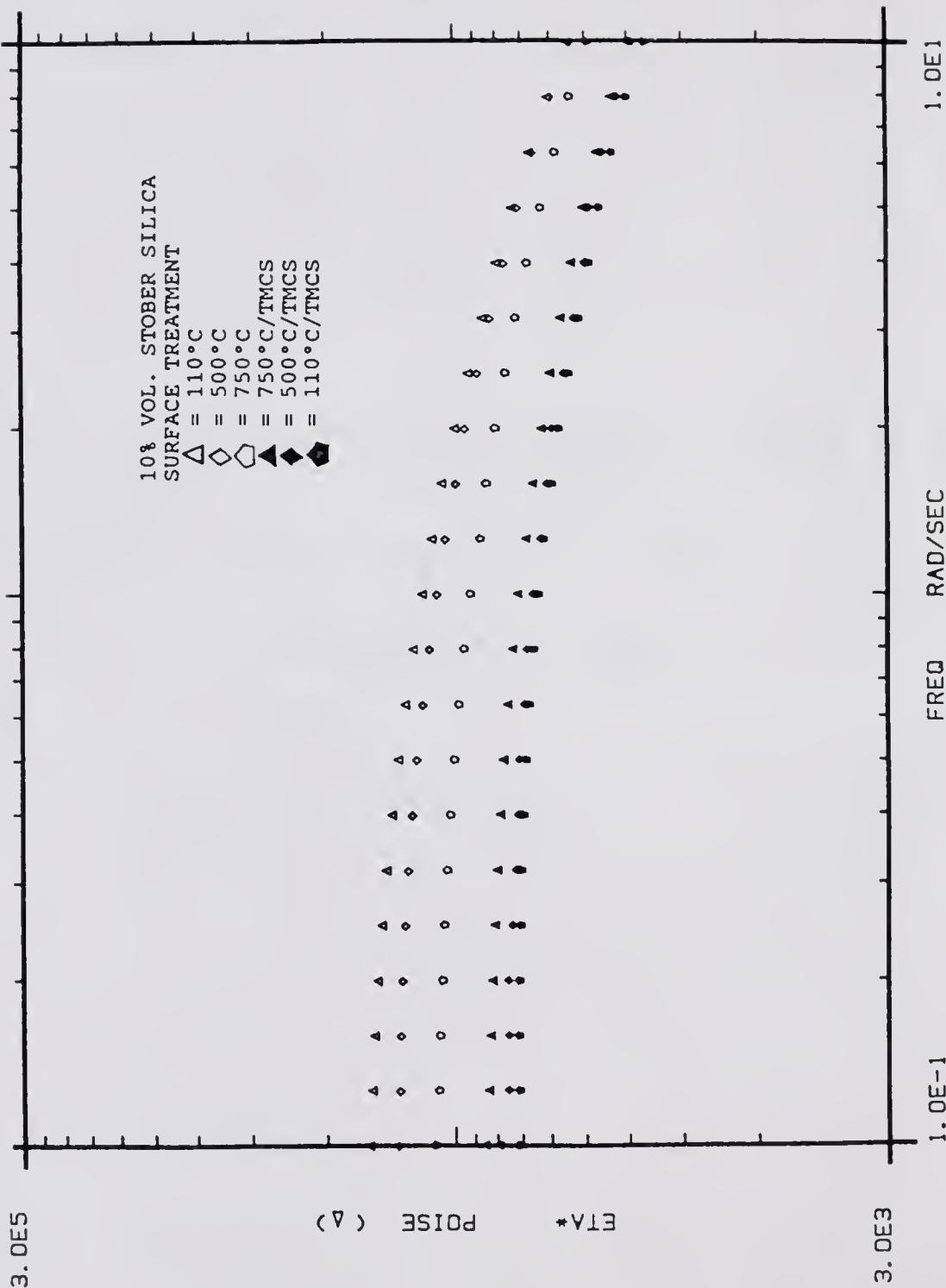
FREQ RAD/SEC

1.0E-1

Figure 5.31 Effect of Frequency and Surface Properties of Silica on the Melt Viscosity of 20% Volume Stöber Filled Copolymer



1.0E-1  
1.0E1  
Effect of Frequency and Surface Properties of Silica on the  
Melt Viscosity of 15% Volume Stöber Filled Copolymer



1.0E-1 1.0E1  
 Effect of Frequency and Surface Properties of Silica on the  
 Melt Viscosity of 10% Volume Stöber Filled Copolymer

3.0E5

3.0E3

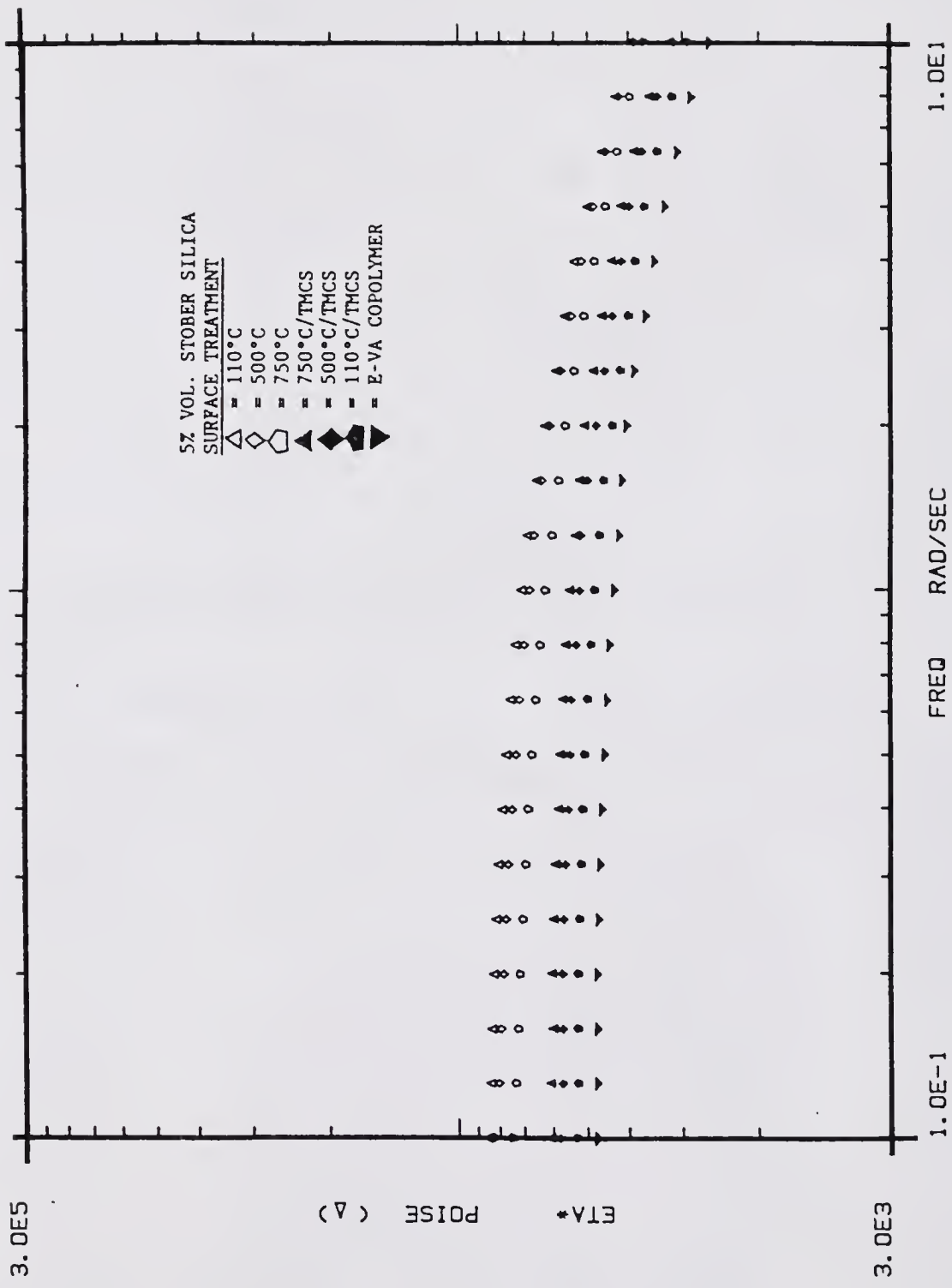


Figure 5.34 Effect of Frequency and Surface Properties of Silica on the Melt Viscosity of 5% Volume Stöber Filled Copolymer

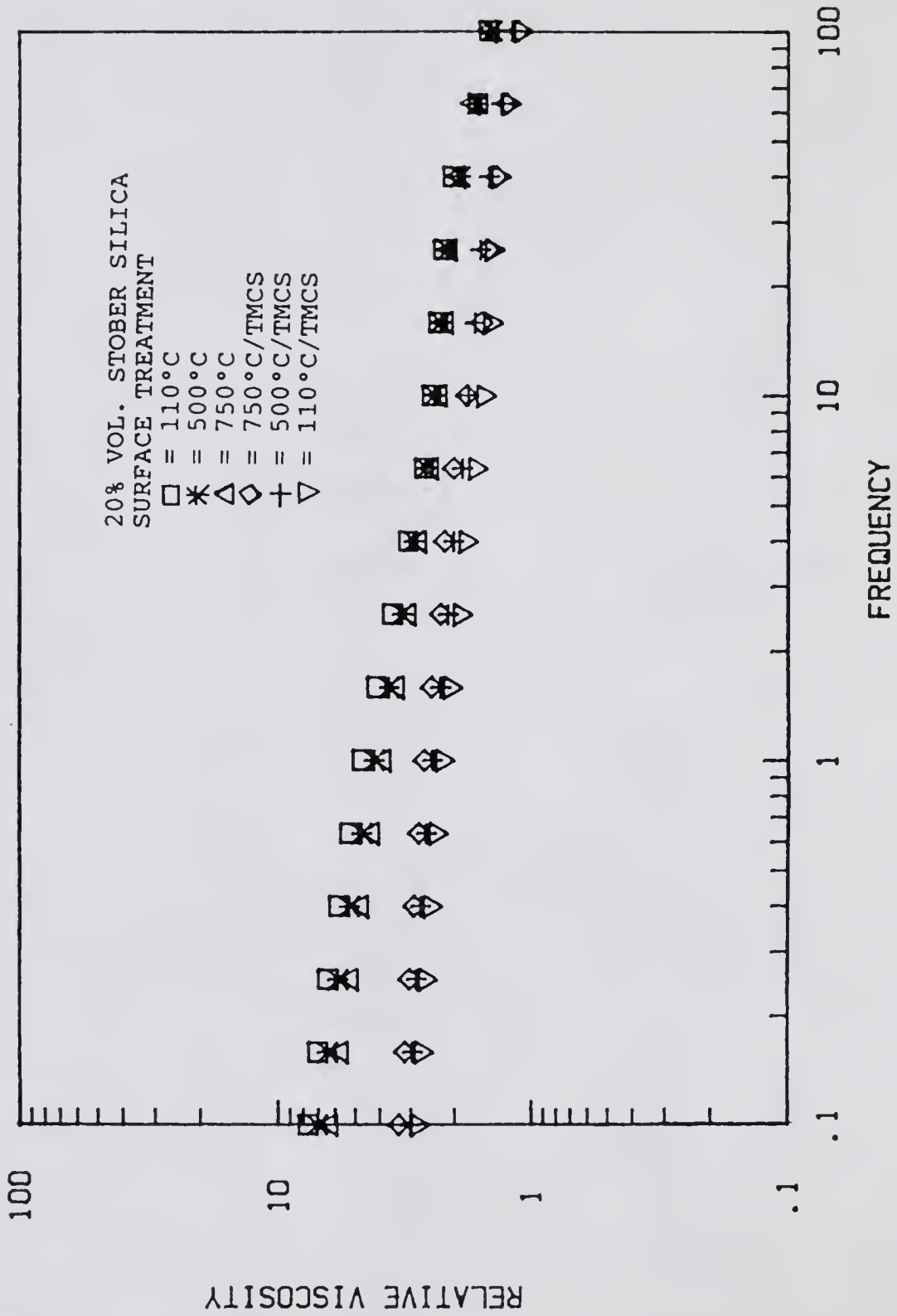


Figure 5.35 Relative Melt Viscosity versus Frequency of Various Surface Properties of 20% Volume Stöber Silica Filled Copolymer

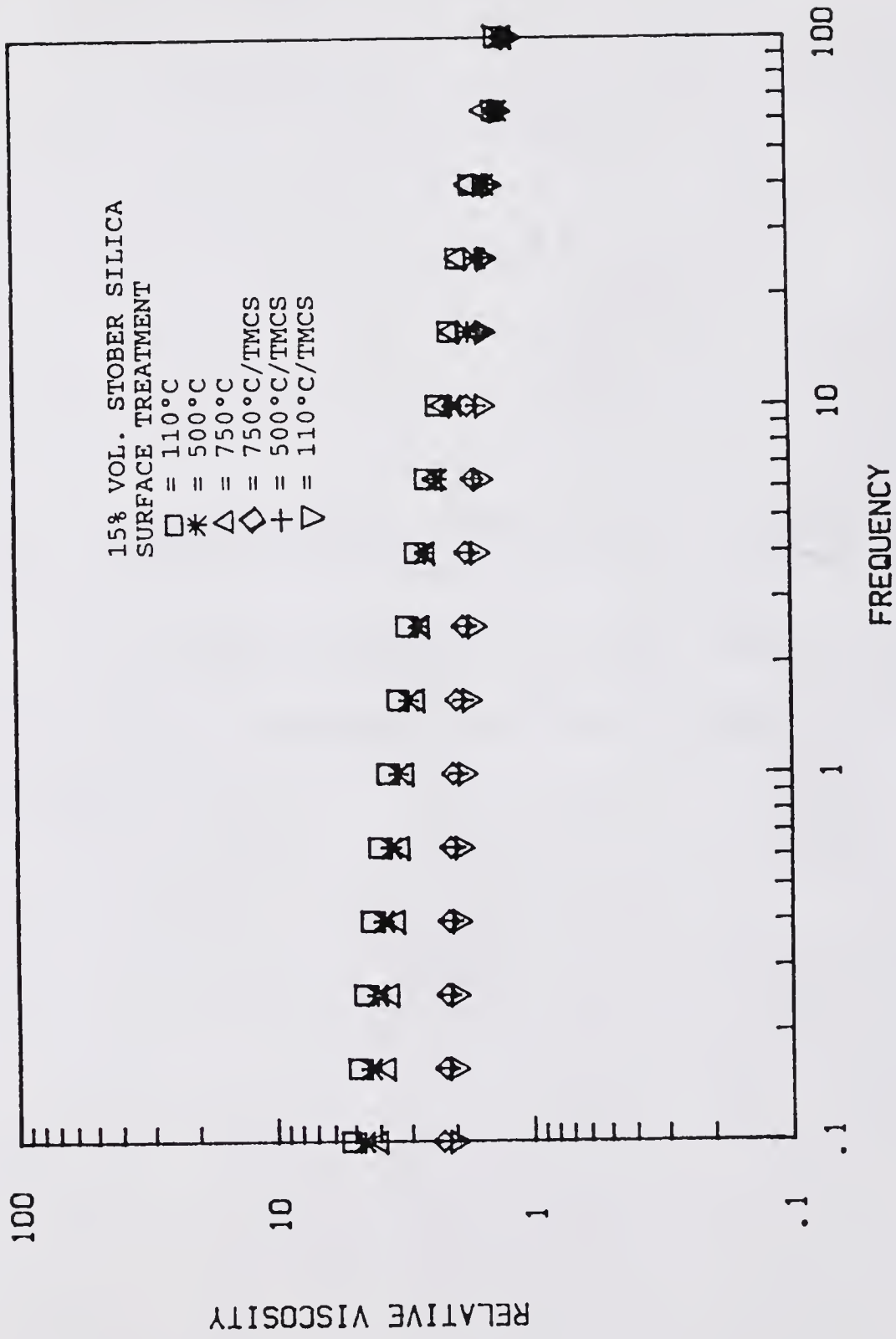


Figure 5.36 Relative Melt Viscosity versus Frequency of Various Surface Properties of 15% Volume Stöber Silica Filled Copolymer

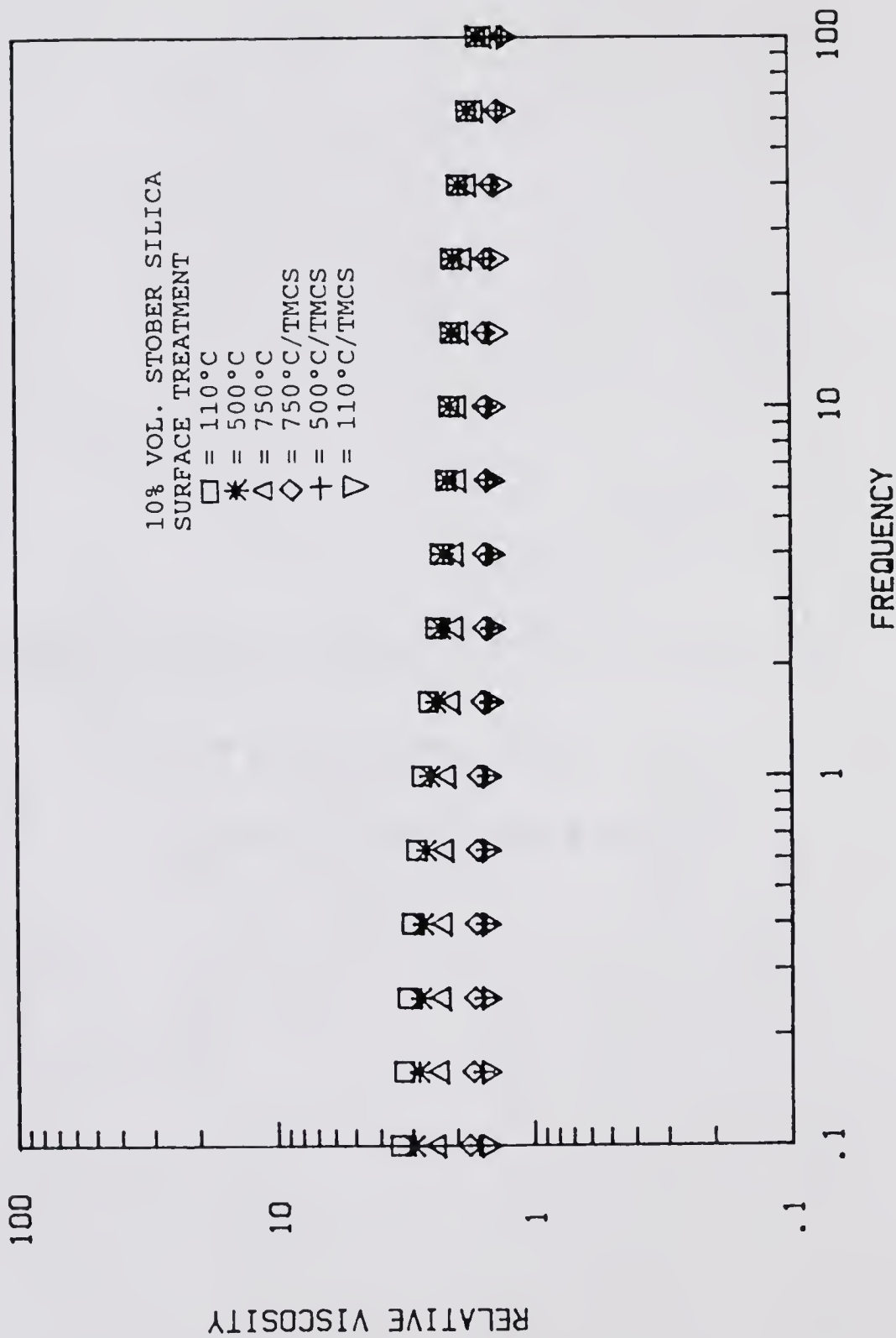


Figure 5.37 Relative Melt Viscosity versus Frequency of Various Surface Properties of 10% Volume Stober Silica Filled Copolymer

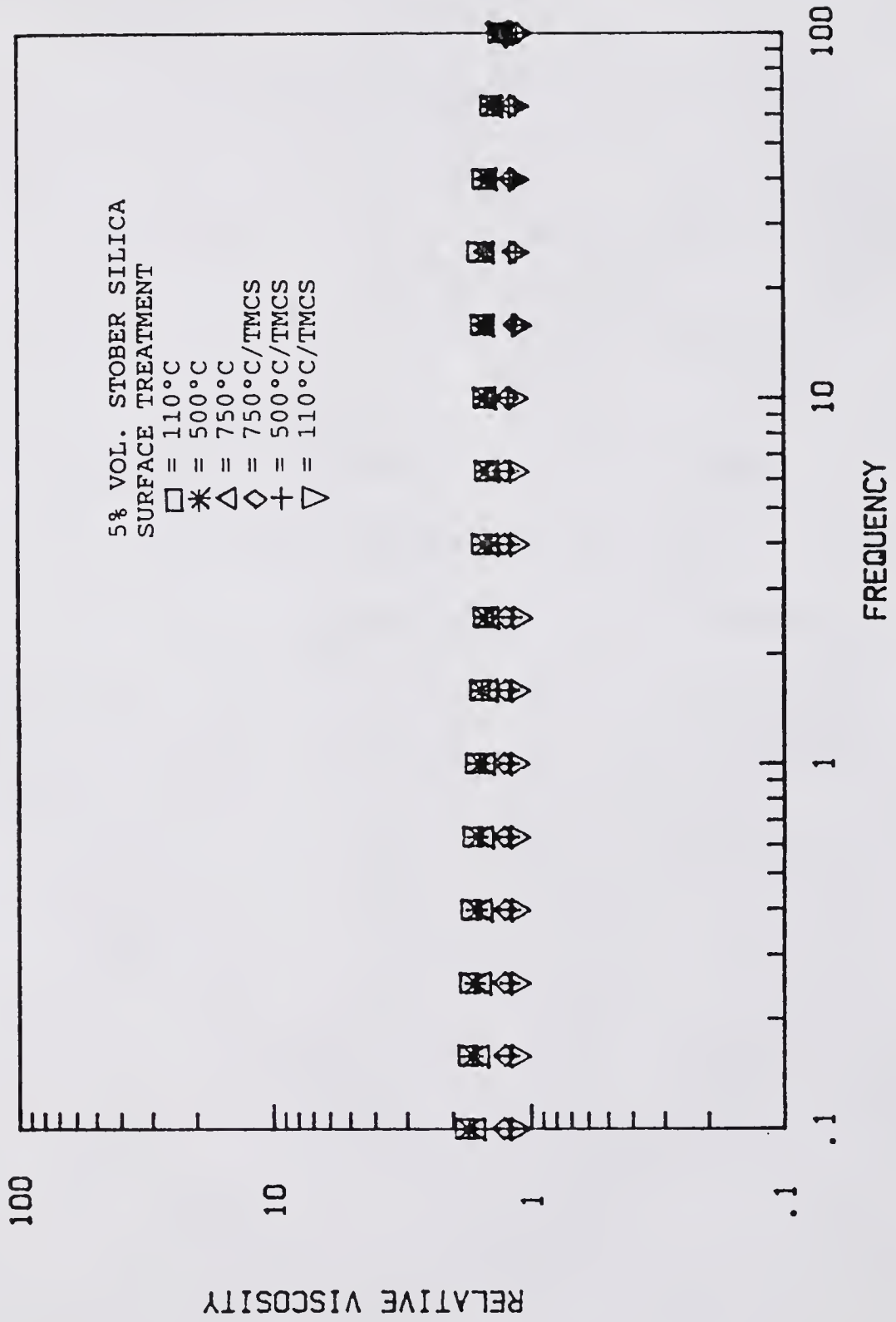


Figure 5.38 Relative Melt Viscosity versus Frequency of Various Surface Properties of 5% Volume Stöber Silica Filled Copolymer

### 5.3.2.2 Dependence of work of adhesion on the melt viscosity

#### 5.3.2.2.1 Cab-O-Sil silica filled composites

Figure 5.39 shows the effect of work of adhesion on the relative melt viscosity of 5% volume Cab-O-Sil silica filled E-Va copolymer. The relative melt viscosity of filled polymer melts is higher when work of adhesion is increased.

Regardless of the frequencies studied, there exists an exponential relationship between the relative melt viscosity of filled polymer and reciprocal work of adhesion. However, the slope value becomes higher with a decrease in frequency. This slope will be defined in Chapter 6 as the apparent surface energy barrier of the relative melt viscosity. In other words, work of adhesion has the greater effect on the relative viscosity of filled melts at a low frequency. At a higher frequency, work of adhesion is not as effective in controlling properties as at a lower frequency.

#### 5.3.2.2.2 Stöber silica filled composites

The effect of interfacial bonding on the relative melt viscosity of the 20% volume fraction of Stöber silica filled E-Va copolymer is shown in Figure 5.40. An exponential relationship is obtained again, and the apparent surface energy barrier of relative melt viscosity is higher when the frequency is lower. The other volume

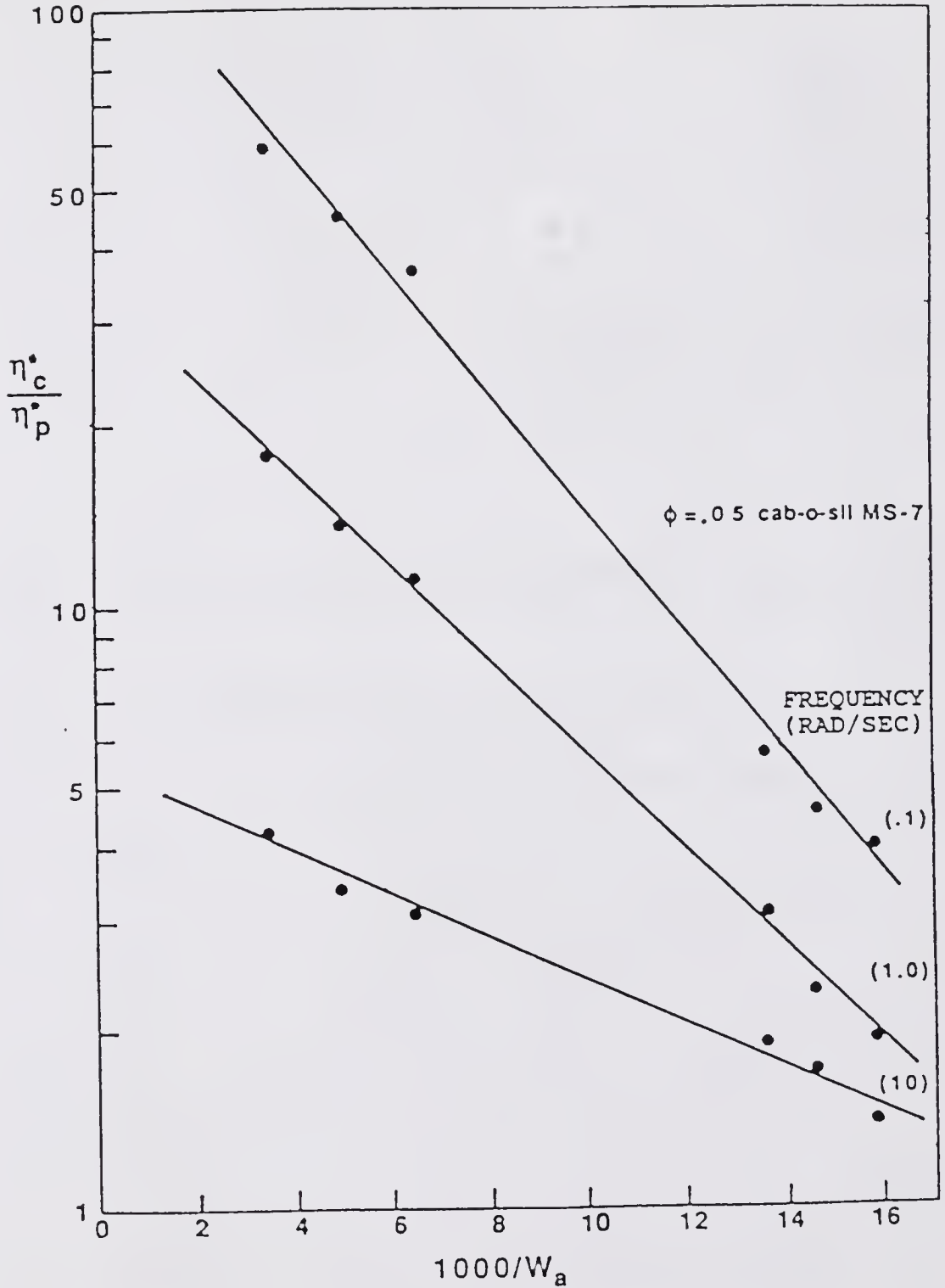


Figure 5.39 Effect of Work of Adhesion and Frequency on the Relative Viscosity of 5% Volume Cab-O-Sil Silica Filled E-Va Copolymer

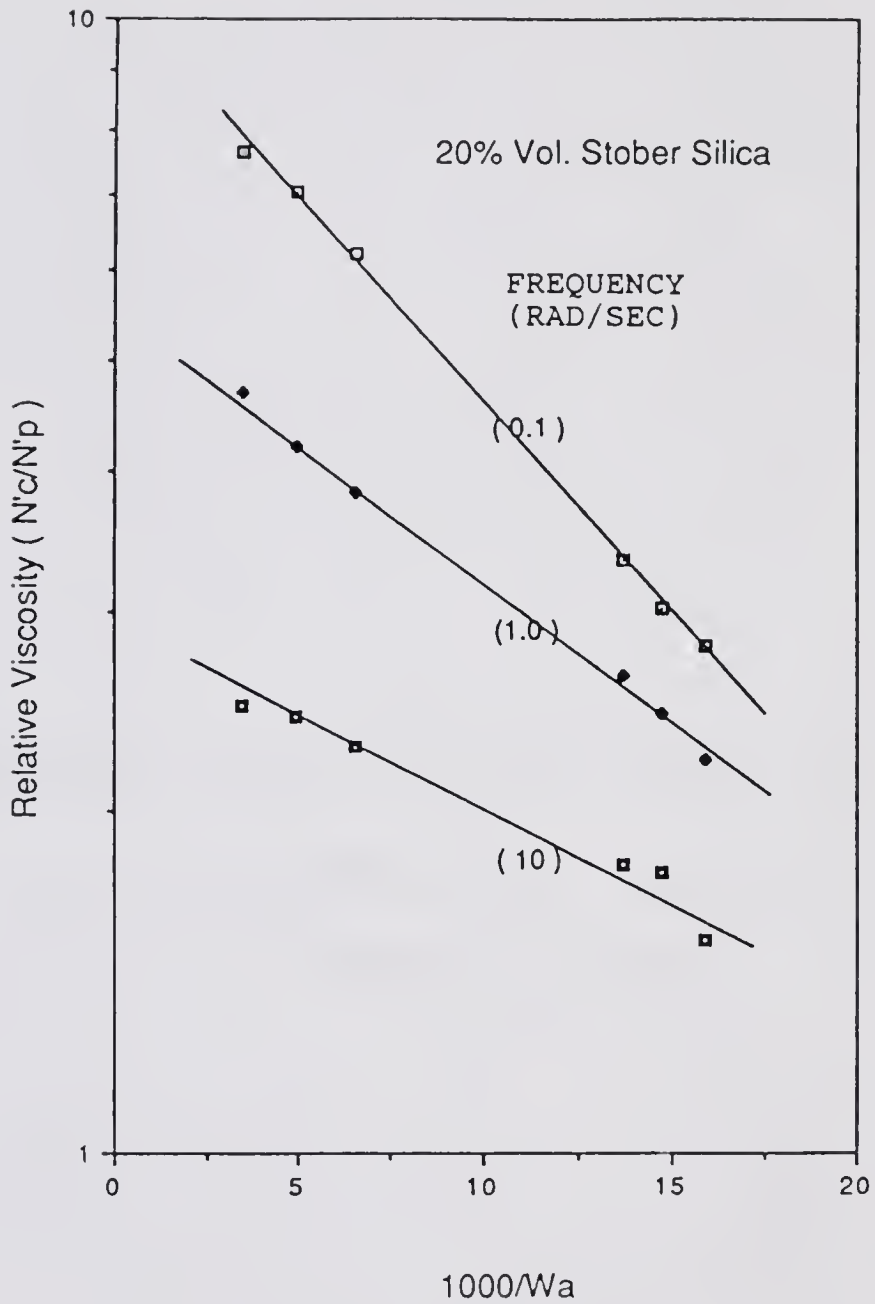


Figure 5.40 Effect of Work of Adhesion and Frequency on the Relative Viscosity of 20% Volume Stober Silica Filled E-Va Copolymer

fractions at 15%, 10% and 5% of Stöber silica filled E-Va copolymer also have exponential relationships between the reciprocal work of adhesion and relative dynamic viscosity, as shown in Figures 5.41 to 5.43.

At a given frequency of dynamic mode, it is interesting to study the effect of work of adhesion on the relative viscosity of various volume fractions of Stöber silica filled E-Va copolymer. Figure 5.44 shows the relative viscosities of different volume fractions of Stöber silica versus reciprocal work of adhesion at frequency of 0.10 rad/sec.

The relative viscosities of filled polymer melts are increased when the volume fractions silica are increased. Furthermore, the apparent surface energy barrier of relative melt viscosity increases with an increase in volume fraction of silica filler. This result is different from the result with the relative shear modulus in section 5.4.1.2, where the apparent surface energy barrier of relative shear modulus is independent of volume fraction of silica in the range of study. When the studied frequencies are changed to 1.0 or 10 rad/sec, in Figure 5.45 and 5.46, respectively, the apparent surface energy barrier of the relative viscosities is also dependent on the volume fraction of Stöber silica.

At a frequency equal to 0.1 rad/sec in Figure 5.44, when the apparent surface energy barrier of the relative

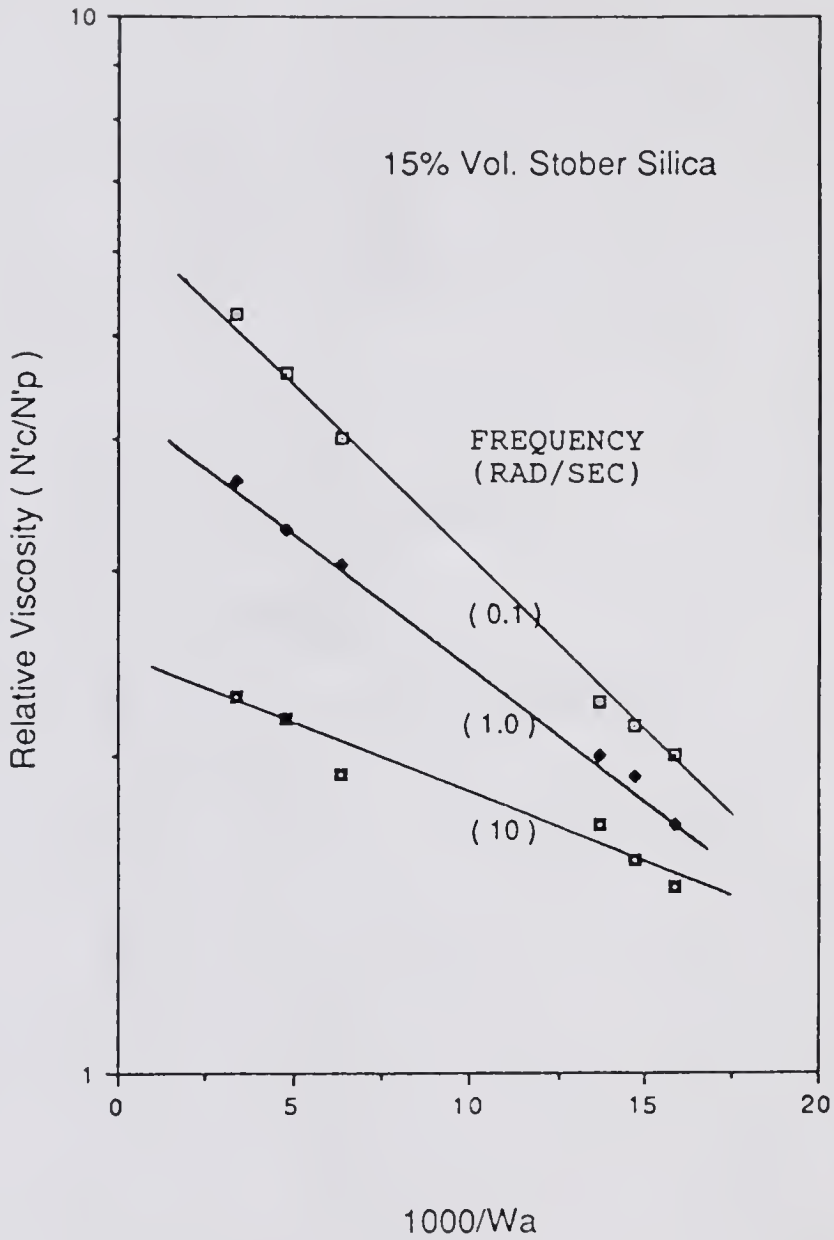


Figure 5.41 Effect of Work of Adhesion and Frequency on the Relative Viscosity of 15% Volume Stober Silica Filled E-Va Copolymer

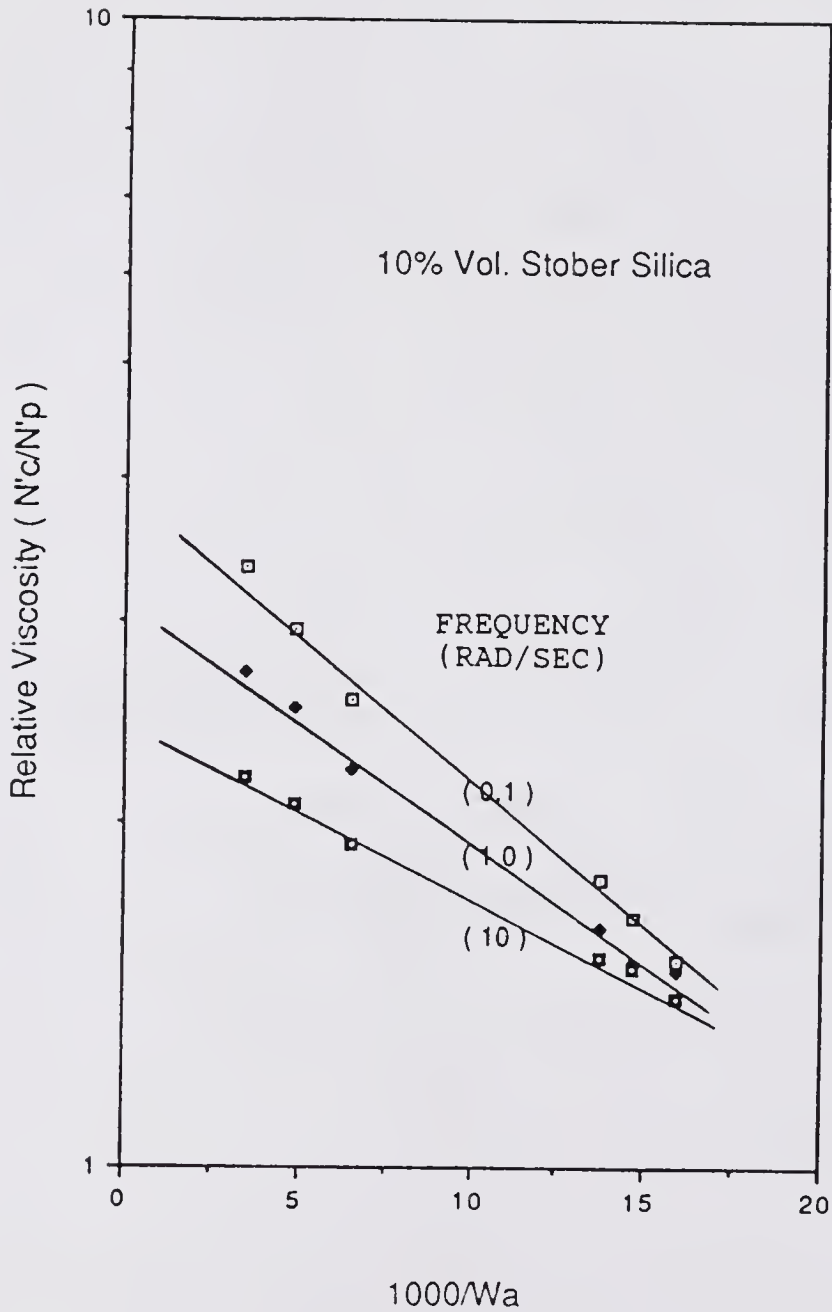


Figure 5.42 Effect of Work of Adhesion and Frequency on the Relative Viscosity of 10% Volume Stober Silica Filled E-Va Copolymer

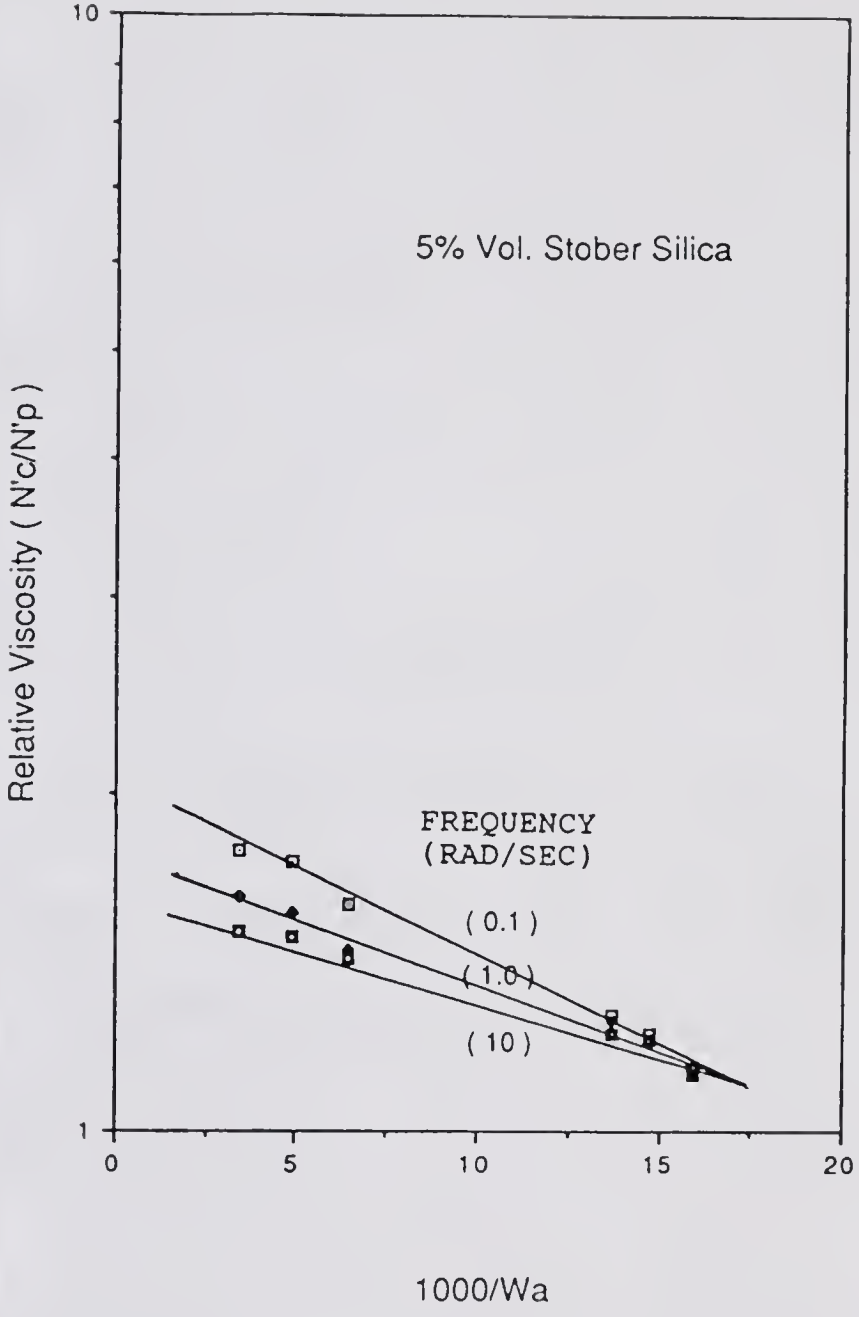


Figure 5.43 Effect of Work of Adhesion and Frequency on the Relative Viscosity of 5% Volume Stober Silica Filled E-Va Copolymer

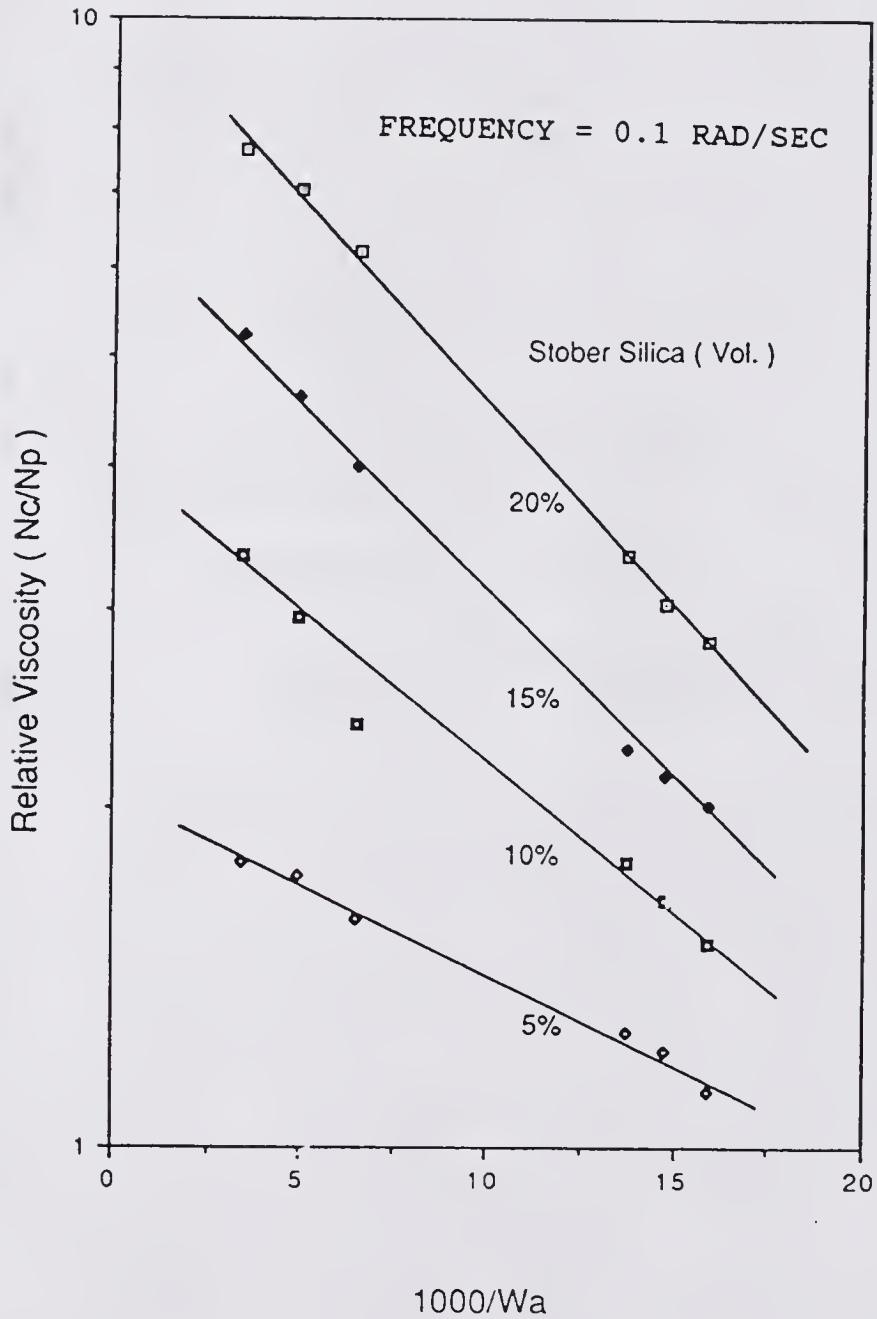


Figure 5.44 Effect of Work of Adhesion and Volume Fraction on the Relative Viscosity of Stober Silica Filled E-Va Copolymer Measured at 0.1 rad/sec

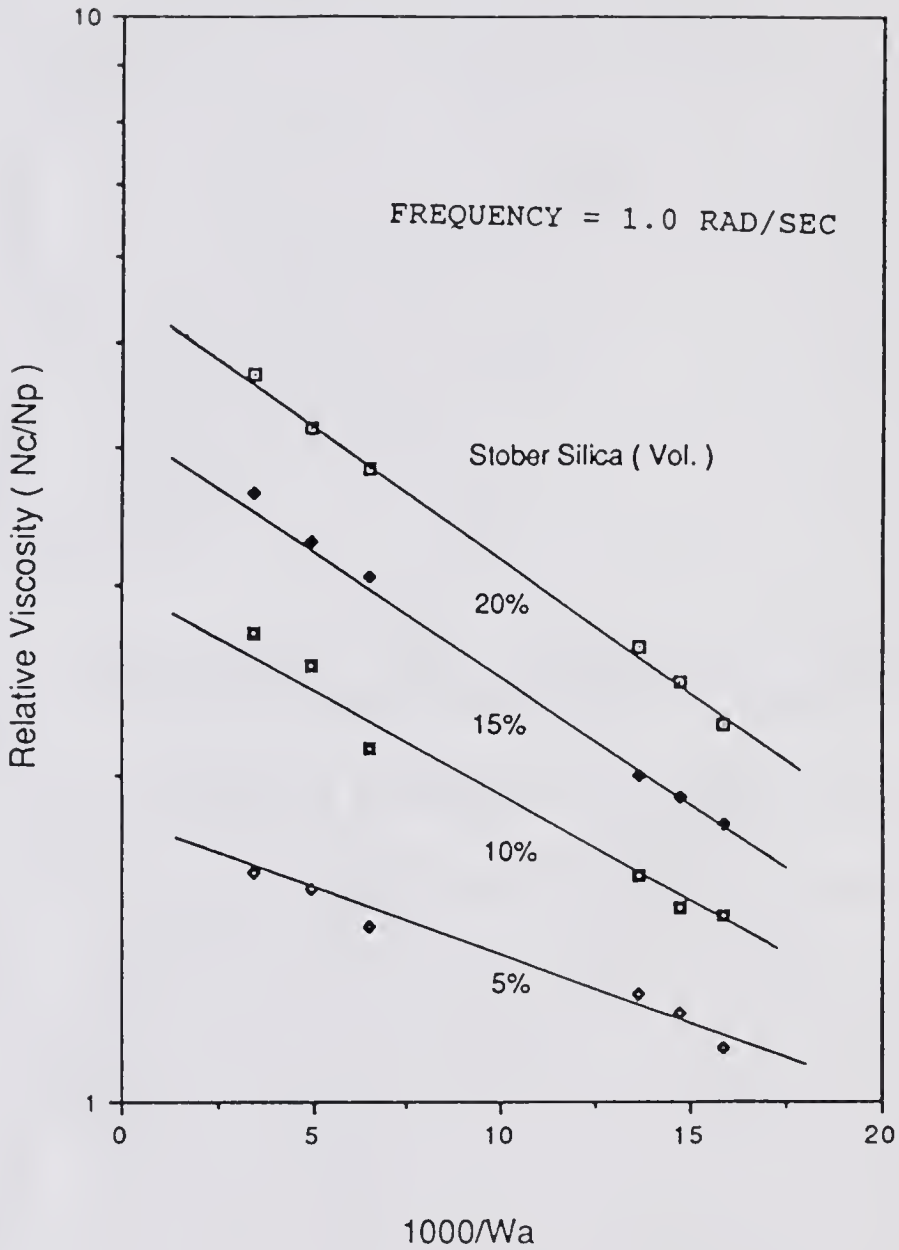


Figure 5.45 Effect of Work of Adhesion and Volume Fraction on the Relative Viscosity of Stober Silica Filled E-Va Copolymer Measured at 1.0 rad/sec

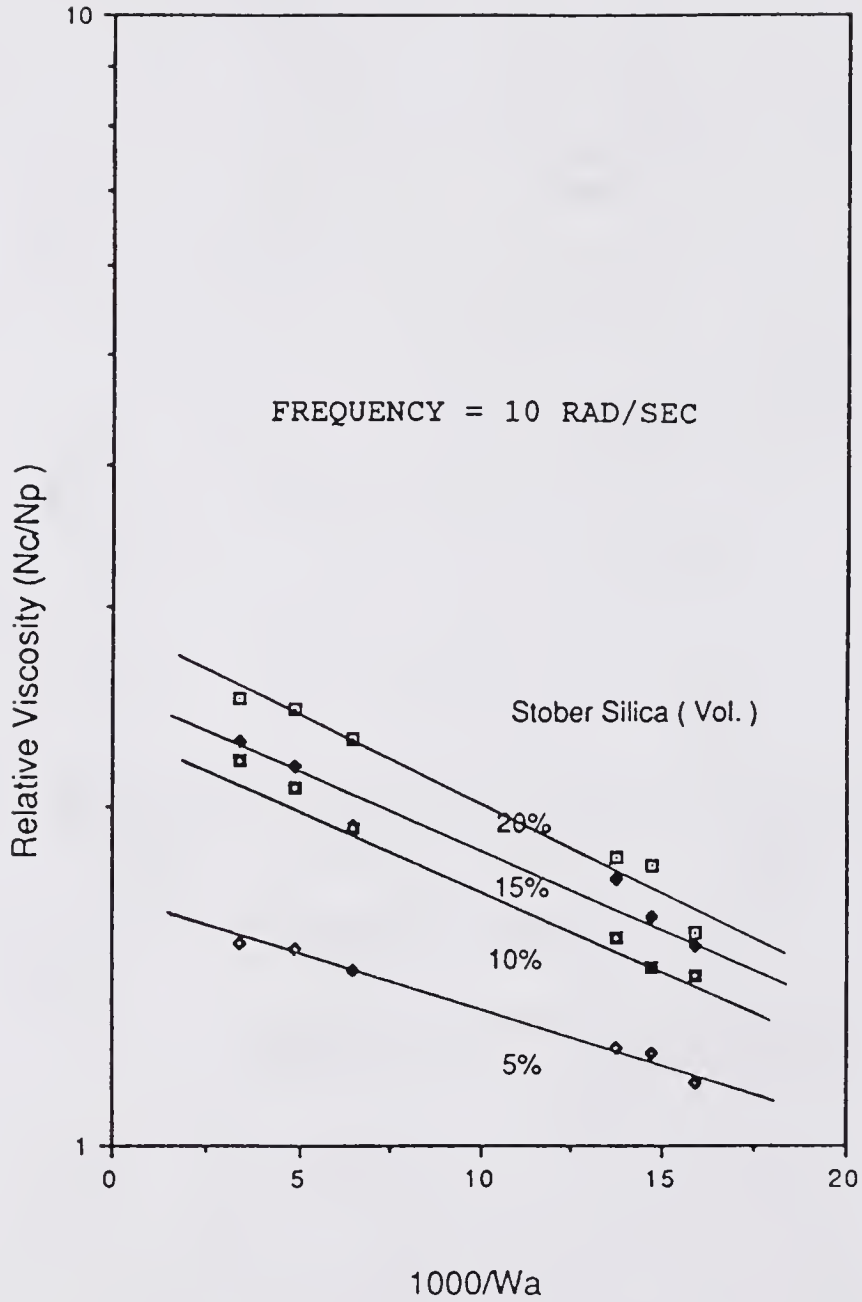


Figure 5.46 Effect of Work of Adhesion and Volume Fraction on the Relative Viscosity of Stober Silica Filled E-Va Copolymer Measured at 10 rad/sec

melt viscosities ( $\eta_c^*/\eta_p^*$ ) versus  $1000/Wa$  is plotted against volume fraction of filler, a linear relationship is obtained. This is shown in Figure 5.47. When the apparent surface energy barrier of relative viscosities versus volume fraction of silica is plotted at other frequencies, such as 0.4, 1.0, 2.4 and 10 rad/sec, they also show linear relationships. However, even though a linear relationship is obtained, each line is not parallel. In Figure 5.47, each of these lines has its own slope. These results suggest that the apparent surface energy barrier of the relative dynamic viscosities is dependent on frequency and volume fraction of Stöber silica in the range of study.

Furthermore, when these slopes in Figure 5.47 are plotted versus logarithm of frequency, a straight line is obtained in Figure 5.48. In other words, the slope (of the apparent surface energy barrier of  $\eta_c^*/\eta_p^*$  versus volume fraction of filler at each studied frequency) is linearly dependent on the logarithm of frequency.

The relationships discussed above between the relative melt viscosity ( $\eta_c^*/\eta_p^*$ ) of filled polymer melts and work of adhesion can be described by a mathematical equation.

From Figure 5.39 to 5.43, the relationship can be expressed as

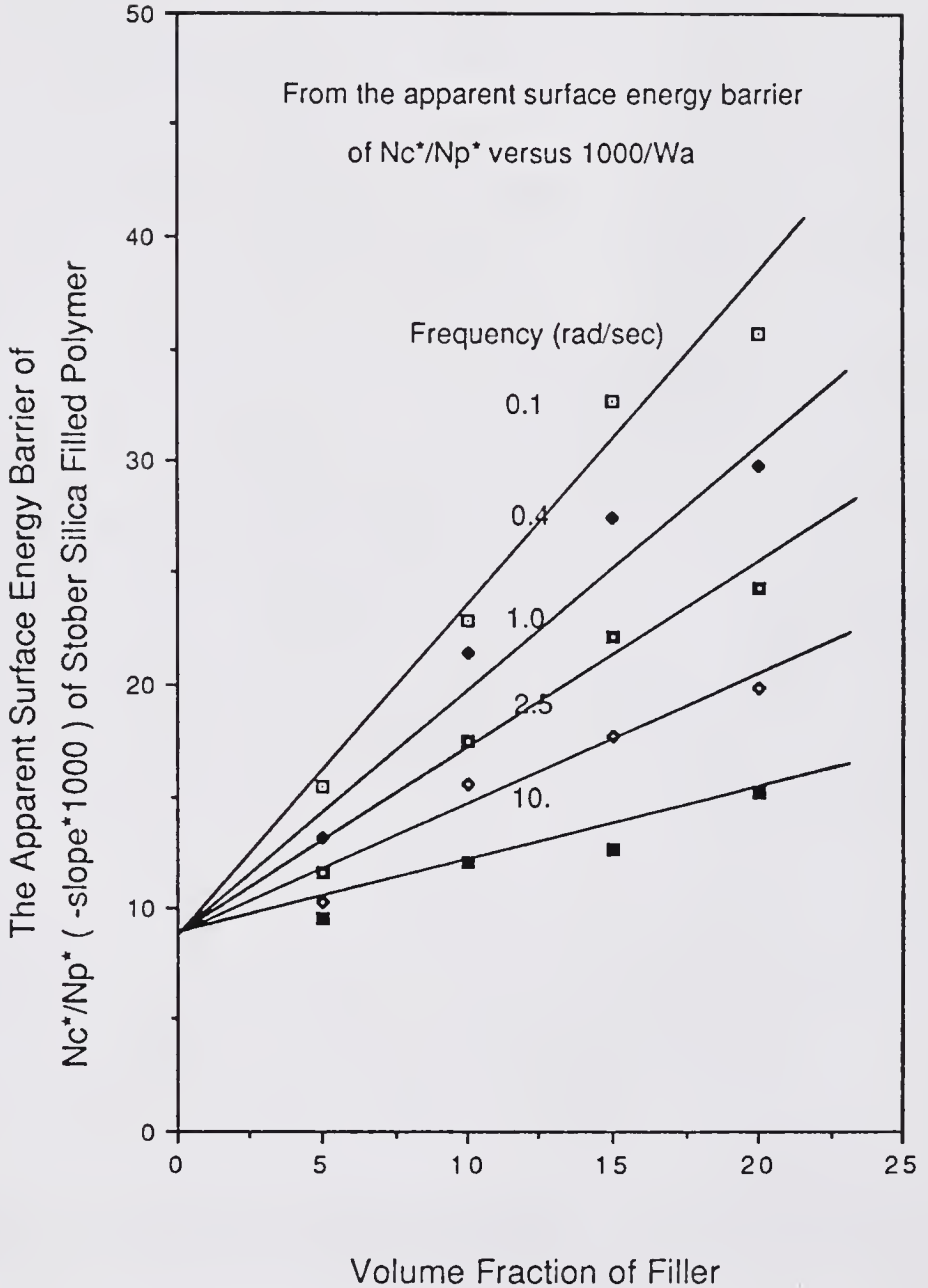


Figure 5.47 Effect of Volume Fraction of Stober Silica and Frequency on the Apparent Surface Energy Barrier of Melt Viscosity

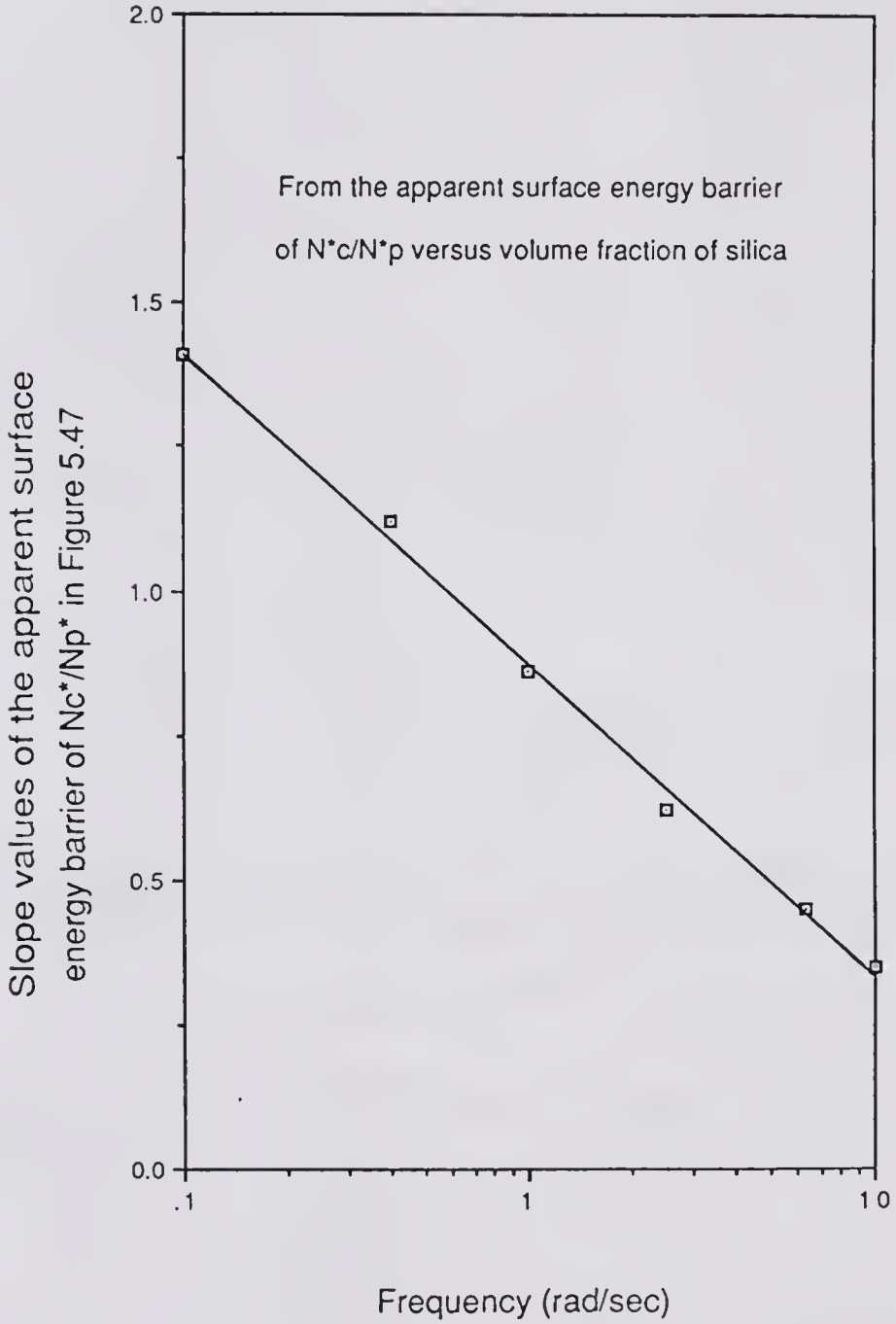


Figure 5.48 Effect of Frequency on the Slope Values in Figure 5.47

$$\frac{\eta_c^*}{\eta_p^*} = C \cdot e^{-K \left( \frac{1}{W_a} \right)} \quad ( 5.17 )$$

where

$\eta_c^*$  = melt viscosity of polymer composite

$\eta_p^*$  = melt viscosity of unfilled polymer

$W_a$  = work of adhesion

$C$  = constant at a given volume fraction of silica

$K$  = slope of  $\eta_c^*/\eta_p^*$  vs.  $1/W_a$ , the apparent surface energy barrier of relative shear modulus

With different surface properties of silica in a given volume fraction silica filled polymer melts, the relative viscosity can be expressed by

$$\frac{\eta_c^*}{\eta_{co}^*} = e^{-K \left( \frac{1}{W_a} - \frac{1}{W_{ao}} \right)} \quad ( 5.18 )$$

where

$\eta_{co}^*$  = dynamic viscosity of a composite with the poorest interfacial bonding ( $W_{ao} = 63$  erg cm<sup>-2</sup> for 110°C/TMCS)

$W_{ao}$  = work of adhesion of the poorest interfacial bonding at the interface

$K$  is a function of frequency, particle size, and volume fraction of filler.

At a constant frequency:

$$k = f( V_f ) \quad ( 5.19 )$$

$$K = P + Q \cdot V_f \quad ( 5.20 )$$

But with varying frequencies:

$$Q = R + n \cdot \log w \quad ( 5.21 )$$

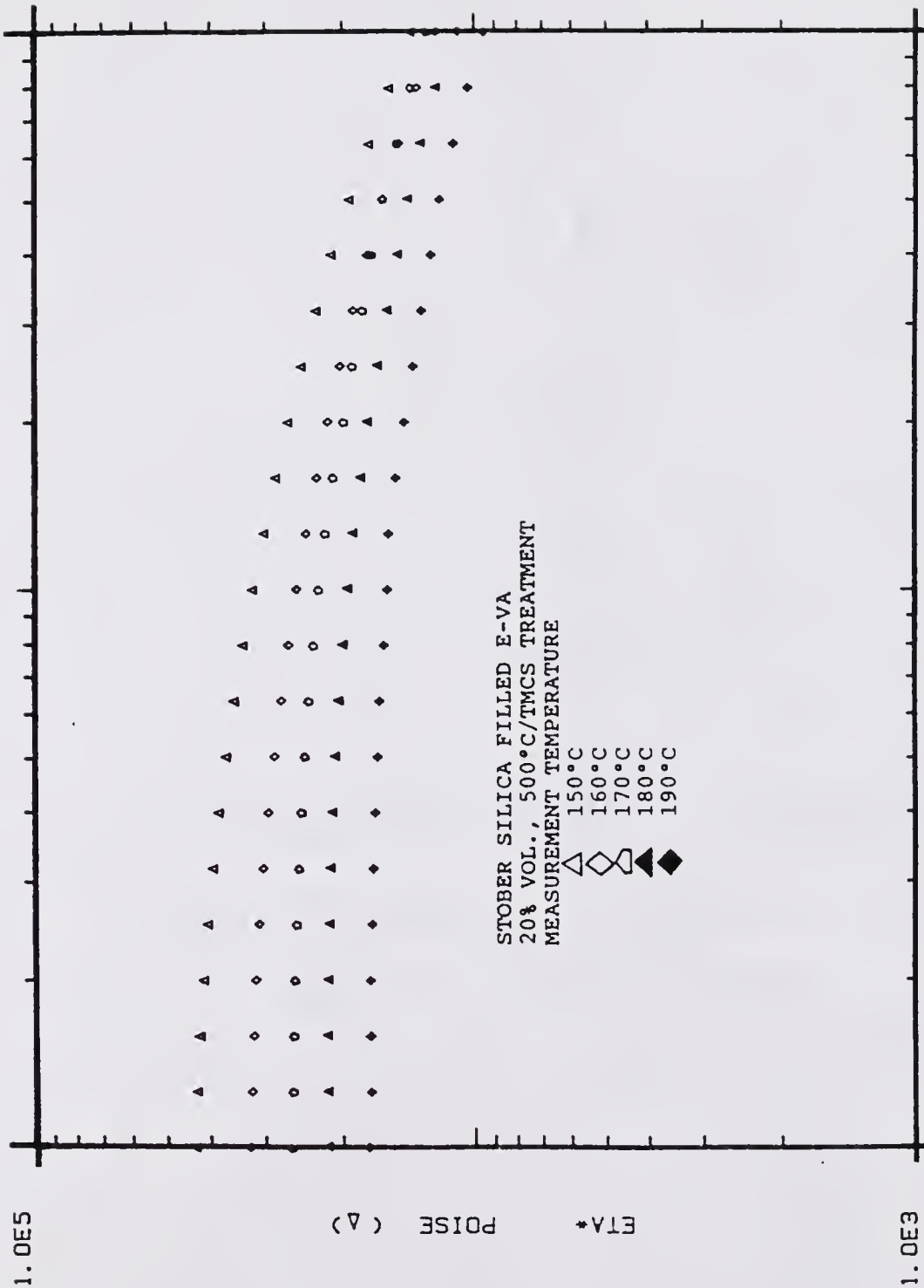
Therefore:

$$K = P + ( R + n \cdot \log w ) \cdot V_f \quad ( 5.22 )$$

where  $w$  is the frequency, and  $R$  and  $n$  are dependent on the particle size of filler.  $P$  is the intercept point at  $V_f = 0$  in Figure 5.47, which is equal to  $-0.008$  in this study. Theoretically,  $P$  should be equal to zero when there are no filler particles in the polymer melt, and it is seen that there is reasonable agreement with the experimental value in this study.

#### 5.4 Effect of Temperature on the Viscosity of Silica Filled Polymer Composites

Figure 5.49 shows that the melt viscosity of 20% volume fraction of Stöber silica filled E-Va copolymer changes with temperature. The viscosity decreases with increasing



1.0E-1      FREQ    RAD/SEC      1.0E1

Figure 5.49 Effect of Frequency and Temperature on the Melt Viscosity of Polymer Filled by 20% Stober Silica with 110°C Treatment

1.0E5

ETA\* POISE (Δ)

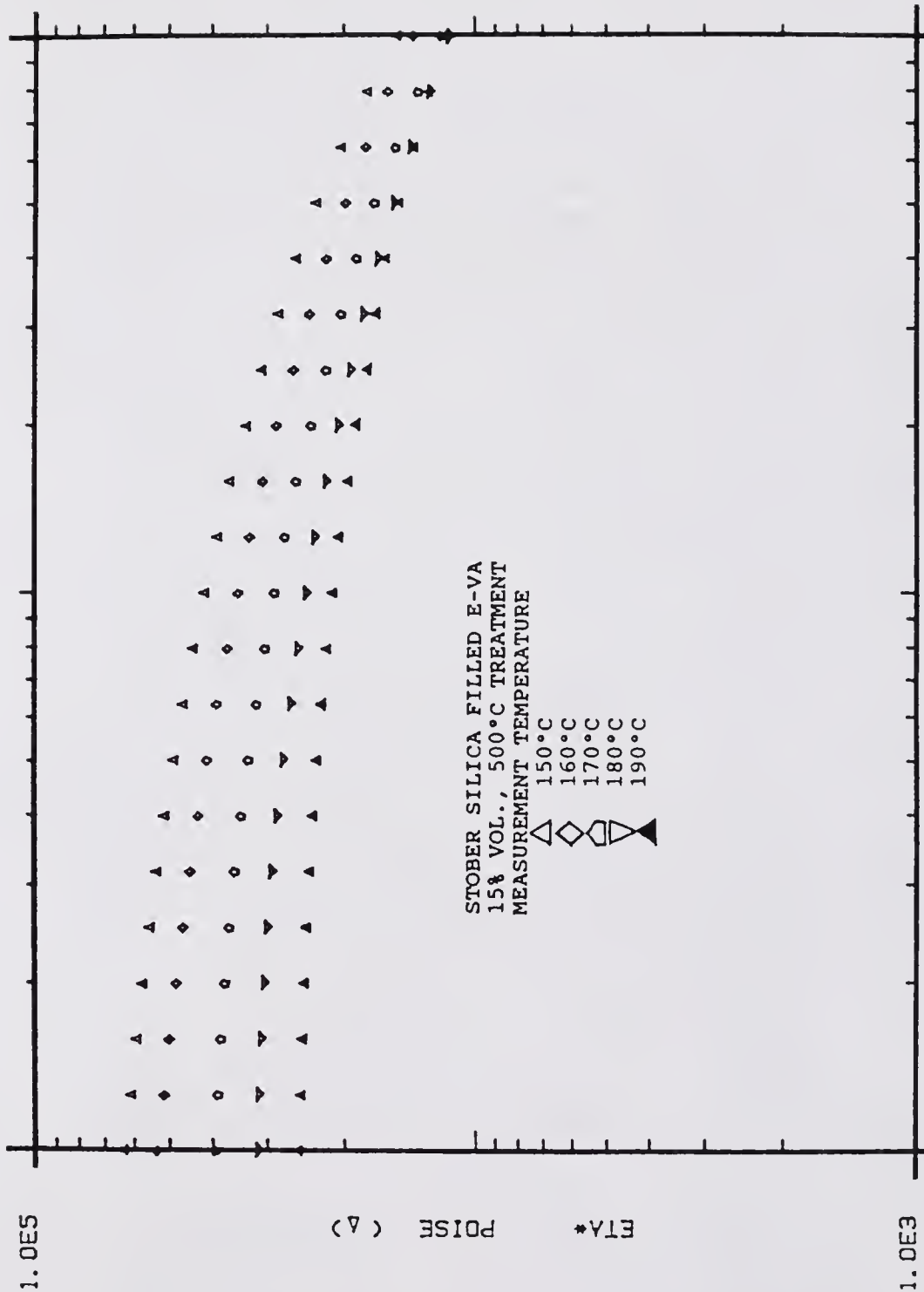
1.0E3

temperature. The change of viscosity with temperature is more pronounced at lower frequencies than at higher frequencies. The change, with temperature, of viscosities of the 15%, 10% and 5% volume fractions of silica filled composites as well as unfilled E-Va copolymer is also shown in Figures 5.50 to 5.53. The trend of temperature dependence of these melt viscosities is similar to the 20% volume fraction of silica in Figure 5.49. However, when studied at higher frequencies, the extent of change in viscosity with temperature increases with a decrease in volume fraction of silica.

#### 5.4.1 Dependence of Volume Fraction of Silica

In Figure 5.54, a linear slope is obtained when the logarithm of melt viscosity at a frequency of 0.1 rad/sec is plotted against reciprocal temperature. From the experimental results, it seems that the filled polymer melts also follow the Arrhenius equation in the range of volume fractions of silica studied. This is due to the low concentrations of Stöber silica particles in the polymer matrix (152,247,248). The activation energy for the flow process of the filled and unfilled polymer melts can be obtained from the slope in Figure 5.54.

The interesting results are that all of slopes are parallel at a frequency equal to 0.1 rad/sec regardless of the silica concentrations of polymer melts and surface properties of the silica particles. This indicates that



1.0E-1  
 Figure 5.50 Effect of Frequency and Temperature on the Melt Viscosity of  
 Polymer Filled by 15% Stober Silica with 500°C Treatment  
 1.0E1

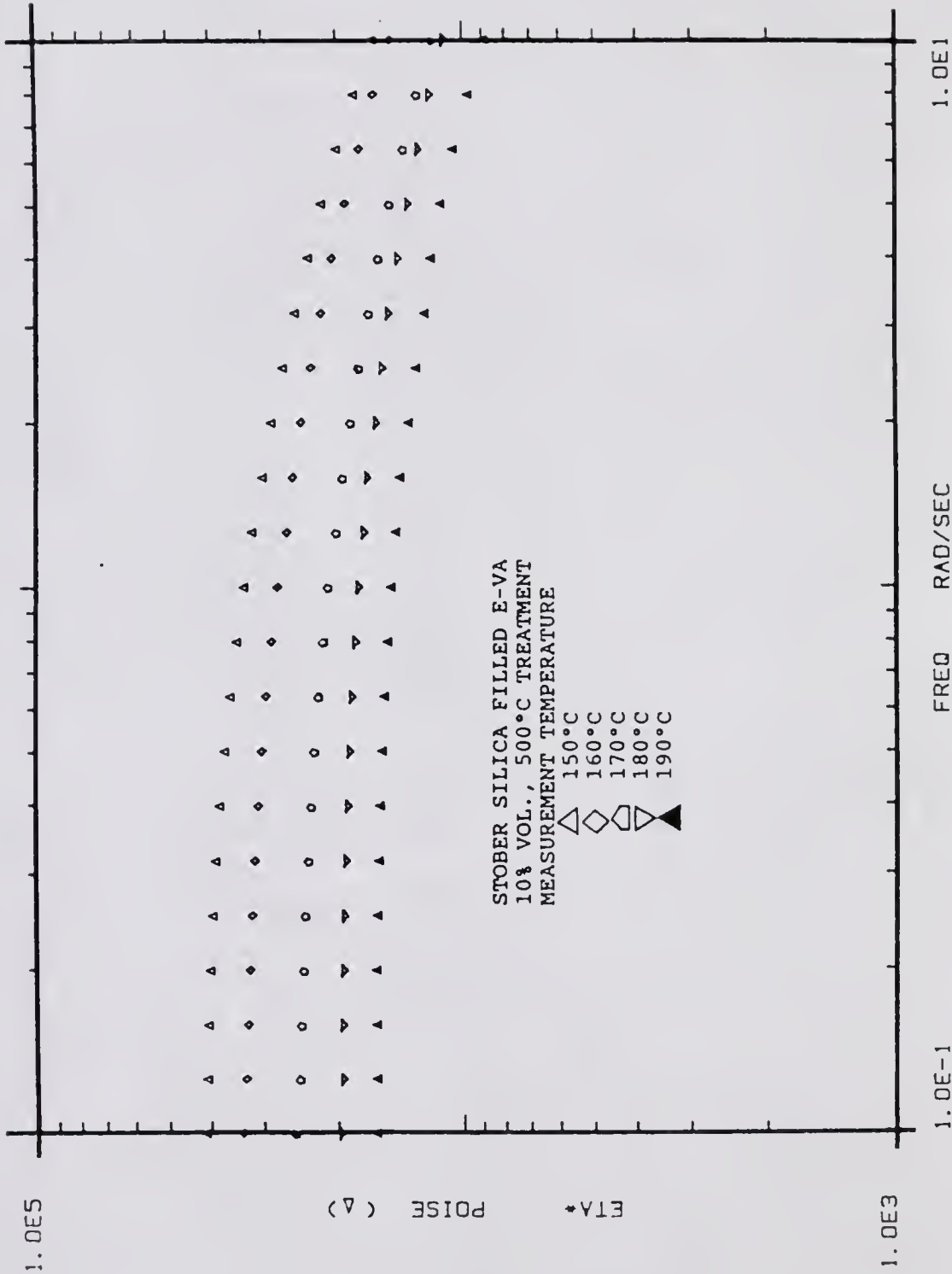
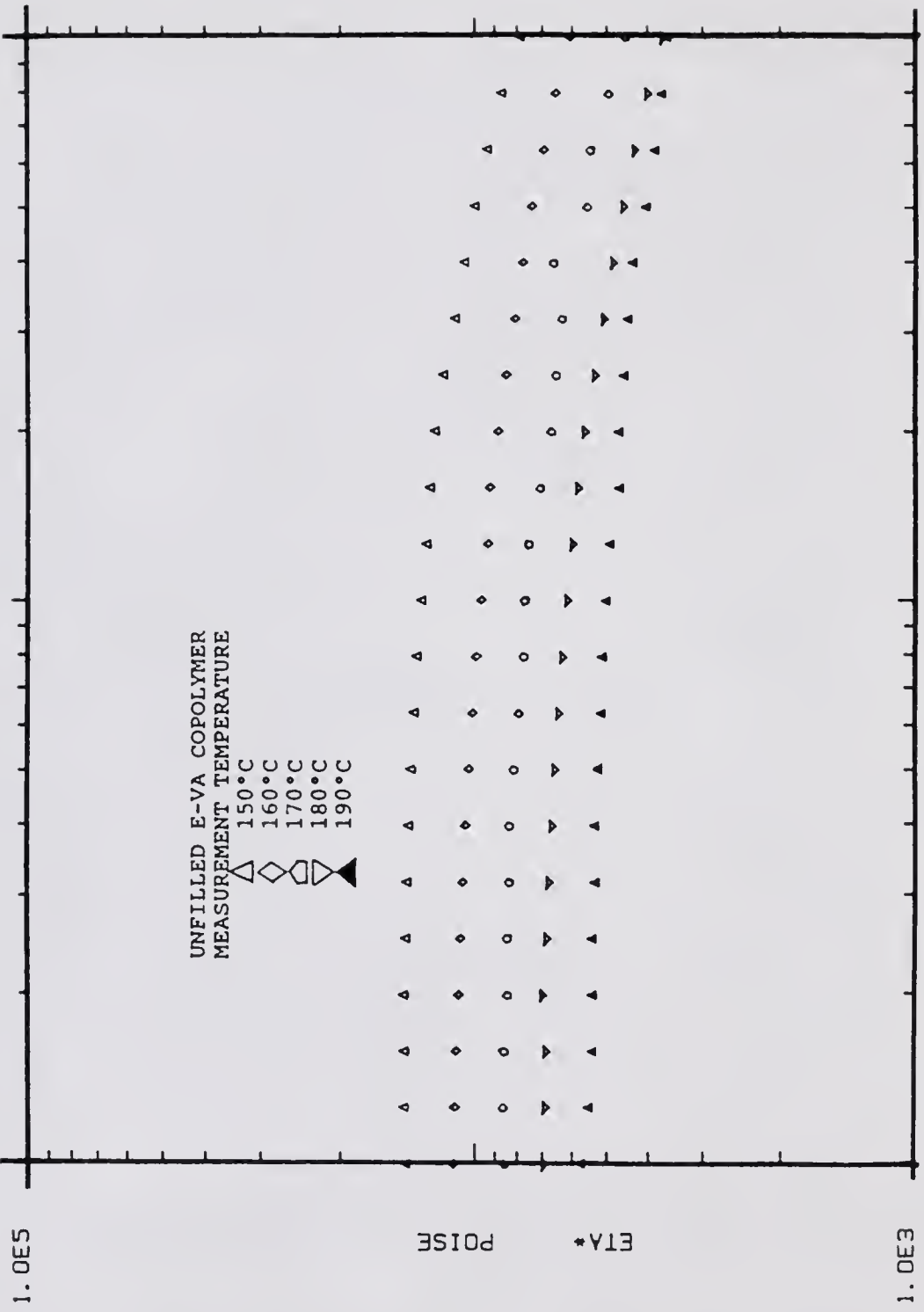


Figure 5.51 Effect of Frequency and Temperature on the Melt Viscosity of Polymer Filled by 10% Stober Silica Treated by 500°C/TMCS





1.0E-1 FREQ RAD/SEC 1.0E1

Figure 5.53 Effect of Frequency and Temperature on the Melt Viscosity of E-Va Copolymer

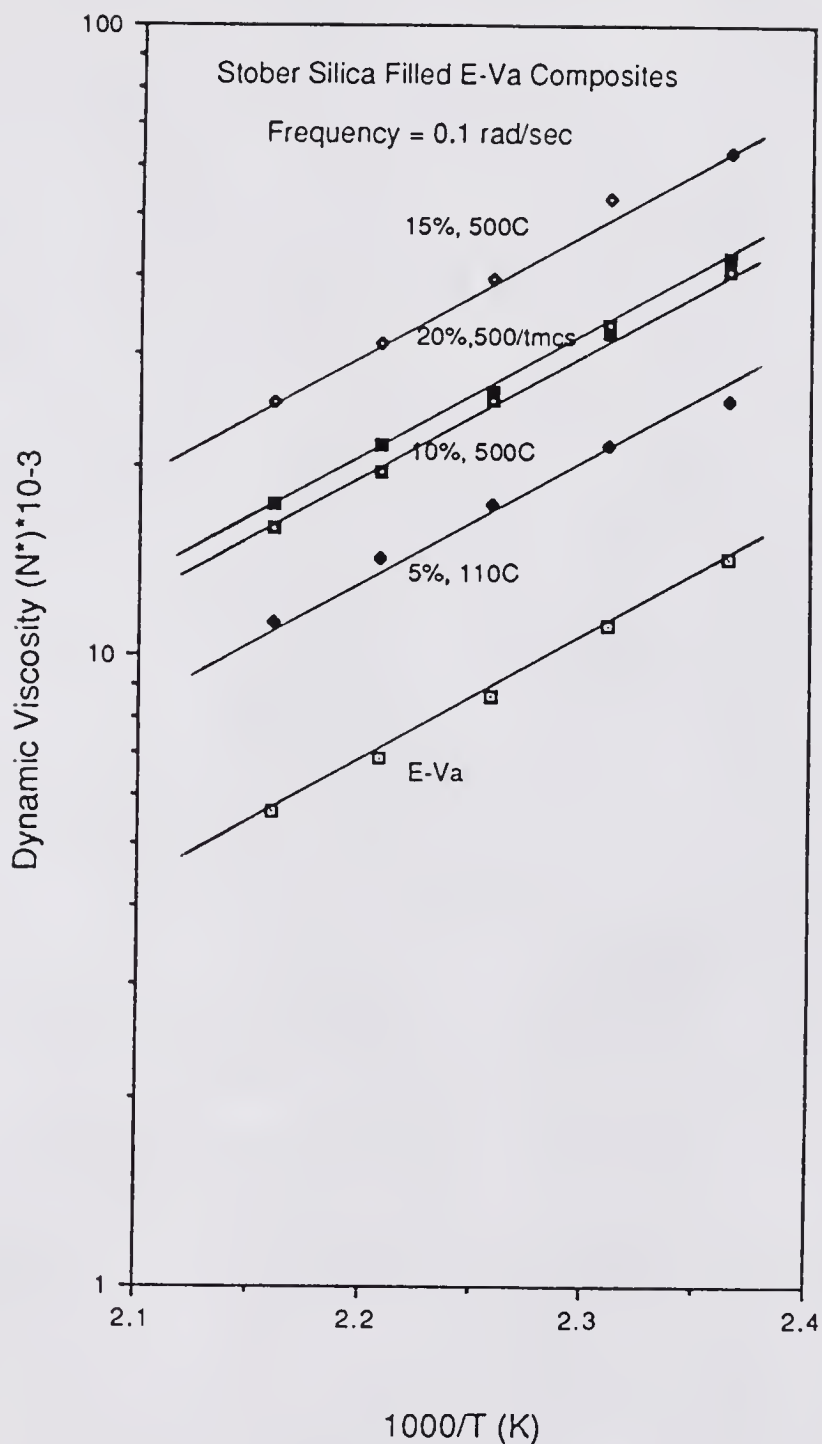


Figure 5.54 Effect of Environmental Testing Temperature and Solid Loading on the Melt Viscosity of Stober Silica Filled Polymer Measured at 0.1 rad/sec

the activation energies are approximately the same at a frequency of 0.1 rad/sec. The values of activation energies at a frequency of 0.1 rad/sec are listed in Table 5.5.

In Figures 5.55 and 5.56, where the frequencies studied are 1.0 and 10 rad/sec, the slope at a high frequency decreases to a low value. Meantime, the slope values of the filled E-Va copolymer decrease with an increase in filler concentration. The values of activation energies at frequencies of 1.0 and 10 rad/sec are listed in Table 5.5, which are obtained from Figures 5.55 and 5.56. The effects of frequency and solid loading on the melt viscosity can be clearly seen in Figure 5.57, which indicates that the melt viscosity of the unfilled polymer is more sensitive to temperature at higher frequencies (270). It is seen that the activation energy is decreased with increasing frequency. However, the change in the activation energy of the unfilled polymer with frequency is small. This change is not as obvious as the change in silica filled polymers.

#### 5.5.2 Dependence of Silica Surface Properties

Figures 5.58 to 5.63 show the change of composite viscosity with temperature, in polymer melts filled by the 20% volume Stöber silica treated with various surface modifications (110°C, 500°C, 750°C, 750°C/TMCS, 500°C/TMCS, 110°C/TMCS). The temperature dependence of melt viscosity at frequency of 0.1 rad/sec is shown in Figure 5.64. All

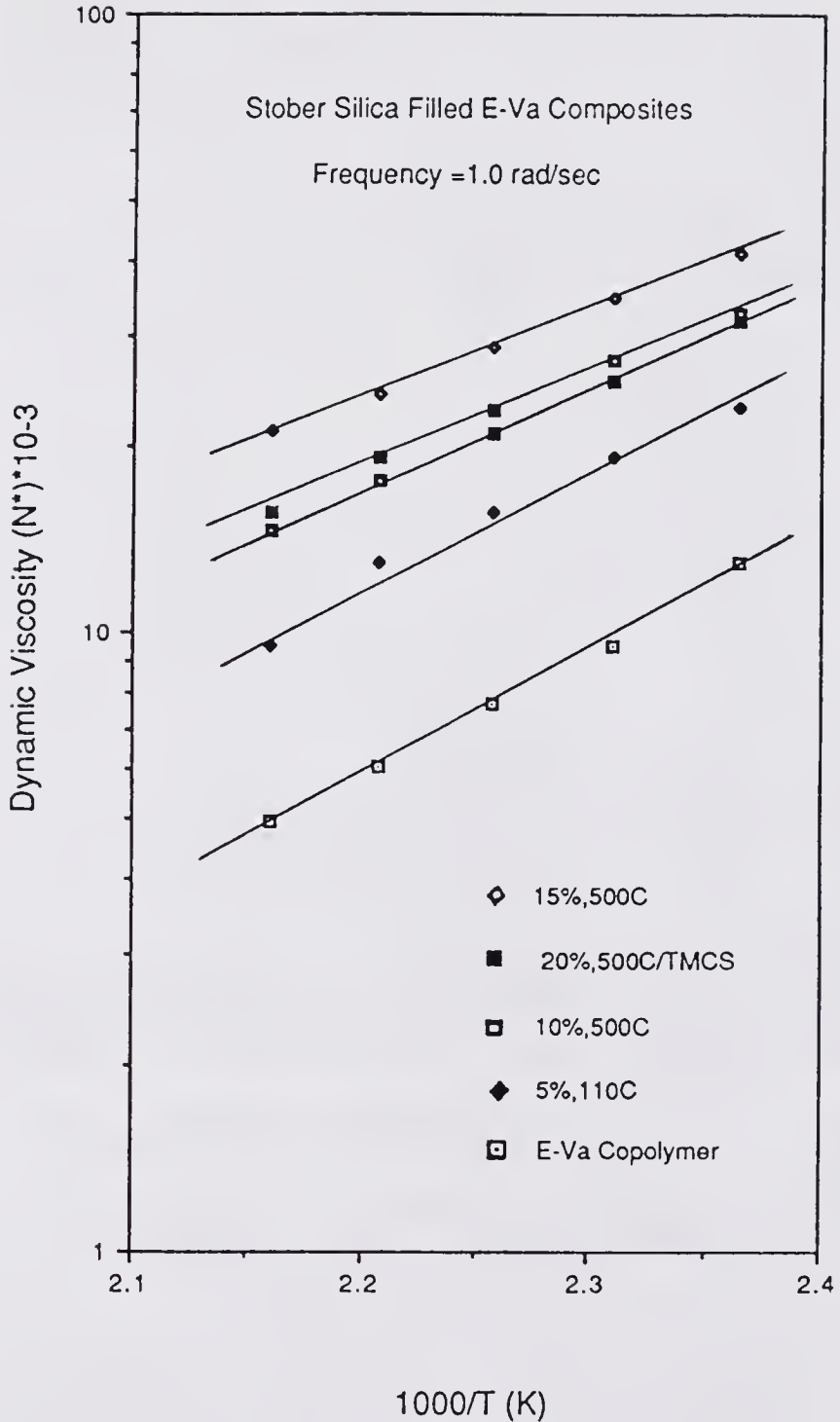


Figure 5.55 Effect of Environmental Testing Temperature and Solid Loading on the Melt Viscosity of Stober Silica Filled Polymer Measured at 1.0 rad/sec

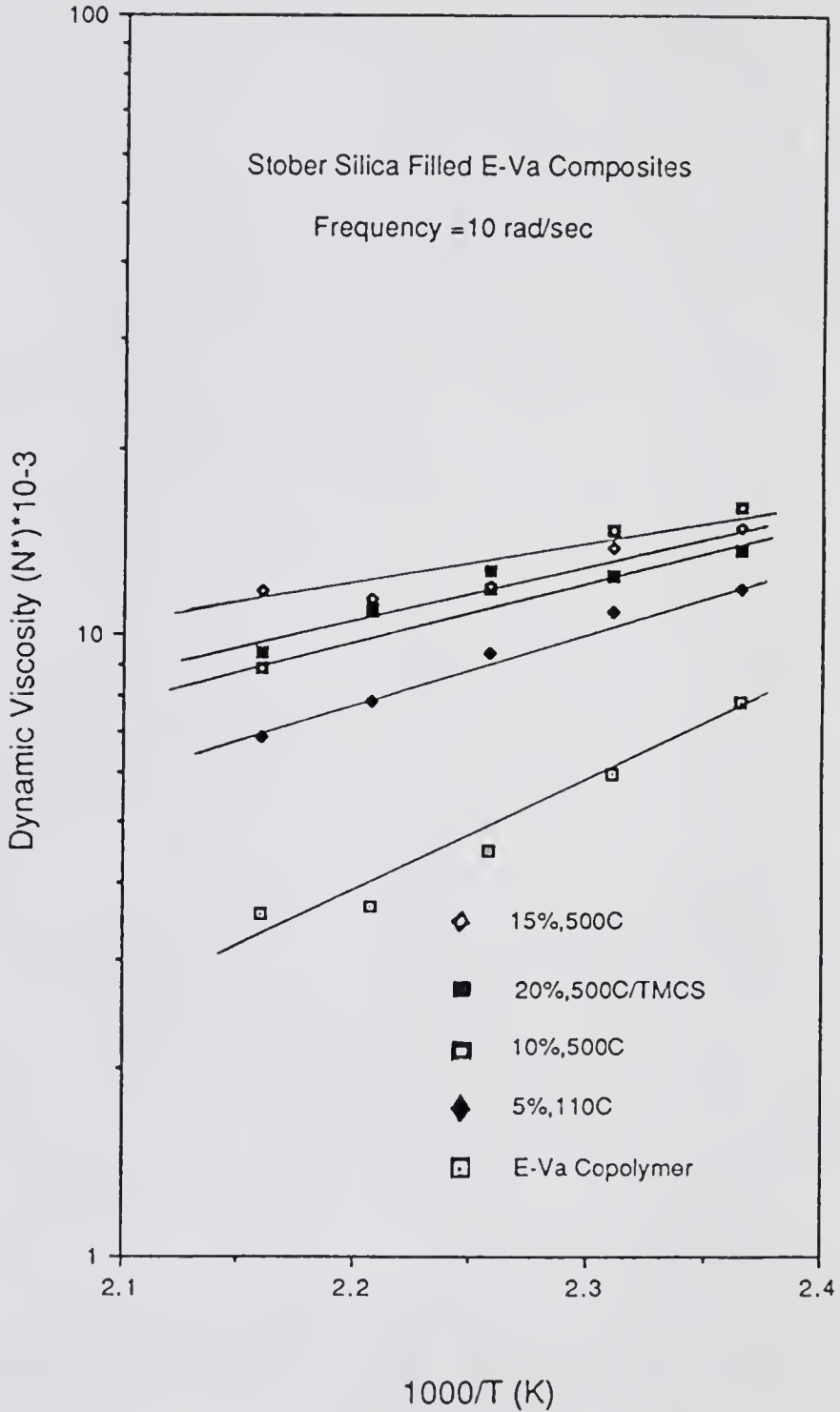


Figure 5.56 Effect of Environmental Testing Temperature and Solid Loading on the Melt Viscosity of Stober Silica Filled Polymer Measured at 10 rad/sec

Table 5.5

ACTIVATION ENERGY OF VISCOSITY OF  
STÖBER SILICA FILLED ETHYLENE-VINYL ACETATE COPOLYMER

Activation Energy ( Kcal/mole )

Volume Fraction of Stöber Silica	Frequency ( rad/sec )		
	0.1	1.0	10
15%, 500°C	9.12	6.60	2.64
20%, 750°C/TMCS	8.66	6.58	3.42
10%, 500°C	9.20	8.03	5.85
5%, 110°C	8.36	8.34	5.60
E-Va	9.00	8.85	8.06

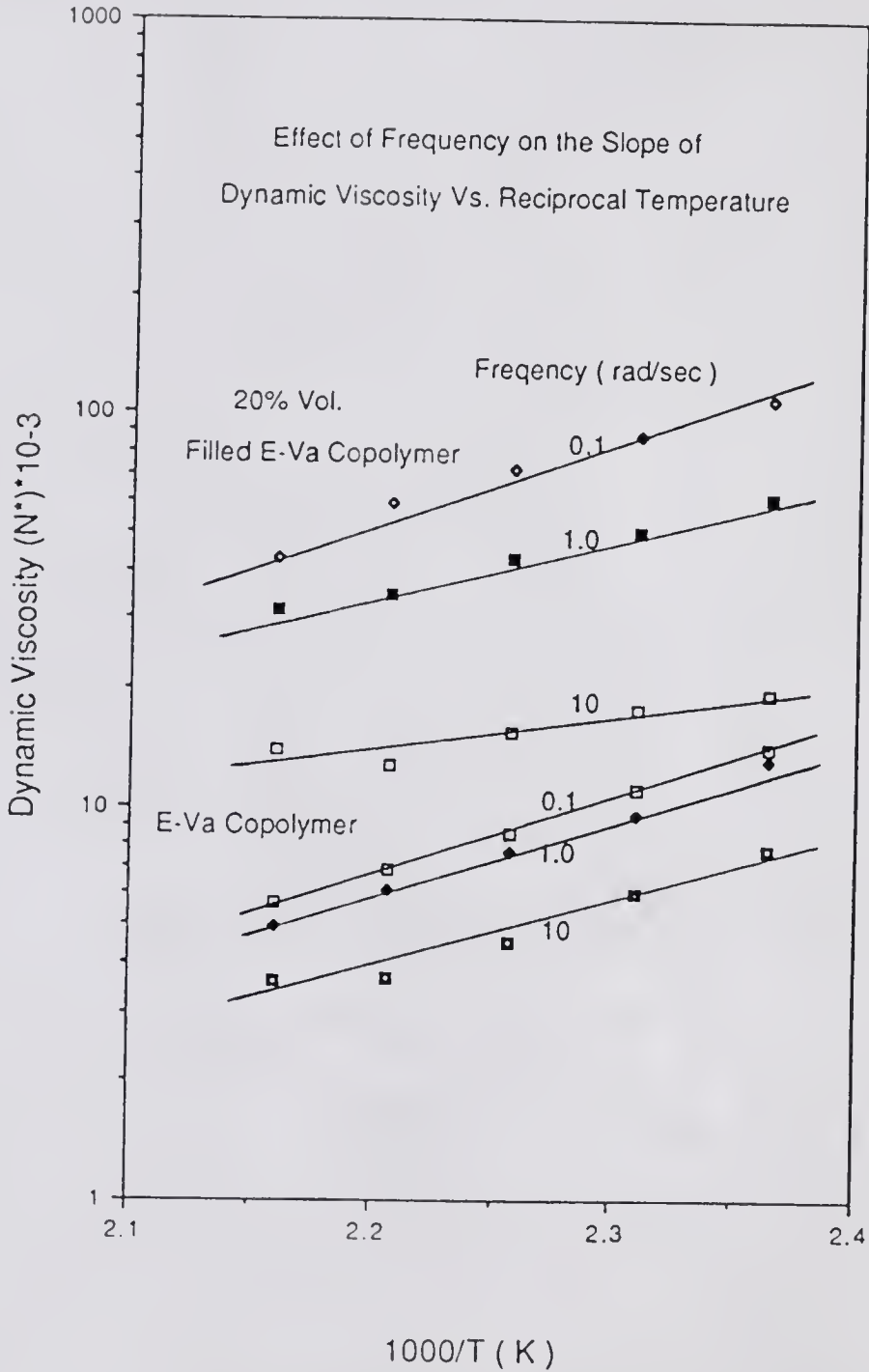


Figure 5.57 Effect of Frequency and Solid Loading on the Change of Melt Viscosity with Temperature

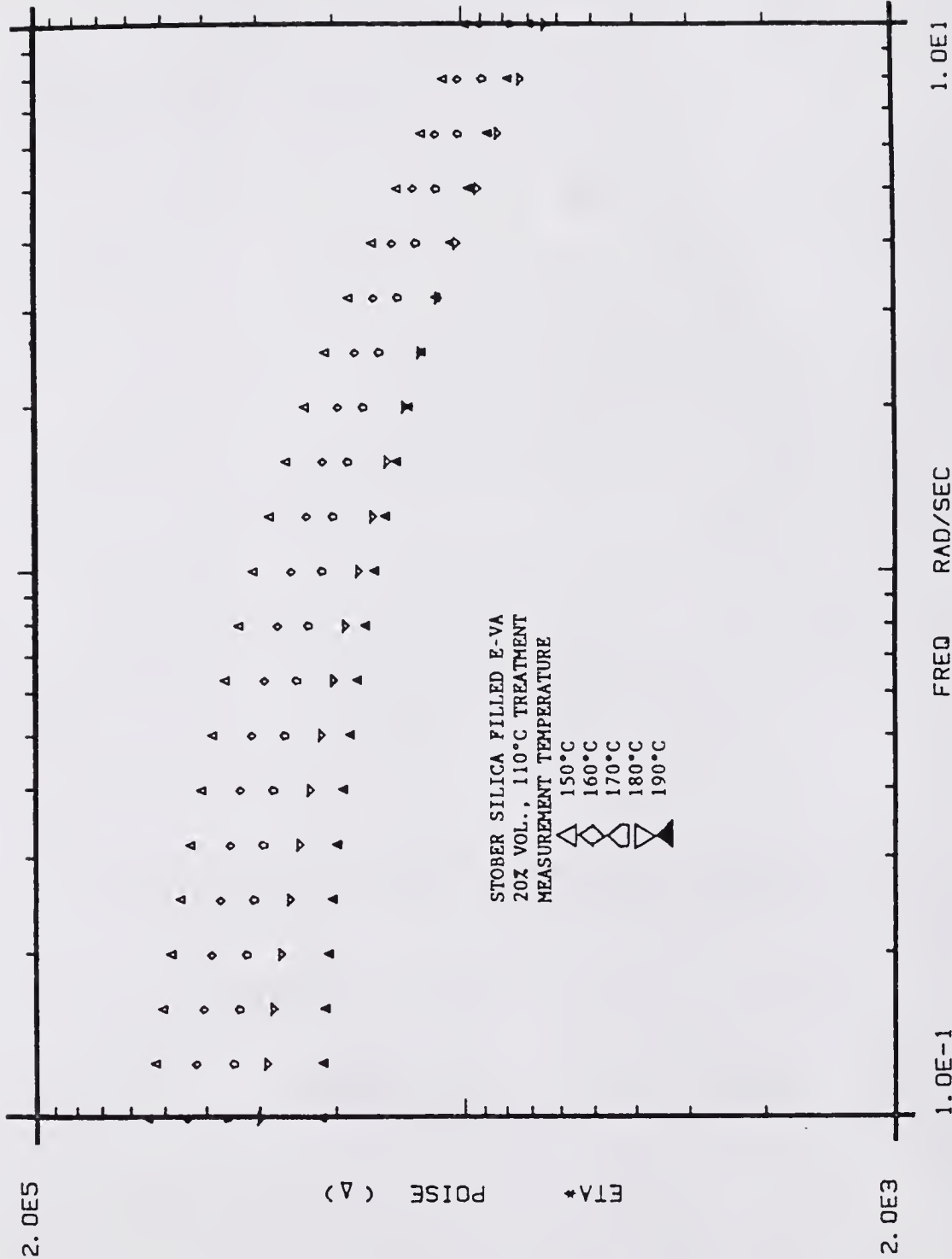


Figure 5.58 Effect of Frequency and Temperature on the Melt Viscosity of Polymer Filled by 20% Stober Silica with 110°C Treatment

2.0E5

ETA' POISE (Δ)

2.0E3

1.0E-1

FREQ RAD/SEC

1.0E1

STÖBER SILICA FILLED E-VA  
 20% VOL., 500°C TREATMENT  
 MEASUREMENT TEMPERATURE

- △ 150°C
- ◇ 160°C
- ◻ 170°C
- ▽ 180°C
- ◼ 190°C

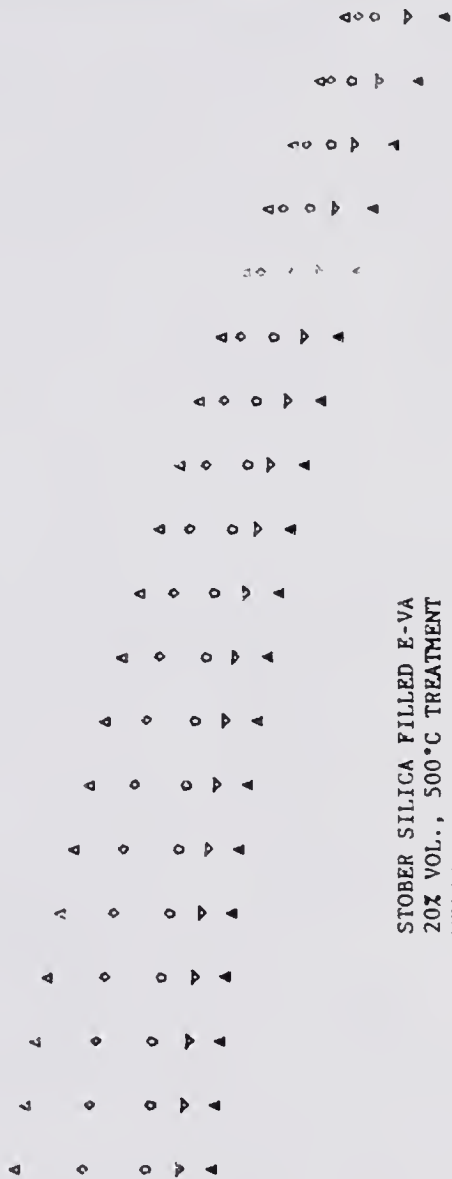


Figure 5.59 Effect of Frequency and Temperature on the Melt Viscosity of Polymer Filled by 20% Stöber Silica with 500°C Treatment

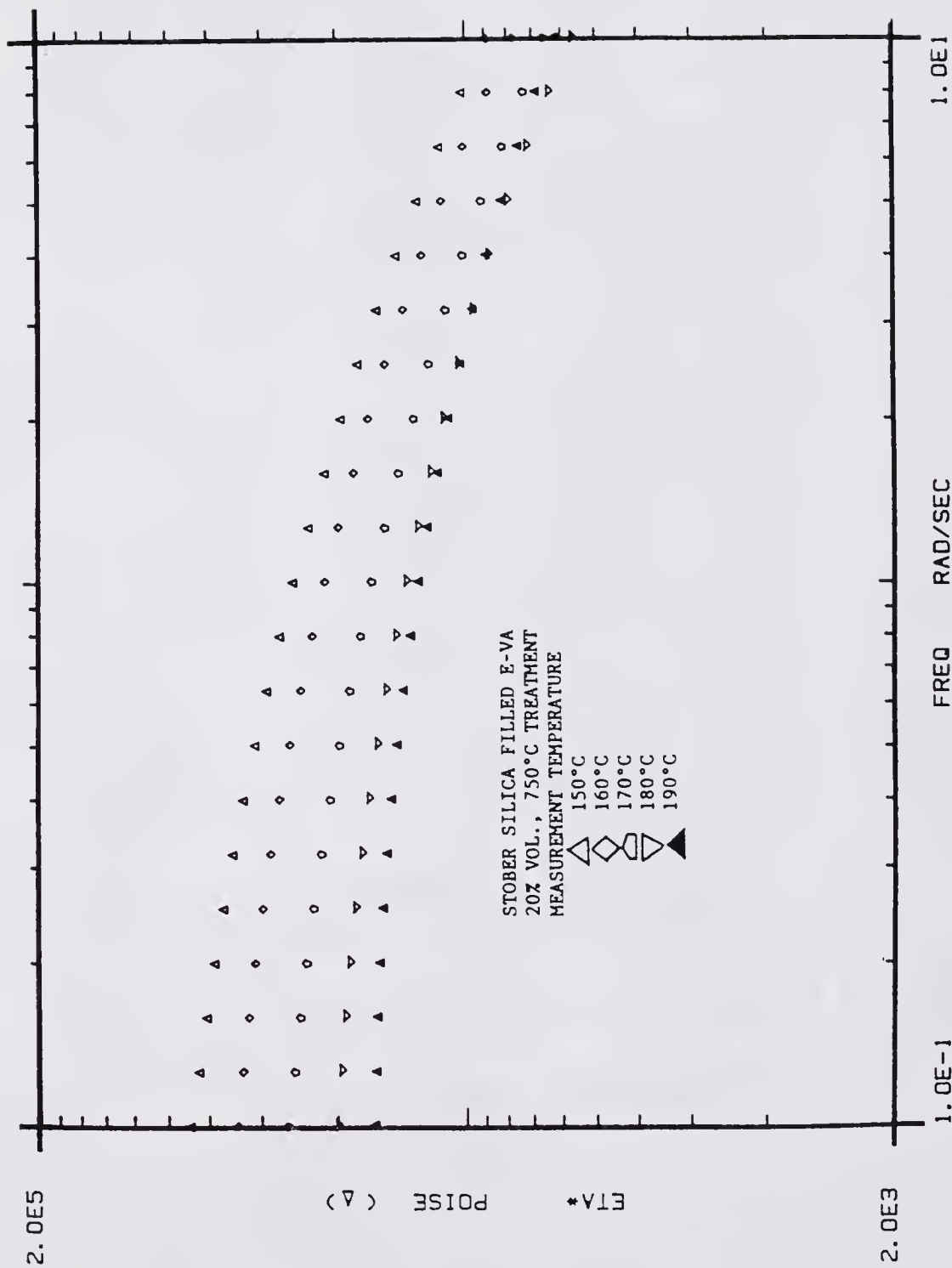


Figure 5.60 Effect of Frequency and Temperature on the Melt Viscosity of Polymer Filled by 20% Stober Silica with 750°C Treatment

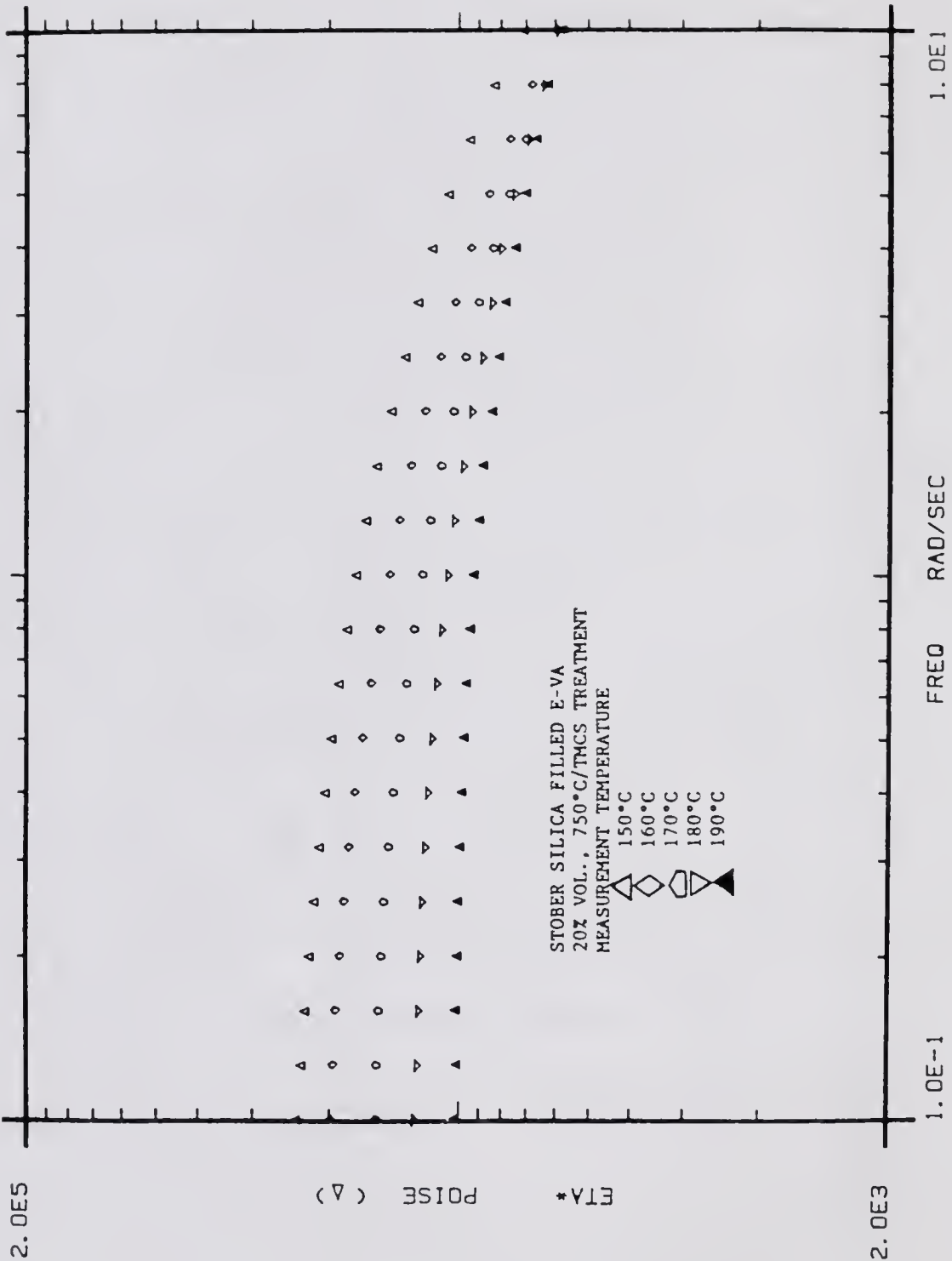


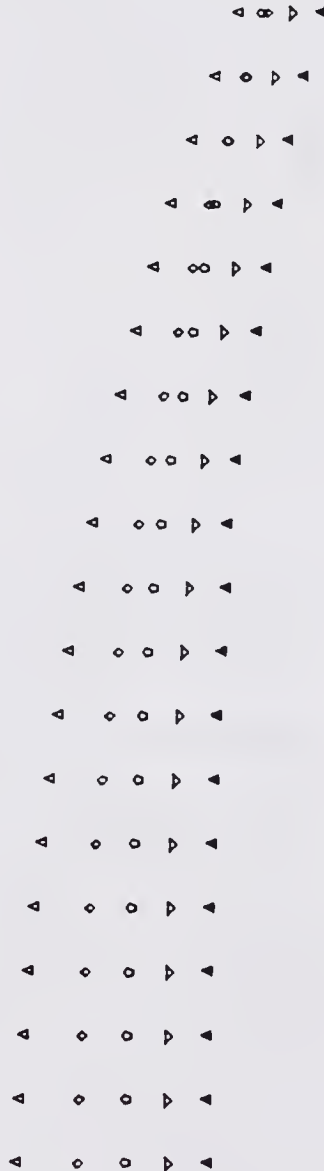
Figure 5.61 Effect of Frequency and Temperature on the Melt Viscosity of Polymer Filled by 20% Stober Silica Treated by 750°C/TMCS

2.0E5

POISE (Δ)

ETA\*

2.0E3



STOBER SILICA FILLED E-VA  
 20% VOL., 500°C/TMCS TREATMENT  
 MEASUREMENT TEMPERATURE

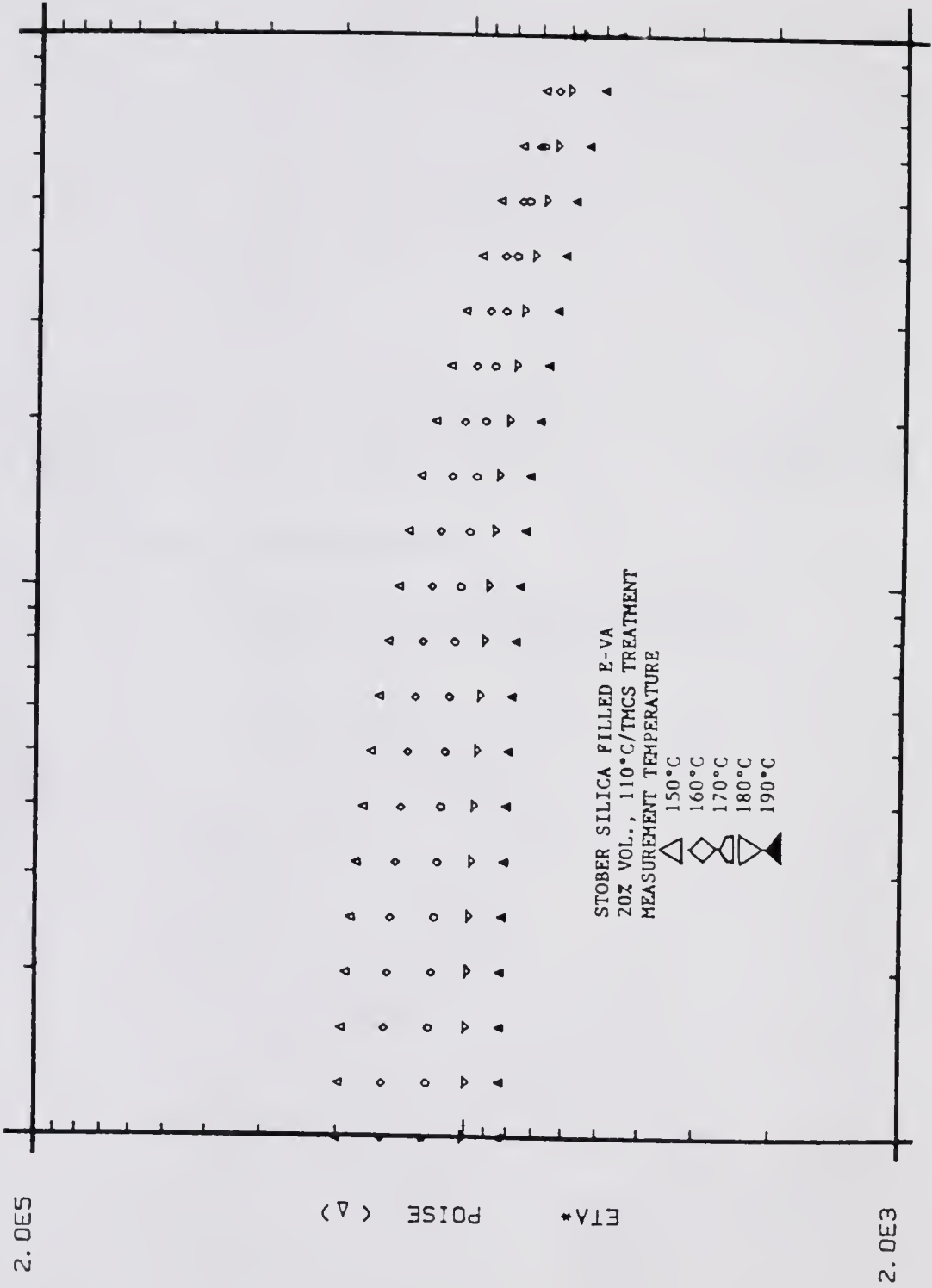
△ 150°C  
 ◇ 160°C  
 ▽ 170°C  
 △ 180°C  
 △ 190°C

1.0E-1

FREQ RAD/SEC

1.0E1

Figure 5.62 Effect of Frequency and Temperature on the Melt Viscosity of Polymer Filled by 20% Stober Silica Treated by 500°C/TMCS



1.0E-1 FREQ RAD/SEC 1.0E1  
 Figure 5.63 Effect of Frequency and Temperature on the Melt Viscosity of  
 Polymer Filled by 20% Stober Silica Treated by 110°C/TMCS

of the slopes are parallel regardless of the interfacial bonding strength. These slopes are also parallel to the slopes in Figure 5.54. When these filled polymer melts are studied at frequencies of 1.0 and 10 rad/sec, Figures 5.65 and 5.66, the slopes are parallel again within the studied surface modifications. However, the activation energies in Figures 5.64 to 5.66 decrease with increasing frequency.

The information in Figures 5.58 to 5.63 can also be used to study the effect of work of adhesion on the melt viscosity at different temperatures. The melt viscosities versus the reciprocal of work of adhesion measured at various temperatures are shown in Figure 5.67 to 5.69.

#### 5.6 Dispersion of Silica Particles in the Polymer Matrix

Dispersion of 15% volume fraction of Stöber silica particles in the E-Va copolymer was investigated by SEM micrographs. The dispersion of the Stöber silica, treated at 110°C, in the polymer matrix is shown in four different magnifications in Figure 5.70. Meanwhile, the dispersion of the Stöber silica, surface modified by 110°C/TMCS, in the polymer matrix is also shown in Figure 5.71 at four different magnifications.

From (a) and (b) of each Figure in 5.70 and 5.71, it is apparent that the state of dispersion of the Stöber silica filler particles in the E-Va copolymer matrix is almost the same regardless of the interfacial bonding strength.

Figures 5.70 (a) and (b) illustrates good interfacial

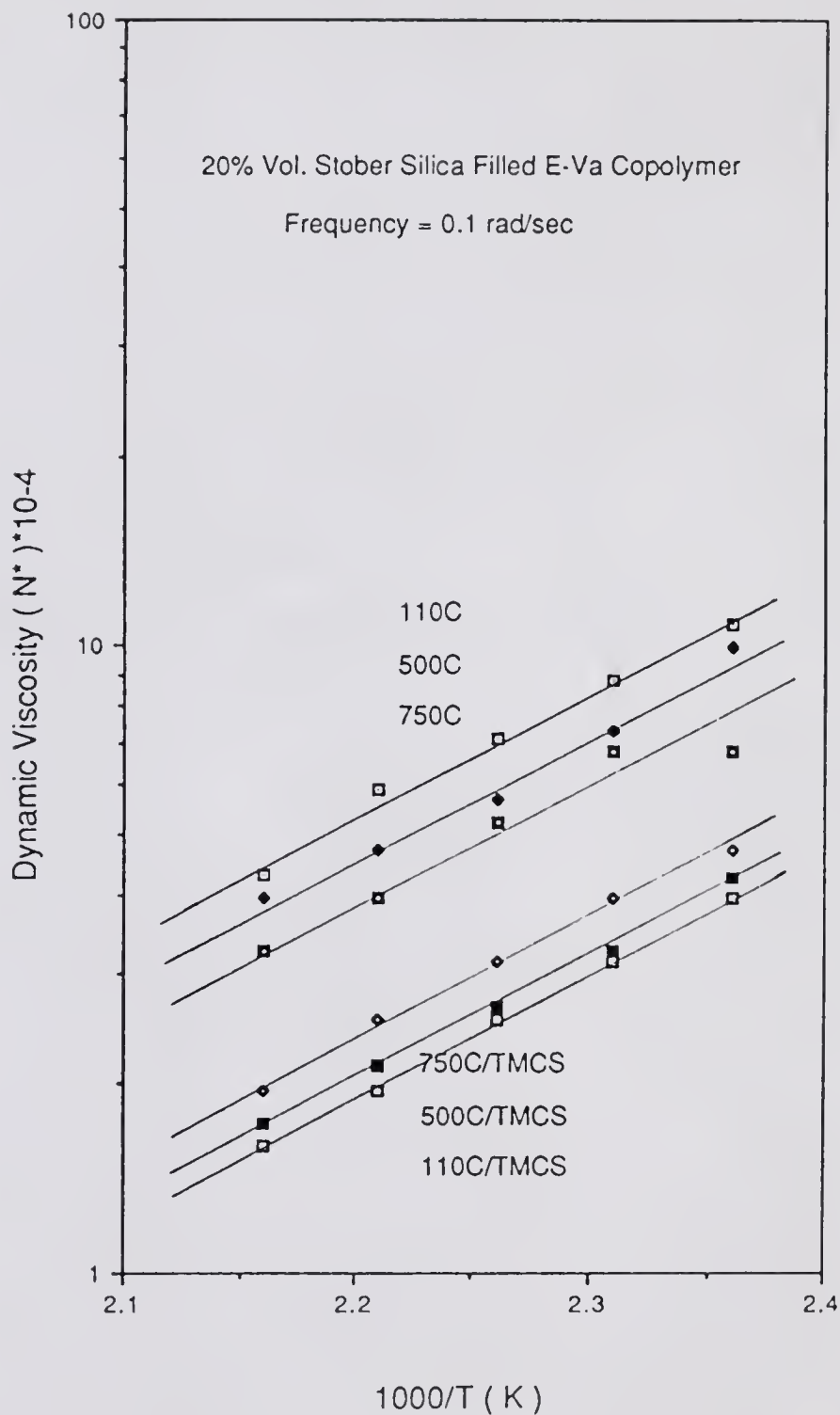


Figure 5.64 Effect of Temperature and Work of Adhesion on the Melt Viscosity of 20% Volume Stober Filled Polymer at 0.1 rad/sec

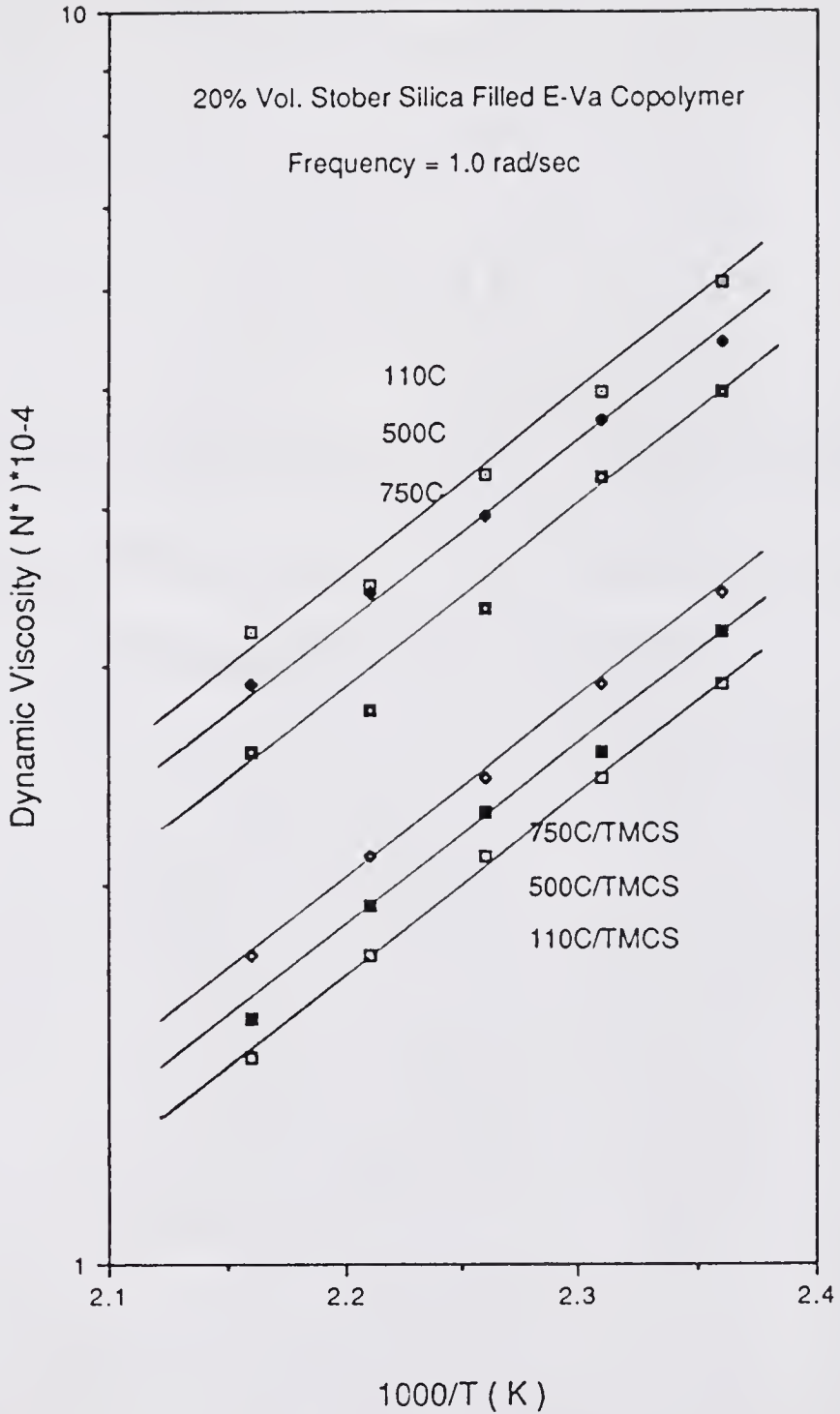


Figure 5.65 Effect of Temperature and Work of Adhesion on the Melt Viscosity of 20% Volume Stober Filled Polymer at 1.0 rad/sec

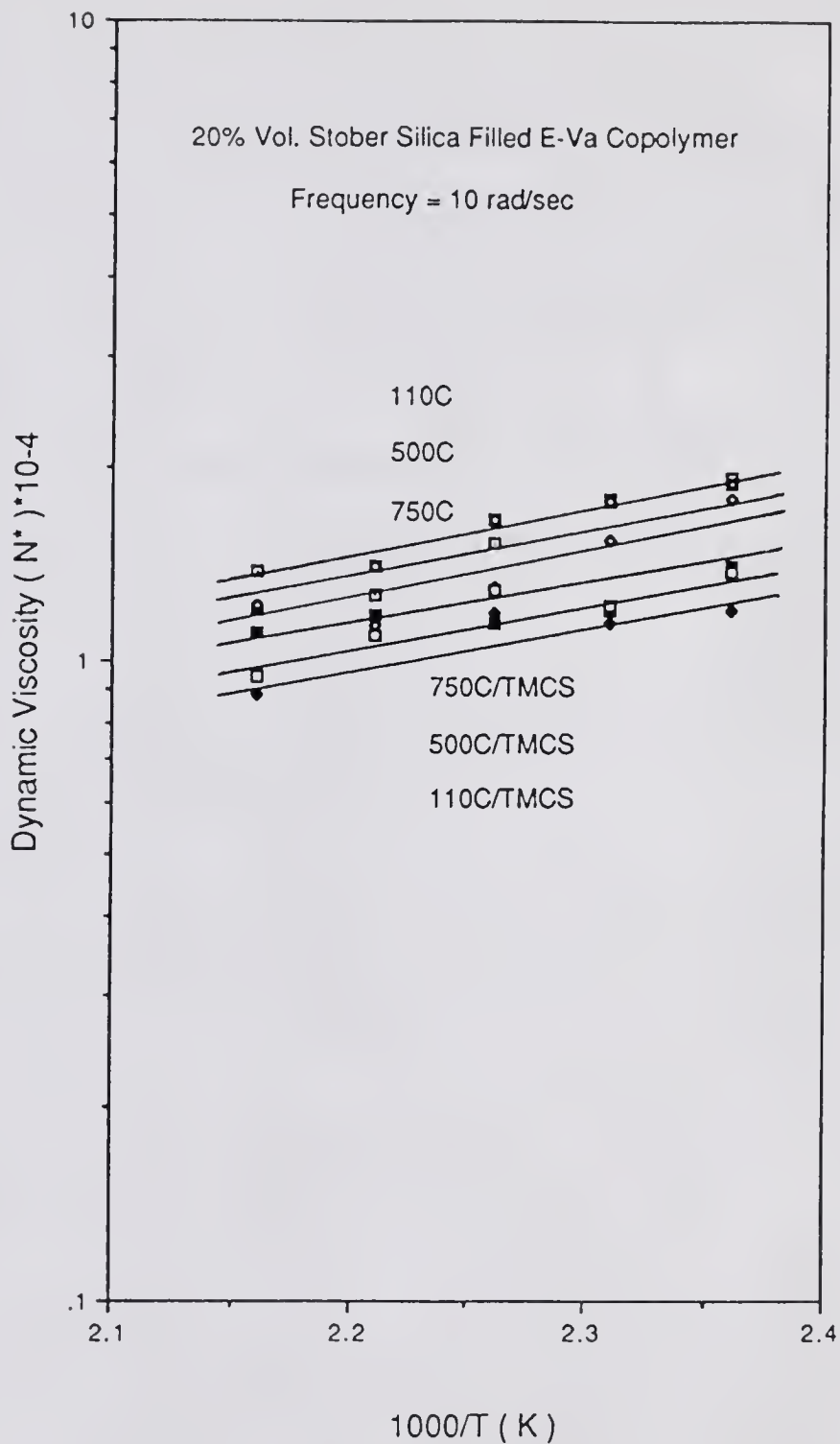


Figure 5.66 Effect of Temperature and Work of Adhesion on the Melt Viscosity of 20% Volume Stober Filled Polymer at 10 rad/sec

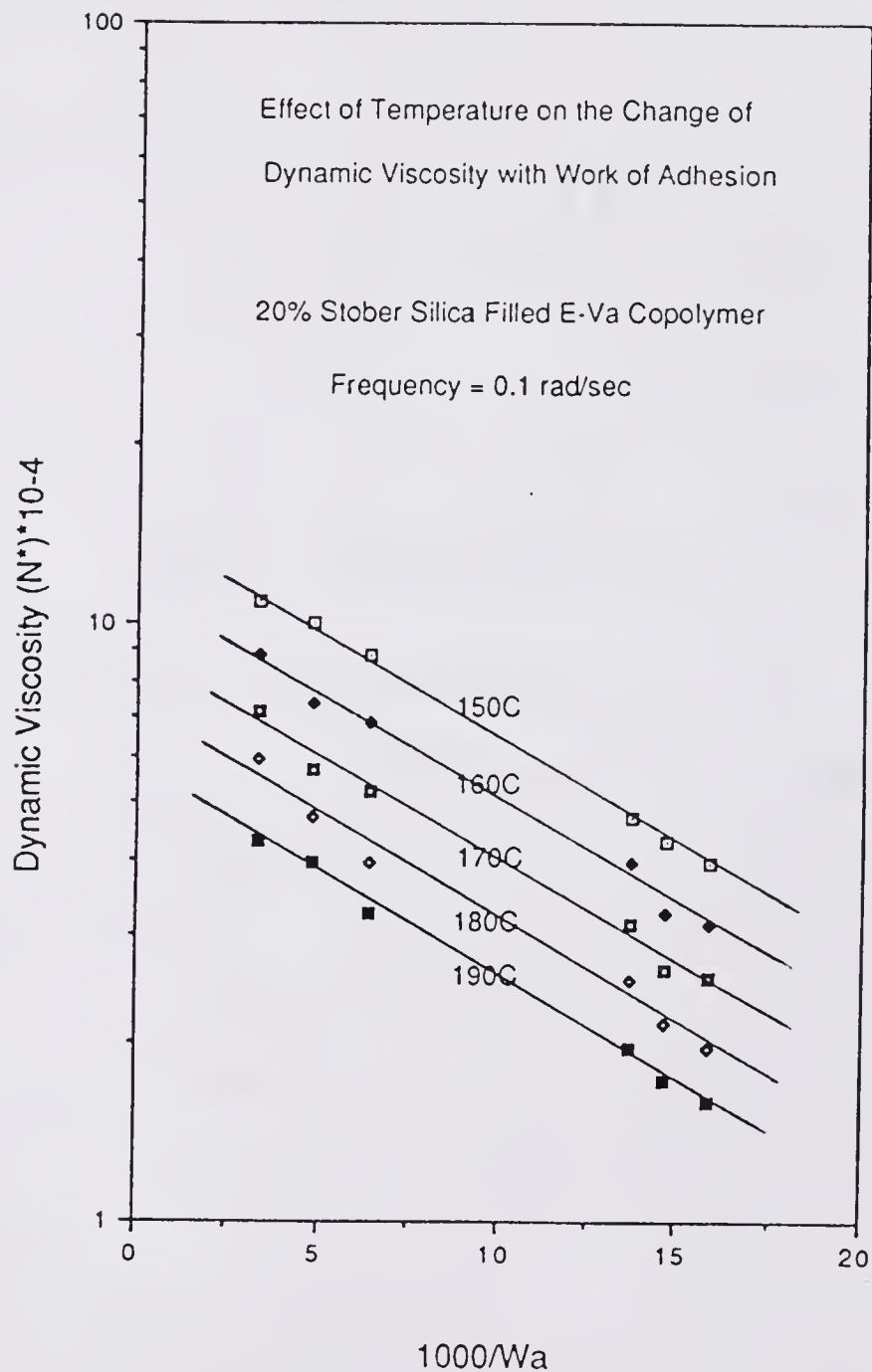


Figure 5.67 Effect of Testing Temperature on the Change of Melt Viscosity with Work of Adhesion for 20% Stober Silica Filled Polymer at 0.1 rad/sec

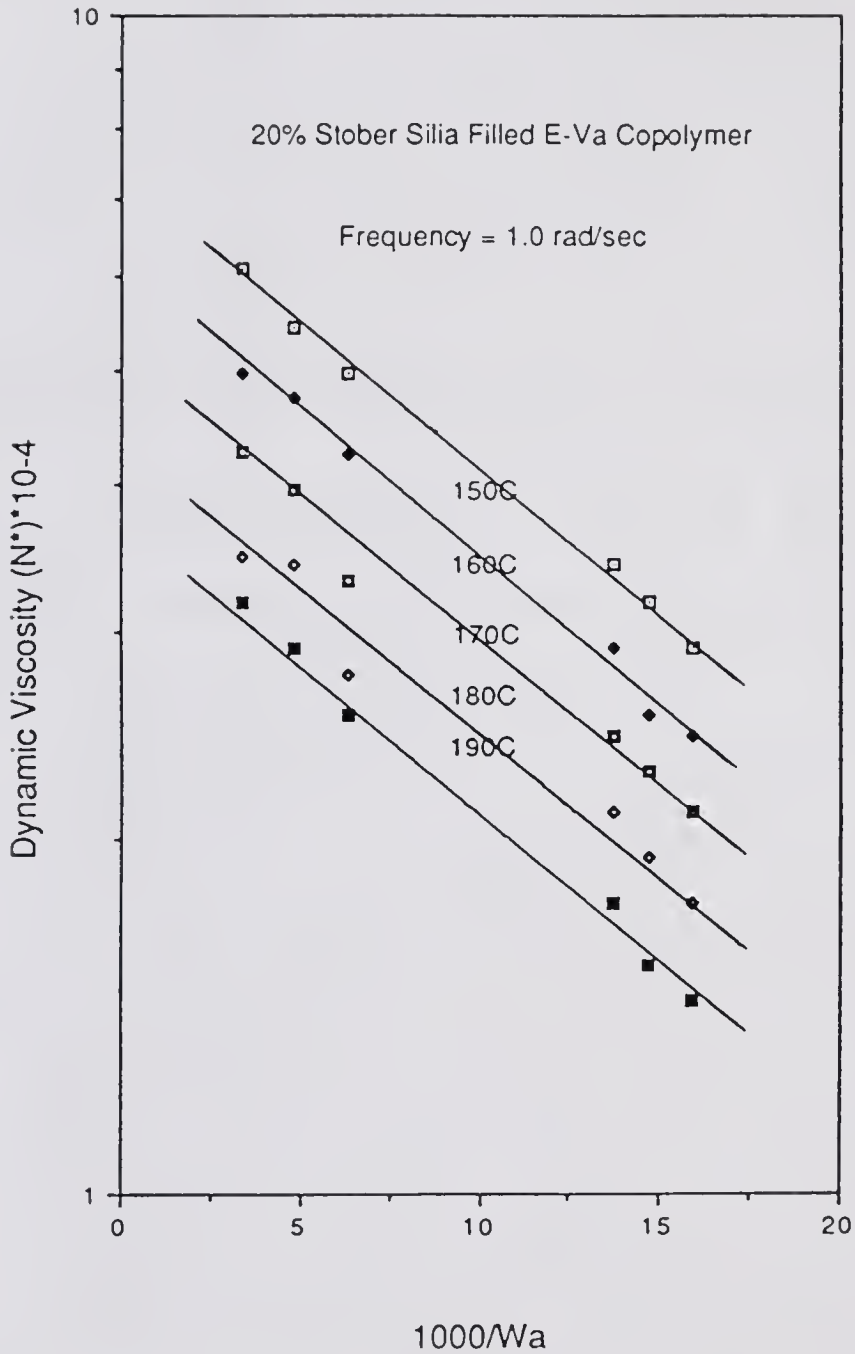


Figure 5.68 Effect of Testing Temperature on the Change of Melt Viscosity with Work of Adhesion for 20% Stober Silica Filled Polymer at 1.0 rad/sec

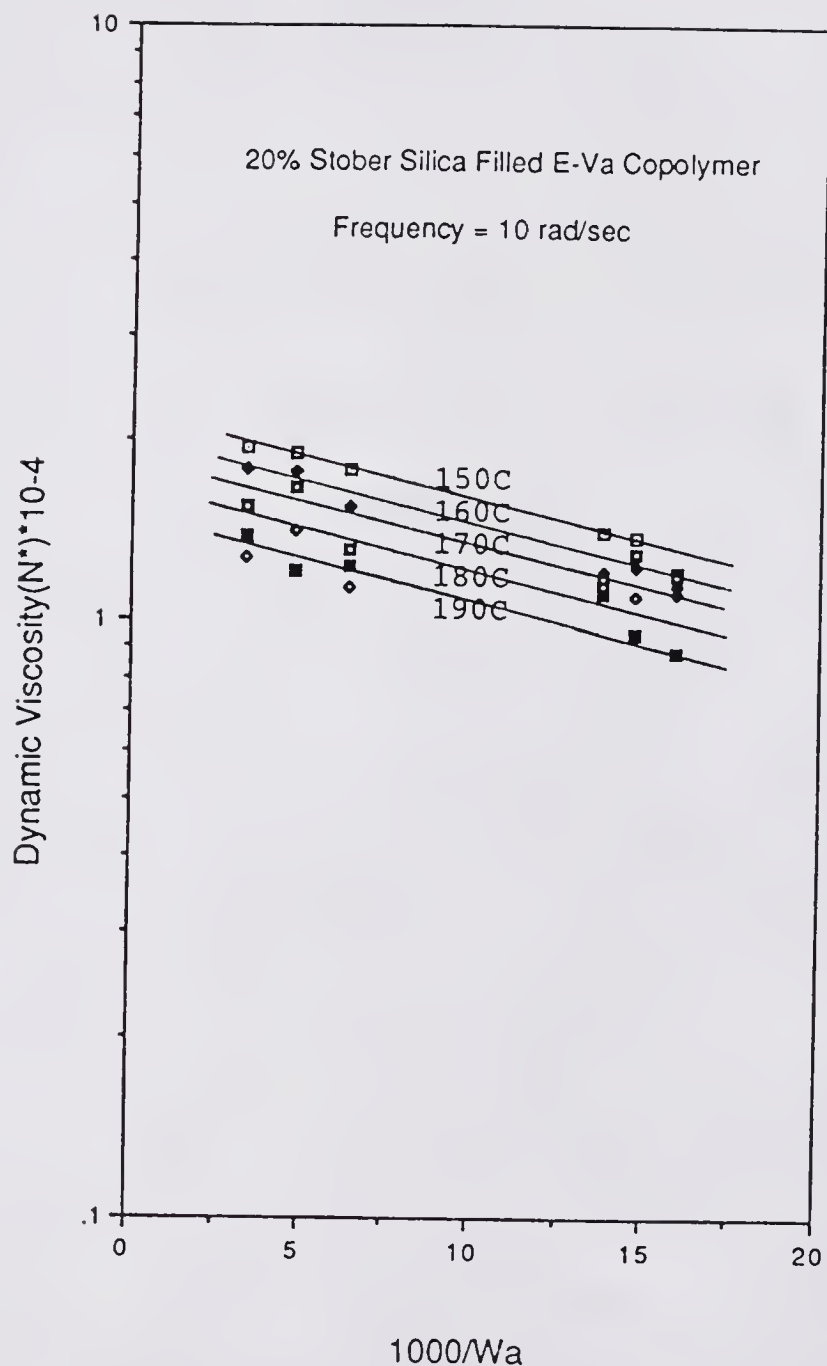
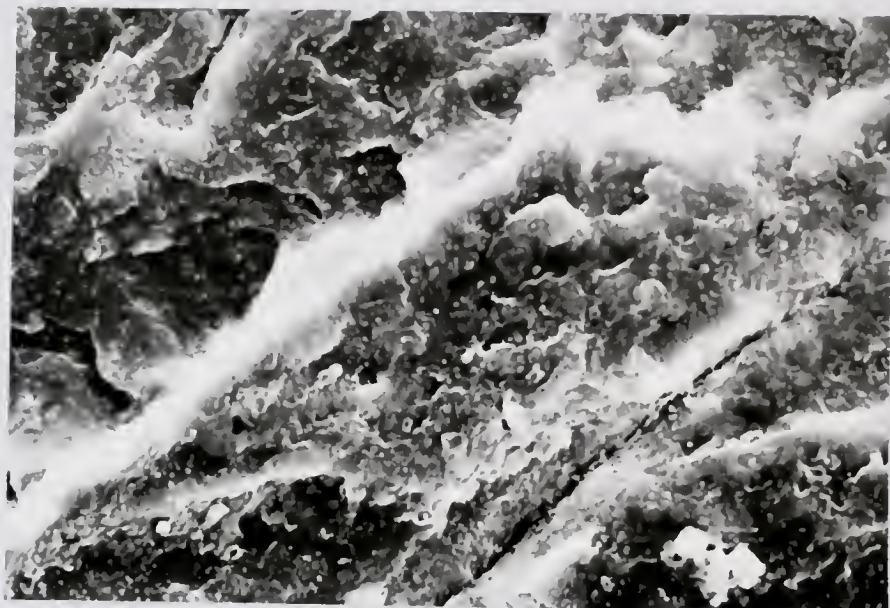
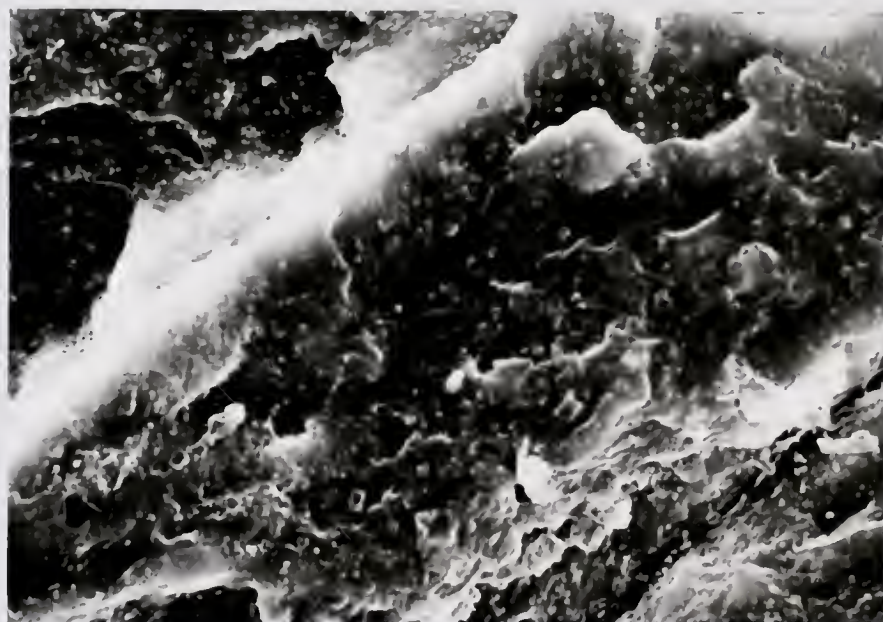


Figure 5.69 Effect of Testing Temperature on the Change of Melt Viscosity with Work of Adhesion for 20% Stöber Silica Filled Polymer at 10 rad/sec



10.0  $\mu\text{m}$

(a)



10.0  $\mu\text{m}$

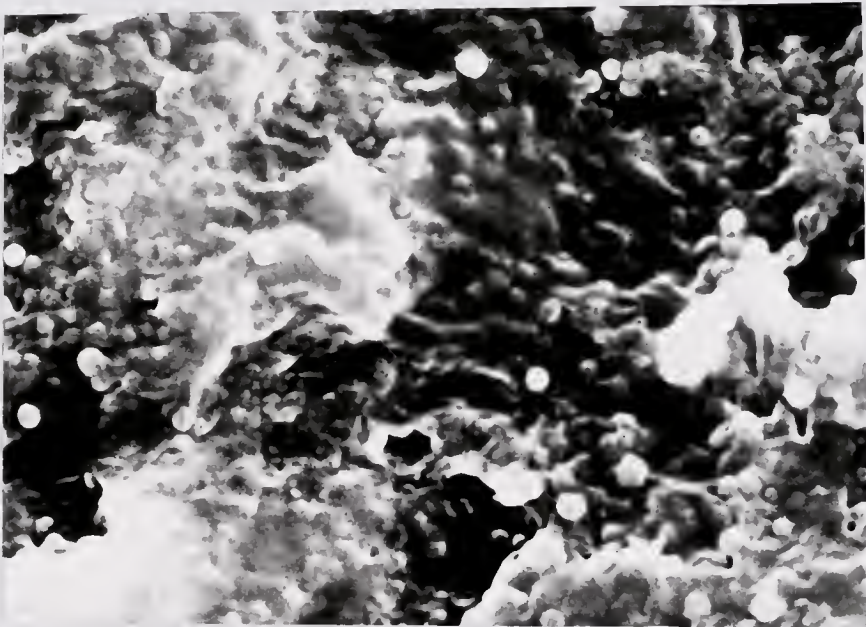
(b)

Figure 5.70 SEM Micrograph of the Brittle Fracture Surface of 15% Volume Stöber Silica Particles in E-Va Copolymer Matrix. Silica Treated at 110°C



10.0  $\mu\text{m}$

(c)



1.0  $\mu\text{m}$

(d)



—  
10.0 $\mu$ m

(a)



—  
10.0 $\mu$ m

(b)

Figure 5.71 SEM Micrograph of the Brittle Fracture Surface of 15% Volume Stober Silica Particles in E-Va Copolymer Matrix. Silica Treated by 110°C/TMCS



10.0  $\mu\text{m}$

(c)



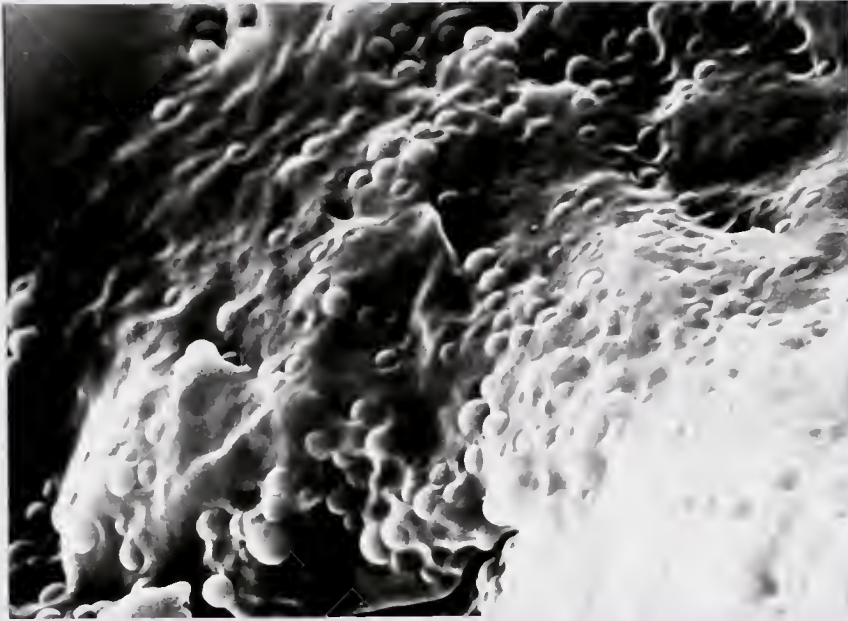
1.0  $\mu\text{m}$

(d)

bonding, while Figures 5.71 (a) and (b) illustrates poor interfacial bonding. From these four SEM micrographs, it can be inferred that the state of dispersion in the other surface modifications within these two extreme surface properties of silica should be similar to these two cases. This is supported by Figure 5.72 where (a) is the 750°C treated silica and (b) is the 750°C/TMCS treated silica.

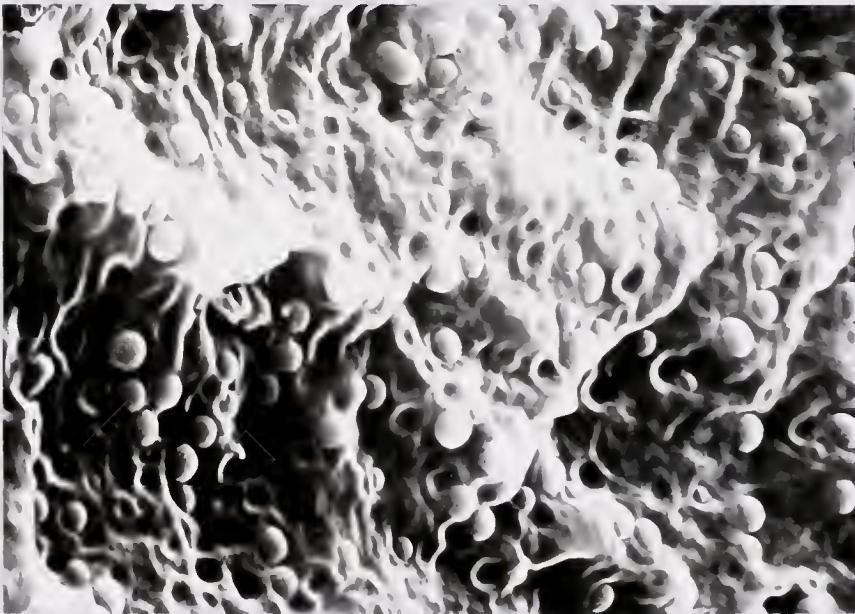
From the SEM micrographs in Figures 5.70 to 5.72, it indicates that the surface modification on the Stöber silica filler particles has little effect on the state of dispersion of these silica particles in the polymer matrix. This similarity can result from the process of sample preparation. The composites are prepared by mixing the silica particles in the polymer solution instead of polymer melt. The individual silica particle can be wetted by the solvent first before polymer is bonded and/or adsorbed on the silica surface. The agglomerate is swollen by the solvent and the individual particle is gradually separated from this agglomerate under the stirring process.

From (c) and (d) in Figure 5.70, it is seen that the Stöber silica particles are bonded and covered by polymer matrix, a composite with the highest value of work of adhesion investigated in this study. However, from the fracture surface in Figures 5.71 (c) and (d), a composite with the lowest work of adhesion, most of the Stöber silica particles are less bonded and covered by polymer matrix.



—  
1.0 μm

(a)



—  
1.0 μm

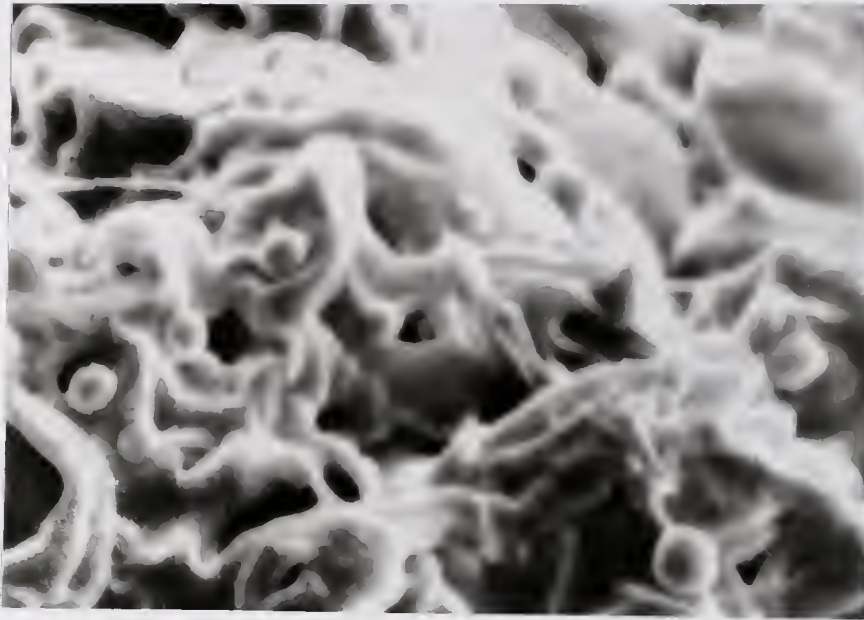
(b)

Figure 5.72 SEM Micrograph of the Brittle Fracture Surface of 15% Volume Stober Silica Particles in E-Va Matrix. Silica at (a) 750°C (b) 750°C/TMCS

The micrographs of (a) and (b) in Figure 5.72 show moderate interfacial bonding because the values of work of adhesion of these two surface treated silica particles are in between two extreme values.

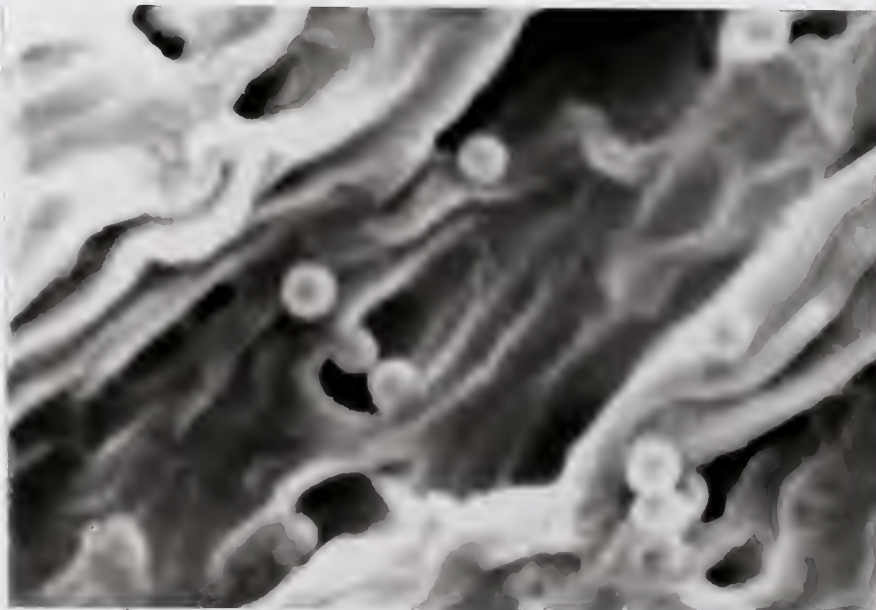
It is apparent from these SEM micrographs that the surface properties of silica do affect the interfacial bonding strength, and thus affect the locus of impact fracture of polymer composites at liquid nitrogen temperature. Further examples are seen in the tensile fracture surface of the 5% and 15% volume Stöber silica filled composites under the stress-strain test at room temperature. Some of the Stöber silica particles are still embedded in the polymer matrix on the tensile fracture surfaces for 5% volume of 110°C treated silica and 15% volume of 750°C treated silica, shown in Figures 5.73 (a) and 5.74 (a), respectively. However, Figures 5.73 (b) and 5.74 (b) show that the Stöber silica particles are almost free from polymer on the tensile fracture surface in the 5% volume of 110°C/TMCS surface modified silica and the 15% volume of 750°C/TMCS surface modified silica.

The state of dispersion of the Cab-O-Sil silica in the E-Va copolymer was also studied by SEM and TEM micrographs. The E-Va copolymer filled with a 5% volume fraction of Cab-O-Sil silica was examined by SEM. The dispersion of silica by 110°C and 110°C/TMCS treatments is shown in Figures 5.75 and 5.76, respectively. The state of dispersion of the



1.0  $\mu\text{m}$

(a)



1.0  $\mu\text{m}$

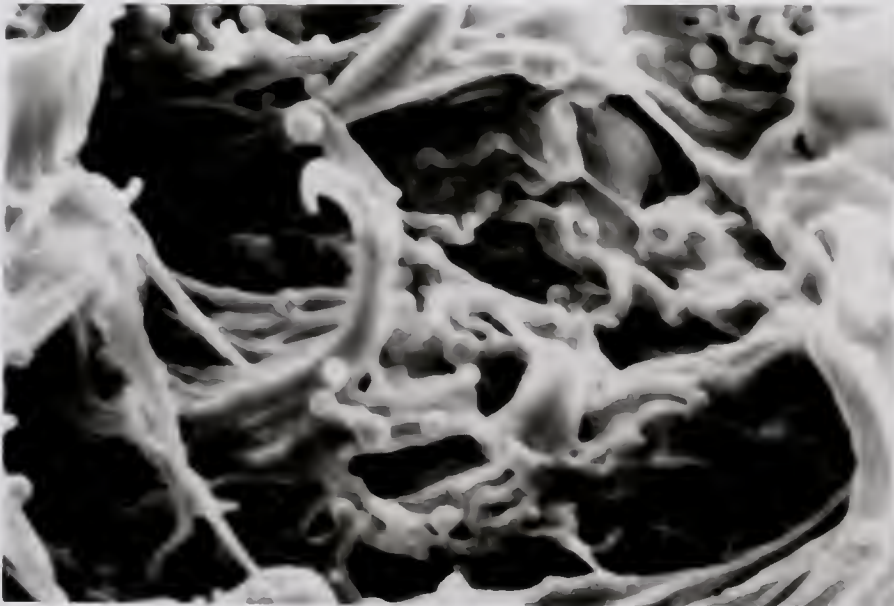
(b)

Figure 5.73 SEM Micrograph of the Tensile Fracture Surface of 5% Volume Stober Silica Particles in E-Va Matrix. Silica at (a) 110°C (b) 110°C/TMCS



1.0  $\mu\text{m}$

(a)



1.0  $\mu\text{m}$

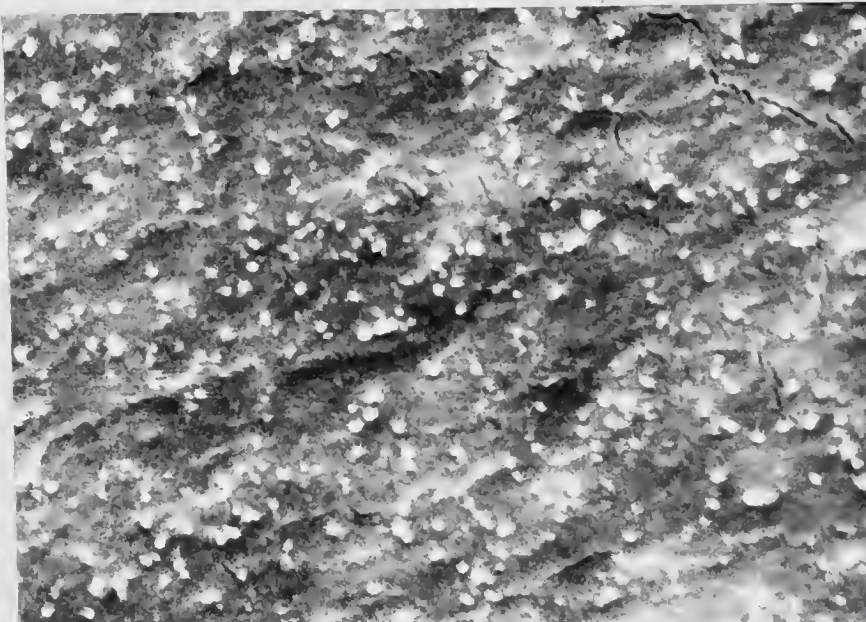
(b)

Figure 5.74 SEM Micrograph of the Tensile Fracture Surface of 15% Volume Stober Silica Particles in E-Va Matrix. Silica at (a) 750°C (b) 750°C/TMCS



1.0  $\mu\text{m}$

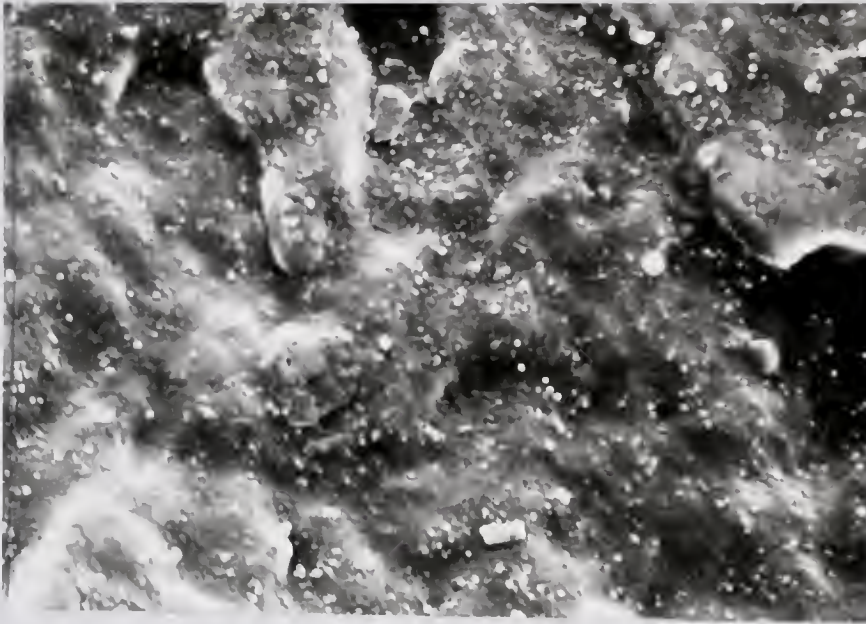
(a)



1.0  $\mu\text{m}$

(b)

Figure 5.75 SEM Micrograph of the Brittle Fracture Surface of 5% Volume Cab-O-Sil Silica in E-Va Matrix. Silica Treated at 110°C



1.0  $\mu\text{m}$

(a)



1.0  $\mu\text{m}$

(b)

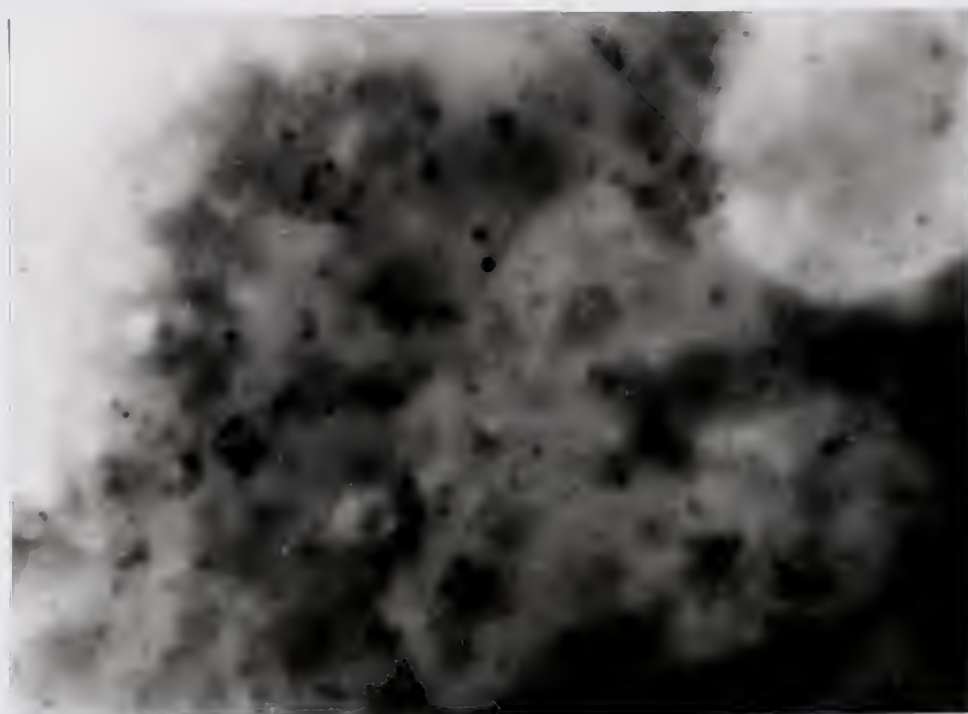
Figure 5.76 SEM Micrograph of the Brittle Fracture Surface of 5% Volume Cab-O-Sil Silica in E-Va Matrix. Silica Treated by 110°C/TMCS

Cab-O-Sil silica in the polymer matrix does not show much difference in either case of surface modification.

Cab-O-Sil silica particle aggregates apparently exist in each surface modification (151,260). From these SEM micrographs, the size of these aggregates is estimated to range from several hundred to a thousand angstroms. As discussed in section 3.1, the aggregate is formed during the manufacturing process and cannot be broken by the mixing procedure during the preparation of the composites. The aggregated particles in the range of submicro centimeter shown on the fracture surface, which was prepared at liquid nitrogen temperature, can then be quantitatively counted. Volume fractions of Cab-O-Sil aggregated silica particles of more than 3% can be identified in each SEM micrographs in Figures 5.75 and 5.76. These aggregates are in the thousand angstroms range. In other words, estimated from SEM pictures, about 70% of Cab-O-Sil silica exists as aggregated particles in the filled composite. Therefore, the dispersion of the Cab-O-Sil silica in the polymer matrix was further studied by TEM.

When the fracture surface is investigated at high magnification, the small silica particles, which cannot be identified by SEM, now can be studied by TEM. These fine silica particles are dispersed around the aggregated silica in the polymer matrix. The state of dispersion of the

Cab-O-Sil silica particles in the polymer matrix with various surface modifications of the silica surface is shown in Figure 5.77. It is seen that the state of dispersion of Cab-O-Sil silica in the polymer matrix is similar in each of surface modified silicas. These individual fine particles can be clearly identified at even higher magnification, as shown in Figure 5.78.



1.0  $\mu\text{m}$

(a)



1.0  $\mu\text{m}$

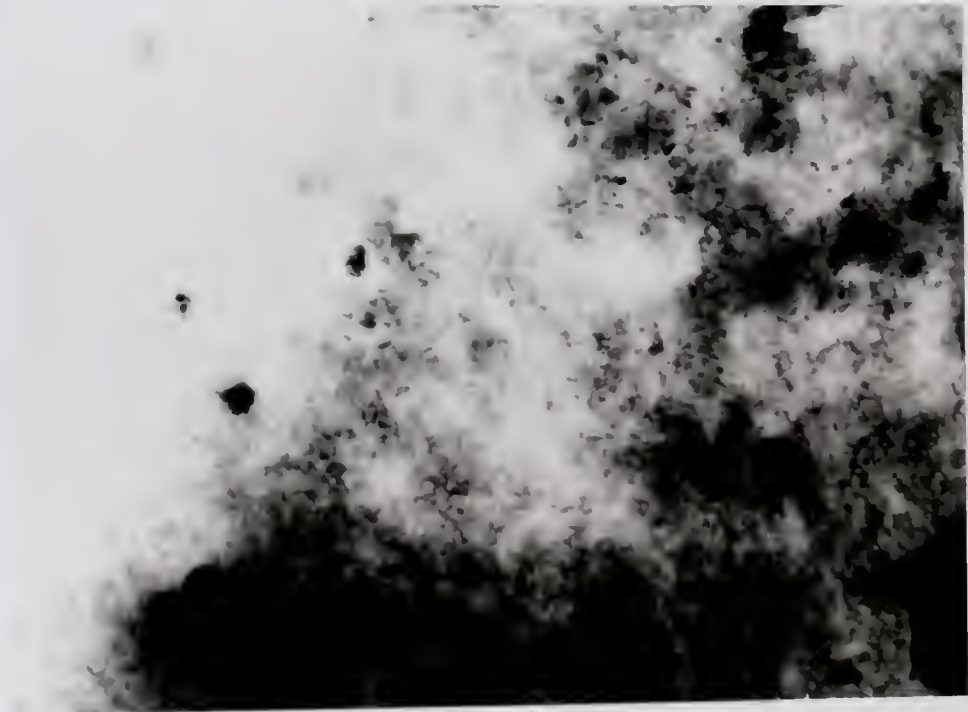
(b)

Figure 5.77 TEM Micrographs of 5% Volume Cab-O-Sil Silica in E-Va Matrix. Silica Surface Modified by (a) 110°C (b) 500°C (c) 750°C (d) 750°C/TMCS (e) 500°C/TMCS (f) 110°C/TMCS



1.0  $\mu\text{m}$

(c)



1.0  $\mu\text{m}$

(d)



—  
1.0 $\mu$ m  
(e)

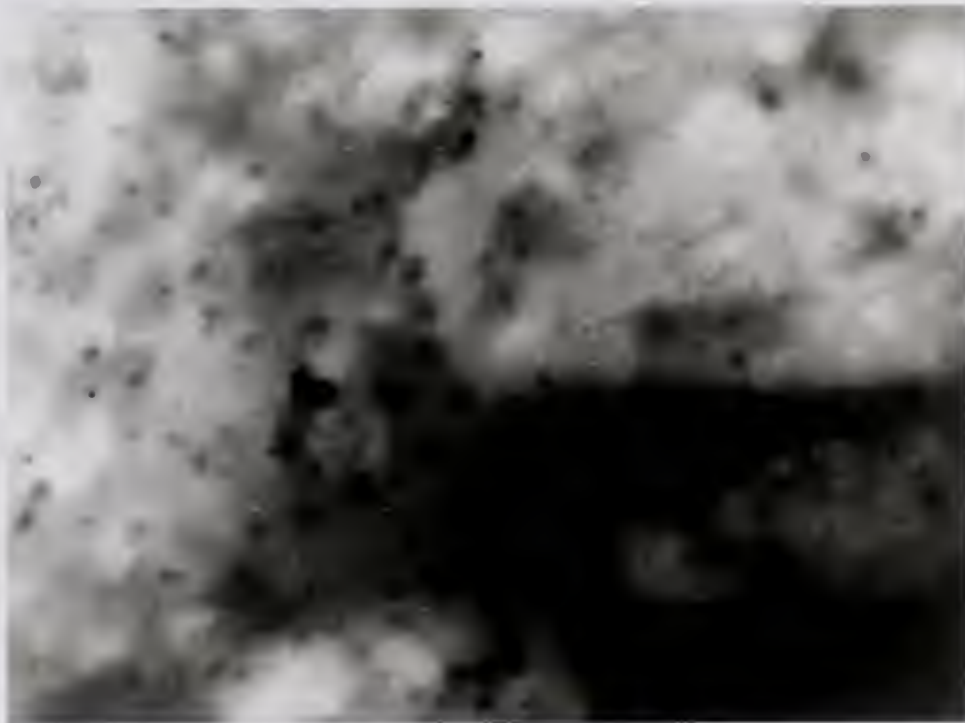


—  
1.0 $\mu$ m  
(f)



1.0  $\mu\text{m}$

(a)



1.0  $\mu\text{m}$

(b)

Figure 5.78 TEM Micrographs of 5% Volume Cab-O-Sil Silica in E-Va Matrix. Silica with Various Surface Modification Studied at High Magnification

## CHAPTER 6 DISCUSSION

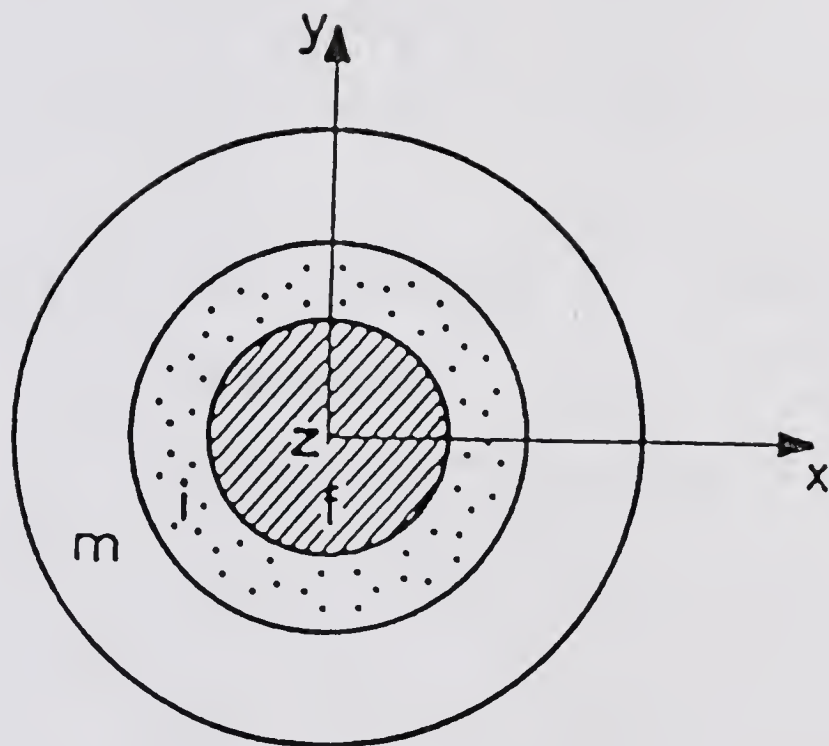
### 6.1 Effective Silica Particle Size

The bonded and/or adsorbed polymer molecules form an interphase layer around the silica particles. The interphase layer combining with a silica filler particle establishes an effective silica particle size (261).

Polymer adsorbed onto the silica surface from solution is studied by FTIR in section 4.4. Even though the studied polymer volume concentrations in Figure 4.15 do not reach the saturated concentration, it can still be seen that there are more polymer molecules bonded and/or adsorbed on heat treated than heat/TMCS treated silica particles.

Figure 4.16 indicates that the extent of polymer bonded and/or adsorbed onto the silica surface from solution increases exponentially with a linear increase in work of adhesion. When silica particles are embedded in a polymer composite, the extent of polymer bonded and/or adsorbed on the silica particles being heat treated should be greater than being heat/TMCS treated.

Figure 6.1 shows that the bonded and/or adsorbed polymer molecules form an interphase layer around a silica particle. Since the thickness of this interphase layer is



f = SILICA FILLER  
i = INTERFACE  
m = POLYMER MATRIX

Figure 6.1 Schematic Representation of the Interface Model

determined by the surface properties of silica particles, the interphase is greater when the work of adhesion is higher. Thus, the effective particle size of silica is increased with an increase in work of adhesion.

The interphase molecules lose their flexibility and mobility since they are restrained on the silica surface by the interfacial bonding. The properties of the polymer within the interphase layer around silica particles are different from the properties of polymer far away from the silica surface.

This phenomenon is similar to silane molecules bonded to a filler surface (11,13,38-40). This silane thin film consists of chemisorbed and physisorbed layers of silane molecules which have structural and compositional gradients (11,13). The silane molecules adjacent to filler particles can form a network structure or orient in a particular direction. Due to these different properties, an interphase layer is formed.

The gradient in the change of properties, such as modulus, within an interphase will depend on the thickness of this interphase. Figure 6.2 shows the variation of gradient of properties with the interphase thickness. The gradient in change of properties within the interphase is slower when the interphase is thicker. The gradient of the change of properties within the interphase is then developed to influence the overall performance of silica

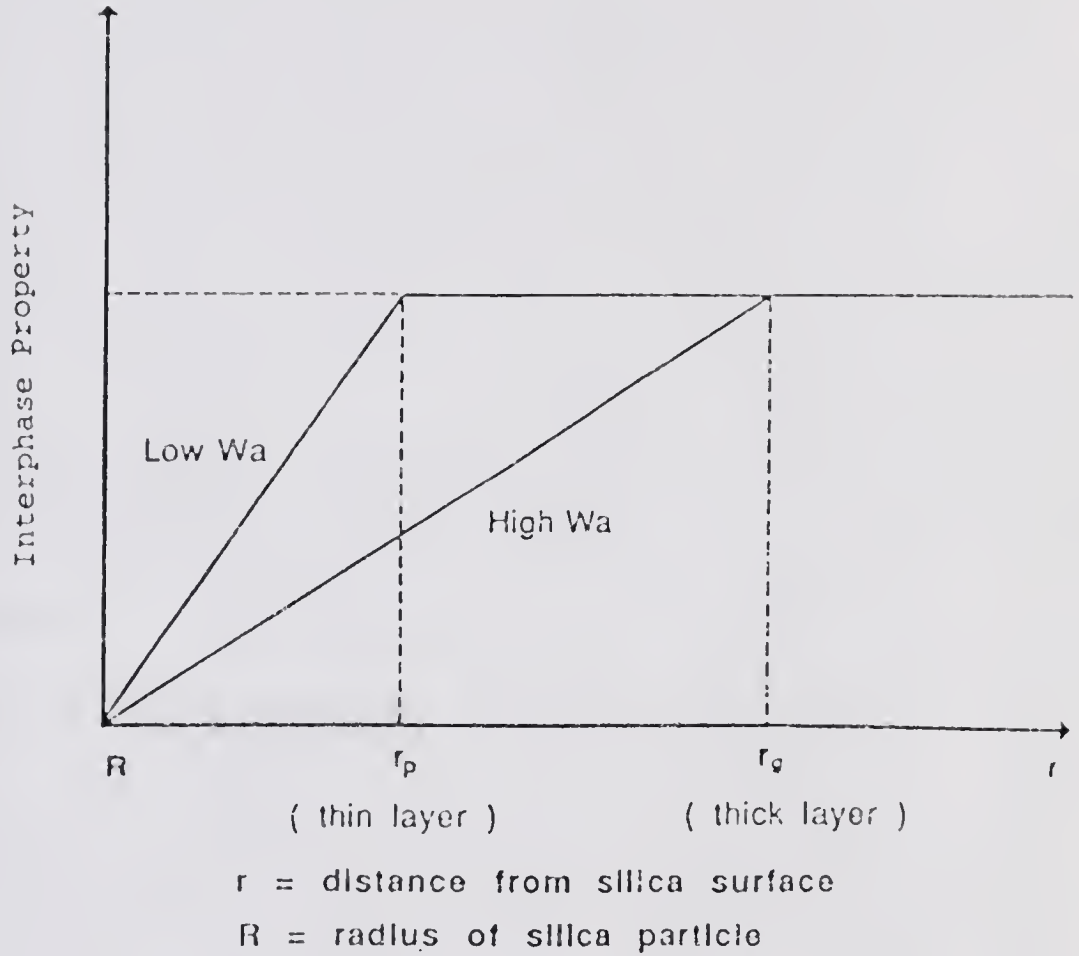


Figure 6.2 Effect of Work of Adhesion on the Gradient of Properties of Polymer within the Interphase Layer

filled polymers. This has been theoretically studied by Theocaris et al. (262-267).

From this discussion, it is evident that the effective particle size of silica filler is important to determine the mechanical and rheological properties of composites.

## 6.2 Interphase Dependence of Mechanical Properties of Polymer Composites

### 6.2.1 Interphase Dependence of Young's Modulus

It is known that Young's modulus increases with an increase in volume fraction of filler.

For a constant volume fraction of filler particles in the polymer matrix, an increase in the effective particle size is equivalent to an increase in filler concentration. This leads to an increase in the modulus of the polymer composite. It is thus seen in Figure 5.7 that the Young's moduli of silica filled composites increase exponentially with work of adhesion.

With the same volume fraction but with various size of silica particles in the polymer matrix, the Cab-O-Sil silica has a higher total filler surface area than Stöber silica. Thus, the polymer fraction included in the interphase layer is higher in the Cab-O-Sil silica (237). This is essentially equal to an increase in volume fraction of filler. It explains why the modulus of the Cab-O-Sil silica filled polymer composite is higher than that of the Stöber silica filled composite.

From Figure 5.7 and Table 5.3, it can be seen that the apparent surface energy barrier of the Young's modulus is higher when the filled silica particle size is small. The concept of the apparent surface energy barrier will be discussed in section 6.4. It indicates that an increase in modulus with work of adhesion occurs faster for the Cab-O-Sil composites than for the Stöber composites. This can be explained by the gradient of polymer fraction included within the interphase. The Cab-O-Sil composites have a higher gradient than the Stöber composites.

The apparent surface energy barrier of Young's modulus in the studied system is dependent on particle size but independent of the volume fraction of silica. This finding may result from the low silica filler concentration. No particle-particle interaction occurs at these concentrations.

The same phenomenon is also seen for the shear modulus in Figure 5.24 to 5.26. The apparent surface energy barrier of shear modulus is independent of volume fraction of silica in the polymer composites, which are seen in equation ( 5.13 ).

Nevertheless, the apparent surface energy barrier of the modulus still depends on other materials characteristics. The size of filler particles used in polymer composites discussed above is one example. Another example is the stress transfer at the interface. The

dependence of modulus on the work of adhesion in fiber reinforced plastics (FRP) is different from particulate filled composites, since fibers have different aspect ratio when compared to spherical silica particle. The mechanism of stress transfer at the interface between particulate filled polymers and fiber reinforced plastics is different. The role of work of adhesion on the mechanical performance of fiber reinforced plastics is therefore different.

### 6.2.2 Interphase Dependence of Tensile Strength

In Figure 5.8, the logarithm of tensile strength is proportional to the reciprocal of work of adhesion. A higher work of adhesion corresponds to a higher tensile strength.

The first two types of polymer molecular links, which were discussed in section 2.7.2.3, play an important role in determining the tensile properties of silica filled composites. The thickness of the interphase layer increases with an increase in the work of adhesion. Within this interphase layer, more polymers are bonded on silica surface and entangled by other bulk polymer molecules. More forces can then be transferred to silica filler when the number of these links at the interphase are increased.

With the same applied stress on a composite, the polymer itself in the composite bears less stress when stress is easily transferred to filler particles. The hydrogen bonding at the interface forms bonds strong enough

to tolerate the applied stresses (58-63), and does not result in a failure at the interface. From Figures 5.73 (a) and 5.74 (a), the tensile fracture surface of the Stöber silica filled E-Va copolymer, it is seen that the silica particles are still somewhat surrounded by polymer. This indicates that the fracture does not occur at the interface, and that the filler can carry some of the applied loads.

In contrast, if the filler does not adhere to the matrix, then the filler particles cannot carry any load. The polymer will sustain all the forces. The silica is free from the polymer matrix when the adhesion is weak as seen in Figures 5.73 (b) and 5.74 (b). This illustrates that filler does not sustain any of the loads applied in the polymer composite.

For strong hydrogen bonds at the interface, the matrix does not detach from a spherical particle. Instead, it undergoes internal rupture near the particle surface, nucleated by a small precursor void within the interphase layer (268,269). The condition for growing the precursor voids to craze is that the applied stress must be higher than the critical stress required to grow the voids (critical stress for cavitation). This critical stress for cavitation is higher than the stress required for dewetting (critical stress for detachment), which occurs in the poor adhesion of silica filler system (268,269).

Since a higher value of stress is required to begin the craze formation for strong hydrogen bonding, a higher tensile strength will be obtained in this composite.

In addition, from Figures 5.5, 5.6 and 5.8, it is shown that the small particles had more pronounced reinforcing properties than the large ones (127-130,270).

As seen in section 2.4.3, the reinforcing phenomenon is related to (a) the interfacial area per unit volume of silica particles, (b) the extent of interaction of stress fields around filler particles, and (c) volume of polymer around an individual filler involved in the debonding process.

The stress fields near a particle are independent of the size of filler particles (101). However, the volume of polymer, which experiences a given value of stress concentration, increases with increasing particle size. When the size of a particle is extremely small, the voids located within the immediate vicinity of the particle must be small in size in comparison with the particle itself (268). The critical stress for cavitation will no longer be given by the value necessary to maintain the deformation or the resistance to expansion. It also needs to meet the value necessary to maintain the surface energy requirement of constraint on the expansion of a void. This means that the surface energy will become important when the size of the void becomes very small. In other words, the critical

stress for cavitation will be very high when the size of the silica particles is very small (268-270).

Meanwhile, the possibility of finding a large flaw within the volume experiencing a given stress increases with an increase in particle size. If a large flaw exists within the region of stress concentration, the tensile strength will be reduced according to Griffith's theory (271). A large void is more detrimental than a small one. A large void may be found around a large filler particle after dewetting occurs at a large deformation. The tensile strength of polymer composites filled by Stöber silica is thus lower than that of those filled by Cab-O-Sil silica.

The extent of interaction of stress fields during a large deformation is a function of volume fraction of filler particles. The interaction of stress fields increases when the volume fraction of silica is increased. These interactions will weaken the materials, which results in a decrease in tensile strength when the volume fraction of filler is increased. As seen in Figure 5.6, when the volume fraction is high enough to result in the interaction of stress fields at large deformations, the tensile strength decreases with an increase in volume fraction of silica. This point is around 4% volume fraction for Cab-O-Sil silica in Figure 5.6. The tensile strength is gradually increased with volume fraction of Cab-O-Sil silica before this volume fraction of filler (272).

The apparent surface energy barrier of the tensile strengths in Figure 5.8 is dependent on the filler particle size and volume fraction of silica. The apparent surface energy barrier of the tensile strength is listed on Table 5.4. As discussed above, for a composite, the polymer fraction involved within the interphase is more in the Cab-O-Sil silica filled composite than in the Stöber silica filled composite. The variation of the polymer fraction involved within the interphase with a change of work of adhesion occurs faster in the Cab-O-Sil silica filled composites.

The change of tensile strength with the variation of work of adhesion might be faster in the Cab-O-Sil silica filled composites. Therefore, the apparent surface energy barrier would be higher for Cab-O-Sil silica filled composites. However, this is not consistent with the trend of the values listed on Table 5.4. This inconsistency can be related to aggregation formation of Cab-O-Sil silica and to the extent that polymer is attached around each individual particle involved in the debonding process.

The aggregates of Cab-O-Sil silica form three dimensional networks. The dependence of tensile strength on the work of adhesion will differ when the aspect ratio of the filler particles is changed, since the mechanism of stress transfer at the interface is different.

When an individual silica particle is considered, the polymer around the particle involved in the dewetting or cavitation process is increased with increasing particle size. Thus, an individual Stöber silica particle has more polymer involved than an individual Cab-O-Sil silica particle, even though the Cab-O-Sil silica filled composite has a higher polymer fraction involved within the interphase.

Furthermore, when the extent of hydrogen bonds at the interface, and thus work of adhesion, is varied, the gradient of molecular structure and packing as well as the thickness of the interphase around each individual particle are changed. These changes with work of adhesion will develop a pronounced effect on the stress transfer between filler particle and polymer matrix. Since tensile stress is the result of a large deformation, the dewetting and void formation around each individual particle will play a very important role in determining the tensile strength of the materials.

Therefore, The Stöber silica filled composites have a higher value of the apparent surface energy barrier than the Cab-O-Sil silica filled composites. The result of this argument is consistent with the values listed on Table 5.4.

Meanwhile, the apparent surface energy barrier of tensile strength of composites is increased with an increase in volume fraction, and can be attributed to the

interaction of stress fields and void at the large deformation.

From the discussion of the apparent surface energy barrier of the Young's modulus and tensile strength, it is seen that work of adhesion has two effects on the mechanical properties of silica filled polymer composites. One is in the overall fraction of polymer involved around the silica particles in the composite. This is the central role of work of adhesion in determining the Young's modulus. The other is in the volume of polymer involved in the dewetting process around each individual silica particle. This is the central role of work of adhesion in determining the tensile strength of polymer composite.

### 6.3 Effect of Temperature on Work of Adhesion

In section 4.5, the effect of environmental temperature on the interfacial bonding is studied by DRIFT technique.

#### 6.3.1 Temperature Dependence of Weak Interfacial Bonding

From equations ( 5.2 ) and ( 5.3 ), each component of the work of adhesion of the weak interfacial bonding can be evaluated from the surface energy of silica and polymer.

Wu showed that the surface energy of polymer decreased linearly with an increase in temperature (76,273-276). However, the change of surface energy of a polymer with change in temperature is much smaller than the change of a small molecule. This is attributed to the conformational restrictions of long-chain polymer molecules (277,278).

The  $W_a^d$  in equation ( 5.2 ) and  $W_a^h$  in equation ( 5.3 ) are, therefore, dependent on temperature since the surface energy of a polymer is temperature dependent.

### 6.3.2 Temperature Dependence of Strong Interfacial Bonding

From equations ( 5.4 ) and ( 5.5 ), the  $W_a^h$  in the strong interfacial bonding is dependent on (a) acid-base interaction energy and (b) amount of hydrogen bonds at the interface.

As discussed in section 4.5.1, the interaction energy of hydrogen bonding at the interface is decreased with increasing environmental temperature since the difference in the wavenumber between the free C=O group and the hydrogen-bonded C=O group becomes small as temperature increases.

Furthermore, it is assumed in the model used to evaluate  $W_a^h$  that all the hydroxyl groups on the silica surface can form hydrogen bonds with carbonyl groups in the polymer chain. However, some of these hydrogen bonds at the interface might not exist at high temperatures since high temperature increases the mobility of polymer molecular chain. This is supported by a decrease in the peak intensity of hydrogen-bonded C=O group in Figures 4.19 and 4.21. Thus, the number of hydrogen bonds at the interface at high temperature is smaller than the number of hydrogen bonds at room temperature.

Thus,  $W_a^h$  is decreased with an increase in temperature. Meanwhile,  $W_a^d$  in the strong interfacial bonding system is also evaluated from equation 5.2.

Therefore, both  $W_a^h$  and  $W_a^d$  in the strong hydrogen bonding system are temperature dependent.

### 6.3.3 Discussion of Temperature Dependence of Work of Adhesion

As discussed above, the work of adhesion in the model used to evaluate the interfacial bonding strength is dependent on temperature.

In a strong hydrogen bonding interface, both the number of interfacial bonds and the acid-base interaction energy are decreased with an increase in temperature. In a weak hydrogen bonding interface, the surface energy is also decreased with an increase in temperature. Therefore, both cases suggest that the work of adhesion is decreased with an increase in temperature (279,280). The main contribution to the change of work of adhesion with temperature comes from the change in  $W_a^h$  since  $W_a^h$  is more sensitive to the temperature change (87,281,282).

The above result is from a system with a thin layer of polymer bonded and/or adsorbed on silica surface. The effect of environmental temperature on the hydrogen bonds is measured by hot stage with DRIFT technique under ambient atmosphere. However, the real conditions of filler-polymer interface of polymer composites are different from the

environmental conditions of the FTIR study. The effect of temperature at the in-situ interface of a composite might not be so great as it would be on the result from a thin layer polymer adsorbed onto silica surface (283). Some possible reasons can cause this difference. One is the low thermal conductivity of the polymer matrix. Another is that the polymer at the interface layer of a composite actually locates inside a bulk of polymeric material, instead of in a thin polymeric film exposed to the ambient atmosphere (283), and there might be a dynamic equilibrium of bonding at the interface.

Hence, the temperature dependence of work of adhesion at the interface of a composite is not easily evaluated precisely due to the complex nature of the system. The calculated values of work of adhesion in sections 5.3 and 5.4 are determined at room temperature, not at the rheological measurement temperature.

However, quantitative studies of the rheological properties of composites versus work of adhesion are still useful and valuable in sections 5.3 and 5.4, even though the values of work of adhesion used in the study are determined at room temperature. This study provided a quantitative technique to evaluate the relationship between interfacial bonding strength and the mechanical as well as rheological properties of polymer composites.

At the same time, from this quantitative study, it is apparent that the effect of work of adhesion on the rheological properties of polymer composites is dependent on test conditions (such as frequency and temperature) and materials characteristics (such as volume fraction and particle size of silica filler).

#### 6.4 Effect of Interphase on the Rheological Properties of Silica Filled Polymer Melt

##### 6.4.1 Frequency Dependence of the Effective Particle Size

Figure 6.3 is proposed to describe how the effective silica particle size changes with the frequency. At a low frequency the dependence of the effective particle size on the work of adhesion is obvious. When the frequency is increased, the adsorbed polymer within the outer layer of interphase gradually loses the entanglements from the bonded polymer at an inner layer of interphase (16). The amount of polymer within the interphase is then reduced. The effective particle size thus decreases with an increase in frequency. It is seen from Figure 6.3 that the rate of polymer reduction at the interphase layer differs with variation in work of adhesion. However, the effective particle size will approach the original silica particle size when the frequency is high enough. Due to this same approximate effective particle size, the work of adhesion will not much influence the rheological properties of a filled polymer at a high frequency.

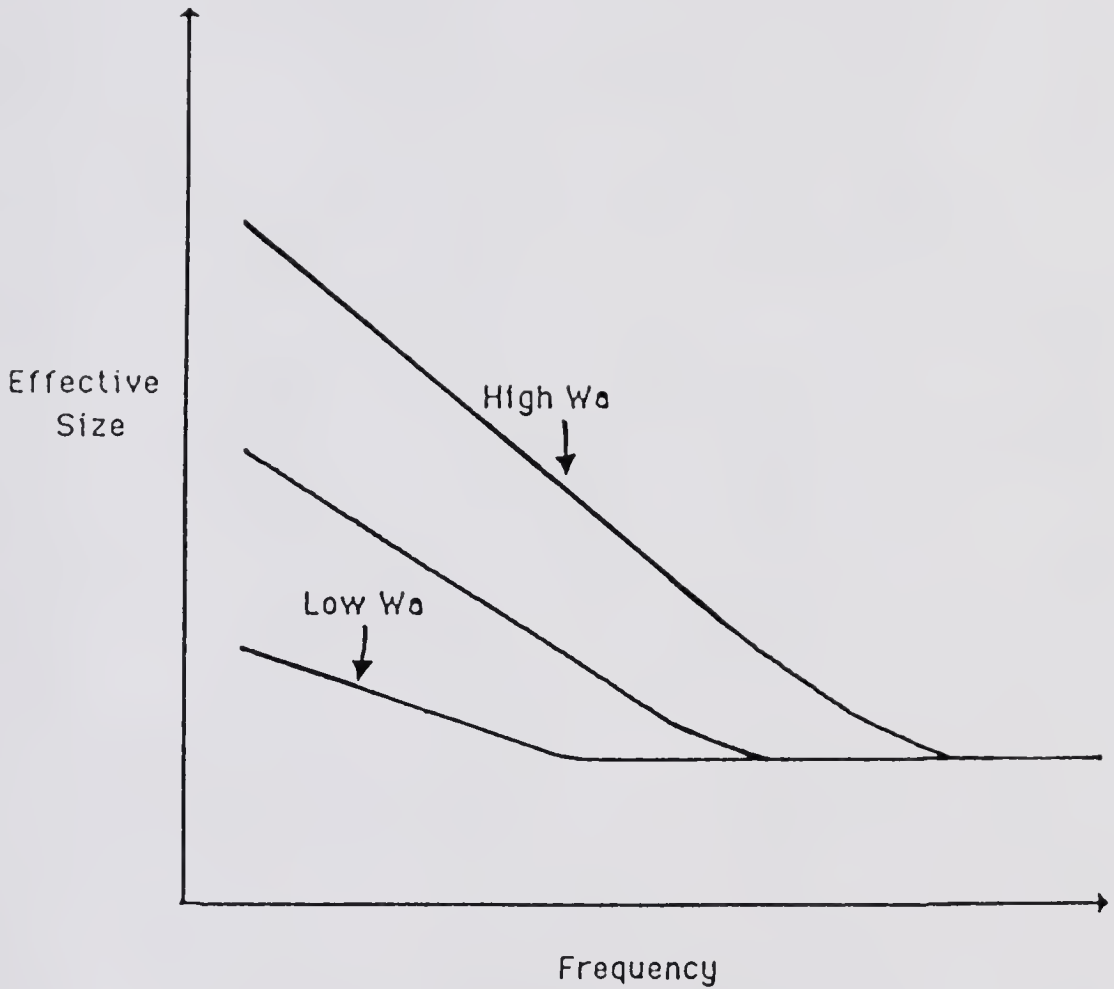


Figure 6.3 The Change of Effective Particle Size of Silica with Frequency at Different Levels of Work of Adhesion

#### 6.4.2 Interphase Dependence of Shear Modulus

The shear modulus of a polymer composite is studied in section 5.4.1. From Figures 5.9 and 5.11 to 5.14, it is seen that at a low frequency the composite material filled with heat treated silica has a higher shear modulus than when filled with heat/TMCS treated silica. This difference is attributed to the effective particle size.

A polymer is a viscoelastic material; during shear, some energy dissipates into heat, while some can be stored as elastic energy of the polymer. At a high frequency, the decrease in viscosity is associated with the development of elasticity in the melt (164). The elasticity can be measured as an elastic modulus. From Figures 5.9 and 5.14, it is seen that the shear modulus of an unfilled polymer melt increases when the frequency is increased.

The properties of a polymer, far away from the silica surface, are similar to the properties of an unfilled polymer. These properties are different from the properties of the polymer within the interphase layer. When a relative value is used to study the elastic properties, the matrix effect can be minimized (167). Figures 5.10 and 5.15 to 5.18 show that the relative shear modulus is lower at a high frequency than at a low frequency, since the effective particle size becomes small and almost has the same size at a high frequency. The relative shear moduli of composites then approach the same

value at a high frequency. On the contrary, the effective particle size is greater at a lower frequency. The relative shear moduli of composites at a low frequency are thus strongly dependent on the surface properties of silica particles. The change in the effective particle size is more sensitive to the variation in the work of adhesion at a low frequency than at a high frequency. Thus, in Figures 5.19 to 5.23 the slope of relative shear modulus versus the reciprocal of work of adhesion is steeper at a low frequency.

### 6.4.3 Interphase Dependence of Melt Viscosity

#### 6.4.3.1 Flow process of a filled polymer melt

With regard to the flow process of a silica filled polymer melt, the polymer far away from the silica particle will move faster than the polymer on the silica surface. The polymers will pass through the silica particles during the flow process. Thus, the polymer molecules at the matrix will move at a relative velocity to the silica particle. When there is a relative movement between these two phases, friction occurs at the interface.

Furthermore, the movement of the polymer within the interphase layer to the silica particle can be described by Figure 6.2. The velocity of polymer within the interphase varies with distance from silica surface.

Regardless of the thickness of the interphase, polymer at the matrix is assumed to flow at one velocity ( $V_p$ ) and

the silica particle moves at another velocity ( $V_f$ ). The gradient in the change of velocity within this interphase layer is slower when the interphase is thicker.

#### 6.4.3.2 Effect of friction factor on melt viscosity

The frequency in dynamic mode is analogous to the shear rate in steady mode or the flow velocity in a flow process. When a laminar flow of a low molecular weight of fluid passes the smooth surface of an object, both skin and form friction factors are variation with the reciprocal of the velocity ( $V$ ) of fluid (32).

$$f \propto \frac{1}{V} \quad ( 6.1 )$$

The relationship between the friction factor and frequency in the dynamic mode may not follow an equation similar to that as shown above. Nevertheless, the friction factor will decrease with an increase in frequency in the dynamic mode. Meanwhile, the effect of the friction factor will become obvious in filled polymer melts since the polymer molecules are macromolecules.

As discussed in section 2.7.2, the form friction factor is determined by the shape of filler particles. The shape of silica does not change after the silica particles are subjected to heat and/or chemical treatments. The extent of polymer bonded and/or adsorbed at the interphase does

depend on the silica surface properties, however, the shape of effective particle size is still spherical.

On the other hand, the skin friction factor is determined by the size of particle or the contact surface area of the solid. In other words, the friction factor changes with the effective particle size of silica.

In addition, the effective silica particle size decreases with an increase in frequency; therefore the effect of the friction factor on composite melt viscosity is dependent on the frequency applied in the melt.

#### 6.4.3.3 Low frequency dependence of surface friction factor

Surface friction factor is one of the important properties in determining the magnitude of the viscosity of silica filled polymer melts.

As studied in the section 5.4.2.2, the effect of work of adhesion on the melt viscosity of a polymer composite at a low frequency is obvious. From Figures 5.39 to 5.43, it is seen that the relative melt viscosity increases with an increase in work of adhesion. This phenomenon can be interpreted by the skin friction factor.

The skin friction factor is increased with an increase in work of adhesion, since the effective particle size is increased with an increase in work of adhesion. When melt viscosity of a silica filled polymer is studied at a low frequency, the polymer being bonded and/or adsorbed around silica particles does not show much loss of entanglement

with the bulk polymer or separation from the outer layer of interphase. The effective particle size at a low frequency is not much different from at rest.

Therefore, the chance of the existence of the first two kinds of links, discussed in section 6.2.2, must be higher when the thickness of interphase layer is increased. The concept of the coupling interaction field on the melt viscosity of an unfilled polymer, originally proposed by Bueche (184,185), can then be apply to the interphase layer. The first two kinds of links are important to these polymers within the interphase layer in determining the melt viscosity of a filled polymer.

The reason is that the entangled coupling interaction field around the silica particles is increased when the thickness of the interphase is increased. The resistance of movement between silica particles and polymer matrix is then increased when the interfacial bonding and coupling interaction fields are strong. The melt viscosity is the result of resistance of flow. The melt viscosity is thus increased with an increase in the thickness of interphase. All these factors demonstrate that skin friction is increased when work of adhesion is increased.

The skin friction factor of a filled polymer is also increased with an increase in contact surface area of filler particles. This can be seen by applying the same concept of polymer included within the interphase layer

discussed in the previous section on mechanical properties. Thus, the Cab-O-Sil silica filled polymer thus has a higher melt viscosity than the Stöber silica filled polymer.

However, no matter what kinds of surface modifications are applied to the silica particles, the segmental friction of the matrix polymer far away from silica surface is the same. Skin friction is thus the dominant factor in determining the relative melt viscosity of a silica filled composite. The relative melt viscosity of a polymer composite at a low frequency is thus increased with an increase in the work of adhesion. The apparent surface energy barrier of the relative melt viscosity also depends on frequency, because skin friction is determined by the frequency applied in a filled polymer melt.

Meanwhile, the skin friction is also increased when the silica concentration in a composite is increased, since there is more contact surface area between the Stöber silica particles and the polymer matrix. In Figure 5.44, it is shown that the apparent surface energy barrier of the relative melt viscosity is higher at a higher volume fraction of the silica filled polymer melt. However, from Figures 5.44 to 5.46, the effect of volume fraction on the apparent surface energy barrier of relative melt viscosity is gradually reduced when frequency is increased. In general, the magnitude of friction in a composite material is determined by the particle size, volume fraction of

silica and work of adhesion when studied at a given frequency.

#### 6.4.3.4 High frequency dependence of surface friction factor

The adhesion at the interface is reduced at a high frequency. The extent of entanglements and the degree of the entangled coupling interaction field of polymer at the interphase are decreased at a high frequency (184,185). Skin friction factor is thus decreased since the resistance of polymer movements in the dynamic mode becomes small. Thus, the skin friction on the melt viscosity at a high frequency does not play as an important role as at a low frequency.

The polymer is oriented and the response of polymer at a high frequency is just in the segmental (or local) part of a polymer chain. Less extents of entanglements of polymer are believed to exist since the response of polymer is a localized at a high frequency. The effect of entanglements on the melt viscosity of polymer is not as greater at a high frequency as at a low frequency. This is also the reason why the melt viscosity of an unfilled polymer decreases with an increase in the frequency.

The skin friction factor at the interface does not play an important role. The segment friction factor of polymer at the matrix is similar whenever polymer is far away from the silica surface. Due to these reasons, the relative

melt viscosity of the Stöber silica filled polymer is thus not much different at a very high frequency. This melt viscosity of a filled polymer at a high frequency is lower since the segmental friction of polymer at a high frequency is reduced. The segmental friction is the dominant factor in determining the viscosity of a silica filled composite at a high frequency.

This conclusion is supported by the results shown in Figures 5.40 to 5.43. Even though the relative melt viscosity of a polymer composite still shows an increase with increasing the work of adhesion at a high frequency, the slope of the relative melt viscosity is much smaller at a high frequency than at a low frequency.

Furthermore, since the skin friction factor does not play an important role at a high frequency, the apparent surface energy barrier of relative melt viscosity should not be sensitive to the volume fraction of silica. This argument is supported by Figure 5.46. The segmental friction is thus the dominant factor in controlling the viscosity of a silica filled composite at a high frequency.

### 6.5 Mathematical Model

The concept of energy barrier is used to study the deformation kinetics of solid polymers and flow process of melt polymers (184,185,284,285). Entanglement restricts the mobility of polymer and thus determines the polymer properties. Most studies of the energy barrier in a

homogeneous system of unfilled polymers are concentrated on the macromolecular entanglements.

It is well known that the interface can affect the performance of a filled polymer composite. Therefore, the interface of a composite can be considered an energy barrier. The concept of energy barrier is proposed and described by Figure 6.4. A model regarding the interface of polymer composites as an energy barrier is described as follows.

First, for the kinetic study of a chemical reaction,

$$R = K_R \cdot \phi_f \quad ( 6.2 )$$

where  $R$  is the reaction rate,  $K_R$  is the rate constant, and  $\phi_f$  is the concentration of reactant. However, rate constant is related to the activation energy, which is an energy barrier the reaction must overcome.

$$K_R = A \cdot \exp \left( \frac{-E_a}{RT} \right) \quad ( 6.3 )$$

Where  $E_a$  is the energy barrier of the reaction,  $RT$  is the kinetic energy of the system which is available to overcome the activation energy of the reaction.  $A$  is called the pre-exponential factor.

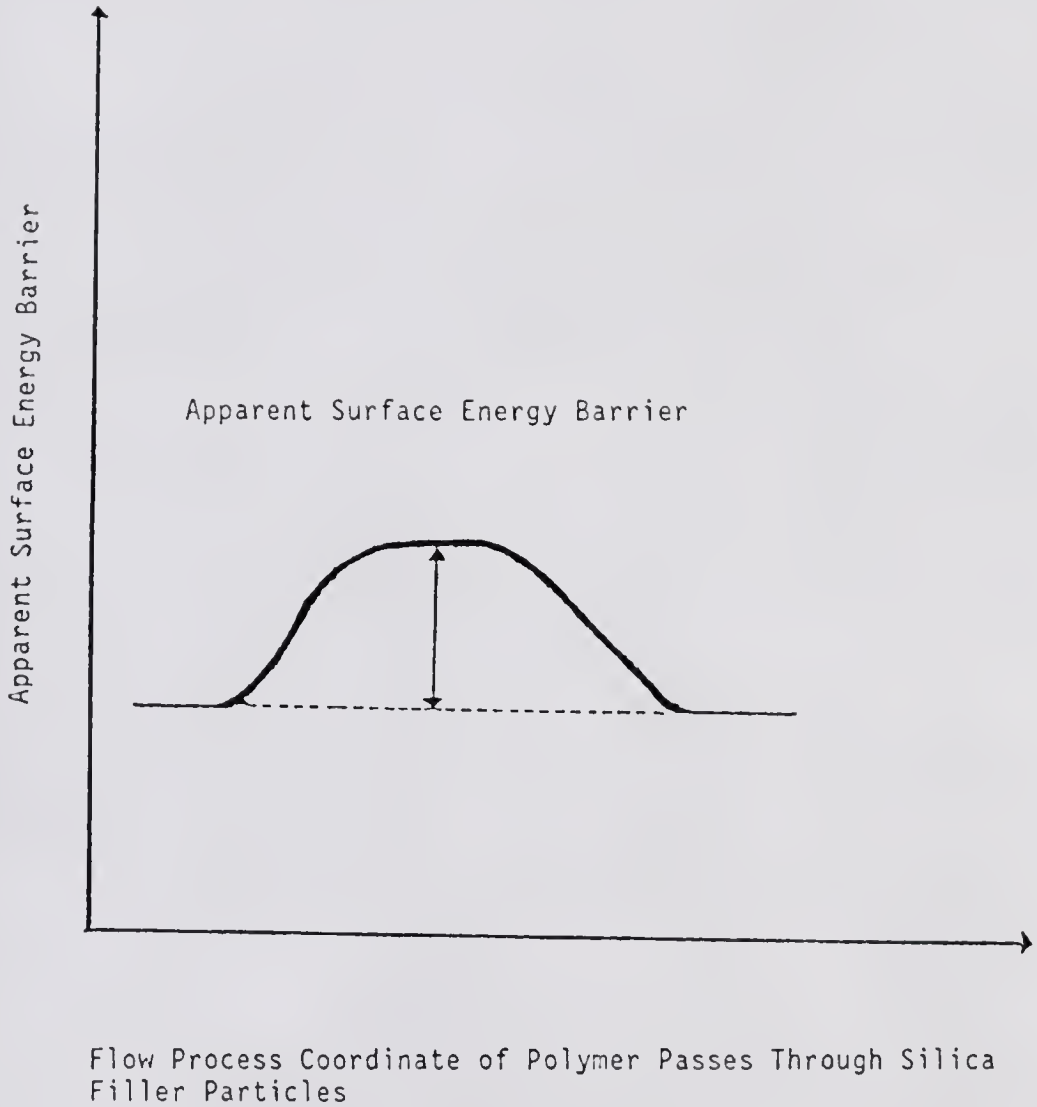


Figure 6.4 The Apparent Surface Energy Barrier of Polymer Flowing Through Different Surface Properties of Silica Filler Particles

The concept of activation energy is also used to study the temperature dependence of the diffusion coefficient (286).

$$D = C \cdot \exp^{-E_a/RT} \quad ( 6.4 )$$

where D is the diffusion coefficient. The vacancy and atomic sizes of compositions will affect the diffusion path, and then affect the activation energy.

Analogously, when filler particles are incorporated to the polymer, the interface is also a barrier during the deformation by an extension or shear process. The elastic deformation of polymer is hindered by silica particles. The hindrance is dependent on the contact surface area between the filler particles and polymer matrix. The interface is thus an energy barrier for the deformation. The energy barrier at the interface is called the apparent surface energy barrier.

The work of adhesion is the energy available by the interface to overcome the energy barrier. It is similar to the kinetic energy (RT), which is available to overcome the activation energy of diffusion. When the kinetic energy is increased, the fraction of molecules which overcomes the energy barrier is increased. Diffusion is thus increased. Analogously, the higher the work of adhesion, the stronger the bond at the interface is. The fraction of polymer

being not deformed is increased, more force is required to deform a composite, and the modulus is thus increased.

For example, the effect of work of adhesion on the Young's modulus of a composite is shown as follows:

$$E_c = C \cdot \exp \left( -K \left( \frac{1}{W_a} \right) \right) \quad ( 5.6 )$$

When this is applied to the interfaces with the various levels of work of adhesion, the experimental result can be expressed by an empirical equation,

$$E_c = E_p \left( 1 + 2.5 V_f + 14.1 V_f^2 \right) \cdot \exp \left( -K \left( \frac{1}{W_a} - \frac{1}{W_{a0}} \right) \right) \quad ( 5.9 )$$

Hence, C in equation ( 5.6 ) will include the modulus of the unfilled polymer and volume fraction of filler. Thus, the rate constant is:

$$K_R = A \cdot \exp \left( \frac{-K}{W_a} \right) \quad ( 6.5 )$$

where K is called the apparent surface energy barrier of the Young's modulus of silica filled composites.

In Chapter 5, it is seen that the apparent surface energy barrier of the Young's modulus or shear modulus is dependent on the particle size since the energy barrier of a silica filled composite increases with an increase in contact surface area (or a decrease in particle size) in a composite.

With respect to the tensile strength of a composite, the interface is a barrier to the stress being transferred. The fraction of the stress which can be transferred through the interface is increased with increasing work of adhesion. The tensile strength is thus increased with an increase in work of adhesion. However, due to the involvement of the plastic deformation in the tensile strength, the apparent surface energy barrier of the tensile strength is dependent on both the particle size and volume fraction of silica, even though the volume fraction is low. Thus, the term

$$\exp \left( \frac{-K}{W_a} \right)$$

is the fraction of the stress which can be transferred through the energy barrier ( $K$ ) by the work of adhesion ( $W_a$ ) available at the interface.

When the concept of the apparent surface energy barrier is used to study the melt viscosity of a filled polymer,

the effect of work of adhesion on the melt viscosity can be also related to the energy barrier at the interface.

Since the particle moves at a relative velocity to the polymer melt during the dynamic test, the interphase layer is a barrier which acts to inhibit the polymer around the silica particles from moving as fast as the polymer at the matrix. The work of adhesion is the energy available for the interface to overcome the apparent surface activation energy of the fluidity in order for a polymer to flow in a filled polymer melt. The empirical equation of melt viscosity from the experimental result is shown as:

$$\frac{\eta_c^*}{\eta_p^*} = C \cdot \exp \left( -K \left( \frac{1}{Wa} \right) \right) \quad ( 5.17 )$$

where

$$\eta_c^* = K_R \cdot (\eta_p^* \cdot C') \quad ( 6.6 )$$

$$C = C' \cdot A$$

Thus, the rate constant is:

$$K_R = A \cdot \exp \left( \frac{-K}{Wa} \right) \quad ( 6.7 )$$

The apparent surface energy barrier (K) of melt viscosity in equation ( 5.17 ) can be related to the energy barrier for the flow process. In this equation,

K = the apparent surface energy barrier which is evaluated from the slope of the logarithm of  $\eta_c^*/\eta_p^*$  vs.  $-1/Wa$ . It is an energy barrier for the polymer around the silica particles to move as fast as polymer at the matrix in the flow process.

$Wa$  = the work of adhesion, which represents the adhesion quality. The work of adhesion is the energy at the interface which is available to overcome the apparent surface energy barrier of the fluidity in order for a polymer to flow in a filled polymer melt. In other words, the  $Wa$  represents the resistance of the fluidity of a polymer around particles to flow. When  $Wa$  is increased, the fraction of polymer around particles which does not move as fast as polymer in the matrix is increased.

$\eta_c^*$  = the melt viscosity of a filled composite with the interfacial bonding strength being equal to  $Wa$ .

$\eta_p^*$  = the melt viscosity of an unfilled polymer.

$C$  = a constant which depends on volume fraction of silica.

$C'$  = constant at a given volume fraction of silica.

$A$  = the possibility with which polymer melt is perfectly bonded to a filler and resistant to move as fast as the polymer in the matrix.

$$\frac{-K}{\exp}$$

$W_a =$  represents the fraction of frequency A. It represents the fraction of the polymer in a silica filled polymer melt that does not move as fast as polymer in the matrix.

The apparent surface energy barrier (K) is increased with an increase in contact surface area, which depends on particle size and volume fraction of filler. Both particle size and volume fraction of filler are materials characteristics. However, apparent surface energy barrier is also dependent on the environmental testing conditions. For example, K is dependent on the test frequency because the effect of adhesion on the melt viscosity depends on the surface friction factor.

However, the apparent surface energy barrier of a flow process studied at a high frequency may not really stand for the surface effects on the melt viscosity of a filled polymer. It is due to the fact that the segment friction factor is the main factor in determining the melt viscosity at a high frequency. The apparent surface energy barrier of a filled polymer at a high frequency is more dependent on the segmental friction factor than on the skin friction factor.

The apparent surface energy barrier might also depend on temperature since temperature is one of the

environmental testing conditions. However, temperature also changes the bulk properties of polymer. It makes the system complex. In Figures 5.67 to 5.69, the experimental results showed that the effect of work of adhesion on the melt viscosity is independent of the studied temperatures.

#### 6.6 Effect of Frequency on the Activation Energy of Polymer Melt

The results in section 5.5 show that the silica filled polymer melt in the range of studied filler concentrations follows the Arrhenius equation. However, the melt viscosity is dependent on frequency also. The activation energy of polymer melt thus depends on frequency (287).

The melt viscosity of a polymer decreases with increasing temperature due to a great free volume available for molecular motion at higher temperatures. Molecular mobility and shear deformation are dependent on the free volume available in the polymer. Table 5.5 shows that the activation energy of E-Va copolymer decreases with an increase in frequency. The same phenomenon has also been observed by other authors (161,287,288,289). In the case of a filled system, the free volume available is limited only to the polymer fraction of composite. When the filler fraction is increased, the filled polymer melt viscosity will be less temperature sensitive than an unfilled melt viscosity. In other words, the activation energy of an unfilled polymer is higher than that of a filled polymer,

especially when studied at higher frequencies (150,248, 287).

Table 5.5 shows that the effect of frequency on the activation energy is also dependent on the silica filler concentration. At the same time, it shows that the activation energy of a lower volume fraction of filled polymer melt has less variation when studied at lower frequencies. The independence of filler concentration on the activation energy has been observed by several authors (152,247,248).

This independence is due to the fact that when ranges of solid loading of the composites are low, the temperature effect on the viscosity of a composite mostly comes from polymer matrix and is evidenced by an increase in free volume. The change of free volume with temperature is not much restricted by the low fraction of silica particles. The activation energy remains approximately the same.

The variation of melt viscosity with temperature at different levels of work of adhesion is shown in Figures 5.64 to 5.66. The result is interesting since the activation energies are independent of surface treatments for the 20% volume fraction of Stöber silica. In other words, the activation energy is independent of the work of adhesion, especially when the frequency is lower. It suggests that the variation of interfacial bonding by temperature is not an important factor in determining the

melt viscosity. The variation of a filled melt viscosity with temperature strongly depends on the free volume.

#### 6.7 The Extended Arrhenius Equation on the Melt Viscosity of Silica Filled Polymer Melts

The Arrhenius equation was originally used to describe the temperature dependence of viscosity in an unfilled polymer melt. This equation is also valid for the low volume fractions of silica filled polymers used in this study (150,152,247,248,287). However, when the Arrhenius equation is used to study a composite's melt viscosity, it does not consider the interfacial bonding effect on the melt viscosity studied at different frequencies and contact surface areas of silica particles. The results from this study, regarding the effect of work of adhesion on the melt viscosity, can be used to extend the Arrhenius equation. The factors influencing the melt viscosity include materials characteristics and testing conditions. That is,

- (a) volume fraction of silica,
- (b) particle size of silica,
- (c) frequency,
- (d) temperature, and
- (e) interfacial bonding.

However, the effect of the interfacial bonding on the melt viscosity is dependent on the above four independent variables.

The Arrhenius equation is written as:

$$\eta = C \cdot \exp \left( \frac{E}{RT} \right) \quad ( 5.23 )$$

where E can be considered an indicator of temperature sensitivity of materials.

The effect of work of adhesion on the melt viscosity is:

$$\frac{\eta_c^*}{\eta_p^*} = C \cdot \exp \left( -K \left( \frac{1}{Wa} \right) \right) \quad ( 5.17 )$$

An extended equation of the Arrhenius equation could then be written as:

$$\eta_c^* = \beta \cdot \exp \left( \frac{-K}{Wa} \right) \cdot \exp \left( \frac{E}{kT} \right) \quad ( 6.8 )$$

Let

$$A = \exp \left( \frac{-K}{Wa} \right), \quad ( 6.9 )$$

which stands for the effect of work of adhesion on the melt viscosity.

Then, let

$$B = \exp\left( -\frac{E}{kT} \right), \quad ( 6.10 )$$

which stands for the effect of temperature on the melt viscosity.

When the apparent surface energy barrier (K) is studied at a constant temperature, K can be related to the particle size, volume fraction of silica and the testing frequency according to equation ( 5.22 ):

$$K = P + ( R + n \cdot \log w ) \cdot V_f \quad ( 5.22 )$$

However, when the apparent surface energy barrier is studied at different temperatures, it is found that K is independent of temperature. This is based on the results from Figures 5.67 to 5.69. The apparent surface energy barrier of  $\sigma^*$  of 20% volume fraction of Stöber silica versus  $1000/Wa$  is independent of the studied temperature. This is due to the fact that the polymer is a dominant component in a low volume fraction of silica filled polymers. The effect of temperature on an increase in the free volume of polymer is more important than on a reduction in the interfacial bonding strength. Thus, the effect of temperature on work of adhesion is not so important when it is compared to the free volume.

Nevertheless, the validity of this argument on other volume fractions of silica needs to be proved.

In other words, the first exponential term on the right hand side of equation ( 6.8 ) is independent of temperature.

$$K \neq ( T ) \quad ( 6.11 )$$

Meanwhile,

$$\tau = \left( \frac{\partial G}{\partial A} \right)_{T,P,n} \quad ( 6.12 )$$

$G$  = the Gibbs free energy of the total system

$A$  = the surface area

$T$ ,  $P$ , and  $n$  are temperature, pressure and component in the system.

$$\Delta G = \Delta H - \Delta TS \quad ( 6.13 )$$

From section 6.3, the  $\Delta S$  of polymer is small, and the range of  $\Delta G$  does not change much when temperatures vary from 150°C to 190°C. The  $\tau$  of polymer then does not change much. The  $W_a^d$  and  $W_a^h$  in equations ( 5.2 and 5.3 ) thus have little change. From Figures 4.19 and 4.21, when temperatures vary from 150°C to 190°C, the  $W_a^h$  in equation

( 5.4 ) also has little change. Therefore, the  $W_a$  is almost independent of temperature in the range of temperatures studied.

On the other hand, in the Arrhenius equation in section 6.5.3, the activation energy (E) is dependent on the volume fraction and frequency. The particle size effect is not studied in section 6.5.3, but it is believed that the E is also dependent on the particle size, since the activation energy is an indicator of the temperature sensitivity, which is also dependent on contact surface area.

$$E = f(\text{ frequency, size, and volume fraction of silica } )$$

( 6.14 )

An increase in temperature in the silica filled polymer melt can decrease (a) the viscosity of polymer itself, and (b) the interfacial bonding at the interface. Furthermore, the effect of interfacial bonding on activation energy has been studied, and shows that activation energy is independent of work of adhesion. This finding is based on the results shown in Figures 5.64 to 5.66. The slopes of  $\ln^*$  of 20% volume fraction of Stöber silica versus  $1000/T$  is independent of surface properties of silica. Again, the validity of this argument on the other volume fraction of silica needs to be proved.

Thus, the second exponential term on the right hand side of equation ( 6.8 ) is independent of work of adhesion.

$$E \neq f( W_a ) \quad ( 6.15 )$$

Therefore, both K and E are individually dependent on:

- (a) volume fraction of silica,
- (b) particle size of silica,
- (c) frequency.

In summary, the extended Arrhenius equation is:

$$\eta_c^* = \beta \cdot \exp\left(\frac{-K}{W_a}\right) \cdot \exp\left(\frac{E}{kT}\right) \quad ( 6.8 )$$

where

$$K = P + ( R + n \cdot \log w ) \cdot V_f \quad ( 5.22 )$$

$$E = f( w, V_f, \text{ and size } ) \quad ( 6.14 )$$

When the relationship of K and E to the frequency, particle size and volume fraction is known,  $\beta$  can be determined by  $\eta_c^*(w_1, T_1)$ . Thus the  $\eta_c^*(w_2, T_2)$  can be evaluated by equation ( 6.8 ).

In other words, for the Stöber silica filled polymer melts, one could say:

- (a) when studied at a constant temperature, the term B is not changed, and the melt viscosity is dependent on the friction factor.
- (b) When studied at a given frequency, melt viscosity is dependent on the volume fraction of silica, temperature, and work of adhesion.

## CHAPTER 7 CONCLUSIONS

1. The interfacial bonding between a silica filler and ethylene-vinyl acetate copolymer can be quantified in terms of work of adhesion ( $W_a$ ). The techniques used to evaluate  $W_a$  combine fourier transform infrared (FTIR) spectroscopy, contact angle measurements, and titration with indicator dyes. The  $W_a^h$  and  $W_a^d$  are obtained from equations 5.1 to 5.5 explained in text of this work.
2. The magnitude of  $W_a$  can be controlled by modifying the surface properties of silica particles. The values of  $W_a$  range from  $63 \text{ erg cm}^{-2}$  to  $301 \text{ erg cm}^{-2}$ .
3. Values of  $W_a^h$  vary greatly from  $260 \text{ erg cm}^{-2}$  to  $13 \text{ erg cm}^{-2}$  when the silica surface is heated and/or chemically treated, however, values of  $W_a^d$  only show a small change from  $41 \text{ erg cm}^{-2}$  to  $53 \text{ erg cm}^{-2}$ .
4. The  $W_a^h$  is the main component to determine the mechanical and rheological properties of the polymer composites in this study.
5. Quantitative study of the effect of work of adhesion on the mechanical and rheological properties of polymer composites is obtained when the interfacial bonding is quantified.

6. There is an exponential relationship between the Young's modulus, tensile strength, shear modulus and melt viscosity of the composites and  $W_a^{-1}$ . At a constant volume fraction of silica filler, the Young's modulus, tensile strength, shear modulus and melt viscosity of composites are directly proportional to  $W_a$ .
7. The effect of  $W_a$  on the mechanical and rheological properties of polymer composites is dependent on the materials characteristics (particle sizes and volume fractions of filler) and test conditions (testing rates and temperatures).
8. An increase in Young's modulus with increasing  $W_a$  occurs faster for the Cab-O-Sil silica filled composites than for the Stöber silica filled composites, since the Cab-O-Sil filled composites have a higher gradient of polymer fraction included within the interphase than the Stöber filled composites.
9. The Cab-O-Sil silica filled E-Va copolymer has higher tensile strength than the Stöber silica filled E-Va copolymer. The tensile strength of the unfilled E-Va copolymer is located in between both silica filled copolymers. This is because Cab-O-Sil silica has a much higher surface area per unit volume than Stöber silica.

10. The extent of the increase in the tensile strength with increasing  $W_a$  is dependent on the filler particles size and volume fraction of silica for both Cab-O-Sil and Stöber silica filled composites in this study.
11. Interfacial bonding strength is decreased with increasing temperature. This is because an increase in temperature reduces both the extent and the interaction energy of the hydrogen bonds at the interface.
12. Work of adhesion has a greater effect on the shear modulus and melt viscosity of a silica filled polymer tested at a low frequency than at a high frequency. However, work of adhesion has little effect on the change of the melt viscosity of a filled polymer with temperature at a given frequency.
13. The extent of the increase in the melt viscosity with increasing  $W_a$  is greater when the volume fraction of silica in the polymer matrix is higher.
14. The thickness of an interphase layer around a silica filler surface is increased with an increase in the interfacial bonding strength. The effective particle size of silica filler is thus increased with increasing work of adhesion.
15. The effective silica particle size becomes smaller when the testing frequency is increased. The effect of  $W_a$  on the melt viscosity of composite is then not obvious when the effective particle size become smaller.

16. Friction factors are proposed to explain the effect of interphase on the melt viscosity of filled polymers during the flow process.
17. Skin friction, dependent on the magnitude of  $W_a$ , is strongly related to the adhesion quality and thus determines, especially at low frequency, the melt viscosity of a filled polymer from a flow process viewpoint.
18. The higher the  $W_a$  at the interface, the stronger the skin friction at the interphase will be. Higher skin friction results from the higher resistance of the polymer flowing through the silica filler particle, and thus gives a higher melt viscosity of composites.

## CHAPTER 8 FUTURE RESEARCH

Some of interesting subjects related to this study can be described as follows.

### 8.1 Silane Coupling Agent at the Interface

Coupling agent is defined as a chemical which has two polymerizable functional groups and can be used to improve the practical adhesive bond at the interface between filler surface and polymer matrix (11). Coupling agent can involve an increase in true adhesion to improve the mechanical and physical properties of polymer composites. At the same time, it can also involve improved wetting, dispersion, rheology, and other properties (1-11).

In addition, coupling agent can polymerize on the surface of filler particles and modify the interphase region to strengthen the organic and inorganic boundary layers. The coupling agent layers are not a simple thin film, but consist of chemisorbed and physisorbed layers with a structural and compositional gradients (13).

Since a coupling agent is an exterior material introduced at the interface, the structure of a coupling agent at the interface depends on the application method, solvent, PH, organofunctionality, concentration, dry

conditions, and temperature of coupling agent treating solution, etc (13,33-39,45-49). The detailed characterization of the molecular structures involved and their corresponding interactions will help to understand the performance of coupling-agent-modified polymer composites (11,13,33-39,45-49,148,152).

However, the quantitative study of the effect of interfacial bonding on the mechanical and physical properties of composites is extremely complex when a coupling agent exists at the interface. Furthermore, it is known that the method of silane treatment and the amount of silane molecules on the reinforcing surface are the important factors for achieving the optimum performance of polymer composite. The quantitative approach, which establishes a calibration curve of silane coupling agent on the filler surface, may be an appropriate method, and this study has just begun (13,38,249).

The calibration curve is characterized by the known extent of silane molecules on the filler surface through a dry mixing versus the peak intensity of a specific functional group of silane molecule. This can be determined from Fourier Transform Infrared (FTIR) spectroscopy by use of the Diffuse Reflectance Infrared Fourier Transform (DRIFT) technique (38,205,249).

The silane coupling agents can be then prepared from any reaction conditions with filler or reinforcing surface.

The thickness of silane molecule layers on the filler surface can be thus evaluated from the calibration curve by comparing the peak intensity of a specific functional group. The mechanical and physical properties of composites can then be quantitatively related to the extent of silane on the filler surface.

However, the orientation and structure of silane molecules on the filler surface depend on the treatment conditions. The orientation and structure of silane molecules on the filler surface may be different even though the extent of silane molecules is the same. Fortunately, this information can be used to study the effect of orientation and structure of silane molecules on the composite performance based on the same amount of silane at the interface.

From the above discussion, It is obviously challenging work to quantitatively relate the extent of silane and method of silane applied on the filler surface to the mechanical and physical properties of composite. This study is very important to the polymer composite industry in determining the optimum conditions for preparing the desired composite materials.

## 8.2 Temperature Effect on the Interfacial Bonding Strength

It is shown in sections 4.5 and 5.5 that temperature can change both the extent and interaction energy of the interfacial bonding at the interface. The interfacial

bonding strength, which is characterized in terms of work of adhesion ( $W_a$ ), therefore decreases when the environmental temperature is increased.

However, the type of relationship which exists between work of adhesion and temperature is not known yet. The quasi-equilibrium constant in section 4.5.3 gives some idea of the extent of hydrogen bonding at the interface varying with temperature. The wavenumber shift of carbonyl groups from the FTIR spectroscopy shows the change of interaction energy of hydrogen bonds with temperature. The challenge is how to correlate this information to the work of adhesion. In other words, the challenge is to establish a model to evaluate the work of adhesion which is temperature dependent.

When the value of work of adhesion at the testing temperature is available, it is interesting to quantitatively study the performance of polymer composites changing with the in-situ work of adhesion.

### 8.3 Crystallinity in the Polymer Composite

Polyethylene will crystallize and form crystallites during the annealing process. It is known that the degree of crystallinity is much reduced when ethylene is copolymerized with another monomer. The higher the comonomer, the lower the crystallinity of copolymer is. The E-Va copolymer (72% wt.-28% wt.) is nearly amorphous. However, when the copolymer is filled by very small size of

filler particles, the crystallinity of polymer can increase due to heterogeneous nucleation. The effect of crystallites can work as filler particles in the polymer matrix. One example of this is the molecule composites of polyethylene. The mechanical properties of silica filled polymers will then depend on the extent and size of the crystallites in the polymer matrix.

The possibility of the formation of crystallites in the unfilled and 5% volume silica filled polymer after the annealing process is studied by DSC. Figures 8.1 to 8.3 indicate the formation of this crystallites by heterogeneous nucleation. It is based on the results showing new peaks formed in the silica filled polymers. It is interesting to note the new peak positions and intensity in the Cab-O-Sil and Stöber silica filled polymers.

The Stöber silica filled polymer has a very small peak at 88°C. It means that the extent of heterogeneously introduced crystallites is few. The peak position is located at a higher temperature than an unfilled E-Va copolymer. It indicated that the lamellar size heterogeneously introduced is larger than the size of lamellar in the unfilled polymer. In contrast, the new peak in Cab-O-Sil silica filled polymer is at 75°C, which is lower than for an unfilled polymer. It shows that the lamellar size is smaller than that formed in an unfilled E-Va copolymer. However, the extent of new formed lamella is

PERKIN-ELMER  
7 Series Thermal Analysis System

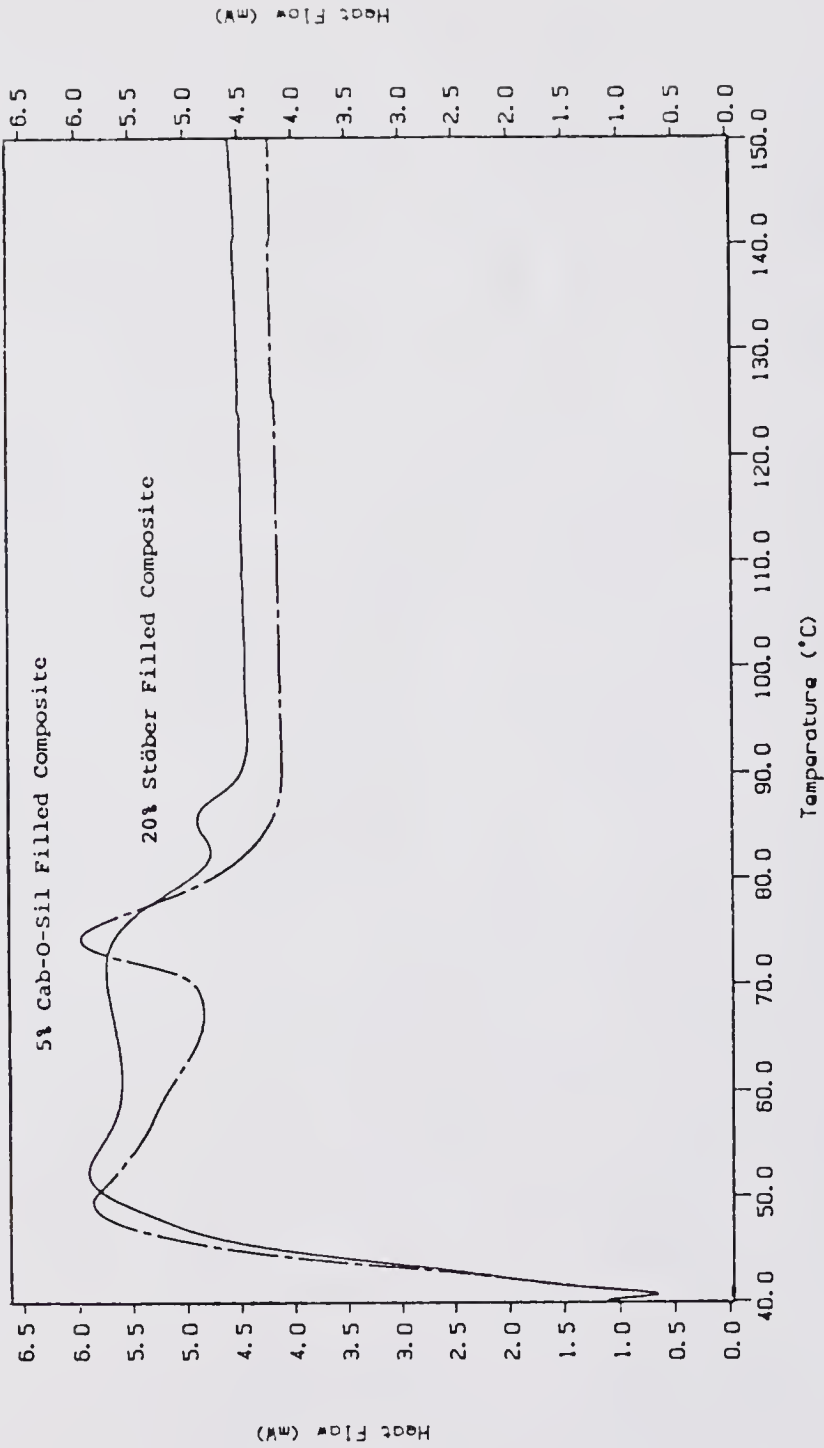


Figure 8.1 DSC Spectrum of 20% Volume Stöber Silica and 5% Volume Cab-O-Sil Filled E-Va Copolymer

PERKIN-ELMER  
7 Series Thermal Analysis System

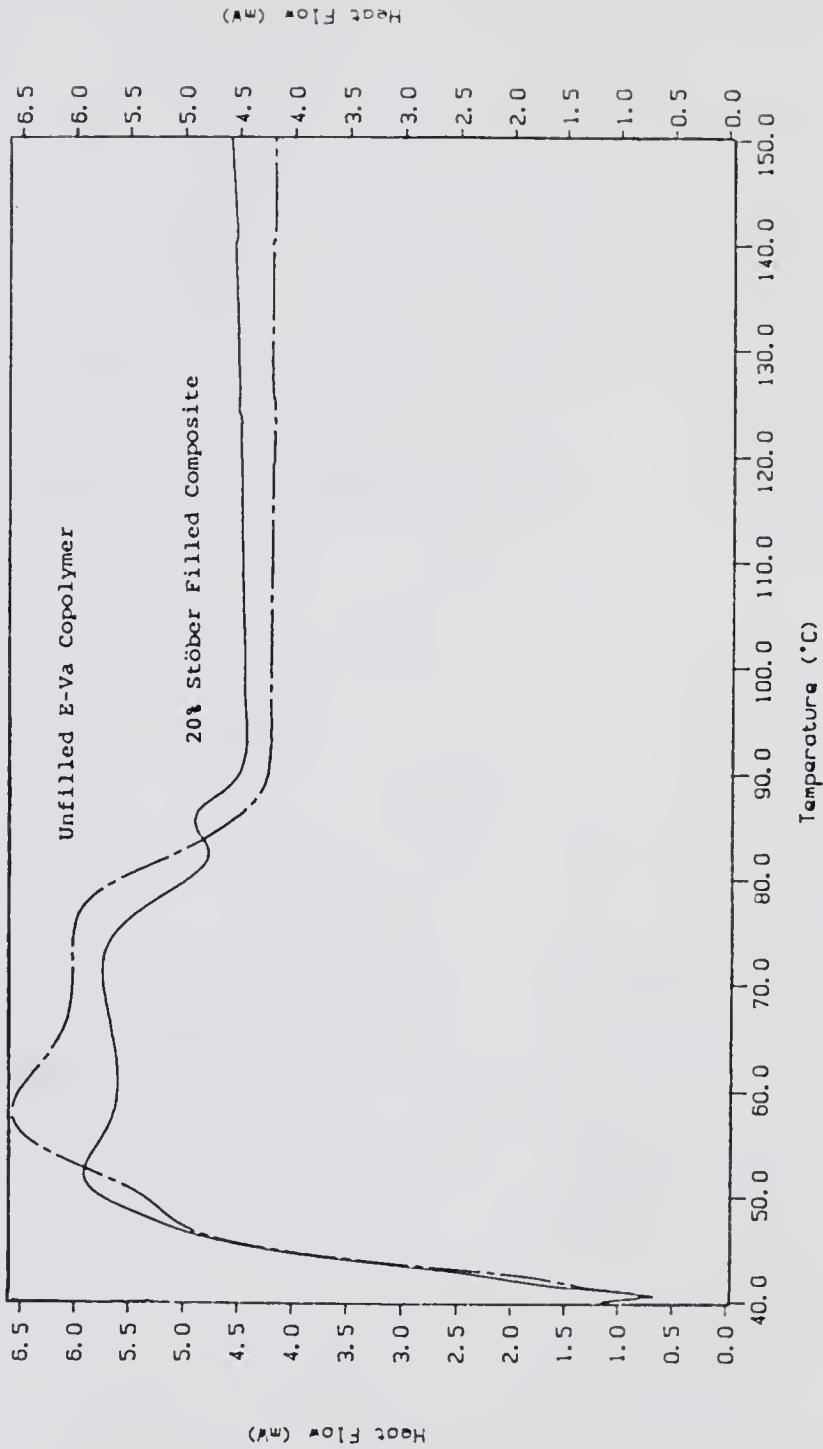


Figure 8.2 DSC Spectrum of Unfilled and 20% Volume Stöber Silica Filled E-Va Copolymer

PERKIN-ELMER  
7 Series Thermal Analysis System

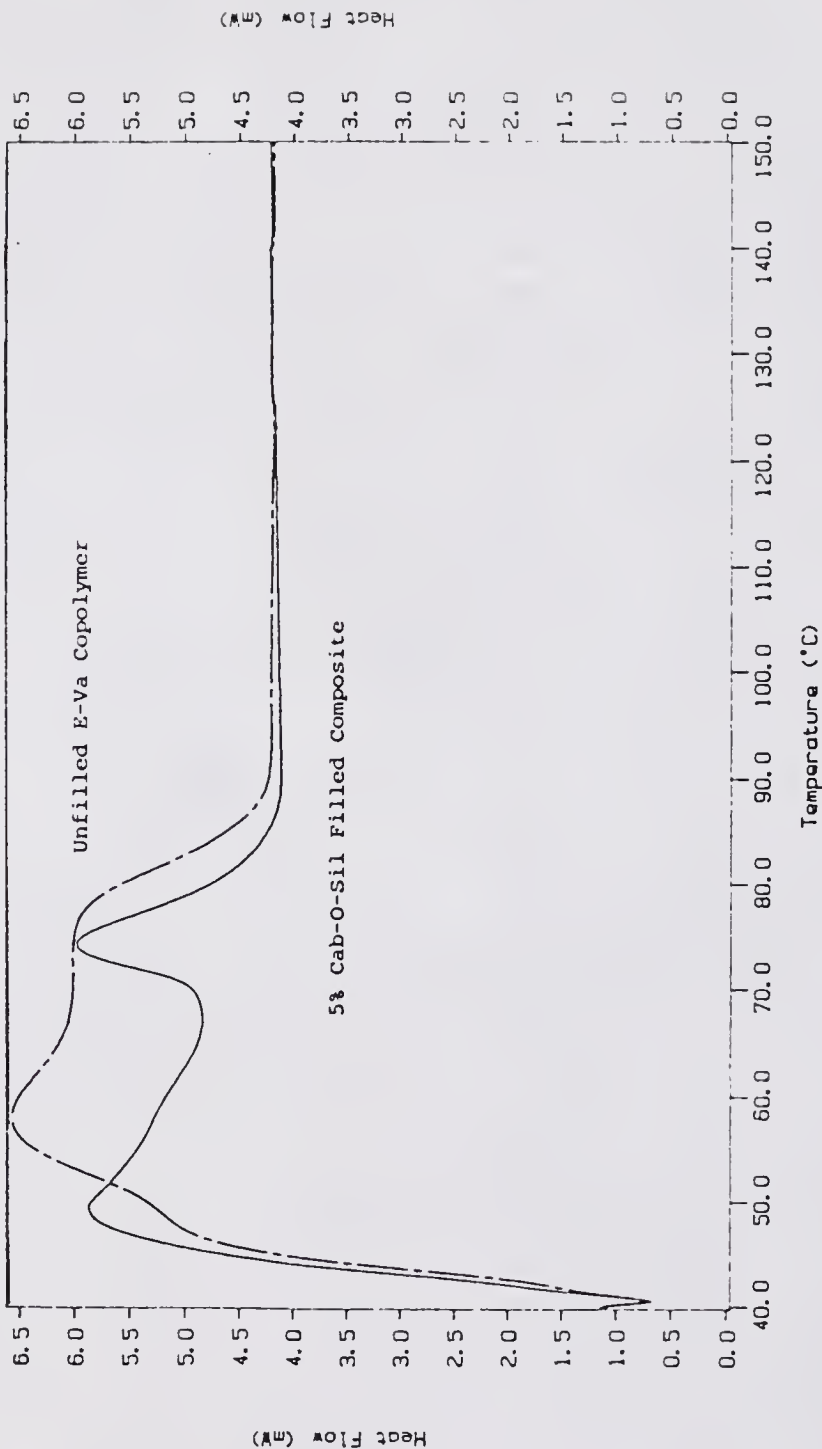


Figure 8.3 DSC Spectrum of Unfilled and 5% Volume Cab-O-Sil Silica Filled E-Va Copolymer

more in Cab-O-Sil silica than in Stöber silica filled polymers since the peak intensity is higher in Cab-O-Sil silica filled polymer.

It is worthwhile to further studied the crystallites which grow on different surfaces of silica, and its effect on the mechanical properties of composites, especially the Cab-O-Sil silica filled polymers.

## REFERENCES

1. Dekkers, M. E. J. and Heikens, D., "The Effect of Interfacial Bonding Adhesion on the Tensile Behavior of Polystyrene-Glass-Bead Composites," J. Appl. Polym. Sci., 28, 3809 (1983)
2. Graf, R. T., Koenig, J. L., and Ishida, H., "The Influence of Interfacial Structure on the Flexural Strength of E-Glass Reinforced Polyester," J. Adhesion, 16, 97 (1983)
3. Boluk, M. Y. and Schreiber, H. P., "Interfacial Interactions and Properties of Filled Polymers: I. Dynamic-Mechanical Responses," Polym. Compos., 7, (5), 295 (1986)
4. Trotignon, J. P., Sanachagrin, B., Piperaud M., and Verdu, J., "Mechanical Properties of Mica-Reinforced Polypropylene Composites," Polym. Compos., 3, (4), 230 (1982)
5. Mandell, J. F., McGarry, F. J., Huang D. D., and Li, C. G., "Some Effects of Matrix and Interface Properties on the Fatigue of Short Fiber-Reinforced Thermoplastics," Polym. Compos., 4, (1), 32 (1983)
6. Chang, H. L., Han, C. D., and Mijovic, J., "Effect of Coupling Agents on the Rheological Behavior and Physical/Mechanical Properties of Filled Nylon 6," J. Appl. Polym. Sci., 28, 3387 (1983)
7. Boaira, M. S. and Chaffey, C. E., "Effect of Coupling Agents on the Mechanical and Rheological Properties of Mica-Reinforced Polypropylene," Polym. Eng. Sci., 17, (10), 715 (1977)
8. Suetsugu, Y. and White, J. L., "The Influence of Particle Size and Surface Coating of Calcium Carbonate on the Rheological Properties of Its Suspensions in Molten Polystyrene," J. Appl. Polym. Sci., 28, 1481 (1983)

9. Smith, J. C., Kermish, G. A., and Fenstermaker, C. A., "Separation of Filler Particles from the Matrix in a Particle-Loaded Composite Subjected to Tensile Stress," J. Adhesion, 4, 109 (1972)
10. Wambach, A., Trachte, K., and DiBenedetto, A. T., "Fracture Properties of Glass Filled Polyphenylene Oxide Composites," J. Compos. Mater., 2, (3), 266 (1968)
11. Plueddemann, E. P., Chapter 5: Nature of Adhesion through Silane Coupling Agents, p. 111-139, Silane Coupling Agents, Plenum Press, New York (1982)
12. Katz, H. S. and Milewski, J. V., Section II: Coupling Agents, p. 65-115, Handbook of Fillers for Plastics, Van Nostrand Reinhold Company, New York (1987)
13. Ishida, H., "Structure Gradient in the Silane Coupling Agent Layers and its Influence on the Mechanical and Physical Properties of Composites," in Molecular Characterization of Composite Interfaces, p. 25-50, eds., Ishida, H. and Kumar, G., Plenum Press, New York (1985)
14. Sohn, J. E., "Improved Matrix-Filler Adhesion," J. Adhesion, 19, 15 (1985)
15. Chahal, R. S. and St. Pierre, L. E., "Interfacial Phenomena in Macromolecular Systems. I. Heats of Adsorption of Polysiloxanes on Modified Silica Surfaces," Macromolecules, 1, (2), 152 (1968)
16. Chahal, R. S. and St. Pierre, L. E., "Interfacial Phenomena in Macromolecular Systems. II. Relaxation Modulus of Uncross-Linking Silica-Polydimethylsiloxane Composites," Macromolecules, 2, (2), 193 (1969)
17. Hull, D., Chapter 3, p. 36-58, An Introduction to Composite Materials, Cambridge Solid State Science Series, Cambridge University Press, Cambridge (1981)
18. Fowkes, F. M. and Mostafa, M. A., "Acid-Base Interaction in Polymer Adsorption," Ind. Eng. Chem. Prod. Res. Dev., 17, (1), 3 (1978)
19. Fowkes, F. M., "Acid-Base Interaction in Polymer Adhesion," Physicochemical Aspects of Polymer Surface, Vol. 2, p. 583-603, ed., Mittal, K. L., Plenum, New York, (1983)

20. Fowkes, F. M., "Acid-Base Interactions in Polymer Adhesion," Microscopic Aspects of Adhesion and Lubrication, Vol. 7, p. 119-137, ed., Georges, J. M., Elsevier, Amsterdam (1982)
21. Fowkes, F. M., "Donor-Acceptor Interactions at Interfaces," Recent Advances in Adhesion, Proc. Am. Chem. Soc. Symp., p. 39-44, ed. by Lee, L. H., Gordon and Breach, London (1973)
22. Fowkes, F. M., "Determination of Interfacial Tensions, Contact Angles, and Dispersion Forces in Surfaces by Assuming Additivity of Intermolecular Interactions in Surfaces," J. Phys. Chem., 66, 382, (1962)
23. Fowkes, F. M., "Donor-Acceptor Interactions at Interfaces," J. Adhesion, 4, 155 (1972)
24. Fowkes, F. M., McCarthy, D. C., and Tischler, D. O., "Predicting Enthalpies of Interfacial Bonding of Polymers to Reinforcing Pigments," in Molecular Characterization of Composite Interface, p. 401-411, eds., Ishida, H. and Kumar, G., Plenum Press, New York (1985)
25. Manson, J. A., "Interfacial Effects in Composites," Pure & Appl. Chem., 57, (11), 1667 (1985)
26. Drago, R. S., Vogel, G. C., and Needham, T. E., "A Four-Parameter Equation for Predicting Enthalpies of Adduct Formation," J. Am. Chem. Soc., 93, 6014 (1971)
27. Drago, R. S., Parr, L. B., and Chamberlain, C. S., "Solvent Effects and Their Relationship to the E and C Equations," J. Am. Chem. Soc., 99, 3203 (1977)
28. Fowkes, F. M., Chapter 9, "Interface, Acid-Base/Charge-Transfer Properties, in Surface and Interfacial Aspects of Biomedical Polymer, Vol. 1, p. 337-372, ed., Andrade, J. D., Plenum Press, New York (1985)
29. Marmo, M. J., Mostafa, M. A., Jinnal, H. and Fowkes, F. M., "Acid-Base Interaction in Filler-Matrix Systems," Ind. Eng. Chem. Prod. Res. Dev., 15, (3), 206 (1976)
30. Williams, J. W. and Shang, S. W., "Effect of Work of Adhesion on the Mechanical Properties of Silica Filled Ethylene-Vinyl Acetate Copolymer," Polym. Preprint, Div. Polym. Chem., A.C.S., 28 (2), 44 (1987)

31. Williams, J. W., Shang, S. W., and Sacks, M. D., "Quantitative Studies of the Effect of Adhesion on the Mechanical and Physical Properties of Polymer Composites," Mat. Res. Soc. Symp. Proc., Vol. 119: Adhesion in Solids, p. 17-23, eds., Mattox, D. M., Baglin, J. E. E., Gottschall, R. J., and Batich, C. D., Materials Research Society, Pittsburgh, PA (1988)
32. Foust, A. S., Wenzel, L. A., Clump, C. W., Maus, L., and Andersen, L. B., Chapter 13: Fundamentals of Turbulent Transfer, p. 154-165, Principles of Operations, Wiley, New York (1980)
33. Bird, R. B., Stewart, W. E., and Lightfoot, E. N., Chapter 6: Interphase Transport in Isothermal Systems, p. 180-207, Transport Phenomena, Wiley, N.Y. (1960)
34. Nielsen, L. E., "Mechanical Properties of Particulate Filled Systems," J. Compos. Mater., 1, 100 (1967)
35. Culler, S. R., Ishida, H., and Koenig, J. L., "The Silane Interphase of Composites: Effects of Process Conditions on  $\gamma$ -Aminopropyltriethoxysilane," Polym. Compos., 7, (4), 231 (1986)
36. Ishida, H., "A Review of Recent Progress in the Studies of Molecular and Microstructure of Coupling Agents and Adhesive Joints," Polym. Compos., 5, (2), 101 (1984)
37. Ishida, H., and Koenig, J. L., "The Reinforcement Mechanism of Fiber-Glass Reinforced Plastics under Wet Conditions: Review," Polym. Eng. & Sci., 18, (2), 128 (1978)
38. Boerio, F. J., Armogan, L., and Cheng, S. Y., "The Structure of  $\gamma$ -Aminopropyltriethoxysilane Films on Iron Mirrors," J. Colloid Interface Sci., 73, (2), 416 (1980)
39. Ishida, H. and Miller, J. D., "Cyclization of Methacrylate-Functional Silane on Particulate Clay," J. Polym. Sci. Polym. Phys. Ed., 23, 2227-2242 (1985)
40. Ishida, H. and Koenig, J. L., "Fourier Transform Infrared Spectroscopic Study of the Structure of Silane Coupling Agent on E-Glass Fiber," J. Colloid Interface Sci., 64, (3), 565-576 (1978)

41. Miller, J. D., Ishida, H., and Maurer, F. H. J., "The Effect of Additives on the Structure and Mechanical Properties of Polypropylene-Filled Systems," in Polymer Composites, p. 449-456, ed., Sedláček, B., Walter de Gruyter, New York (1986)
42. Good, R. J., "Intermolecular and Interatomic Forces," in Treatise on Adhesion and Adhesives, Vol. 1, p. 9-68, ed., Patrick, R. L., Marcel Dekker, New York (1967)
43. Wake, W. C., "Theories of Adhesion and Uses of Adhesives: A Review," Polymer, 19, 291 (1978)
44. Solomon, G., Chapter 1: Adhesion, p. 3-8, Adhesion and Adhesives, Vol. 1, eds., Houwink, R. and Salomon, G., Elsevier, Amsterdam (1965)
45. Erickson, P. W. and Plueddemann, E. P., Chapter 1: Historical Background of the Interface, p. 1-30, Interface in Polymer Matrix Composites, ed., Plueddemann, E. P., Academic Press, New York (1974)
46. Sung, N. H., Kaul, A., Chin, I., and Sung, C. S. P., "Mechanistic Studies of Adhesion Promotion by  $\gamma$ -Aminopropyl Triethoxy Silane in  $\alpha$ -Al<sub>2</sub>O<sub>3</sub>/Polyethylene Joint," Polym. Eng. Sci., 22, 637 (1982)
47. Kaas, R. L. and Kardos, J. L., "The Interaction of Alkoxy Silane Coupling Agents with Silica Surfaces," Polym. Eng. Sci., 11, (1), 11 (1971)
48. Chen, T. M. and Brauer, G. M., "Solvent Effects on Bonding Organo-Silane to Silica Surfaces," J. Dent. Res., 61, (12), 1439 (1982)
49. Chiang, C. H. and Koenig, J. L., "Fourier Transform Infrared Spectroscopic Study of the Adsorption of Multiple Amino Silane Coupling Agents on Glass Surfaces," J. Colloid Interface Sci., 83, (2), 361 (1981)
50. Hirschfelder, J. O., Curtiss, C. F., and Bird, R. B., Chapter 1: Interaction and Background Information, p. 22-35, Molecular Theory of Gases and Liquids, Wiley, New York (1954)
51. McMillin, D. R., Drago, R. S., "E and C Parameters for Ionic Interactions," Inorg. Chem., 11, (4), 872 (1972)
52. Kemball, C., Adhesion, p. 19, ed., Eley, D. D., Oxford University Press, London (1961)

53. Huntsberger, J. R., "The Mechanisms of Adhesion," Treatise on Adhesion and Adhesives, Vol. 1, p. 119-149, ed., Patrick, R. L., Marcel Dekker, New York (1967)
54. Margenau, H., Kestner, N., Chapter 1: History of Intermolecular Forces, p. 1-14, Theory of Intermolecular Forces, 3rd. ed., Pergamon Press, London (1971)
55. Krupp, H., "Particle Adhesion Theory and Experiment," Adv. Colloid Interface Sci., 1, 111 (1967)
56. Wu, S., Chapter 2: Molecular Interpretations, p. 35-40, Polymer Interface and Adhesion, Marcel Dekker, New York (1982)
57. Pauling, L., The Nature of Chemical Bonds, Connel University Press, New York (1960)
58. Huntsberger, J. R., "The Nature of Adhesion," Adhesives Age, 13 (11), 43 (1970)
59. Orowan, E., "The Physical Basis of Adhesion," J. Franklin Inst. 290, 493 (1970)
60. Tabor, D., "Basic Principles of Adhesion," Reports on Prog. Appl. Chem., 36, 621, (1951)
61. Bailey, R., and Castle, J. E., "XPS Study of the Adsorption of Ethoxysilanes on Iron," J. Mater. Sci., 12, 2049 (1977)
62. Gettings, M., and Kinloch, A. J., "Surface Analysis of Polysiloxane/Metal Oxide Interfaces," Surface Interference Analysis, 1, 1899 (1980)
63. Koenig, J. L., Shih, P. T. K., "Raman Studies of the Glass Fiber-Silane-Resin Interface," J. Colloid Interface Sci., 36, 247 (1971)
64. Dupré, A., Chapter 6: Théorie des Gaz, p.60-87, Théorie Mécanique de La Chaleur, Gsuthier-Villars, Paris (1869)
65. Harkins, W. D., Chapter 2: Films on Liquids, p. 94-198, The Physical Chemistry of Surface Film, Reinhold, New York (1952)
66. Osipow, I. L., Chapter 10: Wetting, p. 232-294, Surface Chemistry: Theory and Industry Applications, Krieger, New York (1977)

67. Cherry, B. W., Chapter 2: The Solid-Liquid Interface, p. 18-33, Polymer Surface, Cambridge University Press, London (1981)
68. London, F., "Zur Theorie und Systematik der Molekularkräfte," Z. Phys., 63, 245 (1930)
69. London, F., "The General Theory of Molecular Forces," Trans. Faraday Soc., 33, 8 (1937)
70. Salem, L., "Attractive Forces between Long Saturated Chains at Short Distances," J. Chem. Phys., 37, 2100 (1962)
71. Debye, P. J. W., Chapter 1: Fundamental Electrostatic Field Relations, p. 1-15, Polar Molecules, Chemical Catalog, New York (1929)
72. Keesom, W. H., "Die Berechnung der Molekularen Quadrupolmomente," Phys. Z., 23, 225 (1923)
73. Debye, P. J. W., "Die van der Waalsschen Kohäsionskräfte," Phys. Z., 21, 178 (1920)
74. Debye, P. J. W., "Molekularkräfte Undihre Elektrische Deutung," Phys. Z., 22, 302 (1923)
75. Latimer, W. M. and Rhoadbush, W. H., "Polarity and Ionization from the Standpoint of Lewis Theory of Valence," J. Am. Chem. Soc., 42, 1419 (1920)
76. Wu, S., "Calculation of Interfacial Tension in Polymer Systems," J. Polym. Sci., C34, 19 (1971)
77. Wu, S., "Polar and Nonpolar Interactions in Adhesion," J. Adhesion, 5, 39 (1973)
78. Girifalco, L. A. and Good, R. J., "A Theory for the Estimation of Surface and Interfacial Energies. I. Derivation and Application to Interfacial Tension," J. Phys. Chem., 61, 904, (1957)
79. Wu, S., Chapter 3: Interfacial and Surface Tensions of Polymer Melts and Liquids, p. 98-104, Polymer Interface and Adhesion, Marcel Dekker, New York (1982)
80. Owens, D. K. and Wendt, R. C., "Estimation of the Surface Free Energy of Polymer," J. Appl. Polym. Sci., 13, 1741 (1969)

81. Batich, C. D. and Wendt, R. C., "Chemical Labels to Distinguish Surface Functional Groups Using X-Ray Photoelectron Spectroscopy (ESCA)," in Photon, Electron, and Ion Probes of Polymer Structure and Properties, p. 221-235, eds., Dwight, D. W., Fabish, T. J., and Thomas, H. R., ACS Symposium Series, ACS, Washington, D. C. (1981)
82. Hildebrand, J. H., "Solubility. 12. Regular Solution," J. Am. Chem. Soc., 51, 66 (1929)
83. Hildebrand, J. H. and Scott, R. L., Chapter 21: Surface Phenomena, p. 401-405, The Solubility of Nonelectrolytes, Reinhold, New York (1950)
84. Wu, S., "Estimation of the Critical Surface Tension for Polymers from Molecular Constitution by a Modified Hildebrand-Scott Equation," J. Phys. Chem., 72, 3332 (1968)
85. Small, P. A., "Some Factors Affecting the Solubility of Polymers," J. Appl. Chem., 3, 71 (1953)
86. Hamilton, W. C., "A Technique for the Characterization of Hydrophilic Solid Surfaces," J. Colloid Interface Sci., 40, 219 (1972)
87. Hamilton, W. C., "Measurement of the Polar Force Contribution to Adhesive Bonding," J. Colloid Interface Sci., 47, 672 (1974)
88. Fowkes, F. M., "Additivity of Intermolecular Forces at Interfaces. I. Determination of the Contribution to Surface and Interfacial Tensions of Dispersion Forces in Various Liquids," J. Phys. Chem., 67, 2538 (1963)
89. Tamai, Y., Makuuchi, K., and Suzuki, M., "Experimental Analysis of Interfacial Forces at the Plane Surface of Solids," J. Phys. Chem., 71, 4176 (1967)
90. El-Shimi, E. and Goddard, E. D., "Wettability of Some Low Energy Surfaces. II. Oils on Solids Submerged in Water," J. Colloid Interface Sci., 48, 249 (1974)
91. Ottewill, R. H., and Vincent, B., "Colloid and Surface Chemistry of Polymer Lattices," J. C. S. Faraday I, 68, 1533 (1972)
92. Corkhill, P. H., Chapter 5: Surface Properties of Hydrogel Copolymers, p. 121-164, Novel Hydrogel Polymers, Ph. D. Dissertation, The University of Aston in Birmingham, England (1988)

93. Adamson, A. W., Chapter 10: The Solid-Liquid Interface—Contact Angle, p. 341-344, Physical Chemistry of Surfaces, 4th ed., Wiley, New York (1982)
94. Bikerman, J. J., Chapter 5: Solid Surfaces, p. 187-207, Physical Surface, Academic Press, London (1970)
95. Fowkes, F. M., Tischler, D. O., Wolfe, J. A., and Halliwell, M. J., "Acid-Base Complex of Polymers with Solvents," Org. Coating Appl. Polym. Sci. Proc., 46, 1 (1982)
96. Schreiber, H. P., Wetheimer, M. R., and Lambla, M., "Surface Interactions and Some Properties of Filled Polymers," J. Appl. Polym. Sci., 27, 2269 (1982)
97. Schreiber, H. P. and Li, Y., "Aid-Base Interactions, Surface Modifications by Plasma Treatment and the Properties of COposites," Polym. Prep., 24, (1), 219 (1983)
98. Nielsen, L. E., "Generalized Equation for the Elastic Moduli of Composite Materials," J. Appl. Phys., 41, 4626 (1970)
99. Lewis, T. B. and Nielsen, L. E., "Dynamic Mechanical Properties of Particulate-Filled Composites," J. Appl. Polym. Sci., 14, 1449 (1970)
100. Nielsen, L. E., Chapter 2: Elastic Moduli, p. 39-66, Mechanical Properties of Polymer and Composites, Vol. 1, Marcel Dekker, New York, (1974)
101. Nielsen, L. E., Chapter 7: Particulate-Filled Polymers, p. 379-452, Mechanical Properties of Polymer and Composites, Vol. 2, Marcel Dekker, New York (1974)
102. Manson, J. A. and Sperling, L. H., Chapter 12: Particle-and Fiber-Reinforced Plastics, p. 373-457, Polymer Blend and Composites, 3rd Printing., Plenum Press, New York (1981)
103. Ahmred, M., Chapter 6: Dispersion of Pigments in Plastics, p. 89-108, Coloring of Plastics, Reinhold Company, New York (1979)
104. Kraus, G., "Interactions of Elastomers and Reinforcing Fillers," Rubber Chem. Technol., 38, 1070 (1964)
105. Peiffer, D. G. and Nielsen, L. E., "Preparation and Mechanical Properties of Thick Interlayer Composites," J. Appl. Polym. Sci., 23, 2253 (1979)

106. Peiffer, D. G., "Impact Strength of Thick-Interlayer Composites," J. Appl. Polym. Sci., 24, 1451 (1979)
107. Broutman, L. J., and Agarwal, B. D., "A Theoretical Study of the Effect of an Interfacial Layer on the Properties of Composites," Polym. Eng. Sci., 14, 581 (1974)
108. Newman, S., Chapter 13: Rubber Modification of Plastics, p. 84-88, Polymer Blends, eds., Paul, D. R. and Newman, S., Vol. 2, Academic Press, New York (1978)
109. Kumamaru, F., Oono, J., Kajiyama, T., and Takayanagi, M., "Interfacial Interaction between Poly(p-phenylene terephthalamide) Filament and Nylon 6 Matrix Crystallized from Melts," Polym. Compos., 4, (2), 141 (1983)
110. Kardos, J. L., Cheng, F. S., and Tolbert, T. L., "Tailoring the Interface in Graphite-Reinforced Polycarbonate," Polym. Eng. Sci., 13, 455 (1973)
111. Kinloch, A. J. and Young, R. J., Chapter 11: Toughened Multiphase Plastics, p. 448-452, Fracture Behavior of Polymer, Applied Science, New York (1983)
112. Bucknall, C. B., Chapter 6: Deformation Mechanisms in Glassy Polymers, p. 137-181, Toughened Plastics, Applied Science, London (1977)
113. Folkes, M. J., Chapter 7: Design Aspects, p. 160-167, Short Fiber Reinforced Thermoplastics, Research Studies Press, Wiley, New York (1982)
114. Agarwal, B. D. and Broutman, L. J., Chapter 2: Behavior of Unidirectional Composites, P. 15-70, Analysis and Performance of Fiber Composites, Wiley, New York (1980)
115. Carling, M. J., Manson, J. A., and Hertzberg, R. W., Proc. 43rd SPE Ann. Tech. Conf., p. 396-398, Washington D. C. (1985)
116. Lipatov, Y. S., and Sergeeva, L. M., Chapter 7: Adsorptional Interaction on the Interface and the Properties of the Boundary Layer, p. 140-165, Adsorption of Polymer, Translation from Russian of Adsorbtsiya Polimerov, Wiley, New York (1974)

117. Lipatov, Y. S., Chapter 4: Mechanical Properties of Filled Polymers, p. 132-135, Physical Chemistry of Filled Polymers, International Polymer Science and Technology Monograph No. 2, Translated from Russian by Moseley, R. J., The British Library (1977), Originally Published 'Khimiya, Moscow (1977)
118. Peyser, P. and Bascom, W. D., "The Effect of Filler and Cooling Rate on the Glass Transition of Polymers," Polym. Prepr., 17, (2), 157 (1976)
119. Manson, J. A., Marmo, M., and Williams, J. W., "Acid Base Interaction and Mechanical Behavior in Filled Polymer," Orig. Coat. Plast. Chem. Preprints, 38, (1), 190 (1978)
120. Eastmond, G. C. and Mucciariello, G, "Polymer-Filler Interactions in Composites with Grafted Filler Particles," Polymer, 23, 164 (1983)
121. Vollenberg, P. H. T. and Heikens, D., "The Effect of Particle Size on the Mechanical Properties of Composites," Composite Interface, p. 171-175, eds., Ishida, H., and Koenig, J. L., Elsevier Sci., New York (1986)
122. Sumita, M., Ookuma, T., Miyasaka, K., and Ishikawa, K., "Effect of Ultrafine Particles on the Elastic Properties of Oriented Low-Density Polyethylene Composites," J. Appl. Polym. Sci., 27, 3059 (1982)
123. Guth, E., "Theory of Filler Reinforcement," J. Appl. Phys., 16, 20 (1945)
124. Smallwood, H. M., "Limiting Law of the Reinforcement of Rubber," J. Appl. Phys., 15, 758 (1944)
125. Einstein, A. "Eine neue Bestimmung der Molekul-dimensionen," Ann. d. Physik, 19, 289 (1906)
126. Einstein, A., "Berichtigung zu Meiner Arbeit: Eine neue Bestimmung der Molekul-dimensionen" Ann. d. Physik, 34, 591 (1911)
127. Voet, A., "Reinforcement of Elastomers by Fillers: Review of Period 1967-1976," J. Polym. Sci., 15, 327 (1980)
128. Landon, G., Lewis, G., and Boden, G. F., "The Influence of Particle Size on the Tensile Strength of Particle-Filled Polymer," J. Mater. Sci., 12, 1605 (1977)

129. Alter, H., "Filler Particle Size and Mechanical Properties of Polymers," J. Appl. Polym. Sci., 9, 1525 (1965)
130. Leidner, J. and Woodhams, R. T., "The Strength of Polymeric Composites Containing Spherical Fillers," J. Appl. Polym. Sci., 13, 1639 (1974)
131. Kerner, E. H., "The Elastic and Elastic Properties of Composite Media," Proc. Phys. Soc., London, B69, 808 (1956)
132. Halpin, J. C., "Stiffness and Expansion Estimates for Oriented Short Fiber Composites," J. Compos. Mater., 3, 732 (1969)
133. Tsai, S. W., Halpin, J. C., and Pagano, N. J., "Invariant Properties of Composite Materials," Composite Materials Workshop, p. 233-253, Stamford, Conn., Technomic Publishing Co. (1969)
134. Ashton, J. E., Halpin, J. C., and Petit, P. H., Chapter 5: Structure Property Relationship for Composite Materials, p. 72-94, Primer on Composite Materials: Analysis, Stamford, Conn., Technomic Publishing Co. (1969)
135. Eiler, H., "Die Viskosität von Emulsionen Hochviskoser Stoffe als Funktion der Konzentration," Kolloid-Z., 313 (1941)
136. Landel, R. F., "The Dynamic Mechanical Properties of a Model Filled System: Polyisobutylene-Glass Bead," Trans. Soc. Rheol., 2, 53 (1958)
137. Mooney, M., "The Viscosity of a Concentrated Suspension of Spherical Particles," J. Colloid Sci., 6, 162 (1951)
138. Wagner, M. P., "Silica-Filled Ethylene-Vinyl Acetate Resins," in Additives for Plastics, Vol. 2, p. 25-38, ed., Seymour, R. B., Academic Press, New York (1978)
139. Bigg, D. M., "Mechanical, Thermal, and Electrical Properties of Metal Fiber-Filled Polymer Composites," Polym. Compos., 19, (16), 1188 (1979)
140. Bigg, D. M., "Mechanical Properties of Particle Filled Polymers," Polym. Compos., 8, (2), 115 (1987)

141. Mitsuishi, S., Kodama, S., and Kawasaki, H., "Mechanical Properties of Polyethylene/Ethylene Vinyl Acetate Filled with Calcium Carbonate," Polym. Compos., 9, (2) 112, (1988)
142. Piggott, M. R., "The Effect of the Interface/Interphase of Fiber Composite Properties," Polym. Compos., 8, (5), 291 (1987)
143. Nicolais, L. and Narkis, M., "Stress-Strain Behavior of Styrene-Acrylonitrile/Glass Bead Composites in the Glassy Region," Polym. Eng. Sci., 11, (3), 194 (1971)
144. Narkis, M. and Nicolais, L., "Stress-Strain Behavior of SAN/Glass Bead Composites Above the Glass Transition Temperature," J. Appl. Polym. Sci., 15, 469 (1971)
145. Moehlenpah, A. E., Ishai, O., and DiBenedetto, A. T., "The Effect of Time and Temperature on the Mechanical Behavior of Epoxy Composites," Polym. Eng. Sci., 11, (2), 129 (1971)
146. Smith, T. L., "Volume Change and Dewetting in Glass Bead-Polyvinyl Chloride Elastomeric," Trans. Soc. Rheol., 3, 113 (1959)
147. Smith, T. L. and Stedry, P., "Time and Temperature Dependence of Ultimate Properties of an SBR Rubber at Constant Elongations," J. Appl. Phys., 31, 1982 (1960)
148. Bigg, D. M., "Rheological Behavior of Highly Filled Polymer Melts," Polym. Eng. Sci., 23, (4), 206 (1983)
149. Bigg, D. M., "Rheological Analysis of Highly Loaded polymeric Composites Filled with Non-Agglomerating Spherical Filler Particles," Polym. Eng. Sci., 22, (8), 512 (1982)
150. Saini, D. R., Shenoy, A. V., and Nadkarni, V. M., "Effect of Surface Treatment on the Melt Rheology and Mechanical Properties of Ferrite-Filled Styrene-Isoprene-Styrene Block Copolymers," Polym. Compos., 7, (4), 193 (1986)
151. Nielsen, L. E. and Lewis, T. B., "Viscosity of Dispersed and Aggregated Suspensions of Spheres," Trans. Soc. Rheol., 12, 421 (1968)

152. Maiti, S. N., and Mahapatro, P. K., "Melt Rheological Properties of Nickel Powder Filled Polypropylene Composites," Polym. Compos., 9, (4), 291 (1988)
153. Cantu, T. S., and Caruthers, J. M., "Viscometric Properties of Poly(Dimethylsiloxane) Filled with Spherical Silica Particles," J. Appl. Polym. Sci., 27, 3079 (1982)
154. Lanel, R. F., Moser, B. G., and Bauman, A. J., "Rheology of Concentrated Suspensions: Effect of a Surfactant," Proc. 4th Internat. Congr. Rheol., Part 2, p. 663, ed., Lee, E. H., Interscience, New York (1965)
155. Chong, J. S., Christiansen, E. B., and Bare, A. D., "Rheology of Concentrated Suspensions," J. Appl. Polym. Sci., 15, 2007 (1971)
156. Collins, E. A., and Hoffmann, D. J., "Rheology of PVC Dispersions I. Effect of Particles and Particle Size Distribution," J. Colloid Interface Sci., 71, (1), 21 (1979)
157. Faulkner, D. L., and Schmidt, L. R., "Glass Bead-Filled Polypropylene Part I: Rheological and Mechanical Properties," Polym. Compos., 17, (9), 657 (1977)
158. Mills, N. J., "The Rheology of Filled Polymers," J. Appl. Polym. Sci., 15, 2791 (1971)
159. Boaira, M. S., and Chaffey, C. E., "Effects of Coupling Agents on the Mechanical and Rheological Properties of Mica-Reinforced Polypropylene," Polym. Eng. Sci., 17, (10), 715 (1977)
160. Cross, M. M., "Kinetic Interpretation of Non-Newtonian Flow," J. Colloid Interface Sci., 33, 30 (1970)
161. Bestul, A. B., and Belcher, H. V., "Temperature Coefficients of Non-Newtonian Viscosity at Fixed Shearing Stress and at Fixed Rate of Shear," J. Appl. Phys., 24, (6), 696 (1954)
162. Ferry, J. D., Chapter 11: Dependence of Viscoelastic Behavior on Temperature and Pressure, p. 307-320, Viscoelastic Properties of Polymers, 2nd ed., Wiley, New York (1970)

163. Eyring, H., "Viscosity, Plasticity, and Diffusion as Examples of Absolute Reaction Rates," J. Chem. Phys., 4, 283 (1936)
164. Nielsen, L. E., Chapter 4: Effects of Rate of Shear on Polymer Rheology, p. 47-68, Polymer Rheology, Marcel Dekker, New York (1977)
165. Shenoy, A. V., and Saini, D. R., "Quantitative Estimation of Matrix-Filler Interactions in Ferrite-Filled-Styrene-Isoprene-Styrene Block Copolymer," Polym. Compos., 7, (2), 96 (1986)
166. Svehlová, V., "Microscopic Methods Characterizing the Dispersion in Mineral-Filled Thermoplastics," in Polymer Composites, p. 607-614, ed., Sedláček, B., Walter de Gruyter, New York (1986)
167. Sacks, M. D., Khadilkar, C. S., Scheiffele, G. W., Shenoy, A. V., Dow, J. H., and Sheu, R. S., "Dispersion and Rheology in Ceramic Processing," Advances in Ceramics, Vol. 21: Ceramic Powder Science, p. 495-515, the American Ceramic Society (1987)
168. Dow, J. H., Sacks, M. D., and Shenoy, A. V., "Dispersion of Ceramic Particles in Polymer Melts," Advances in Ceramics, Vol. 21: Ceramic Powder Science, p. 495-515, the American Ceramic Society (1987)
169. Adamson, A. W., Chapter 12: Friction and Lubrication—Adhesion, p. 402-432, Physical Chemistry of Surfaces, 4th ed., Wiley, New York (1982)
170. Cherry, B. W., Chapter 6: Friction and Adhesion," p. 95-122, Polymer Surface, Cambridge University Press, London (1981)
171. Kendall, K., "Inadequacy of Coulomb's Friction Law for Particle Assemblies," Nature, 319, 203 (1986)
172. Johnson, K. L., Lendall, K., and Roberts, A. D., "Surface Energy and the Contact of Elastic Solids," Proc. R. Soc., A324, 301 (1971)
173. Savkoor, A. R. and Briggs, G. A., "The Effect of Tangential Force on the Contact of Elastic Solids in Adhesion," Proc. R. Soc., A356, 103 (1977)
174. Briscoe, B. J. and Kremnitzer, S. L., "A Study of the Friction and Adhesion of Polyethylene-Terephthalate Monofilaments," J. Phys. D: Appl. Phys., 12, 505 (1979)

175. Jones, J. W. and Eiss, N. S. Jr., "Effect of Chemical Structure and Wear of Polyimide Thin Films," in Polymer Wear and Its Control, p. 135-148, ed., Lee, L. H., ACS Symposium Series 287, American Chemical Society, Washington, D.C. (1985)
176. Czichos, H., "Contact Deformation and Static Friction of Polymers: Influence of Viscoelasticity and Adhesion," in Polymer Wear and its Control, p. 1-26, ed., Lee, L. H., ACS Symposium Series 287, American Chemical Society, Washington, D.C. (1985)
177. Lavrentev, V. V., "Theory of Friction of Elastomers," in Advances in Polymer Friction and Wear, p. 759, ed., Lee, L. H., Plenum Press, New York (1974)
178. Tanaka, K. and Yamada, Y., "Effect of Temperature on the Friction and Wear of Some Heat-Resistant Polymers," in Polymer Wear and Its Control, p. 103-128, ed., Lee, L. H., ACS Symposium Series 287, American Chemical Society, Washington, D.C. (1985)
179. Fusaro, R. L., "Tribological Properties and Thermal Stability of Various Types of Polyimide Films," ASLE Trans., 25, 465-477 (1982)
180. Fusaro, R. L., "Molecular Relaxations, Molecular Orientation and Friction Characteristics of Polyimide Films," Trans. ASLE, 20, 1-14 (1977)
181. Peyser, P., and Little, R. C., "The Drag Reduction of Dilute Polymer Solutions as a Function of Solvent Power, Viscosity, and Temperature," J. Appl. Polym. Sci., 15, 2623 (1971)
182. Wasan, D. T., Gupta, L. and Vora, M. K., "Interfacial Shear Viscosity at Fluid-Fluid Interfaces," AIChE Journal, 17, (6), 1287 (1971)
183. Reynolds, O., "An Experimental Investigation of the Circumstances which Determine whether the Motion of Water shall be Directed or Sinuous, and of the Law of Resistance in Parallel Channels," Phil. Trans. Roy. Soc. London, A174: 935 (1883)
184. Hiemenz, P. C., Chapter 2: The Viscous State, p. 75-132, Polymer Chemistry: The Basic Concepts, Marcel Dekker, New York (1984)
185. Bueche, F., Chapter 4: Segmental Motion and the Glass Temperature, p. 85-111, Physical Properties of Polymers, Interscience, New York (1962)

186. Stöber, W., Fink, A., and Bohn, E., "Controlled Growth of Monodisperse Silica Sphere in the Micro Size Range," J. Colloid Interface Sci., 26, 62-69 (1968)
187. Cab-O-Sil Properties and Functions, Cabot Corporation, Tuscola, Illinois (1989)
188. Tan, C. G., Bowen, B. D., and Epstein, N., "Production of Monodisperse Colloidal Silica Spheres: Effect of Temperature," J. Colloid Interface Sci., 118, 290 (1987)
189. Salyer, I. O., "Structure and Properties Relationship in Ethylene-Vinyl Acetate Copolymers," J. Polym. Sci.: Part A-1, 9, 3083 (1971)
190. Lamb, R. N., and Furlong, D. N., "Controlled Wettability of Quartz Surface," J. Chem. Soc., Faraday Trans., 78, (1), 61 (1982)
191. Tsutsumi, K., and Takahashi, H., "Studies of Surface Modification of Solid," Colloid Polym. Sci., 263, 506 (1985)
192. Mack, G. L., "The Determination of Contact Angles from Measurements of the Dimensions of Small Bubbles and Drops," J. Phys. Chem., 40, 159 (1936)
193. Bartell, F. E. and Zuidema, H. H., "Wetting Characteristics of Solids of Low Surface Tension Such as Talc, Waxes and Resins," J. Am. Chem. Soc., 58, 1449 (1936)
194. Johnson, O., "Acidity and Polymerization Acidity of Solid Catalysts," J. Phys. Chem., 59, 827 (1955)
195. Benesi, H. A., "Acidity of Catalyst Surface: Acid Strength from Colors of Adsorbed Indicators," J. Phys. Chem., 78, 5490 (1956)
196. Benesi, H. A., "Acidity of Catalyst Surface: Amine Titration Using Hammett Indicators," J. Phys. Chem., 61, 970 (1957)
197. Blitz, J. P., Murthy, R. S. S., and Leyden, D. E., "Comparison of Transmission and Diffuse Reflectance Sampling Techniques for FT-IR Spectrometry of Silane-Modified Silica Gel," Appl. Spectrosc., 40, 829 (1986)

198. Benesi, H. A., and Jones, A. C., "An Infrared Study of the Water-Silica Gel System," J. Phys. Chem., 63, 179 (1959)
199. Shreedhara Murthy, R. S., and Leyden, D. E., "Quantitative Determination of (3-Aminopropyl) Triethoxysilane on Silica Gel Surface Using Diffuse Reflectance Infrared Fourier Transform Spectrometry," Anal. Chem., 58, 1228 (1986)
200. Koenig, J. L., "Application of Fourier Infrared Spectroscopy to Chemical System," Appl. Spectrosc., 29, 293 (1975)
201. Culler, S. R., Ishida, H., and Koenig, J. L., "The Use of Infrared Methods to Study Polymer Interface," Ann. Rev. Mater. Sci., 13, 363 (1983)
202. Fuller, M. P., and Griffiths, P. R., "Diffuse Reflectance Measurements by Infrared Fourier Transform Spectrometry," Anal. Chem., 50, 1906, (1978)
203. Maulhardt, H., and Kunath, D., "A Simple Device for Diffuse Reflectance Fourier Transform Infrared Spectroscopy," Appl. Spectrosc., 34, 383 (1980)
204. Shreedhara Murthy, R. S., Blitz, J. P., and Leyden, D. E., "Quantitative Variable-Temperature Diffuse Reflectance Infrared Fourier Transform Spectroscopic Studies of Modified Silica Samples," Anal. Chem., 58, 3167 (1986)
205. Hattori, T., Shirai, K., Niwa, M., and Murakami, Y., "Quantitative Interpretation of Infrared Diffuse Reflectance Spectra over Whole Concentration Range," Bull. Chem. Soc. Jpn., 54, 1964 (1981)
206. Leyden, D. E., Shreedhara Murthy, R. S., and Blitz, J. P., "Computer-Interfaced Temperature Controller for FT-IR Diffuse Reflectance Cell," Appl. Spectrosc., 41, 920 (1987)
207. Devries, K. L., Igarashi, M., Chao, F., "Molecular Degradation of Polymers," J. Polym. Sci., Polym. Sympo., 72, 111 (1985)
208. Bakht, M. F., "Thermal Degradation of Copolymers of Vinyl Alcohol and Vinyl Butyl," Pakistan J. Sci. Ind. Res., 26, (1), 35 (1983)

209. Fuoss, R. M., "Evaluation of Rate Constants from Thermogravimetric Data," J. Appl. Polym. Sci., Part A, 2, 3147 (1964)
210. Hirate, T., Kashiwagi, T., and Brown, J. E., "Thermal and Oxidative Degradation of Poly(Methacrylate) Weight Loss," Macromolecules, 18, (7), 1410 (1985)
211. Tadros, T. F., "Adsorption of Polyvinyl Alcohol on Silica at Various PH Values and its Effect on the Flocculation of the Dispersion," J. Colloid Interface Sci., 64, (1), 36 (1978)
212. Killmann, E., Eisenlauer, J., and Korn, M., "The Adsorption of Macromolecules on Solid/Liquid Interfaces," J. Polym. Sci., Polym. Sympo., 61, 413 (1977)
213. Thies, C., "The Adsorption of Polystyrene-Poly(Methyl methacrylate)," J. Phys. Chem., 70, (12), 3783 (1966)
214. Hasegawa, M. and Low, M. J. D., "Infrared Study of Adsorption in situ at the Liquid-Solid Interface. II. Adsorption of Stearic Acid on Zinc Oxide," J. Colloid Interface Sci., 29, (4), 593 (1969)
215. Lipatov, Y. and Sergeeva, L. M., "Adsorption of Polymers from Concentrated Solutions," Advances in Colloid and Interface Sci., 6, 1 (1976)
216. Utracki, L. A. and Fisa, B., "Rheology of Fiber- or Flake-Filled Plastics," Polym. Compos., 3, (4), 193 (1982)
217. Schulken, R. M., Cox, R. H., and Minnick, L. A., "Dynamic and Steady-State Rheological Measurements on Polymer Melts," J. Appl. Polym. Sci., 25, 1341 (1980)
218. Sacks, M. D. and Tseng, T. Y., "Preparation of SiO<sub>2</sub> Glass from Powder Compacts: I, Formation and Characterization of Powders, Suspensions and Green Compacts," J. Am. Ceram. Soc., 67, (8), 526 (1984)
219. Sacks, M. D. and Tseng, T. Y., "Preparation of SiO<sub>2</sub> Glass from Model Powder Compacts: II, Sintering," J. Am. Ceram. Soc., 67, (8), 532 (1984)
220. Tseng, T. Y. and Yu, J. J., "Various Atmosphere Effects on Sintering of Compacts of SiO<sub>2</sub> Microspheres," J. Mater. Sci., 21, 3615 (1986)

221. Barringer, E.A. and Bowen, H.K., "Formation, Packing and Sintering of Monodisperse  $\text{TiO}_2$  Powder," J. Am. Ceram. Soc., 65, (12), C119 (1982)
222. Yasuo, O. and Hattori, E., "Preparation of Translucent  $\text{SiO}_2$  from Monosized Particles," The First International Conference on Ceramic Powder Processing Science, Orlando, FL., Nov. 1-4 (1987)
223. Cheng, Y. C., The Effect of Surface Hydration on the Adsorption and Flocculation of a Model Silica Suspension using Polyethylene Oxide, MS. thesis, p. 34-51, University of Florida (1985)
224. Söderholm, K.-J., "Filler Systems and Resin Interface," Posterior Composite Resin Dental Restorative Materials, p. 139-160, eds., Vanherle, G., and Smith, D. C., Peter Szulc Publishing Co., Netherlands (1985)
225. Wagner, M. P., "Nature and Synthetic Silicas in Plastics," Additives for Plastics, Vol. 1, p. 9-28, ed., Seymour, R. B., Academic Press, New York (1978)
226. Katz, H. S. and Ehrenreich, L., "Glass Filler," Additives for Plastics, Vol. 2, p. 17-24, ed., Seymour, R. B., Academic Press, New York (1978)
227. Hair, M. L., Chapter 4: Silica Surface, p. 79-137, Infrared Spectroscopy in Surface Chemistry, Marcel Dekker, New York (1967)
228. Hair, M. L., "Silica Surface," Silanes, Surfaces, and Interfaces, p. 25-41, from Silanes, Surfaces, Interfaces Symposium (1985: Snowmass, Colo.), ed., Leyden, D. E., Gordon and Breach Sci., Amsterdam (1986)
229. Hair, M. L. and Hertl, W., "Reaction of Chlorosilanes with Silica Surface," J. Phys. Chem., 73, 2372 (1969)
230. Evans, B. and White, T. E., "Adsorption and Reaction of Methylchlorosilanes at an Aerosil Surface," J. Catalysis, 11, 336 (1968)
231. Hertl, W., "Mechanism of Gaseous Silane Reaction with Silica. I," J. Phys. Chem., 72, 1248 (1968)
232. Hertl, W., "Mechanism of Gaseous Silane Reaction with Silica. II," J. Phys. Chem., 72, 3993 (1968)

233. Zhuravlev, L. T., "Concentration of Hydroxyl Groups on the Surface of Amorphous Silica," Langmuir, 3, 316 (1987)
234. Friprat, J. J. and Uytterhoeven, J., "Hydroxyl Content in Silica Gel Aerosil," J. Phys. Chem., 66, 880 (1962)
235. Maron, S. H. and Lando J. B., Chapter 10: Chemical Equilibrium, p. 377-380, Fundamentals of Physical Chemistry, Macmillan, New York (1974)
236. Bolger, J. C., "Acid Base Interactions between Oxide Surfaces and Polar Organic Compounds," in Adhesion Aspect of Polymer Coating, p. 3-18, ed., Mittal, K. L., Plenum Press, New York (1981)
237. McCrum, N. G., Buckley, C. P., and Bucknall, C. B., Chapter 6: Reinforced Polymers, Principles of Polymer Engineering, p. 212-213, Oxford University Press, New York (1988)
238. Hess, W. M., Ban, L., and McDonald, G. C., "Carbon Black Morphology: I. Particle Microstructure. II. Automated EM Analysis of Aggregate Size and Shape," Rubber Chem. Technol., 42, 1209 (1969)
239. Medalia, A. I. and Heckman, F. A., "Morphology of Aggregates. VII. Comparison Chart Method for Electron Microscopic Determination of Carbon Black Aggregate Morphology," J. Colloid Interface Sci., 36, 173 (1971)
240. Hess, W. M., McDonald, G. C. and Urban, E., "Specific Shape Characterization of Carbon Black Primary Units," Rubber Chem. Technol., 46, 204 (1973)
241. Boonstra, B. B. and Medalia, A. I., "Effect of Carbon Black Dispersion on the Mechanical Properties of Rubber Vulcanizates," Rubber Age, 92, 892 (1963)
242. Boonstra, B. B. and Medalia, A. I., "Effect of Carbon Black Dispersion on the Mechanical Properties of Rubber Vulcanizates, continued from preceding issue," Rubber Age, 93, 82 (1963)
243. Kraus, G. and Gruver, J. T., "Thermal Expansion, Free Volume, and Molecular Mobility in a Carbon Black-Filled Elastomer," J. Polym. Sci., Part A-2, 8, 571 (1970)

244. Kraus, G., "A Structure-Concentration Equivalence Principle in Carbon Black Reinforcement of Elastomers," J. Polym. Sci., Part B, 8, 601 (1970)
245. Kraus, G., "Interactions of Elastomers and Reinforcing Fillers," Rubber Chem. Technol., 38, 1070 (1965)
246. Kraus, G., "Structure-Concentration Equivalence in Carbon Black Reinforcement of Elastomers. III. Application to Tensile Strength," J. Appl. Polym. Sci., 15, 1679 (1971)
247. Han, C.D., "Rheological Properties of Calcium Carbonate-Filled Polypropylene Melts," J. Appl. Polym. Sci., 18, 821 (1974)
248. Kambe, H. and Takano, M., "Viscoelastic Properties of Concentrated Dispersions in a Molten Polymer," Proceedings of the Fourth International Congress on Rheology, Part 3, p. 557-572, ed., Lee, E. H., Interscience, New York (1963)
249. Tanaka, H. and White, J., "Experimental Investigations of Shear and Elongational Flow Properties of Polystyrene Melts Reinforced With Calcium Carbonate, Titanium Dioxide, and Carbon Black," Polym. Eng. Sci., 20, (14), 949 (1980)
250. Lobe, V. M. and White, J., "An Experimental Study of the Influence of Carbon Black on the Rheological Properties of A Polystyrene Melt," Polym. Eng. Sci., 19, (9), 617 (1979)
251. White, J. M. and Crowder, W., "The Influence of Carbon Black on the Extrusion Characteristics and Rheological Properties of Elastomers: Polybutadiene and Butadiene-Styrene Copolymer," J. Appl. Polym. Sci., 18, 1013 (1974)
252. Minagawa, N. and White, J. M., "The Influence of Titanium Dioxide on the Rheological and Extrusion Properties of Polymer Melts," J. Appl. Polym. Sci., 16, 501 (1976)
253. Luo, H. L., Han, C. D., and Mijovic, J., "Effects of Coupling Agents on the Rheological Behavior and Physical/Mechanical Properties of Filled Nylon 6," J. Appl. Polym. Sci., 28, 3387 (1983)

254. Han, C. D., Villamizar, C. A., and Kim, Y. W., "Morphology and Mechanical Properties of Injection-Molded Specimens of Two Phase Polymer Blends," J. Appl. Polym. Sci., 21, 353 (1977)
255. Han, C. D., "Measurement of the Rheological Properties of Polymer Melts with Slit Rheometer. I. Homopolymer Systems," J. Appl. Polym. Sci., 15, 2567 (1971)
256. Han, C. D., Yu, T. C., Kim, K. U., "Rheological Properties of Molten Polymers. I. Homopolymer Systems," J. Appl. Polym. Sci., 15, 1149 (1971)
257. Lem, K. W., Han, C. D., "Rheological Behavior of Concentrated Suspensions of Particles in Unsaturated Polyester Resin," J. Rheology, 27, (3), 263 (1983)
258. Han, C. D., Sandford, C., and Yoo, H. J., "Effects of Titanate Coupling Agents on the Rheological and Mechanical Properties of Filled Polyolefins," Polym. Eng. Sci., 18, (11), 849 (1978)
259. Han, C. D., Weghe, V. D., Shete, P., and Haw, J. R., "Effects of Coupling Agents on the Rheological Properties, Processability, and Mechanical Properties of Filled Polypropylene," Polym. Eng. Sci., 21, (4), 196 (1981)
260. Galanti, A. V. and Sperling, L. H., "Morphology and Structure of Silica Agglomerates in Silica-Reinforced Silicone Rubber," J. Appl. Polym. Sci., 11, 2785, (1970)
261. Kozicki, W., Hanna, M. R., and Tiu, C., "Polymer Adsorption in Packed Bed Flow," J. Rheology, 32, (6), 593 (1988)
262. Papanicolaou, G. C., Theocaris, P. S., and Spathis, G. D., "Adhesion Efficiency between Phases in Fiber-Reinforced Polymers by Means of the Concept of Boundary Interphase," Colloid and Polymer Sci., 258, 1231 (1980)
263. Sideridis, E., Theocaris, P. S., and Papanicolaou, G. C., "The Elastic Modulus of Particulate Composites Using the Concept of a Mesophase," Rheol. Acta., 25, 350 (1986)
264. Theocaris, P. S., "The Concept and Properties of Mesophase in Composites," Composite Interfaces, p. 329-349, eds., Ishida, H. and Koenig, J. L., Elsevier Science, New York (1986)

265. Sideridis, E., "The Dynamic Moduli of Particulate-Filled Polymers as Defined by the Concept of Interphase," Compos. Sci. Technol., 27, 305 (1986)
266. Spathis, G., Kontou, E., and Theocaris, P. S., "Dynamic Mechanical Properties of an Iron-Epoxy Particulate Composite," J. Rheol., 28, (2), 161 (1984)
267. Theocaris, P. S. and Spathis, G. D., "Glass-Transition Behavior of Particle Composites Modeled on the Concept of Interphase," J. Appl. Polym. Sci., 27, 3019 (1982)
268. Gent, A. N., "Fracture Mechanics Applied to Elastomeric Composites," Rubber Chem. & Technol., 56, (5), 1011 (1983)
269. Gent, A. N., "Detachment of an Elastic Matrix from a Rigid Spherical Inclusion," J. Mater. Sci., 15, 2884 (1980)
270. Wagner, M. P., "Reinforcing Silicas and Silicates," Rubber Chem. & Technol., 49, 703 (1976)
271. Griffith, A. A., "The Phenomena of Rupture and Flow in Solids," Phil. Trans. Royal Soc., London, A221, 163 (1920)
272. Parkinson, D., Chapter 5: Influence of Carbon Black on the Properties of Vulcanized Rubbers, p. 13-24, Reinforcement of Rubbers, Lakeman, London (1957)
273. Wu, S., Chapter 3: Interfacial and Surface Tensions of Polymer Melts and Liquids, p. 67-132, Polymer Interface and Adhesion, Marcel Dekker, New York (1982)
274. Padday, J. F., Part 1: The Theory of Surface Tension, Surface and Colloid Science, Vol. 1, p. 39-99, ed., Matijevic, E., Wiley, New York (1969)
275. Wu, S., "Surface and Interfacial Tensions of Polymer Melts. II. Poly(methyl methacrylate), Poly(n-butyl methacrylate), and Polystyrene," J. Phys. Chem., 74, 632 (1970)
276. Roe, R. J., "Surface Tension of Polymer Liquids," J. Phys. Chem., 72, 2013 (1968)
277. Wu, S., Chapter 6: Interfacial Energy, Structure, and Adhesion between Polymers, p. 243-293, Polymer Blend, Vol. 1, eds., Paul, D. R. and Newman, S., Academic Press, New York (1978)

278. Wu, S., "Interfacial and Surface Tensions of Polymers," J. Macromol. Sci., C10, 1 (1974)
279. Baszkin, A., Nishino, M., and Ter-Minassian-Saraga, L., "Solid-Liquid Adhesion of Oxidized Polyethylene Films. Effect of Temperature," J. Colloid Interface Sci., 54, (3) 317 (1976)
280. Baszkin, A., Nishino, M., and Ter-Minassian-Saraga, L., "Solid-Liquid Adhesion of Oxidized Polyethylene Films. Effect of Temperature on Polar Forces," J. Colloid Interface Sci., 59, (3) 516 (1977)
281. Kloubek, J., "Interaction of Polar Forces and Their Contribution to the Work of Adhesion," J. Adhesion, 6, 293 (1974)
282. Baszkin, A. and Ter-Minassian-Saraga, L., "Effect of Surface Polarity on Self-Adhesion of Polymers," Polymer, 19, 1083 (1978)
283. Malpass, V. E., Kempthorn, J. T., and Dean, A. F., "Estimating Thermoforming Behavior of Mineral-Filled Polypropylenes," Plastics Engineering, January, 27 (1989)
284. Ree, T. and Eyring, H., Chapter 3: The Relaxation Theory of Transport Phenomena," Rheology: Theory and Applications, Vol. 2, ed., Eirich, F. R., Academic Press, New York (1958)
285. Krausz, A. S. and Eyring, H., Chapter 4: Special Topics, p. 338-351, Deformation Kinetics, Wiley, New York (1975)
286. Askeland, D. R., Chapter 5: Atom Movement in Materials, p. 99-100, The Science and Engineering of Materials, Wadsworth, New York (1984)
287. Vinogradov, G. V., Malkin, A. Ya., Chapter 2: Shear Viscosity, p. 104-142, Rheology of Polymers, Mir Publishers, Moscow (1980), Translated from the revised version of Reologia Polimerov, Khimia, Moscow, 1977, by Artavaz Beknazarov.
288. Lupton, J. M., "Flow of Polymer Melts," Polymer Processing, ed., Fear, J. V. D., Chem. Eng. Progr. Symp. Ser., 60, (49), 17, (1964)
289. Williams, D. J., Chapter 12: Interaction to Polymer Melt Rheology, p. 340-371, Polymer Science and Engineering, Englewood Cliffs, New Jersey (1974)

## BIOGRAPHICAL SKETCH

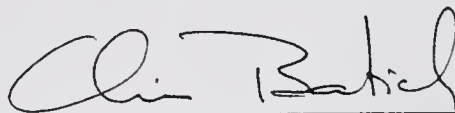
Shaye-Wen ("Sherwin") Shang was born May 19, 1957, in Taiwan, Republic of China. He graduated from National Central University, Taiwan, with a degree of Bachelor of Science in chemical engineering in June 1980. Following graduation, he served the nation two years in army to fulfill mandatory military service.

For seeking a higher education, he was admitted to the graduate school at the University of Florida in August 1982 and received the degree of Master of Science in chemical engineering in August 1983.

For pursuing the advanced study in polymer materials, he entered the Department of Materials Science and Engineering at the University of Florida after he received his M.S. degree. The field of his doctor research is in the polymer composite materials, emphasizing on the understanding the interfacial bonding between two phases.

He is a member of the American Chemical Society and the Society of Plastic Engineers.

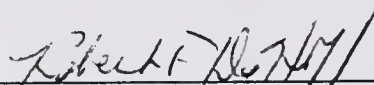
I certify that I have read this study and that in my opinion it conforms to acceptable standards of scholarly presentation and is fully adequate, in scope and quality, as a dissertation for the degree of Doctor of Philosophy.



---

Christopher D. Batich, Chair  
Professor of Materials Science  
and Engineering

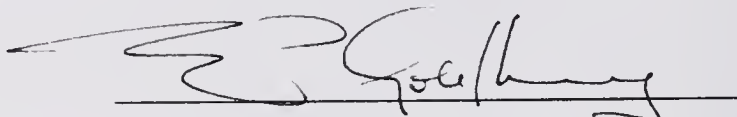
I certify that I have read this study and that in my opinion it conforms to acceptable standards of scholarly presentation and is fully adequate, in scope and quality, as a dissertation for the degree of Doctor of Philosophy.



---

Robert T. DeHoff, Cochair  
Professor of Materials Science  
and Engineering

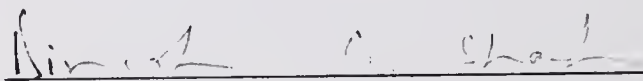
I certify that I have read this study and that in my opinion it conforms to acceptable standards of scholarly presentation and is fully adequate, in scope and quality, as a dissertation for the degree of Doctor of Philosophy.



---

Eugene P. Goldberg  
Professor of Materials Science  
and Engineering

I certify that I have read this study and that in my opinion it conforms to acceptable standards of scholarly presentation and is fully adequate, in scope and quality, as a dissertation for the degree of Doctor of Philosophy.



---

Denish O. Shah  
Professor of Chemical Engineering

I certify that I have read this study and that in my opinion it conforms to acceptable standards of scholarly presentation and is fully adequate, in scope and quality, as a dissertation for the degree of Doctor of Philosophy.



---

Kevin S. Jones  
Assistant Professor of Materials  
Science and Engineering

This dissertation was submitted to the graduate Faculty of the College Engineering and to the Graduate School and was accepted as partial fulfillment of the requirements for the degree of Doctor of Philosophy.

August, 1989



---

Dean, College of Engineering

---

Dean, Graduate School



